Repurposing Drug Scaffolds:
A Tool for Developing Novel Therapeutics with Applications in Malaria and Lung Cancer

A Thesis Submitted by:

Hannah Elizabeth Cook

In partial fulfilment of the requirements for the degree of:

Doctor of Philosophy

September 2018

Supervisors: Professor Matthew J. Fuchter & Professor Anthony G. M. Barrett

Department of Chemistry

Imperial College London

Declaration of Originality

I, Hannah Cook, hereby confirm that the work presented within this thesis is entirely my own, conducted under the supervision of Professor Matthew J. Fuchter and Professor Anthony G. M. Barrett, at the Department of Chemistry, Imperial College London, unless otherwise stated. All work performed by others has been acknowledged within the text and referenced where appropriate.

Hannah E. Cook

September 2018

Copyright Declaration

The copyright of this thesis rests with the author and is made available under a Creative Commons Attribution Non-Commercial No Derivatives licence. Researchers are free to copy, distribute or transmit the thesis on the condition that they attribute it, that they do not use it for commercial purposes and that they do not alter, transform or build upon it. For any reuse or redistribution, researchers must make clear to others the licence terms of this work.

Abstract

The definition of repurposing in the context of drug discovery encompasses a variety of strategies designed to redirect current therapeutic knowledge towards new disease indications. This approach can be successful for the design of new drugs to treat diseases of the developing world such as Malaria, where there are limited resources to fund new drug discovery campaigns. Moreover, it can be used to decrease the drug development time for diseases in which there is high drug attrition rates coupled with high mortality rates, which is the case for some cancers.

To this end, two separate medicinal chemistry projects are presented herein which are both based on current drug scaffolds originally used for alternative therapeutic indications. The first is the design of an inhibitor of *Plasmodium Falciparum* Myosin A (*Pf*MyoA), a motor protein implicated in the blood stage invasion of Malaria. Structural predictions of the myosin structure have been made in the form of a homology model using the crystal structure of a well characterised homologue, myosin II and its inhibitor, (*S*)-Blebbistatin. *Plasmodium* specific inhibitors were designed *in silico* based on the structure of (*S*)-Blebbistatin and synthesised for validation of the model using biological testing of their effect on myosin activity and importantly, on parasite invasion. Interestingly, compounds were found to reduce parasitaemia in red blood cells, independently of *Pf*MyoA, suggesting interaction with an alternative essential myosin.

The second project described is the synthesis of compounds that inhibit 90-kDa ribosomal S6 kinase 4 (RSK4), a promotor of lung cancer metastasis and resistance to chemotherapeutic treatments. Inhibitors were synthesised based on the structures of fluoroquinolone antibiotics Moxifloxacin and Trovafloxacin which were identified as moderately potent inhibitors of RSK4. Derivatives were designed with enhanced solubility and tested in a cell-based assay in which 10 novel compounds were identified that inhibit RSK4 activation by at least 50%.

Acknowledgements

First and foremost, I would like to thank my two supervisors, Professor Matthew Fuchter and Professor Anthony Barrett for granting me the opportunity to work on two interesting and unique projects, and for their continued support throughout my PhD. I would also like to thank Jochen Brandt and Sandeep Sundriyal for their guidance and reassurance in my early days in the lab. In addition, special thanks must also go to Ainoa Zubiaurre who has always gone the extra mile to help me, especially during my write up period.

I'd also like to thank Professor Jake Baum and his group at Imperial College for their work on the biological aspects of the Myosin A project. In particular, I thank Tom Blake and Linda Makhlouf who carried out the biological assays and provided me with their invaluable insights. Thanks also to Dr Olivier Pardo and Professor Michael Seckl for offering their expertise and guidance at the beginning of the RSK4 project.

Thanks should also go to the analytical staff at Imperial College; Dr Lisa Haigh, Dick Sheppard and especially Pete Haycock who kindly ran samples for me during the hectic departmental move to White City.

During my PhD I have had the pleasure to work with many people from the Fuchter and Barrett group, and I would like to extend my thanks to past and present members for keeping me sane over the years. A special mention must go to Alex, Luiza, Katie and Melis who have been with me since the beginning and have supported (and commiserated with) me the whole way through.

Finally, I'd like to thank George for his endless patience and belief in me, and my family for their continued encouragement. It has been a long journey and I am so grateful to have had you all by my side.

Contents

Declaration of Originality 3

Copyright Declaration 3

Abstract 4

Acknowledgements 5

Abbreviations 10

1. General Introduction 14

1.1. Repurposing Strategies in Drug Discovery 14

1.1.1. Target Repurposing 15

1.1.2. Drug Repurposing 17

Investigating *Plasmodium Falciparum* Myosin A 19

2. Introduction 20

2.1. Malaria 20

2.1.1. Malaria Cause and Transmission 20

2.1.2. The Invasive Parasite: Merozoites 22

2.1.3. Antimalarials Past and Present 23

2.1.4. Challenges to Current Treatment 26

2.2. Myosin: The Muscle Motor Protein 27

2.2.1. Structure and Function 27

2.2.2. Inhibitors of Myosin 31

2.2.3. (*S*)-Blebbistatin 33

2.2.4. Limitations and Derivatives of (*S*)-Blebbistatin 34

2.3. *Plasmodium Falciparum* Myosin A 38

2.3.1. Parasite Invasion 38

2.3.2. The *Pf*MyoA Motor Complex 40

2.4. (*S*)-Blebbistatin and *Plasmodium Falciparum* Invasion 42

2.5. Project Aims 44

3. Results and Discussion 45

3.1. Part 1: Development of a Homology Model 46

3.1.1. Structure Based Drug Design 46

3.1.2. Generation of a *Pf*MyoA Homology Model 48

3.1.3. Redesigning (*S*)-Blebbistatin 52

3.2. Part 2: Synthesis of 1st Generation (*S*)-Blebbistatin Analogues 58

3.2.1. Synthetic Route A – Hydroxylation and Lactam Reduction 58

3.2.2. Synthetic Route B – Cyanohydrin Formation and N-Arylation 65

3.2.3. Synthetic Route C – Amide Derivatives 69

3.2.4. Synthetic Route D – Acyl Anion Equivalents for Ketone Synthesis 80

3.2.5. Synthetic Route E - Ketone Derivatives 86

3.3. Part 3: Synthesis of 2nd Generation (*S*)-Blebbistatin Analogues 90

3.3.1. A Structural Biologist's Perspective 90

3.3.2. Synthesis of Derivatives with Smaller Amidine Substituents 93

3.3.3. Synthesis of Open Ring Derivative 103

3.3.4. Synthesis Towards Quinolone Derivative 103

3.4. Part 4: Biological Assessment 107

3.4.1. Invasion and Growth Inhibition Assays 107

3.4.2. *Pf*MyoA ATPase Assay 109
3.5. Conclusions and Future Work 113
Synthesis of Fluoroquinolone Derivatives as Inhibitors of RSK4 115
4. Introduction 116
4.1. Lung Cancer 116
4.1.1. Lung Cancer Pathogenesis 117
4.1.2. Current Treatments of NSCLC 119
4.2. The Ribosomal S6 Kinase Family 122
4.2.1. RSK Structure and Function 122
4.2.2. RSKs in Cancer 124
4.2.3. RSK Inhibitors 125
4.2.4. The RSK4 Isoform 127
4.2.5. RSK4 vs. RSK1 in Lung Cancer: Discovery of a Novel Therapeutic Target . 129
4.2.6. Inhibitors of RSK4: The Fluoroquinolones 132
4.3. Project Aims 137
5. Results and Discussion 138
5.1. Part 1: Synthesis of Moxi/Trovafloxacin Derivatives 139
5.1.1. Combinational Derivative Design 139
5.1.2. Synthesis of Moxifloxacin Derivatives 141
5.2. Part 2: Biological Assessment 154
5.2.1. RSK4 Biochemical Assay 154
5.2.2. RSK4 Cell-based Assay 154
5.3. Conclusions and Future Work 158

6. Final Remarks 159

7. Experimentals 160

7.1. General Methods 160

7.2. Synthetic Procedures: Part 1 162

7.3. Synthetic Procedures: Part 2 221

7.4. Biological Testing – Part 1 272

7.4.1. Ex vivo Parasite Experiments 272

7.4.2. *In vitro* ATPase Assay 273

7.5. Biological Testing: Part 2 274

7.5.1. RSK4 Cell-based Assay 274

8. References 275

Abbreviations

Å	Angstrom (10^{-10} metres)
Ac	Acetyl
ACT	Artemisinin-based combination therapy
ADDP	1,1'-(Azodicarbonyl)dipiperidine
ADP	Adenosine diphosphate
Aq.	Aqueous
Atm	Atmosphere (unit)
ATP	Adenosine triphosphate
BDM	2,3-Butanedione monoxime
BINAP	2,2'-bis(Diphenylphosphino)-1,1'-binaphthyl)
Bleb	(*S*)-Blebbistatin
Bn	Benzyl
Boc	*tert*-Butyloxycarbonyl
bp	Boiling point
BTS	*N*-Benzyl-*p*-toluene sulfonamide
Bu	Butyl
CAN	Cerium ammonium nitrate
CDK	Cyclin-dependent kinase
conc.	Concentration
CTKD	Carbon-terminal kinase domain
CytoD	Cytochalasin D
DCC	*N*,*N*'-Dicyclohexylcarbodiimide
DCE	1,2-Dichloroethane
DCM	Dichloromethane
***DD*MyoII**	*Dictyostelium discoideum* myosin II
DIAD	Diisopropyl azodicarboxylate
DIPEA	*N*,*N*-Diisopropylethylamine
DMF	*N*,*N*-Dimethylformamide
DMSO	Dimethyl sulfoxide
EC_{50}	Concentration of a drug where the response is reduced by half
EDC	1-Ethyl-3-(3-dimethylaminopropyl)carbodiimide
EGFR	Epidermal growth factor receptor
EI	Electron ionisation

Equiv.	Equivalent
ERK	Extracellular-signal-regulated kinase
Erα	Estrogen receptor α
ES	Electrospray
Et	Ethyl
EtOH	Ethanol
FDA	Food and Drug Administration
GFP	Green fluorescent labelling protein
GIA	Growth inhibition assay
Gly	Glycine
h	Hours
HOBt	1-Hydroxybenzotriazole hydrate
HPLC	High-performance liquid chromatography
HRMS	High resolution mass spectrometry
HTRF	Homogenous time resolved fluorescence
HTS	High through-put screening
Hz	Hertz
i	*iso*
IC_{50}	Half maximal inhibitory concentration
IIA	Invasion inhibition assay
IMC	Inner membrane complex
IR	Infrared
LC-MS	Liquid chromatography-mass spectrometry
LDA	Lithium diisopropylamide
Leu	Leucine
M	Molar (mol dm^{-3})
m/z	Mass-to-charge ratio
***m*CPBA**	*meta*-Chloroperoxybenzoic acid
Me	Methyl
MeCN	Acetonitrile
MeOH	Methanol
min	Minutes
Moxi	Moxifloxacin
mp	Melting point
MS	Mass spectrometry

MW	Microwave
MyoII	Myosin II
NAD	Nicotinamide adenine dinucleotide
NBS	*N*-Bromosuccinimide
NMR	Nuclear magnetic resonance
NMT	*N*-Myristoyltransferase
NSCLC	Non-small cell carcinoma
NTD	Neglected tropical diseases
NTKD	Amino-terminal kinase domain
OTf	Triflate
PBS	Phosphate-buffered saline
PDB	Protein data bank
PDK	Phosphoinositide-dependent kinase
***Pf*MyoA**	*Plasmodium falciparum* myosin A
Ph	Phenylalanine
Phe	Phenylalanine
Phyre2	Protein homology recognition engine V 2.0
Pi	Inorganic phosphate
pIC_{50}	The negative log of the IC_{50} value when converted to molar
PIFA	Bis(trifluoroacetoxy)iodobenzene
PMP	*Para*methoxyphenyl
ppm	Parts per million
PPS	Pre-power stroke
Rb	Retinoblastoma gene
RBC	Red blood cell
RNAi	RNA interference
RSK	90-kDa Ribosomal S6 kinase
rt	Room temperature
s	Seconds
SAR	Structure activity relationships
Sc	Scramble
SCLC	Small cell carcinoma
Ser	Serine
SiRNA	Small interfering RNA
SM	SWISS-MODEL

t	*tert*
TBAB	Tetrabutylammonium bromide
TBAF	Tetrabutylammonium fluoride
TFA	Trifluoroacetic acid
THF	Tetrahydrofuran
Thr	Threonine
TIPS	Triisopropylsilyl
TLC	Thin layer chromatography
TMS	Trimethylsilyl
Trova	Trovafloxacin
Tyr	Tyrosine
UV	Ultraviolet
WHO	World Health Organisation
X	Halide

1. General Introduction

1.1. Repurposing Strategies in Drug Discovery

Repurposing drug discovery strategies generally refers to a range of approaches designed to identify novel therapeutic indications for drugs, lead compounds and targets beyond their original purpose.[1] This alternative approach has grown in popularity over the years, largely due to the high cost of running drug discovery programmes combined with the very low market output, with only 5% of candidate drugs receiving approval following clinical trials.[2]

Repurposing chemical matter is attractive to pharmaceutical companies and academia alike as it can make development of a programme from hit to clinical candidate much quicker and therefore cheaper. Since safety and pharmacokinetic profiles may already be known, synthetic pathways may already have been mapped out and extensive knowledge of the biological target may already have been thoroughly investigated.[3]

Furthermore, for neglected tropical diseases (NTDs) such as human African trypanosomiasis (HAT) and Malaria, much of the drug discovery and hit to lead optimisation process is carried out in academia, as there is little incentive for for-profit organisations to invest in this area as the patient population is usually from regions of poverty that cannot afford medication.[4] With limitations such as a lack of technical support and man power that pharmaceutical companies yield, academic groups must employ alternative tools for drug development and often re-use existing target and chemical knowledge, as well as data from previous development campaigns.[2]

There are a number of approaches that can be used for repurposing drug discovery strategies and these can be grouped into the following areas: lead repurposing, target class repurposing, target repurposing and drug repurposing, though there are some strategies that fall outside these categories.[2] Lead repurposing involves taking a class of lead compounds in the early stage of development, usually identified in high through-put screening (HTS),

and exploiting the structural and chemical information available. This can be more useful than an unbiased HTS screen as the compounds that are identified often come from compound libraries designed to be more drug-like. Target class repurposing is used in cases where the target within a species of interest, for example a malarial parasite, is unknown, however it may carry out cellular functions that are homologous to another species' target class. Phenotypic assays are frequently used for this type of repurposing to ascertain whether a drug has the desired effect.

Although all classes can be effective for different cases, target and drug repurposing usually provide the best starting points in terms of the availability of information, and have the greatest potential for swift lead to optimisation and success in the clinic. For the purpose of this thesis, these approaches are of most interest and will therefore be discussed in further detail.

1.1.1. Target Repurposing

Target repurposing can be employed when the target in question with an undefined structure exists in a given species of interest, and has a well-defined and structurally characterised homolog in another. For example, a target protein present in the malaria parasite that has a well characterised close human homolog. If there are compounds that target the human protein, this provides a good starting point for a medicinal chemistry programme targeting the uncharacterised homologous protein of the other species.[2] Structural optimisation is required following identification of a lead compound, including improvements to the selectivity of the drug for the desired species over the original. Target repurposing is particularly attractive in NTD drug discovery as it can provide an economical and accelerated path to new therapies.[5]

An important advantage of this approach over target class repurposing is that the target protein is known, therefore medicinal chemistry programmes do not have to rely on a phenotypic effect for drug development. This also allows for structure-based drug design

programmes, either using X-ray crystallography if the purified target protein is available in large enough quantities, or the construction of homology models. The challenge of achieving selectivity between species can be alleviated since there is often considerable amounts of information available on the interactions between the human homolog and its active compounds, therefore these can be disrupted during optimisation of the compounds for the desired target.[2]

A shortcoming of target repurposing is the requirement of species homologs. Some therapeutic targets in humans do not exist in other species, such as the kinetoplastid parasite *Toxoplasma Brucei* which does not express G-protein coupled receptors, a commonly exploited family of receptors in humans.[6] Additionally, it is likely that a compound optimised for targeting the human homolog will be only moderately active against the target of interest, therefore it is often necessary to completely redevelop the compounds building on newly observed structure activity relationships (SAR).

Target repurposing was employed by a large consortium of chemistry groups at Imperial College London after finding that *N*-myristoyltransferase (NMT) is an essential target in *Plasmodium falciparum* (*P*. *falciparum*), the deadliest malarial parasite.

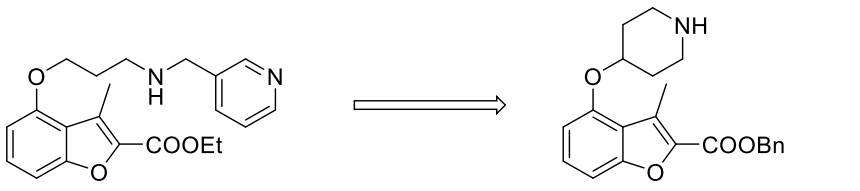


Figure 1: Antifungal NMT inhibitor **1** shown to inhibit *Pf*NMT selectively over the human NMT, *Hs*NMT1 and the resulting optimised molecule **2** with high *Pf*NMT potency as well as antiparasitic activity shown by the EC_{50} value.

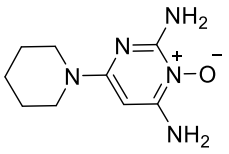
To develop an inhibitor of the desired target, they first created a homology model based on the closely related *Plasmodium Vivax* (*P. vivax*) NMT and the human NMT (HsNMT1), which was later aided by the resolution of the *P. falciparum* NMT (*Pf*NMT) X-ray crystal structure.

These were used to optimise the structure of the Roche anti-fungal NMT inhibitor **1** (Figure 1).[7]

1.1.2. Drug Repurposing

Drug repurposing can be characterised as redirecting molecules to an alternative indication from the one that was originally intended, without the requirements of structural modification as properties such as safety, toxicity and pharmacokinetics will already have been optimised for the original purpose. These include Food and Drug Administration (FDA) approved drugs, and those that have been discontinued or never made it to registration due to failures in clinical trials. Currently it takes 12-16 years for a drug to reach the market starting from development, which takes an average 3-6 years, and then preclinical and clinical trials which can span 8-10 years.[8] Due to high rates of attrition, most drugs do not make it to the market, therefore finding new uses for abandoned drugs, as well as those that were successful for a particular therapeutic indication, but have been archived, can be extremely valuable.

One example of successful drug repurposing is the deployment of Minoxidil (Figure 2), first as a treatment for ulcers before its discovery as an effective antihypertensive medication.[9] It was then later approved by the FDA as a treatment for androgenic alopecia, proving that one drug can have many biological outcomes.[1]



Minoxidil

Figure 2: Structure of the repurposed drug Minoxidil.

For the two projects described in this thesis, repurposing strategies have been successfully employed to initiate drug discovery programmes. The first project relies on the repurposing of a human myosin target and known inhibitor towards inhibition of a malaria parasite

myosin, using computer aided drug design. The second uses a slightly altered version of drug repurposing, with a class of antibiotics identified from an HTS of FDA approved drugs against a kinase target implicated in lung cancer. The general structure of this family of antibiotics was altered in an attempt to improve potency while also generating new IP space.

PART 1

Investigating *Plasmodium Falciparum* Myosin A: Exploring its Role in Malaria Using *in Silico* Inhibitor Design and Synthesis

2. Introduction

2.1. Malaria

Malaria remains one of the world's most devastating infectious diseases, placing a considerable burden on the developing world.[10] In 2016 there were 216 million cases of malaria reported from 91 countries worldwide, an increase of 5 million compared to the previous year. There were 445,000 reported deaths that resulted from malaria infections with 80% of casualties and cases occurring in sub-Saharan Africa and in children under 5 years old.[11] Although the general trend of malaria case incidence and mortality rates have been declining since 2010, progress appears to be stalling and in some regions have even reversed. This is a result of challenges associated with developing treatments and prevention strategies, such as the emergence of drug and insecticide resistance, as well as unstable international and domestic funding. More than ever, novel research and development needs to address issues with current therapies to prevent the spread of resistance to regions of endemic Malaria in Africa.

2.1.1. Malaria Cause and Transmission

Malaria is caused by the Apicomplexan parasite of the genus *Plasmodium*. This is a single-celled eukaryotic microorganism of which there are six species that can be transmitted to humans. These are *P. falciparum*, *P. vivax*, *P. knowlesi*, *P. ovale curtisii*, *P. ovale wallikeri* and *P. malariae*.[12] As mentioned previously, *P. falciparum* is the most dangerous as it is the most prevalent in sub-Saharan Africa and has the highest mortality and morbidity rates.

The *Plasmodium* parasite has two hosts, the female anopheles mosquito and a vertebrate host such as a human. Transmission of the parasite to the human occurs when an infected mosquito takes a blood meal (Figure 3). The parasites, in the form of sporozoites then rapidly invade hepatocytes in the liver where thousands of merozoites are formed through replication over several days.[12] Following the rupture of infected hepatocytes, these are

subsequently released into the blood stream where erythrocyte invasion occurs. This asexual blood stage forms a cycle of invasion, development through ring, trophozoite and mature schizont stages with replication to generate new merozoites, which cause erythrocytes to rupture and burst as they are released back into the blood stream, enabling continuation of the asexual cycle. It is at this stage that symptoms of malaria are apparent as the replicating intracellular merozoites cause erythrocytes to dramatically change shape, develop rigidity and lose deformability, enabling adherence to a variety of cell types. In cases of *P. falciparum* infection, symptoms can include; fever, anaemia, lactic acidosis, coma and in severe cases, death.[13]

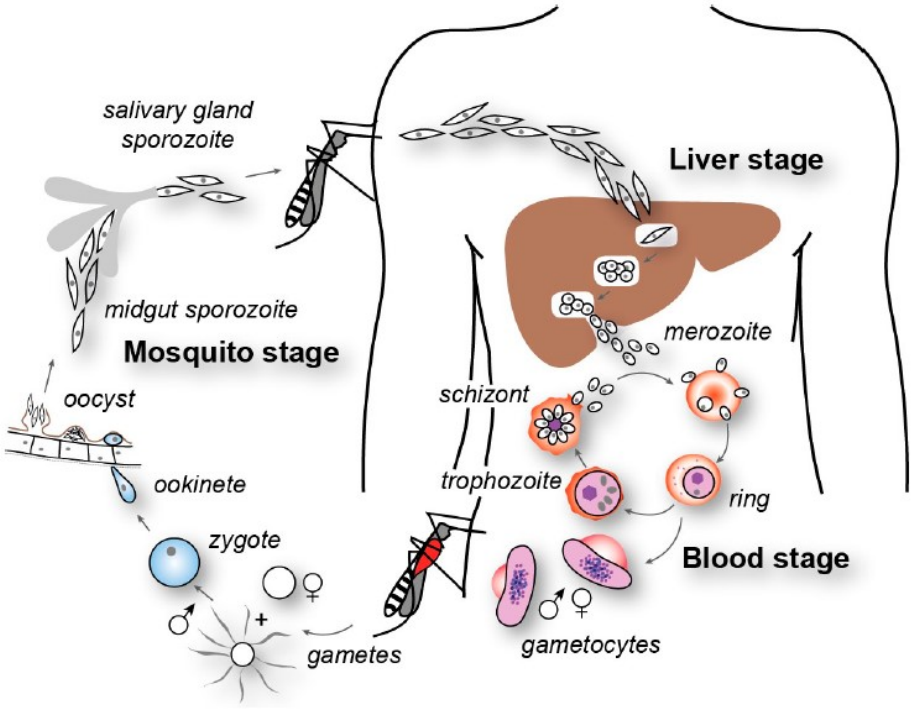


Figure 3: The lifecycle of a malaria parasite within the female anopheles mosquito and human hosts. Image taken from Cowman *et al.*[13]

During the blood stage, gametocytes (macro- and micro- gametocytes) can also develop which are the sexual forms of the parasite (Figure 3). These are passed onto another mosquito during a blood meal, where they mature to become female and male gametes in the insect gut. Fusion of the gametes leads to the generation of zygotes which develop into invasive ookinetes and translocate to the insect midgut where they become oocysts. It is

from oocysts that sporozoites are released into the salivary gland of the mosquito and infection of a vertebrate is able to occur once again during a blood meal.[12]

2.1.2. The Invasive Parasite: Merozoites

During the symptomatic intraerythrocytic stage of the *Plasmodium* parasitic cycle, merozoites exist purely for the purpose of invading red blood cells (RBCs). This is because they are unable to replicate outside of a host cell and therefore must rapidly invade erythrocytes to minimise the window of opportunity for the host immune response to eradicate them.[14] As a result, merozoites are able to invade RBCs at high speed; in less than two minutes from the moment of their release as measured by video microscopy.[15] They also employ several other defence mechanisms to hide from the host immune system, allowing enough time for invasion to occur.

Blood stage merozoites are ovoid in shape and have a typical size of 1-2 μm which make them the smallest cells within the parasitic lifecycle. They also exhibit fast directional motility of 1-10 μm/sec. Observations of the mechanism of erythrocyte invasion were first reported using video and electron microscopy studies more than thirty years ago.[16] When a merozoite first comes into contact with an erythrocyte, they associate at any point on the merozoite surface. This is followed by swift host cell deformation and merozoite reorientation so that the apical part of the merozoite cell is pointing directly into the membrane of the host cell, allowing for tight attachment (Figure 4). The parasite's apical end contains some specialised secretory organelles; rhoptries, dense granules and micronemes, which facilitate invasion following erythrocyte-merozoite engagement. These deploy their contents at the site of contact and the ligands released interact with the surface receptors of the RBC forming a tight junction. This junction then moves from the apical to the posterior end over the merozoite surface driven by an actomyosin motor which is located on the inner membrane complex (IMC) of the merozoite, described further in section 2.3.2. Invasion is accomplished when the moving tight junction reaches the posterior pole as the adhesive proteins at the

junction are proteolytically removed to enable resealing of the membrane and the creation of a parasitophorous vacuole, within which the merozoite cell is enveloped.[13,14,17]

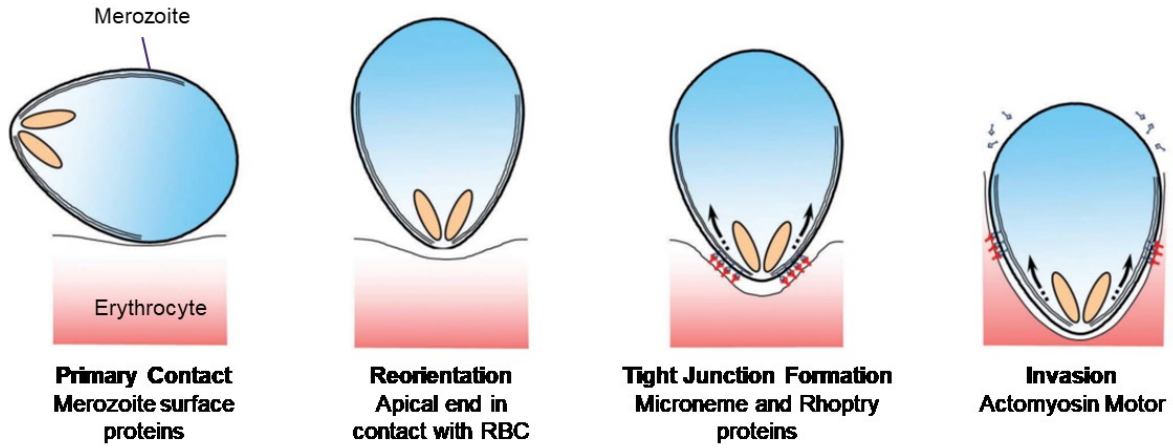


Figure 4: A cartoon to illustrate the stages of erythrocyte invasion by the *Plasmodium* merozoite. Adapted from Wright *et al.*[14]

The ability of the malaria parasite to invade red blood cells is central to disease pathogenesis as well as parasite survival. Invasion is therefore an attractive process to target as this is the only part of the life cycle that initially occurs extracellularly, thus during this short amount of time the parasite is vulnerable to the host immune system and therapeutic intervention is possible.

2.1.3. Antimalarials Past and Present

The first antimalarial agent widely used was extracted from the bark of the *Cinchona calisaya* tree in the 1600's and is known as quinine (Figure 5).[18] It is an aryl-amino alcohol alkaloid and was the first-line therapy for malaria treatment until the 1920's when it was replaced with more effective and safer alternatives.[19] It acts by destroying mature malarial schizonts present within RBCs, an action believed to be caused by accumulation of the drug in the digestive vacuole (DV) leading to inhibition of the detoxification of haem, an essential parasitic process.[20] Development of parasitic resistance to quinine has been slow due to its relatively short half-life of 8-10 hours, and therefore it is still used to treat cases of severe

malaria, and in combination with antibiotics, as a second line treatment against resistant malaria.[21]

A few derivatives of quinine have been developed over the years including chloroquine which was introduced in the late 1940's (Figure 5). It has a 4-aminoquinoline structure and was the first line malaria therapy for many years due to its high efficacy, affordability and safety profile, and is thought to cause parasite death in the same way as quinine. It has a long half-life of approximately 60 days which is likely to have contributed to the development of parasitic resistance, as the parasites are exposed to the drug for extended periods of time when the concentration has dropped below the therapeutic threshold.[21] It is now almost ineffective as an antimalarial agent and is currently used, along with chloroquine analogues, as treatment of other infectious diseases, as well as cancerous, immunological and rheumatic diseases.[22]

Other quinoline derivatives designed to replace chloroquine include; amodiaquine, mefloquine and halofantrine, developed in the United States, and lumefantrine, piperaquine and pyronaridine, developed in China.[18] Although useful for short amounts of time, all have developed parasitic resistance.

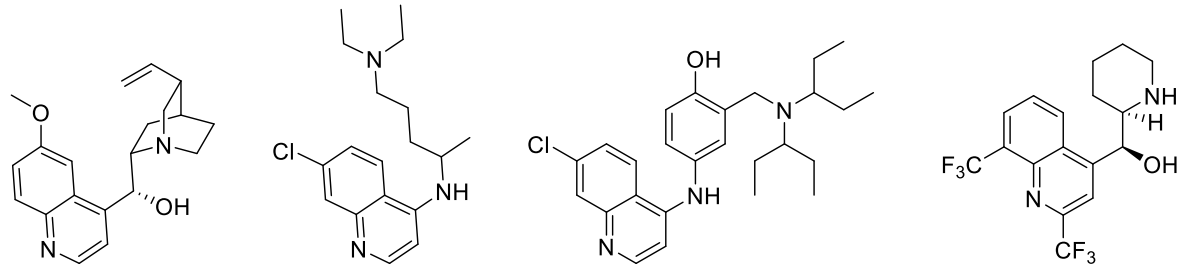
Inhibitors of *P. falciparum* dihydropteroate synthetase (*Pf*DHPS) and dihydrofolate reductase (*Pf*DHFR) have been developed to exploit the inability of parasites to salvage folate, despite the requirement of this cofactor for methylation reactions.[18] Sulfadoxine is an inhibitor of *Pf*DHPS and can be used in combination with *Pf*DHFR inhibitors such as pyrimethamine and proguanil (Figure 5). The combination of sulfadoxine-pyrimethamine was introduced as a promising antimalarial treatment in the 1970's, however resistance rapidly emerged due to point mutations in both targeted enzymes, therefore it is now mostly used as prophylactic therapy.[23]

Artemisinin, a natural product isolated from the *Artemisia annua* plant, was introduced in 1972 by Chinese scientists following the emergence of resistance to most quinoline and

antifolate drugs against *P. falciparum*. It is a sesquiterpene lactone containing an endoperoxide which is essential for antimalarial activity, and has high potency against chloroquine and sulfadoxine–pyrimethamine resistant *P. falciparum* parasites (Figure 5).[24] As a result of poor solubility, artemisinin derivatives such as Artemether and Artesunate have been developed to increase suitability for intravenous and oral administration, as well as potency. It was found that this new genre of antimalarials killed all blood stage parasites effectively, leading to the resolution of symptoms such as fever much more quickly than previously administered drugs. Moreover, they reduced transmission as gametocytes were also targeted.[25] Although the mechanism of action is not fully characterised, it is thought that the endoperoxide bond is cleaved by reduced haem iron to generate carbon radicals which can alkylate important biomolecules.[24] Following a period of dominance in antimalarial drug selection, a decrease in the efficacy of artemisinin-type drugs has been observed along the Thai-Cambodian border and is associated with their wide-spread use in Southeast Asia.

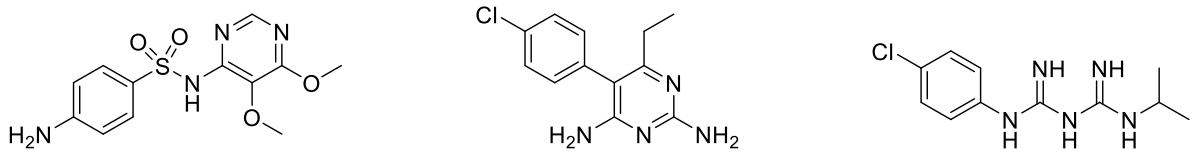
To prolong the use of artemisinin-type drugs and reduce the risk of developing resistance, they are now used in combination with at least one other type of antimalarial drug with different resistance mechanisms.[26] This is known as artemisinin-based combination therapy (ACT). Combining artemisin-type drugs which are rapidly metabolised, with drugs that have a much higher half-life also reduces the treatment time and can also increase the chance of complete parasite clearance.[27] Current combinations include artemether–lumefantrine (the most commonly used therapy to date), artesunate–sulfadoxine–pyrimethamine, artesunate–mefloquine and artesunate–amodiaquine.[21] Presently, ACT's are the first-line treatment for uncomplicated *falciparum* malaria in all regions where the disease is endemic, as recommended by the World Health Organisation (WHO).[28]

Quinoline Derivatives



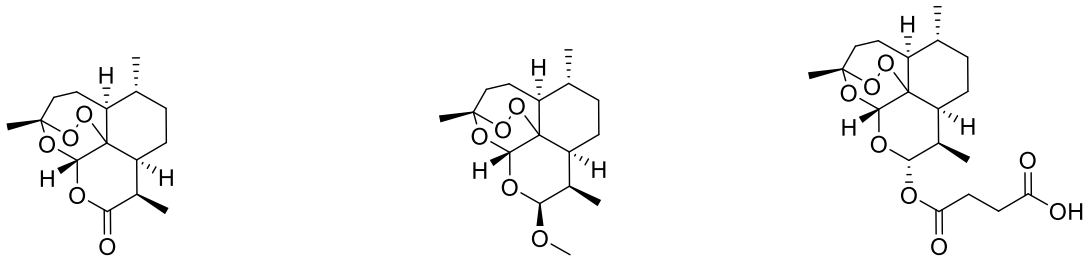
Quinine Chloroquine Amodiaquine Mefloquine

Antifolate Drugs



Sulfadoxine Pyrimethamine Proguanil

Artemisinin Derived Antimalarials



Artemisinin Artemether Artesunate

Figure 5: Common antimalarial drugs used in the last 100 years.

2.1.4. Challenges to Current Treatment

Despite several significant breakthroughs in antimalarial drug discovery over the past 100 years, emergence of parasite resistance to drugs continues to be an unyielding challenge. Artemisinin resistance was first reported in western Cambodia and has since spread to, or developed independently in mainland Southeast Asia including areas of eastern Myanmar, Thailand and southern Vietnam.[29] Although ACT's are faring better in the war against

resistance, their efficacy is beginning to wane as a result of increasing reliance on the partner drug. At some point in the future, the malarial parasites might become resistant to these as well. Alarmingly, there has now been a small number of reported cases of *P. falciparum* resistance to ACT's in Africa, where malaria is most wide spread.[30] As ACT's are the last line of defence against malaria, there has been a recent drive to identify novel targets and develop new drugs in order to prevent the spread of parasitic resistance to major endemic regions in Africa. At this time there are few promising antimalarial molecules in the pipeline as a result of inevitable drug development attrition, and those that have made it through clinical trials tend to be ACT's, highlighting the need for novel approaches.[31]

2.2. Myosin: The Muscle Motor Protein

2.2.1. Structure and Function

Myosin is part of a superfamily consisting of at least 35 classes of molecular motor proteins that are powered by adenosine triphosphate (ATP) hydrolysis.[32] They function by attaching to the cytoskeletal protein actin, and using it as a track on which they move along, generating or sensing mechanical forces, or moving cargoes.[33] Myosins are ubiquitously expressed in eukaryotic cells and are implicated in diverse cellular processes such as muscle contraction, membrane trafficking, cell locomotion, cytokinesis, and cytoskeletal structure to name a few.[34,35]

Myosins exist as monomers, dimers or oligomers and are typically made up of one or two heavy chains and a number of light chains, depending on the myosin subtype.[36] The heavy chains contain three structurally and functionally distinct domains; the head, neck and tail regions.[37] The globular head domain, otherwise known as the N-terminal motor or catalytic domain, is the most conserved of the myosin regions and contains ATP- and actin- binding sites where force and movement is generated. The α-helical neck region lies adjacent to the head domain and contains IQ motifs that are involved in light chain or calmodulin binding and are important for providing the myosin with a rigid structure and a lever arm for myosin

motion.[38] The C-terminal tail domain facilitates the globular head's task by positioning it for actin binding. Tail domains vary greatly in length and sequence between subtypes, and are thought to determine the protein specificity for actions such as cargo binding and dimerization (Figure 6).[32,37,39]

Most knowledge of structure, mechanism and properties of myosins has been obtained by studies carried out on conventional myosin II (MyoII), which is found in muscle cells and in the contractile ring of non-muscle cells.[40] All other types are known as unconventional and are grouped into different classes based on a comparison of their motor domain sequences (Figure 6). The MyoII found in muscle contains two identical heavy chains, each with a globular motor domain, and two pairs of light chains.[41] The α-helical regions of each heavy chain twist around each other forming a dimeric structure of coiled coils.

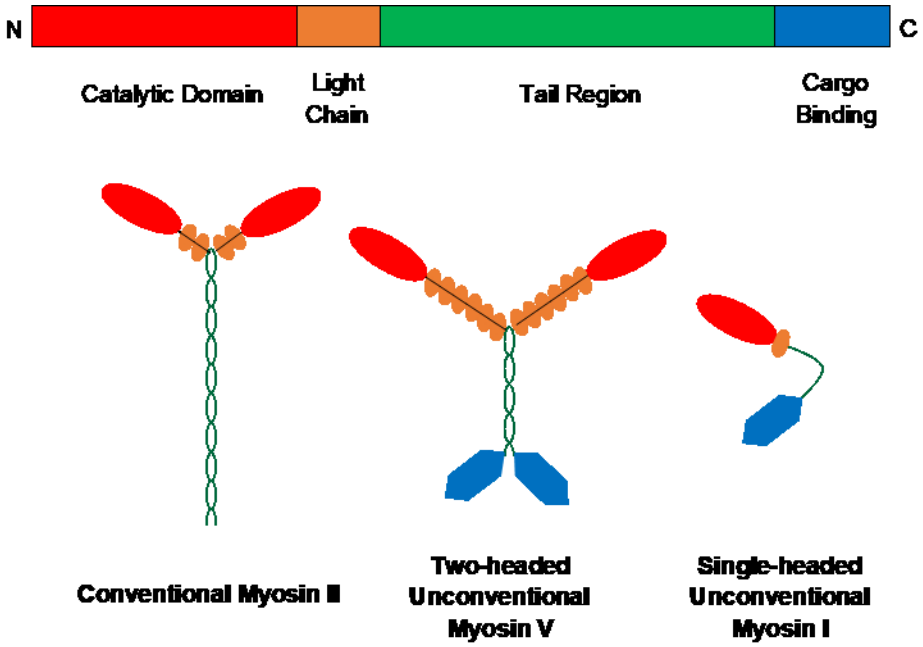


Figure 6: A representation of different myosin structures. The differences in structure are highlighted here with the comparison of the structures of conventional MyoII with double-headed unconventional myosin V and single-headed unconventional myosin I. Adapted from Kalhammer and Bähler.[42]

Skeletal muscle MyoII has been shown to generate muscle contraction through the formation of bipolar myosin filaments that glide along actin filaments of muscle cells in opposite

directions.[43] Non-muscle MyoII is involved in a wide range of fundamental roles including cytokinesis and cell migration.[34]

Within the MyoII head domain there are four subdomains; the upper 50 kDa subdomain, the lower 50 kDa subdomain, the N-terminal subdomain and the converter subdomain (Figure 7).[44] Between the upper and lower 50 kDa subdomains there is a large hydrophobic 50 kDa cleft. The actin binding site lies in the outer cleft region, while the ATP binding site is situated in the inner cleft region in between the upper 50 kDa subdomain and the N-terminal subdomain and is made up of a P-loop and switch I.[45] Interaction of binding sites is mediated by the switch II connector with the 50 kDa cleft. There is also a central β-sheet made up of seven strands which functions as a transducer region.[46]

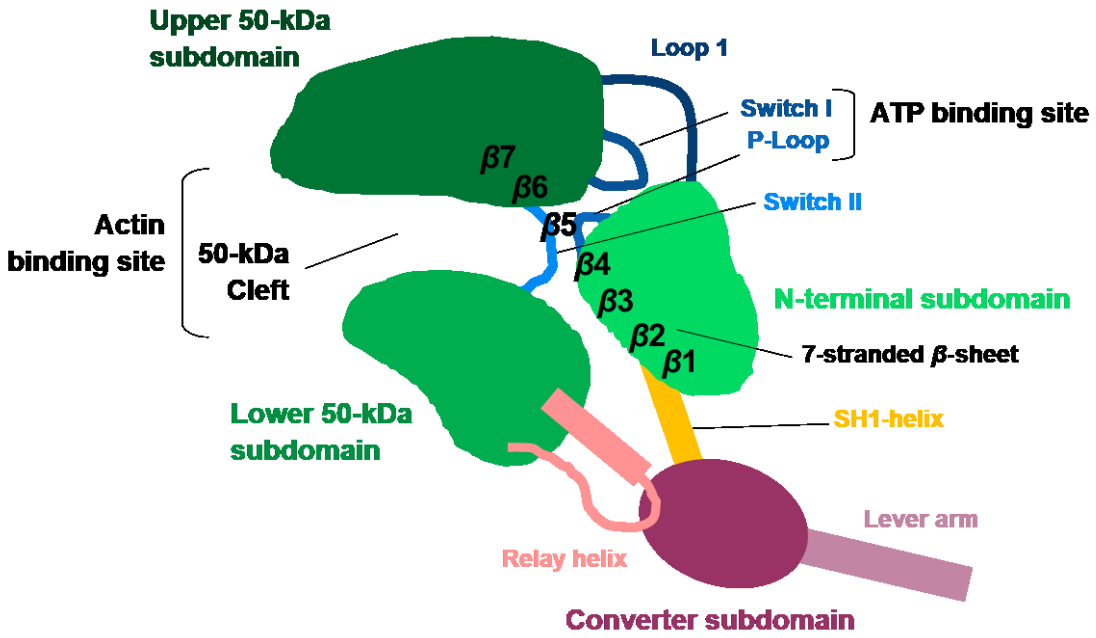


Figure 7: A schematic of the MyoII head domain. Adapted from Roman *et al*.[46]

Myosin motors convert chemical energy into mechanical energy using ATP hydrolysis. This process commences when myosin is tightly bound to actin in the actomyosin rigor state and an ATP molecule binds to it (Figure 8). This leads to a number of head domain conformational changes triggered by the γ-phosphate group of the ATP interacting with the P-loop of the ATP-binding site.[44] The P-loop and switch I enclose the molecule of ATP

causing the β-sheet to twist and open the 50 kDa cleft where actin is bound. This leads to decreased actin affinity and therefore dissociation of actin.[33] Switch II then closes to allow hydrolysis of ATP while the converter subdomain rotates and the relay helix bends, priming the lever arm. The products of ATP hydrolysis, adenosine diphosphate (ADP) and inorganic phosphate (Pi) bind to myosin and form a stable myosin-ADP-Pi intermediate in a conformation known as the pre-power stroke (PPS) state. The cleft then closes, enabling strong re-binding of the myosin head with the actin filament in a new position, which causes the release of Pi. Transmission of rearrangements within the motor domain to the lever arm occurs via the converter subdomain leading to a lever arm swing known as the power stroke, during which the myosin head pulls the actin approximately 5-10 nm.[41] Following this, ADP dissociates leaving myosin in its original rigor state conformation, primed for the cycle to start again.

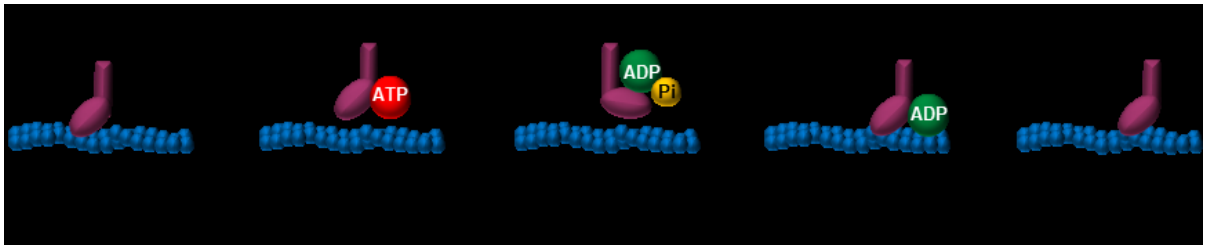


Figure 8: The stepwise process of myosin-mediated conversion of chemical energy into mechanical energy. Adapted from Bond *et al*.[34]

While conventional MyoII plays important roles in muscle contraction, cytokinesis and cell migration, unconventional myosins are involved in a variety of cellular processes including intracellular transport, anchoring, actin organisation, cell motility and adhesion as well as plasma membrane tension sensing.[40] As a result, the superfamily of myosins is implicated in a number of medical conditions including familial hypertrophic cardiomyopathy, liver fibrosis, cancer metastasis, deafness and malaria.[32,47]

2.2.2. Inhibitors of Myosin

Over the years, considerable effort has gone towards the discovery of small molecules that inhibit myosins broadly and specifically. Despite this, there is still only a small number that have been developed and very few provide the specificity required for practical use.[34] This may be due in part to the highly conserved nature of the myosin active site, which makes it an impractical target. As a result, allosteric sites that influence motor activity have been exploited, as they are much less well conserved.[45] So far, four non-overlapping myosin allosteric sites have been identified and targeted modulators have been designed that are specific to small groups of myosins. These small molecules have served as valuable tools for the investigation of complex cellular mechanisms and can provide starting points for the development of drugs that target motor proteins.

Most myosin inhibitors have been developed to target MyoII and include; (*S*)-Blebbistatin (Bleb), a reversible inhibitor of skeletal and non-muscle MyoII, *N*-benzyl-*p*-toluene sulfonamide (BTS), a non-competitive inhibitor of fast-twitch and skeletal MyoII, and 2,3-butanedione monoxime (BDM), a low affinity inhibitor of skeletal MyoII with a wide range of off-target effects (Figure 9A).[32,48,49] All of these function by blocking the release of Pi (Figure 9B), thereby preventing the power stroke necessary for energy production. BTS also impedes ADP disassociation following the power stroke.

Inhibitors of unconventional myosins have also been discovered such as Pentachloropseudilin (PClP) and Pentabromopseudilin (PBP), which are highly halogenated antibiotics that inhibit myosin I and myosin V respectively. PClP reduces the affinity of actin for the nucleotide binding site, while PBP has a more global effect on ATPase activity.[50] MyoVin-I is another myosin V (MyoV) inhibitor with a pyrazolopyrimidine scaffold, designed based on known kinase inhibitors. It is relatively selective for myosin V and functions by hindering the release of ADP.[51] Myosin VI is inhibited by halogenated phenols such as 2,4,6-

triiodophenol (TIP), and although the mechanism of ATPase inhibition is yet to be elucidated, it reduces the motor activity and is reasonably selective for myosin VI.[52]

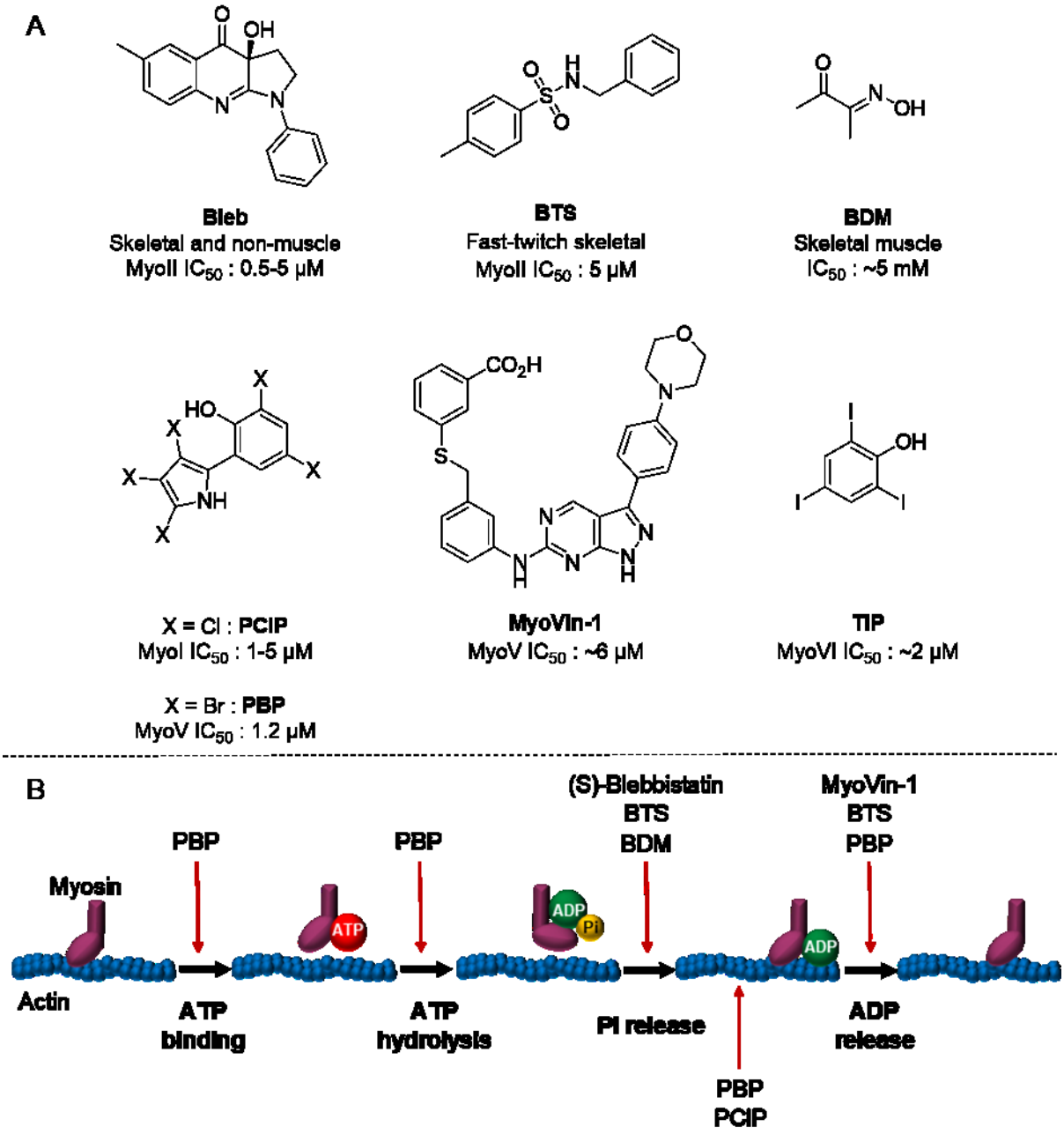


Figure 9A: The structures of myosin inhibitors and their activity for specific myosins given as IC_{50} values;[32,48–52] **B**: Inhibitors of myosin interrupt the motor activity by blocking different mechanisms of the ATPase cycle. Adapted from Bond *et al*.[34]

2.2.3. (*S*)-Blebbistatin

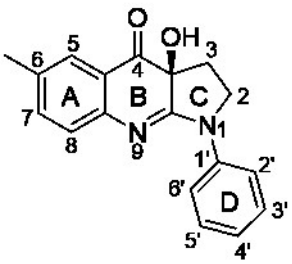
Of the myosin inhibitors described above, Bleb is the best characterised and is widely used due to its selectivity for MyoII. It has been indispensable for the dissection of MyoII actions with respect to associated diseases, and for studying cellular events that MyoII is at the centre of. As a derivative of 1-phenyl-2-pyrrolidinone (Figure 10A), Bleb is a highly cell permeable and moderately potent inhibitor of human and other mammalian skeletal muscle and non-muscle MyoII isoforms, but shows no activity towards smooth muscle MyoII or class I, V or X myosins (Figure 10B).[53,54] It was discovered during a HTS in search of a non-muscle MyoII inhibitors carried out by Cheung *et al*. in 2001.[55]

Bleb derives its inhibitory effect from the hindrance of a critical step in the ATPase cycle.[34] The mechanism of inhibition has been studied using kinetic and structural investigations including blind docking molecular simulations. From these studies Bleb has been shown to inhibit MyoII in an uncompetitive, reversible manner, binding to a hydrophobic pocket near the apex of the 50 kDa cleft, close to the ATP binding site.[32] Bleb binds to the myosin-ADP-Pi complex while the cleft is partially closed thus preventing the following force-producing Pi release responsible for the power stroke.

The co-crystal structure of Bleb bound to the MgADP–vanadate complex of MyoII in *Dictyostelium discoideum* (*Dd*MyoII) was resolved by Allingham *et al*.[32] The orthovanadate ion was used to trap the ADP complex of the myosin head in its metastable PPS state as it mimics the Pi group due to its similar size, charge and adopted conformation.[56] The structure reveals that binding of Bleb is mostly stabilised through hydrophobic interactions with the aromatic ring system, and also the presence of hydrogen bonding between the hydrogen of the main chain amine of Gly240, the carboxylate oxygen of Leu262 and the hydroxyl group of the inhibitor (Figure 10C).[32,57] Bleb also inhibits MyoII in an actin-detached state preventing actomyosin cross-linking, enabling cellular function studies of cytoplasmic MyoII.[53]

(*S*)-Blebbistain is the active enantiomer with a 50% inhibition concentration (IC_{50}) of 4.9 μM measured in *Dd*MyoII while the (*R*)-enantiomer is completely inactive. This can be explained by the presence of the directional hydrogen bonds from the OH group present at the chiral carbon to the carboxylate oxygen of Leu262 and the amine hydrogen of Gly240. The (R)-enantiomer is unlikely to generate these interactions therefore lower activity is expected.[55]

A



B

Myosin	IC_{50} (μM)
DD II	4.9
Non-muscle IIB	1.8
Skeletal II	0.5
Smooth II	79.6
IB	>150

C

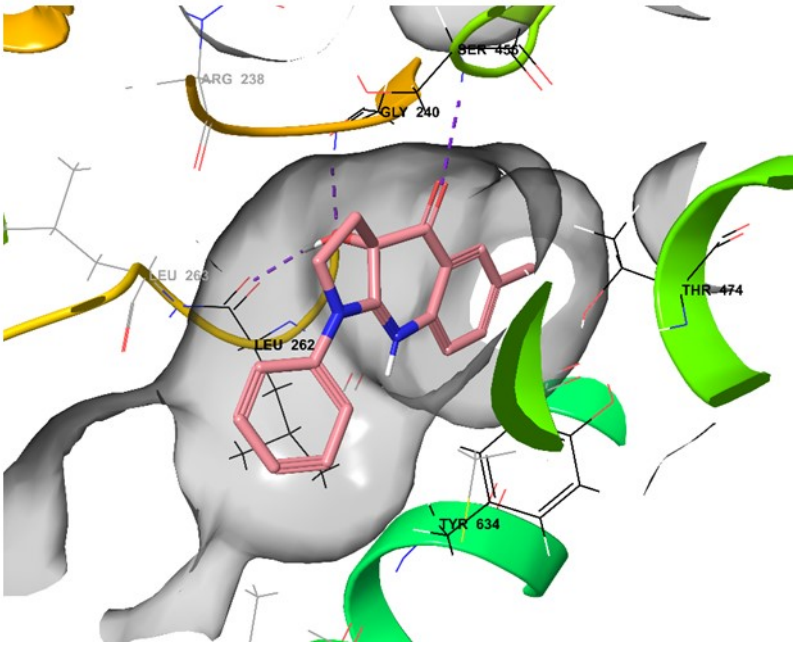


Figure 10A: The structure of Bleb with rings A-D; **B**: The level of inhibition shown for various myosin isoforms; **C**: The co-crystal structure of Bleb (pink) bound to the MgADP–vanadate complex of *Dd*MyoII (PDB accession code 1YV3). Grey shaded area represents Blebbistatin binding cavity and H-bonding interactions to residues are shown with purple dotted lines.

2.2.4. Limitations and Derivatives of (*S*)-Blebbistatin

There are some limitations to the use of Bleb which have prevented its use as a tool for *in vivo* model studies in a therapeutic context. A major restriction is its relatively low activity, which is in the micromolar range, coupled with the lack of selectivity between MyoII isoforms. Additionally, prolonged exposure to wavelengths below 490 nm (blue light) leads to a loss of MyoII activity due to compound degradation, and an irreversible cytotoxic effect on cells of various origins such as HeLa, human blood monocytes and rat cardiac myocytes to name a few.[58,59] Since the degradation is reliant on water mediated initiation, it has been

hypothesised that irradiation of Bleb with blue light in aqueous media may produce peroxy or hydroxyl radicals that induce oxidative degradation. This is problematic as light at this wavelength is commonly used in the excitation of green fluorescent labelling protein (GFP) during fluorescence microscopy, hence this photosensitivity and phototoxicity could have major implications in the experiments used to probe myosin II function, especially in microscopic imaging.[59]

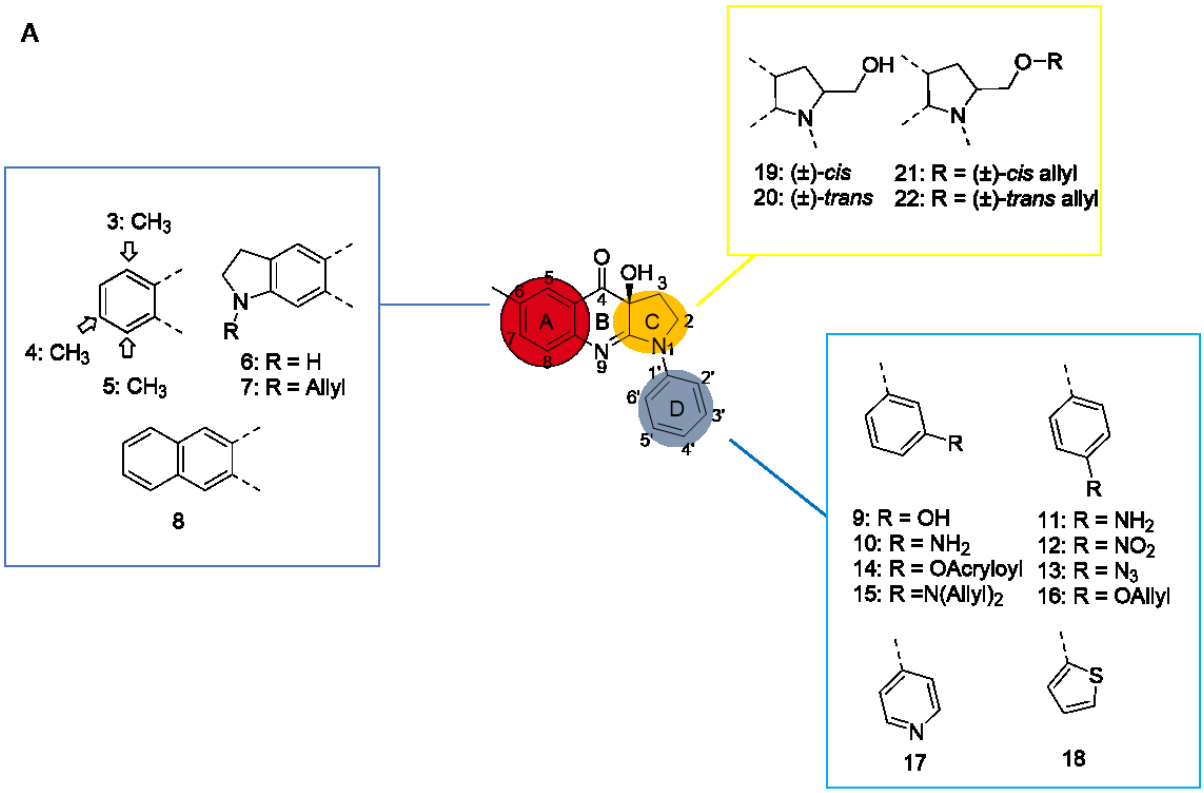
Furthermore, Bleb has been shown to interfere with fluorescent signals. This is caused by poor aqueous solubility which can cause precipitation of Bleb in aqueous media leading to fluorescence hotspots. This makes the use of fluorescent labelling proteins such as GFP even more challenging. Precipitation at concentrations above 10 μM can occur during cellular experiments which render the results meaningless due to ambiguous treatment concentrations.[60]

To overcome these drawbacks, many research groups have investigated derivatives of Bleb. Modification of the A-ring was carried out by Lucas-Lopez *et al*. in which the methyl group was moved to different carbon atoms to explore toleration of the group in different positions (Figure 11 compounds **3**-**5**).[57] In general the change in potency was negligible for these changes, with the exception of compound **5** for which the activity was markedly reduced. In an attempt to increase the potency towards MyoII, the A-ring was also extended from C6 and C7 with rings such as indoline (**6** and **7**) and benzene (**8**) to enhance interactions with hydrophobic residues observed in this part of the binding pocket. These only had negative effects on the ATPase inhibitory potency, suggesting that modification of the A-ring had limited potential for increasing activity.[61]

More success was achieved with analogues that incorporated alterations to the D-ring. Most changes were implemented on the 3'- and 4'-positions due to observation of the 1YV3 co-crystal structure indicating available space for extension at these positions. Improvements to both potency and solubility were achieved with the introduction of polar groups to either position, with (*S*)-3′-hydroxyblebbistatin (**9**), (*S*)-3′-aminoblebbistatin (**10**) and (*S*)-4′-

aminoblebbistatin (**11**) performing the best (Figure 11).[60,62] As a result, these compounds are suitable for assays in which fluorescence interference would be problematic, as at high concentrations, they do not precipitate.

A



B

Compound	MyoII Activity	Compound	MyoII Activity
3	88%[a]	**13**	5.2 ± 0.3 µM[c]
4	90%[a]	**14**	57.6 ± 7.8 µM[b]
5	35%[a]	**15**	>10.8 µM[b]
6	14.5 ± 2.2 µM[b]	**16**	9.41 ± 1.83 µM[b]
7	8.46 ± 1.22 µM[b]	**17**	ND
8	7.97 ± 0.02 µM[b]	**18**	ND
9	19.3 ± 0.5 µM[b]	**19**	>100 µM[b]
10	14.1 ± 0.1 µM[b]	**20**	~75 µM[b]
11	1.0-5.4 µM[b]	**21+22**	>100 µM[b]
12	0.40 µM[b]	**(dr 16 : 84)**	

Figure 11A: A summary of the modifications made to Bleb, with variations on the A, C and D rings; **B**: MyoII activity of Bleb derivatives. [a] Percentage inhibition of *DD*MyoII measured at 50 µM.[57] [b] IC_{50} measured in rabbit skeletal muscle MyoII. [c] IC_{50} measured in *DD*MyoII. [d] Compound precipitation observed at concentrations higher than 10.8 µM. ND : Not determined, dr: diastereomeric excess.[58,60–64]

(*S*)-4′-aminoblebbistatin (**11**) and (*S*)-4′-nitroblebbistatin (**12**) have also been shown to reduce the cytotoxic effect on cells while producing the same MyoII activity as Bleb, therefore they can be used as valid alternatives in cell-based experiments. The addition of electron-withdrawing groups to the D-ring increases the stability of Blebbistatin towards blue light irradiation, with (*S*)-4′-nitroblebbistatin (**12**) providing the greatest stability.[58] Furthermore, irreversible photoreactive covalent inhibitors of MyoII have been developed to enable the complete inhibition of MyoII driven cellular processes, a task unfulfilled by Bleb due to low aqueous solubility. (*S*)-4′-azidoblebbistatin (**13**) was completely covalently bound to *DD*MyoII at low concentration (10 μM) using multiple cycles of compound addition and irradiation.[65]

Several analogues have also been synthesised by Lawson *et al*. that incorporate heterocycles in the place of the phenyl ring such as pyridine (**17**) and thiophene (**18**), although their inhibitory properties against MyoII ATPase have not been measured.[63] Most recently Roman *et al*. have made modifications to the C-ring in order to introduce an extra H-bond interaction with the binding pocket, and to fully occupy the space.[64] A small set of derivatives extending from the C-2 position were synthesised (**19**-**22**), however for all, the MyoII ATPase inhibitory potency was generally lower than for Bleb (Figure 11).

Despite the large body of work carried out exploring the structure of Bleb, MyoII ATPase inhibitory potency and selectivity among MyoII isoforms remain significant challenges and for this reason Bleb and its analogues are unsuitable to be used as therapeutic tools.

2.3. *Plasmodium Falciparum* Myosin A

2.3.1. Parasite Invasion

Actomyosin motors are important for apicomplexan parasite migration through tissue and invasion of vertebrate host cells. Due to the small size of the parasites, they are not able to use common movement-generating organelles such as cilia or flagella, therefore they must continually crawl along the surface of a host cell as they burrow into cells and tissues.[66] For some stages of the lifecycle, gliding motility, a novel form of locomotion is employed that largely depends on an actomyosin motor. This form of motion has been observed in liver stage sporozoites but not in blood stage merozoites, for which the mechanism for generating motility has not been fully elucidated.[67] However, studies have shown that in the absence of gliding motility, merozoite erythrocyte invasion still relies on actomyosin as part of a multiprotein motor complex which is present in all modes of cell motility and invasion across the phylum.[67]

MyoA is one of six Class XIV myosins which are unique to apicomplexans, including *P. falciparum* termed myosin A-F (*Pf*MyoA-F).[68] *Pf*MyoA is the most studied *Plasmodium* myosin due to its homology with the well characterised MyoA of *Toxoplasma Gondii (TG*MyoA), while the remaining 5 are still relatively unexplored. There is a growing interest in *Pf*MyoA as it has been found at the core of the motor complex shown to drive motility and invasion of the *P. falciparum* parasite.[69]

A report by Ménard has shown that actomyosin is important for the invasion and motility of *P. berghei* merozoites and liver stage *P. falciparum* sporozoites, which can be inhibited by actin-filament-disrupting compound Cytochalasin D (CytoD).[70] This finding is corroborated by evidence that myosin ATPase inhibitor BDM inhibits *in vivo* invasion of RBCs by merozoites or schizonts.[71] In addition, the expression of *Pf*MyoA within the erythrocytic cycle is stage specific, with expression observed in mature schizonts just prior to invasion and in merozoites, however it disappears soon after invasion. Using immuno-gold electron

microscopy, Pinder *et al.* were also able to show that *Pf*MyoA is located at the periphery of merozoites within, and liberated from, schizonts. Higher concentrations were found in the area surrounding the apical prominence, which is where the parasite forms a tight junction with the host cell following reorientation, however it was absent from the apical prominence itself. Due to the invasion specific expression and localisation at the functionally invasive apical region of the merozoite, this strongly suggests that *Pf*MyoA is involved in erythrocyte invasion.[71]

Furthermore, conditional knock-out of *Pf*MyoA has recently been shown by our collaborators at Imperial College to almost completely block invasion at a level comparable to CytoD (Figure 12, unpublished work from the Baum group). The conditional knock-out was achieved using a procedure based on the Cre/lox system,[72] modified for use on organisms with few and short introns such as *P. falciparium*.[73] It involved introduction of a loxPint (LP) module into a short intron to form a point of intragenic recombineering which was used to conditionally introduce point mutations.

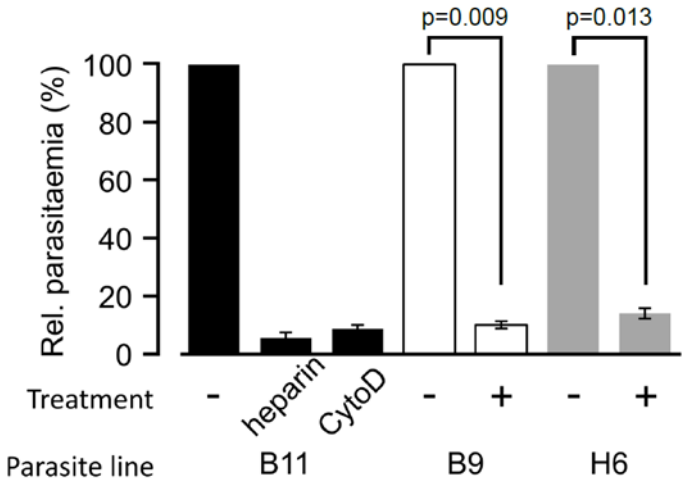


Figure 12: Treatment of schizonts from tagged myosin line (*Pf*MyoA-LP) clones B9 and H6 with rapamycin (+) leads an almost complete block of invasion in the next cycle compared to DMSO control (-). Invasion inhibition observed using heparin or CytoD controls was observed to be greater still. Data was taken as an average of two biological replicates, each with three technical replicates, ± S.D. of biological replicates. Significance evaluated using parametric t-test (paired, two-tailed) (unpublished data by Tom Blake from the Baum group).

This enabled generation of *Pf*MyoA clones (*Pf*MyoA-LP), B9 and H6 of the *P.falciparum* strain B11, a parasite line which steadily expresses a rapamycin-inducible DiCre recombinase. Addition of rapamycin leads to conditional truncation and therefore knock-out of *Pf*MyoA. The ability of the parasites to invade RBCs was significantly impaired when *Pf*MyoA was knocked out, compared to the DMSO control, and the results were akin to the parent parasite line B11 when treated with CytoD and ATPase inhibitor heparin.

2.3.2. The *Pf*MyoA Motor Complex

Due to the conservation of the myosin motor head domain, ATP hydrolysis and the subsequent power stroke of *Pf*MyoA generate directional motion in the same manner as described previously for conventional myosins, propelling itself along actin filaments in a rearward direction. It has been shown using transient kinetic experiments on *TG*MyoA that ATP causes dissociation of MyoA from actin rapidly, and ADP binds to MyoA with low affinity suggesting that the ADP is expelled by MyoA quickly and therefore, this is a fast myosin motor.[74] *Pf*MyoA has also been shown to generate a short-lived power stroke of 5 nm towards the barbed (plus) end of actin filaments.[75]

In the most commonly accepted model, single-headed *Pf*MyoA is attached to the IMC just under the parasite plasma membrane via a number of accessory proteins (Figure 13). The IMC is a flattened membrane structure that maintains the structural integrity of the parasite and is involved in invasion and egress in and out of host cells.[76] Like other myosins, *Pf*MyoA contains a catalytic motor domain which binds MgATP and actin, and a neck region containing two degenerate IQ motifs that bind two light chains and acts as a lever arm, however it has no tail region.[69] The first discovered light chain was myosin tail interacting protein (MTIP), named as such due to its ability to act as the myosin tail, enabling anchoring to glide associated proteins (GAPs) 45 and 50 which are integral membrane proteins within the IMC. The second light chain is known as the essential-type light chain (*Pf*ELC) that requires the presence of MTIP to bind to the heavy chain and is necessary for *Pf*MyoA to

move actin at the greatest velocity, akin to skeletal muscle myosin (~3.8 μm/s measured *in vitro*)[69].

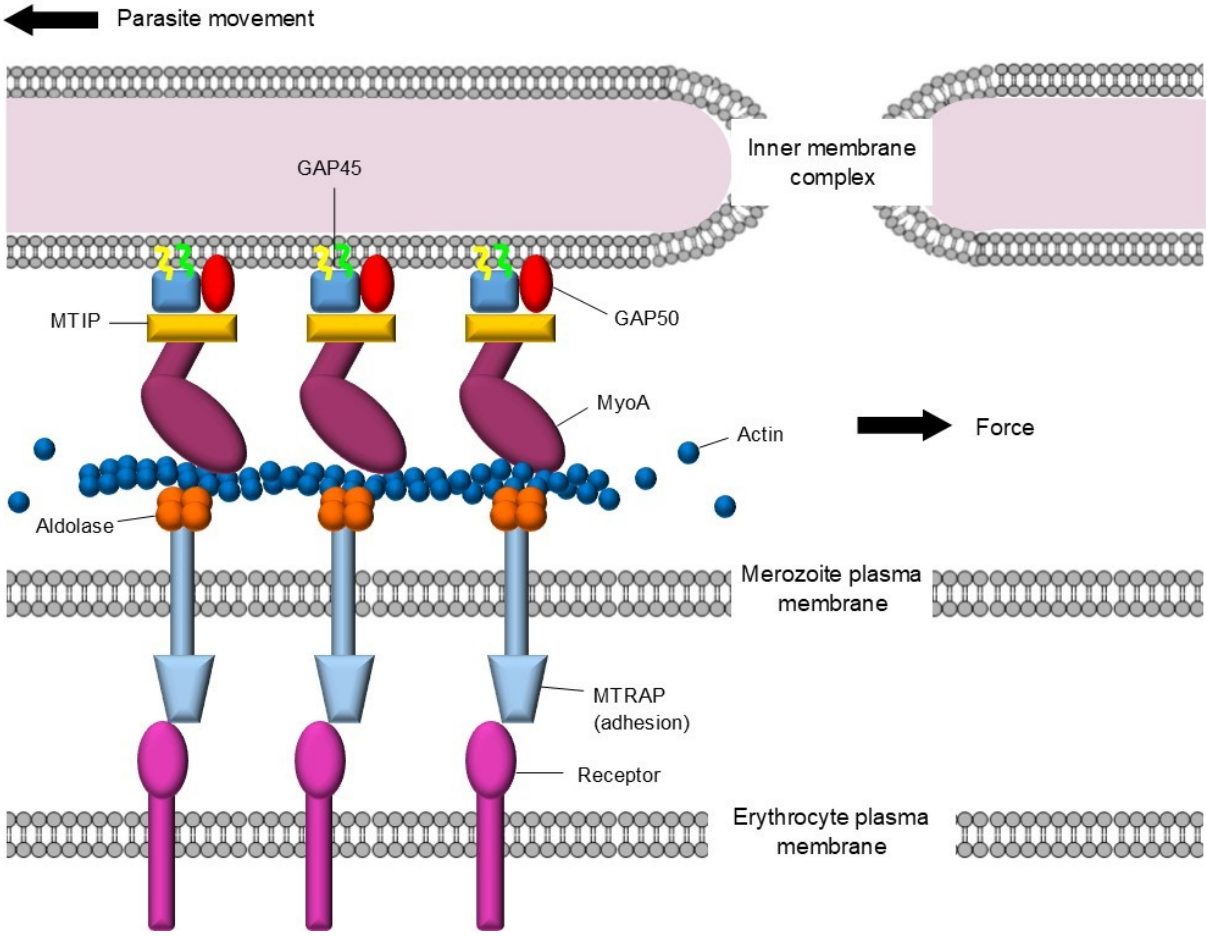


Figure 13: Proposed organisation of the actomyosin motor complex in a merozoite. Adapted from Thomas *et al*.[77]

Although the precise mechanism for actomyosin mediated invasion of erythrocytes by parasites has not been fully defined, it is thought that the micronemes on the apical region of the merozoite, (as described in section 2.1.2.) through stimulation by host cell interaction, release extracellular adhesive proteins including those from the thrombospondin-related anonymous protein (TRAP) family which are responsible for host cell recognition and attachment.[67] These proteins are bound via cytoplasmic tails to short filaments of actin within the motor complex by an actin binding protein, aldolase. When released, TRAPs are translocated in a rearward direction, by the myosin motor, propelling the parasite forward

and driving the movement of the merozoite tight junction that is essential for invasion into the host cell (Figure 13).[14,78]

The motor complex of the *P. falciparum* parasite is closely associated with motility and host cell invasion, both of which are essential for parasite survival and are central to malaria pathogenesis. *Pf*MyoA is postulated to provide the power, in conjunction with actin, that drives the motor complex and has been shown to be indispensable for the function of invasion in the presence of non-specific actin or myosin inhibitors, as well as during conditional *Pf*MyoA knockdown experiments. As novel drugs are urgently required to ease the significant health burden in regions of endemic malaria, *Pf*MyoA is an attractive target for a drug discovery programme as well as for developing a tool to further elucidate its role in host cell invasion.

2.4. (*S*)-Blebbistatin and *Plasmodium Falciparum* Invasion

An investigation into the erythrocytic contribution to the merozoite invasion mechanism was carried out by Zuccala *et al*. in 2015.[47] To determine whether host actin filament dynamics play a significant role in merozoite entry, a series of invasion assays were carried out using actin-filament-disrupting compound CytoD. Broad ATPase inhibitor BDM and more specific MyoII inhibitor Bleb were also used to investigate whether an erythrocyte myosin is involved in this process. Prior to the invasion process, either erythrocytes or merozoites were pre-treated with the desired inhibitor and erythrocytes were washed before merozoite addition. No invasion inhibition was observed for pre-treated erythrocytes, potentially indicating that the host actin filaments or myosin are not involved in the invasion by parasites. However, invasion was strongly inhibited when merozoites were pre-treated with CytoD and BDM. In contrast, pre-treatment of merozoites with Blebbistatin did not have any effect on parasite invasion.[47] As a result of this and observations of *Pf*MyoA dependent invasion as shown in previous conditional knock-out experiments (Figure 12), it was postulated that the MyoII inhibitor, Blebbistatin, does not inhibit *Pf*MyoA.

*Pf*MyoA is present at almost every stage of the malaria parasite's development cycle, both in the human host and the mosquito vector, therefore generation of *Pf*MyoA sensitive inhibitors would aim to prevent the parasite progression and avert onward transmission. Due to the high divergence of the class XIV *plasmodium* myosins from mammalian myosins, compounds that are structurally resolved in their mode of action could be chemically tailored to make them specific to the class XIV myosin motor of the malaria parasite. Given the breadth of structural knowledge available on the binding mode of Bleb in MyoII and its mechanism of inhibition, this previously unsuccessful molecule could be exploited for the development of derivatives sensitive and selective for *Pf*MyoA over MyoII.

2.5. Project Aims

*Pf*MyoA is an essential motor that powers parasite invasion of erythrocytes, a process responsible for symptomatic malaria. Therefore, the focus of this project will be the design and synthesis of *Pf*MyoA inhibitors. As the structure of *Pf*MyoA has not yet been resolved, target repurposing will be employed, exploiting the information available on the structure of conventional MyoII. A homology model of *Pf*MyoA will be developed based on the co-crystal structure of MyoII bound to Bleb to facilitate rational, structure-based drug design. As a well characterised inhibitor of MyoII, the chemical scaffold of Bleb is suggested to be inactive towards *Pf*MyoA. Hence, an investigation to identify the key interactions that govern resistance to this drug will be carried out *in silico* and modifications will be made to the structure to optimise the selective inhibitory activity towards *Pf*MyoA. Once an *in vitro* *Pf*MyoA activity assay has been developed, Bleb and the derivatives will be tested for *Pf*MyoA activity, as well as for *ex vivo* effects on parasite invasion of erythrocytes. This will aim to validate the hypothesis of Bleb inactivity in *Pf*MyoA and to validate the homology model. If successful, these derivatives will be used to probe *P. falciparum* actomyosin motor function within the process of blood stage invasion. Moreover, optimisation of their pharmacokinetic properties could lead to their development as novel therapeutics for the treatment of malaria.

3. Results and Discussion

3.1. Part 1: Development of a Homology Model

3.1.1. Structure Based Drug Design

Structure based drug design is an approach utilized to enable rational drug design using the 3D structure of a protein. Knowledge of the protein structure is important for understanding the specific function and the effect of small molecules on the active site. In the context of drug discovery, once a target protein has been identified, if structural information is available it can be used to identify and optimise interactions between the protein and ligands using computational methodologies.

Protein Structure Determination

There are various methods for obtaining information on the structure of proteins, some of the most notable are; X-ray crystallography, nuclear magnetic resonance (NMR) and electron cryo-microscopy (cryoEM).[79] The most prevalently used method for protein structure determination in drug discovery is X-ray crystallography as structures are often available at high resolution and can be used to identify protein structures of varying sizes. Crystal structures obtained with resolution of 2.5 Å or lower are generally deemed acceptable for use in a drug design programme as this indicates that there is a high level of detail in the diffraction pattern and electron density map, allowing for each atom to be visible.

The number of reported protein sequences with medical relevance far exceed the number of experimentally determined structures available from the Protein Data Bank (PDB) (international repository for 3D structure files) as all experimental methods have limitations. For example, the growth of X-ray quality crystals for X-ray crystallography is paramount for determining the crystal structure, and this is a very difficult technique which, for some proteins is not possible. Moreover, the use of protein NMR is restricted to relatively small proteins (<40 kDa) therefore there is a major limitation to its power of protein structure determination. In general, it also takes a long time to generate meaningful data and most

techniques involve the use of expensive equipment. For these reasons, experimental methods have been supplemented with computational ones.

Homology Modelling

Homology modelling is a useful tool for predicting, to a reasonable degree of accuracy, the protein structure of a "target" protein. This method exploits the fact that the tertiary structure of a protein is more conserved than its amino acid sequence.[80] Therefore, 3D structures of closely related homologous proteins can be used as templates to model proteins with unknown tertiary structure. An alignment of the target protein sequence with the template sequence enables the target residues to be mapped onto the known structure, producing a model of the "target".[81] If the aligned protein sequences have a sequence identity of 30% or more then this is usually considered enough homology between the two sequences to generate a model with a reasonable degree of confidence.

Identification of Target site and Docking

Once structural information has been attained, the binding site of the ligand of interest must be identified. This is usually a hydrophobic pocket with available potential hydrogen bond acceptors and donors, and it may correspond to the active site of the protein, a site at which the ligand interacts with another macromolecule, or a region important for the protein mechanism.[79] A useful tool for identifying the location of a ligand binding site is to co-crystalize the target protein with a known small molecule inhibitor. This can also be a valuable tool when preparing a homology model, as the binding site in a template protein can often be a good estimation of the binding site in the target structure.

With the target structure modelled and the estimated binding site located, computer-aided methods referred to as "docking" can be employed to identify small molecules that will bind effectively in that pocket and hopefully improve potency. This can be accomplished by taking

molecules that are known to bind in the target site and modifying the structure to maximise the interactions between the two. Another method is the use of virtual screening in which a database of small molecules is docked *in silico* into the target binding site and the outcomes are scored based on the acquired interactions. Finally, *de novo* generation of molecules can be used in which fragments such as benzene rings, amides and carbonyl groups are docked into the target site individually. They are then scored based on their interaction with the target site and the best fragments are linked together to generate whole molecules.[79]

It must be kept in mind that all computer-generated results are the sum of a number of approximations and assumptions, therefore should only be used as a guide in medicinal chemistry. All compounds of interest identified from these computational methods should be tested experimentally in biochemical assays to prove that the theoretical models can effectively predict experimental outcome.

3.1.2. Generation of a *Pf*MyoA Homology Model

As the crystal structure of *Pf*MyoA was unavailable, a homology model was required. To that aim the known 3D structure of *DD*MyoII was used as a template, to generate a hypothesis as to why the MyoII inhibitor, Bleb, which binds to *DD*MyoII with an IC_{50} of 4.9 μM, appears to be inactive towards *Pf*MyoA. With knowledge of the predicted structure, Bleb could be redesigned to generate *Pf*MyoA sensitive inhibitors for biochemical and *ex vivo* parasite invasion experiments.

All computational work was carried out in collaboration with postdoctoral associate Dr Sandeep Sundriyal using Schrödinger's Maestro modelling interface.[82] The structure of Bleb bound to the MgADP–vanadate complex of *DD*MyoII (Figure 10C) was available from the PDB (accession code 1YV3) with high resolution of 2 Å. The amino acid sequence of the MyoII heavy chain was aligned with the sequence of *Pf*MyoA (Uniprot, PF3D7_1342600) using Clustal Omega revealing reasonable sequence identity of 32 % (Figure 15). Although

this number is on the low side of the homology model viability threshold, we believed this was high enough for it to provide some insight into the structure of *Pf*MyoA.

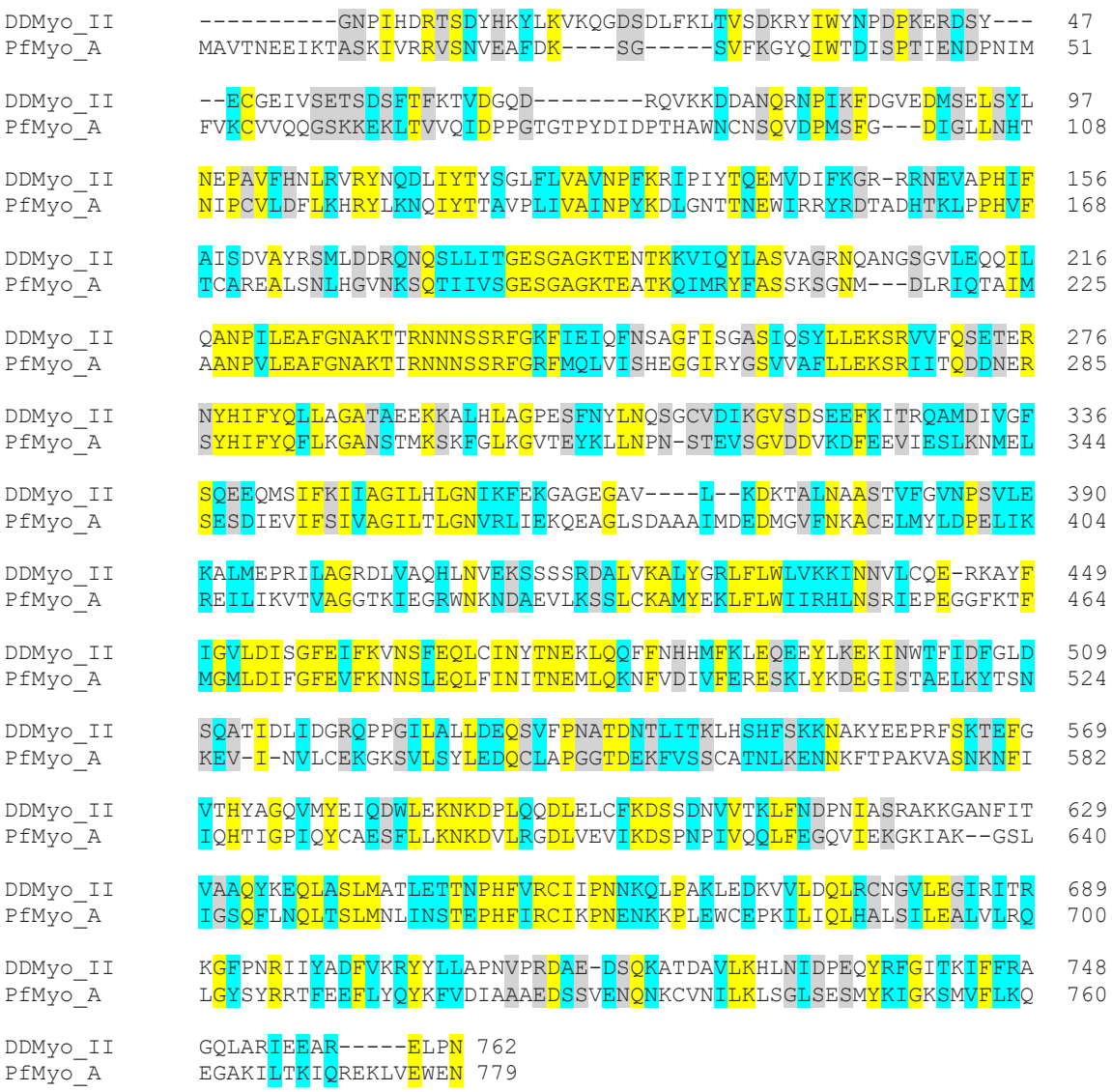


Figure 15: Sequence alignment of template *DD*MyoII (1YV3) and *Pf*MyoA using Clustal Omega.[83] Residues highlighted in yellow indicate a position of residue conservation; Residues highlighted in cyan indicate strong similarity between residues (scoring > 0.5 in the Gonnet PAM 250 matrix); Residues highlighted in grey indicate weak similarity between residues (scoring =< 0.5 in the Gonnet PAM 250 matrix).

Two protein modelling programmes were used to generate homology models; Phyre2 (Protein Homology Recognition Engine V 2.0)[84] and SWISS-MODEL (SM)[85], both of which are fully automated protein structure homology-modelling servers. The docking programme Glide (Grid-based Ligand Docking with Energetics)[86] was then used to generate a receptor

grid (binding site) for each model based on the site at which Bleb is bound in *DD*MyoII. Docking simulations were carried out in flexible docking mode using Glide, which allows for fast ligand docking using a search method that identifies the best-scoring binding pose for a given ligand. This is carried out over a number of hierarchical phases; the first roughly assesses the spatial fit of a ligand in the binding site defined by the grid, and the poses that pass this phase are then evaluated using a flexible energy optimization in the field of the receptor using a standard molecular mechanics energy function, OPLS-AA (Optimized Potentials for Liquid Simulations – All Atoms) non-bonded potential grid.[86] Finally, a Monte Carlo procedure examining pose conformation is used to further refine the selection of best candidates. The outcome of this simulation is multiple solutions with ligands in different poses which are ranked based on their docking score, characterised by GlideScore. GlideScore calculates an approximation of the binding affinity of a ligand to a protein in a certain pose based on complementary shape and electrostatic interactions. A limitation of this is that it assumes that the protein is rigid, however protein and ligand mobility as well as the presence of water molecules are known to play important roles in binding affinity. Moreover, they omit essential thermodynamic considerations such as the free energy of binding. Therefore, docking conformations and poses should be considered more closely than the calculated docking scores. As a general guide, compounds with scores of around -10 kJ/mol are considered ‘very good’ scores that may represent good binding (Schrodinger.com).

Bleb was docked into the Phyre2 model of *Pf*MyoA and was aligned with the 1YV3 structure for direct comparison. When docked into the Phyre2 model, the conformation of Bleb was almost identical to that of 1YV3 and it produced a large negative docking score of -11.1 kJ/mol indicating high affinity docking (Figure 16). Hydrogen bond interactions were observed between the carbonyl oxygen and Phe471, the hydroxyl oxygen and Gly249 as well as the hydroxyl hydrogen with Leu271, all matching the interactions necessary for Bleb activity in 1YV3 but with different amino acid residues.

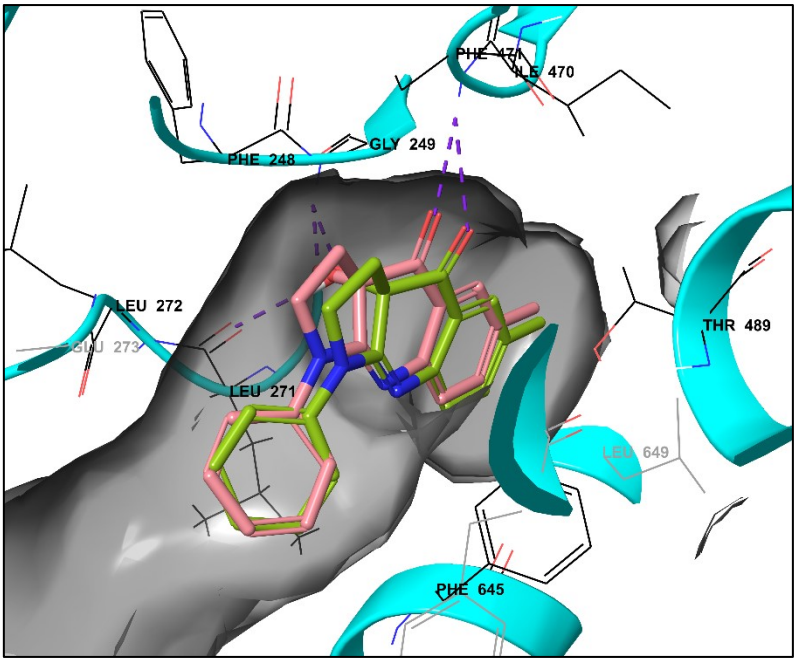


Figure 16: Bleb docked into the Phyre2 model (green) with the 1YV3 Bleb overlaid (pink). Key H-bond interactions shown (purple).

In contrast, Glide would not allow docking of Blebbistatin into the *Pf*MyoA SM model, and an error message appeared every time it was attempted. This was an interesting outcome and it was postulated that this model could be a closer representation of the structure of *Pf*MyoA as it was consistent with the experimental results indicating that Bleb does not bind to *Pf*MyoA. The SM model was aligned with the 1YV3 structure and the most striking difference was the size of the binding cavity which appeared much smaller in the SM model. This was attributed to two protruding residues present in the homology model which were Phe485 and Phe645 (Figure 17A), replacing Cys470 and Tyr634 of *DD*MyoII.

To explore further, the SM model was aligned with the Phyre 2 model with Bleb docked, and in general the residues surrounding the inhibitor that were implicated in binding were conserved. A major difference in their structure was that the Phe485 and Phe645 of each were present in different conformations depending on the model. These are represented in blue (Phyre2 model) and yellow (SM model) in Figure 17B. A potential clash is observed between the aromatic tricyclic region of Bleb and Phe485 of the SM model. The Phyre2

model shows both the Phe485 and the Phe645 in alternative positions, twisted away from Bleb posing no potential clash.

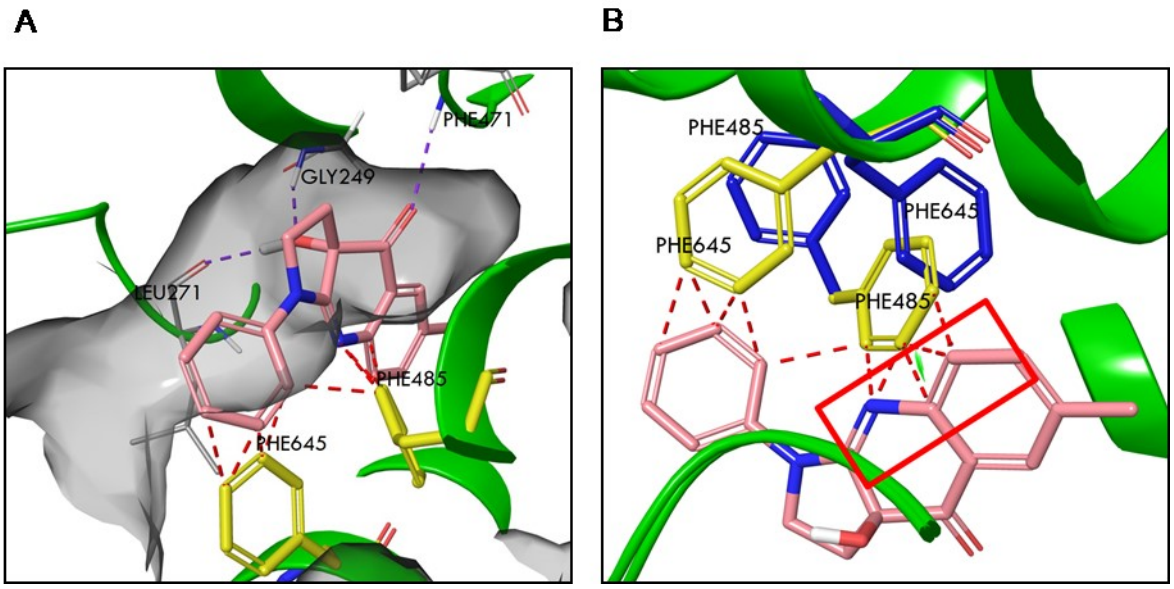


Figure 17A: Two orientations of Phe485 and Phe645 from homology models Phyre2 (blue) and SM model (yellow) when aligned. The clash of the SM model Phe485 and Phe645 with Bleb in the 1YV3 conformation are highlighted (pink); **B**: The SM model predicts that the *Pf*MyoA binding cavity is much smaller than that of the 1YV3 structure which could explain why Bleb is inactive.

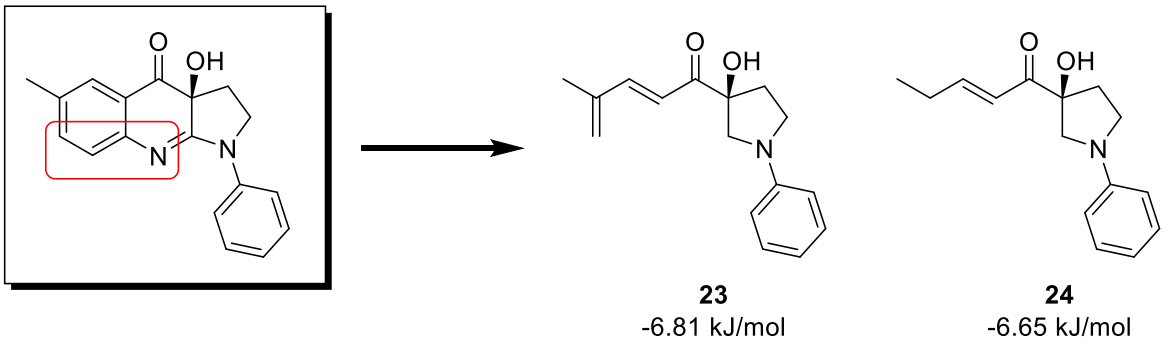
The SM model provides the best hypothesis as to why Bleb is inactive towards *Pf*MyoA. The much smaller binding cavity compared to that of *DD*MyoII, combined with the rigid and conformationally restrained structure of Bleb means it cannot be accommodated by the active site (Figure 17B). For this reason, it was postulated that changing the structure of Bleb to reduce the steric clashes with Phe485 and Phe645, thereby reducing the size and rigidity of the molecule, may provide an inhibitor of *Pf*MyoA.

3.1.3. Redesigning (*S*)-Blebbistatin

The structure of Bleb could be altered to minimise the clash between the molecule and Phe485 and Phe645. We thought that disrupting the rigid tricyclic aromatic system by removing the quinolone nitrogen and the neighbouring carbon chain that make up half of the adjacent benzene ring, may enable docking within the SM model of *Pf*MyoA. This would

increase flexibility of the molecule, allowing for the possibility of conformations that avoid the observed steric clashes.

Consequently, structures **23** and **24** (Figure 18) were designed to probe this hypothesis. Docking simulations in the SM model were carried out with these designs, and in this case the software was able to dock these compounds into the model, providing a few alternative docking modes with varying scores.



23
-6.81 kJ/mol

24
-6.65 kJ/mol

Figure 18: Removal of the highlighted section of Bleb to generate derivatives **23** and **24**, and the docking scores for each.

Overall the lowest energy docking conformations adopted by **23** and **24** were very similar to that of Bleb bound to *DD*MyoII and docked in the Phyre2 model (-11.1 kJ/mol). With the removal of the rigid aromatic system, the unsaturated chain is able to rotate and avoid clashes with the protein. Derivative **23** generates potentially important hydrogen bond interactions with Gly249 and Leu271 and presents the hydroxyl group in the same orientation as Bleb bound to *DD*MyoII. However, the carbonyl group points away from Phe471 and therefore does not acquire this predicted hydrogen bond, perhaps due to the new freedom of rotation which has enabled the terminal alkene to be positioned to avoid the clash with Phe485 (Figure 19A).

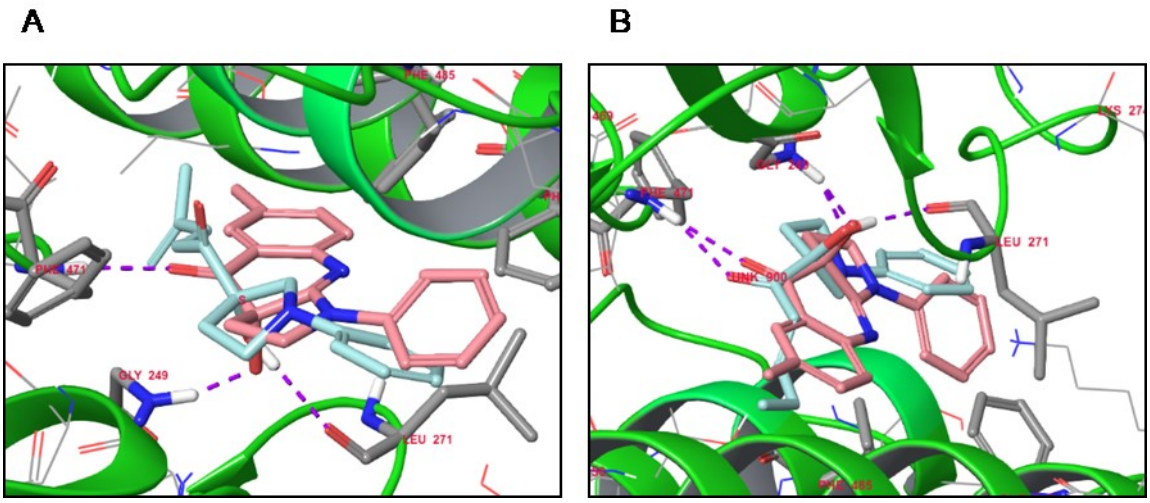


Figure 19A: Compound **23** docked into the SM model of *Pf*MyoA (turquoise) with superimposed 1YV3 Bleb (pink); **B**: Compound **24** docked into the SM model *Pf*MyoA (turquoise) with superimposed 1YV3 Bleb (pink)

Derivative **24** was designed to recover the hydrogen bonding between the carbonyl group and the protein by removing the terminal alkene, and when docked into the *Pf*MyoA SM model it was predicted to maintain all the necessary Bleb hydrogen bonding as hypothesised (Figure 19B). The issue with the structure of **24** is the presence of an α,β-unsaturated ketone which can act as a Michael acceptor. As a potential alkylating agent this structure is undesirable as a non-covalent drug molecule. A library of analogues was devised with variations in this position and some also with alterations to the aniline substituent to gain knowledge of what can be tolerated according to this model.

Figure 20 summarises the variety of structures selected for the docking screen. More than 60 compounds were docked in the SM *Pf*MyoA model, with initial variations made to the groups extending from the carbonyl, looking at compounds that could mimic the hydrophobic and hydrogen bond interactions of Bleb and retain a certain amount of rigidity. Ketones and amides with saturated and unsaturated chains, as well as various aromatic and aliphatic rings of different sizes were incorporated. The compounds were mostly judged based on the poses adopted and their ability to form important H-bond interactions, as docking scores were variably representative of how well a compound docked. It appeared that size was a limiting factor, with only small unsaturated chains and aryl rings tolerated.

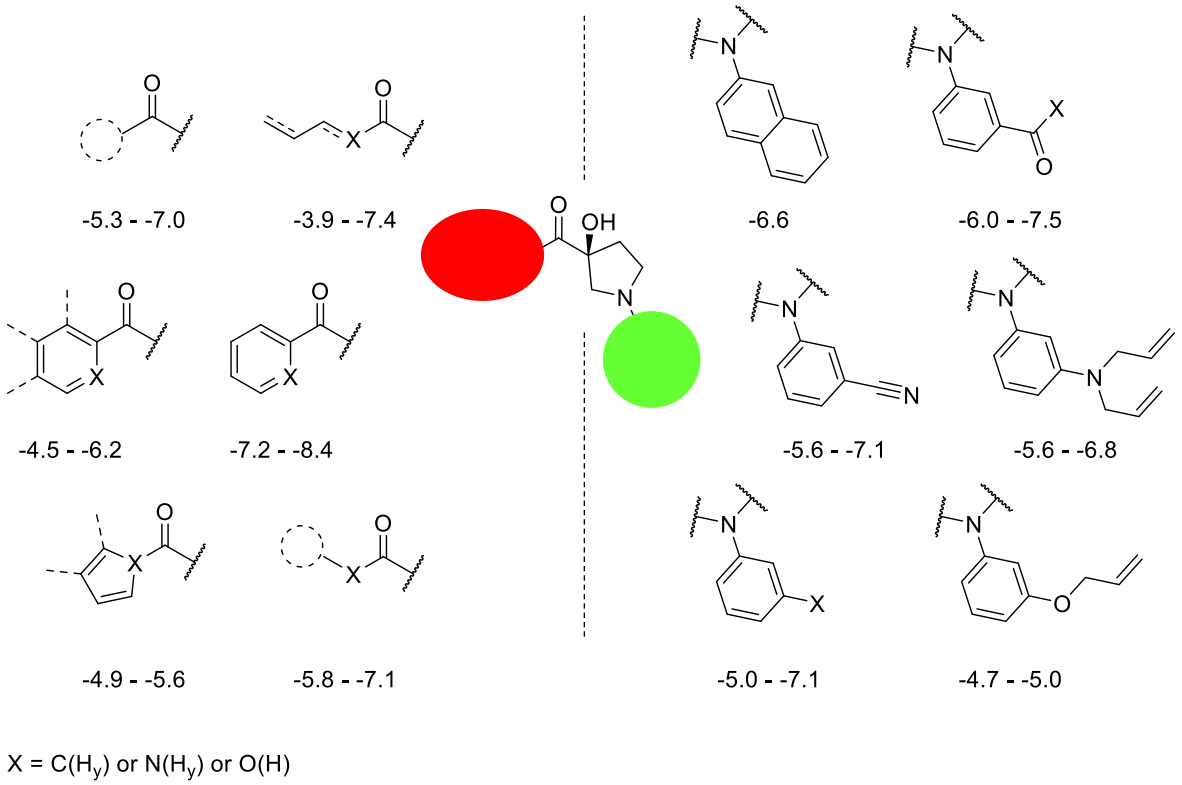


Figure 20: A summary of the various structural changes made to derivative **24** for docking studied in the SM model of *Pf*MyoA with docking scores ranges in kJ/mol.

In a 2017 paper, Verhasselt *et al.* described the synthesis of Bleb derivatives that improved the physicochemical properties and research tool characteristics while maintaining MyoII activity by introducing polar substituents in the meta position on the *N*-phenyl ring.[62] These appendages were also added to the analogues in the docking study as there also appeared to be space in this region of the cavity. However, any extension of the phenyl ring reduced the docking score and the conformations suggested were not consistent with the Bleb binding in 1YV3.

From this screen of compounds, 4 molecules of interest were identified in which the carbonyl group is either a ketone or an amide (Figure 21). Compounds **25** and **26** differ only in the atom adjacent to the carbonyl, while **27** and **28** are both aromatic ketones with either a benzene or pyridine ring.

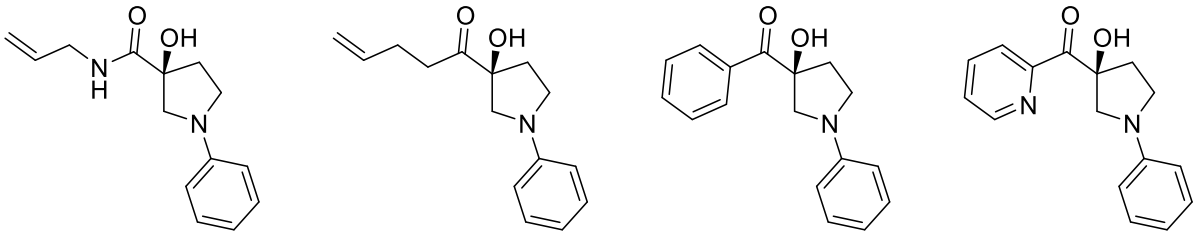


Figure 21: The structures of the best compounds identified from the docking screen with their docking scores (kJ/mol).

It was thought that introduction of an amide may provide some rigidity to the compounds, better mimicking the rigid cyclic structure of Bleb. When unsaturated chains alpha to an amide or an acyl group were incorporated for direct comparison, the docking conformations adopted were very close to that of Bleb in 1YV3 (Figures 22A and 22B).

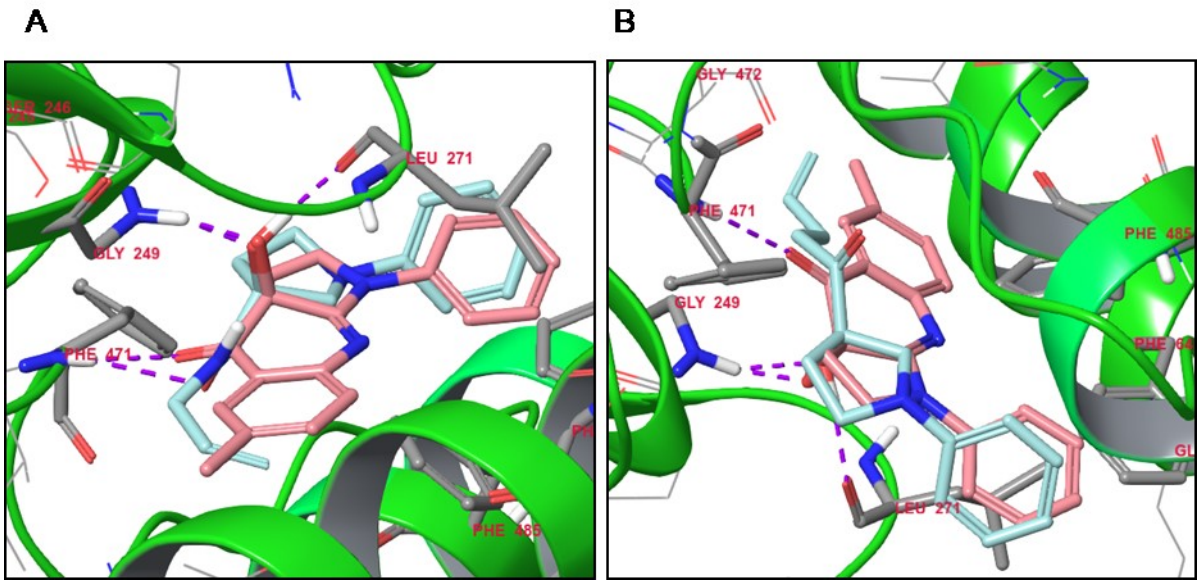


Figure 22A: Compound **25** docked into the SM model of *Pf*MyoA (turquoise) with superimposed 1YV3 Bleb (pink); **B**: Compound **26** docked into the SM model of *Pf*MyoA (turquoise) with superimposed 1YV3 Bleb (pink).

Relatively high docking scores were achieved for amide **25** and ketone **26** scoring -6.4 and -7.3 kcal/mol respectively. H-bonding is maintained in both cases from the hydroxyl group to Gly249 and Leu271, however the carbonyl group of **26** is oriented in a different direction, preventing H-bonding to Phe471. Docking of phenyl ketone derivative **27** into the SM

*Pf*MyoA model produced conformations that very closely mimicked that of Bleb in 1YV3 with a docking score of -7.3 kJ/mol (Figure 23A).[32] Replacement of the phenyl group with a pyridine ring (**28**) gave the greatest docking score of -8.5 kcal/mol which corresponded well to its docking pose in which the three predicted hydrogen bond interactions are observed (Figure 23B).

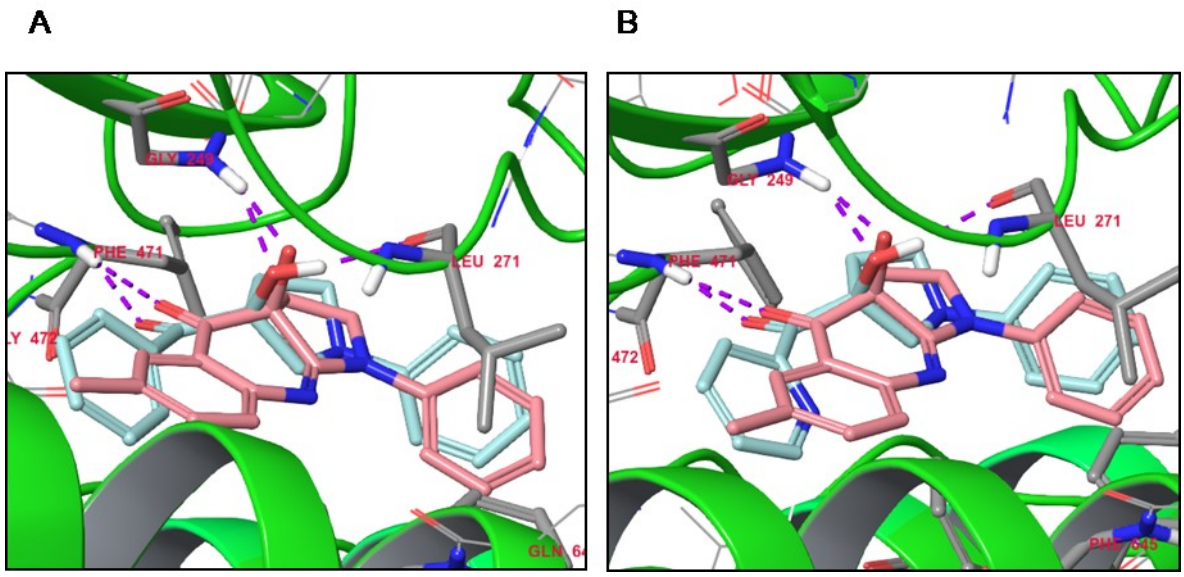


Figure 23A: Compound **27** docked into the SM model of *Pf*MyoA (turquoise) with superimposed 1YV3 Bleb (pink); **B**: Compound **28** docked into the SM model of *Pf*MyoA (turquoise) with superimposed 1YV3 Bleb (pink)

To validate the SM homology model of *Pf*MyoA, these four compounds of interest needed to be synthesised and their biological activity tested against *Pf*MyoA. Once the model has been validated, it can then be used to generate further analogues and to develop some SAR of the *Pf*MyoA binding pocket.

3.2. Part 2: Synthesis of 1st Generation (*S*)-Blebbistatin Analogues

3.2.1. Synthetic Route A – Hydroxylation and Lactam Reduction

Retrosynthetic Analysis

With compounds **25**-**28** identified as promising starting points from the *Pf*MyoA docking studies, the synthesis of these for homology model validation was important. The general structure of these compounds comprises of a core pyrrolidine ring with a phenyl ring attached to the nitrogen (Figure 24A). A carbonyl side chain is attached at C-3 with an adjacent tertiary alcohol.

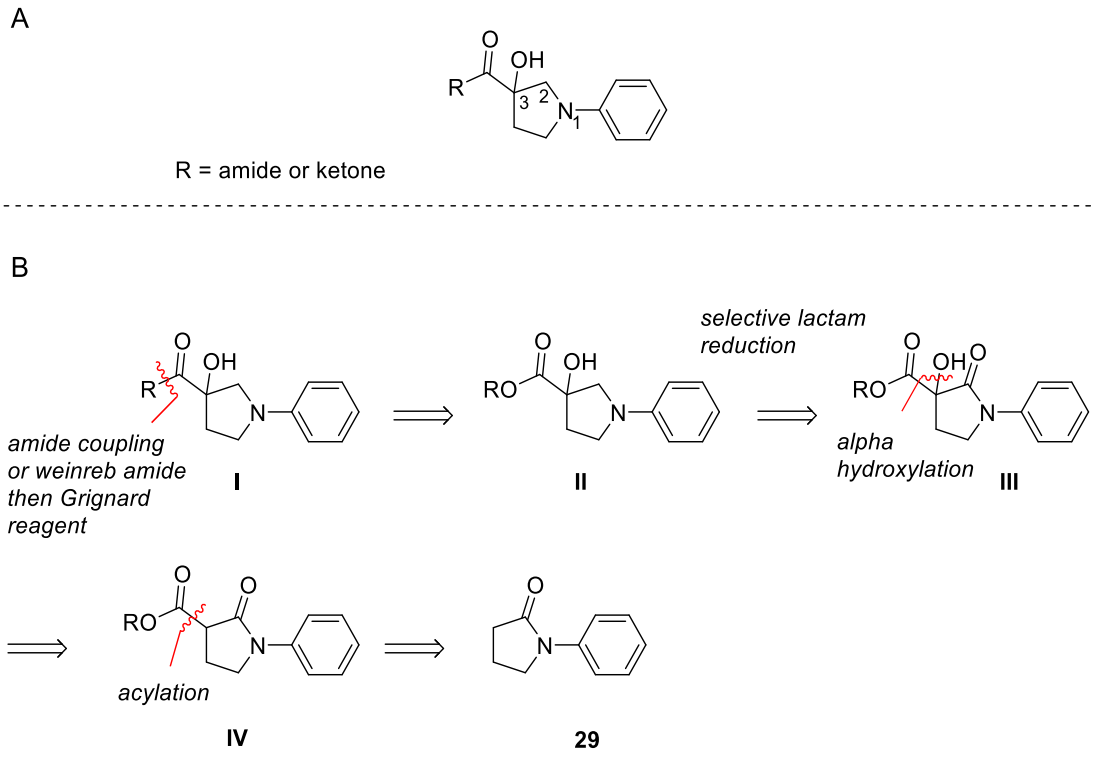


Figure 24A: General structure of promising docking designs; **B**: Initial retrosynthetic analysis of Bleb derivatives.

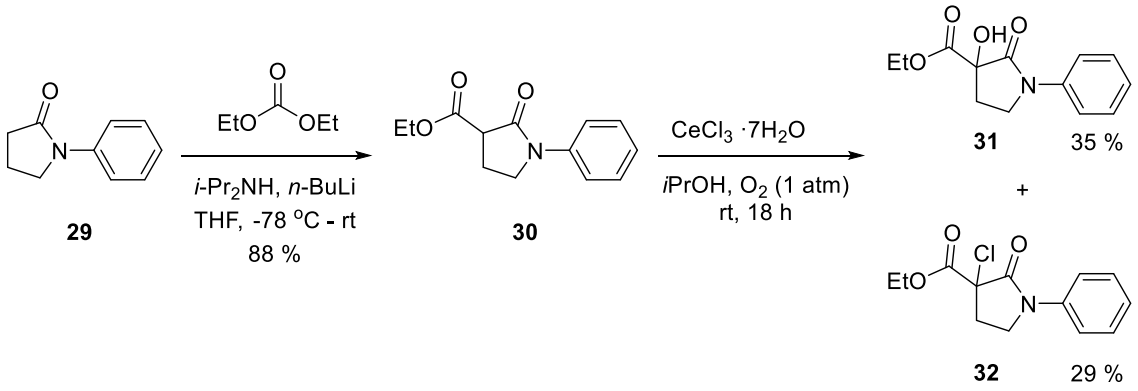
A seemingly simple structure, it was envisaged through retrosynthetic analysis that the synthesis could be carried out in 5 steps starting from commercially available 1-phenyl-2-

pyrrolidinone (**29**) (Figure 24B). Installation of the side chain at C-3 (**IV**) could be achieved by exploiting enolate chemistry followed by α-hydroxylation facilitated by the presence a 1,3-dicarbonyl group (**III**). Selective lactam reduction to generate intermediate **II** would then be employed followed either by amide coupling or formation of the Weinreb amide for derivatisation using Grignard reagents, depending on the analogue.

α-Hydroxylation

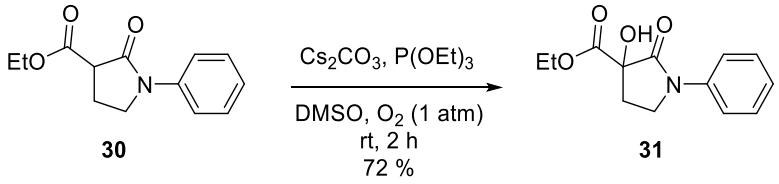
Acylation of 1-phenyl-2-pyrrolidinone was carried out using lithium diisopropylamide (LDA) formed *in situ* to form the enolate, followed by the addition of diethyl carbonate to generate 1,3-dicarbonyl **30** (Scheme 1). At this early stage in the project it was decided that the hydroxyl group would be introduced non-stereoselectively for initial biological assessment before testing the individual enantiomers if any compounds exhibited activity. It was thought that hydroxylation could be facilitated by the presence of the 1,3-dicarbonyl due to the increased acidity of the alpha protons, therefore several methods were investigated.

One way of achieving alpha-hydroxylation is to harness molecular oxygen as an oxidant using metal catalysis, a method regarded as economical and environmentally benign. Cerium (III) chloride heptahydrate was initially used for the hydroxylation of 1,3-dicarbonyl **30** under an oxygen atmosphere (Scheme 1). This is a non-toxic pre-catalyst which is oxidised by oxygen to Ce(IV) when co-ordinated with 1,3-dicarbonyl ligands. Although the mechanism is not fully understood, studies have been carried out to try and identify the source of the α-hydroxyl group which is believed to originate from molecular oxygen itself rather than nucleophilic attack of water.[87] In this case the reaction was low yielding and a significant amount of chlorinated side-product **32** was generated.



Scheme 1: Acylation of 1-phenyl-2-pyrrolidinone (**29**) followed by 1,3-dicarbonyl hydroxylation using $CeCl_3 \cdot 7H_2O$ in oxygen.

Other conditions investigated were the use of caesium carbonate and triethyl phosphite which also utilised molecular oxygen as the sole oxidant. The use of caesium carbonate as a catalyst in this reaction is advantageous as it is inexpensive and, unlike for some transition metal catalysts, it can be easily removed by aqueous work-up, simplifying subsequent purification steps.[88] Hydroxylation of 1,3-dicarbonyl **30** was successful using these conditions and the reaction was complete after 2 hours with no side-product formation and a yield of 72% was achieved following column chromatography (Scheme 2).



Scheme 2: 1,3-dicarbonyl hydroxylation using catalytic Cs_2CO_3 and $P(OEt)_3$ with molecular oxygen as the oxidant.

Following a number of mechanistic experiments, including isotopic labelling, Jiao *et al.* proposed the mechanism for this reaction shown in Figure 25.[88] Deprotonation of the position alpha to the 1,3-dicarbonyl with Cs_2CO_3 would first occur forming carbanion **A** which would react with molecular oxygen to generate superoxide anion **B**. This could obtain a proton from another molecule of 1,3-dicarbonyl **30** to form superoxide **C** which would be reduced by $P(OEt)_3$ to generate hydroxylated compound **31**. This mechanism is plausible as

Jiao *et al.* also identified $P^{18}O(OEt)_3$ as a side-product during the ^{18}O labelling experiments using mass spectrometry.

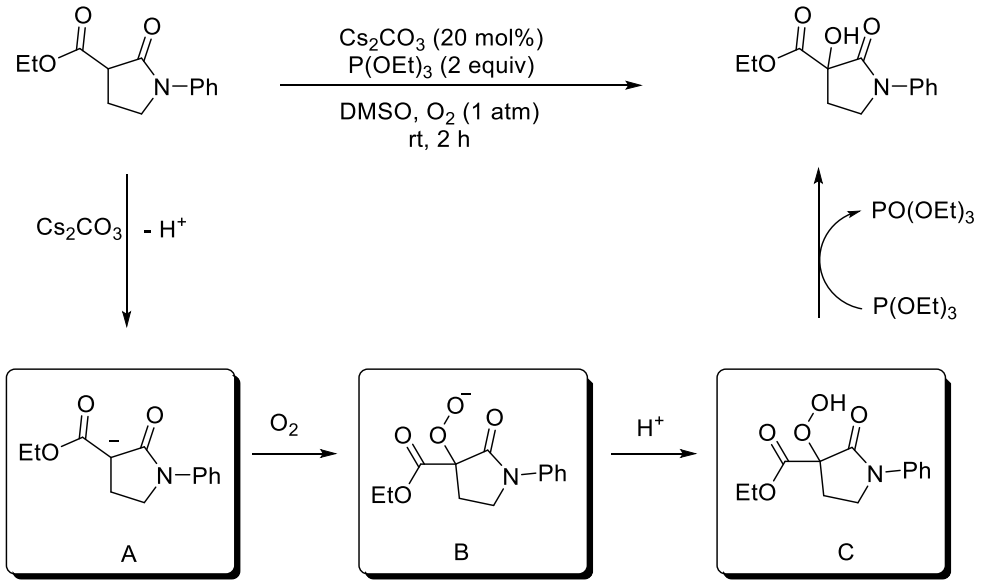
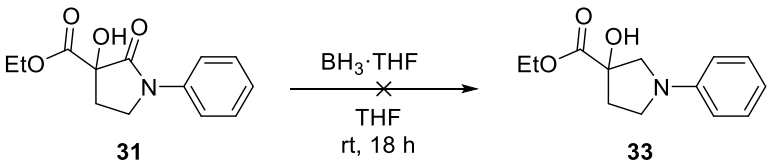


Figure 25: Proposed mechanism for the hydroxylation of 1,3-dicarbonyl **30** by Jiao *et al.*[88]

Selective Lactam Reduction

Following generation of the hydroxylated intermediate **31**, selective lactam reduction was initially attempted using borane-tetrahydrofuran complex (BH_3·THF). It has been reported that it is possible to reduce an amide selectively in the presence of an ester using these conditions,[89–91] however in this case the crude ^1H NMR suggested that a mixture of products was generated, including ester reduction to the corresponding aldehyde with no observed formation of the desired product (Scheme 3).

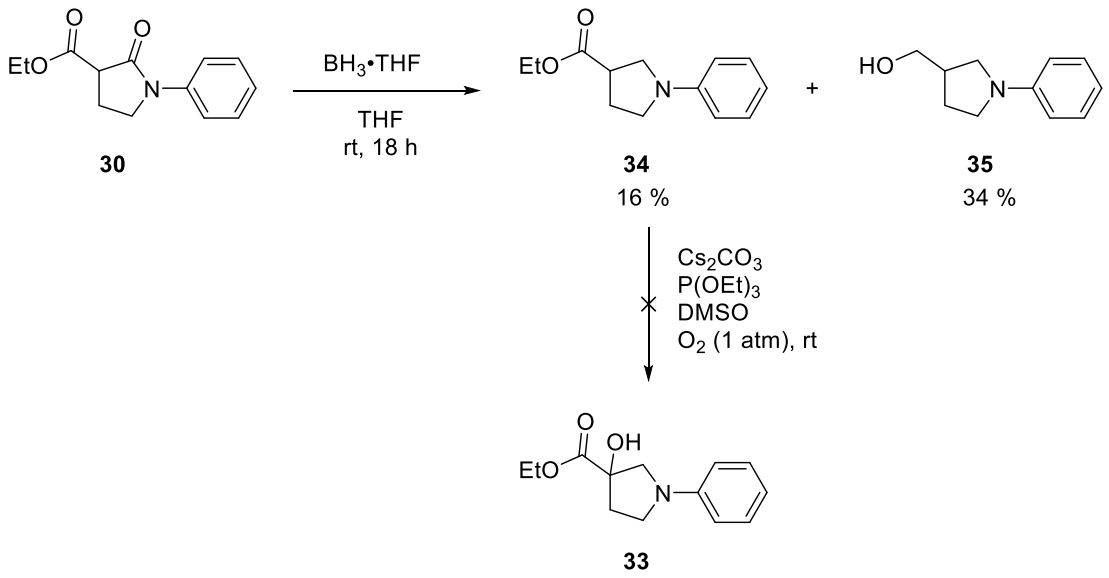


Scheme 3: Attempted selective lactam reduction of 1,3-dicarbonyl **31** using BH_3·THF.

A rationale for the lack of chemoselectivity in this reaction may be a result of competition between the ester and lactam reduction induced by co-ordination between the ester carbonyl

oxygen and the boron thereby increasing the electrophilic nature of the ester carbonyl carbon. It should also be mentioned that the reaction relies on harsh quenching conditions in which methanolic hydrochloric acid is added and refluxed in order to hydrolyse residual borane and amine-boron complexes therefore it is unsurprising that side reactions such as ester hydrolysis occurred.[91]

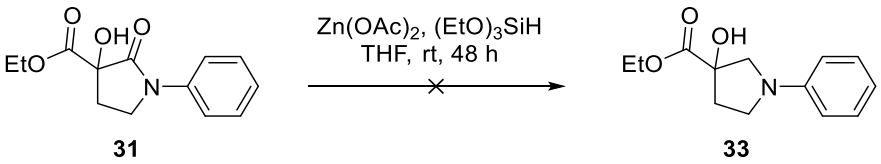
This reactivity was also observed when reduction of 1,3-dicarbonyl **30** was attempted using the same conditions in an attempt to discover whether the hydroxyl group was affecting the reaction. It was found that at room temperature using 1.5 equivalents of borane, a small quantity of the desired amino ester **34** could be isolated however full reduction to the amino alcohol **35** appeared to be favoured (Scheme 4).



Scheme 4: Reduction of 1,3-dicarbonyl followed by the attempted hydroxylation of resulting ester **34** using previously investigated conditions.

With the small quantity of amino ester **34** isolated, hydroxylation was attempted using the conditions that were previously successful for 1,3-dicarbonyl **30**, however no reaction was observed (Scheme 4). This may be due to the increase in pK_a of the proton alpha to the ester of **34** which would be approximately 25 compared to that of the 1,3-dicarbonyl **30** which would have been around 15.

As well as the use of hydride reagents, catalytic amide reductions can be very effective and there are many examples of the hydrosilylation of amides using precious metal catalysts such as Rh, Ru, Pt, Ir and Pd.[92–94] Additionally, Beller *et al*. showed that tertiary amides can be reduced chemoselectively over some esters and ketones using zinc catalysis with triethoxysilane.[95]



Scheme 5: Attempted lactam reduction by hydrosilylation using catalytic $Zn(OAc)_2$ with $(OEt)_3SiH$.

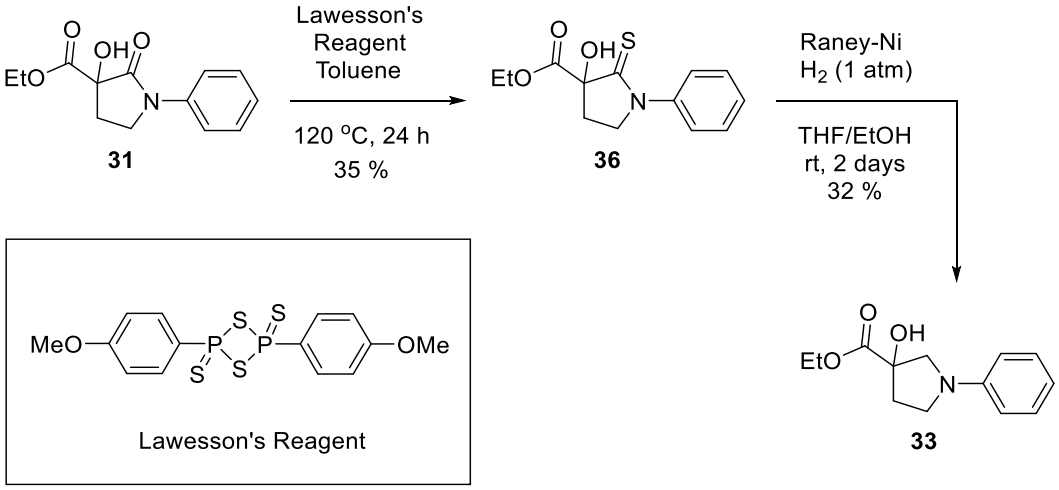
Unfortunately, using the conditions outlined by Beller *et al.* (Scheme 5), ester hydrolysis was observed while amide reduction did not take place. Although Beller *et al.* had explored the tolerance of ester functionality adjacent to aromatic groups, aliphatic esters which are more easily hydrolysed were not included in their scope study and in this case the ester was hydrolysed.

Thiolactam Approach

Another well-established method for the reduction of amides/lactams is a two-step process in which the oxo group of the lactam is first converted to the corresponding thio derivative which is then desulfurized by Raney nickel to give the corresponding amine. Thionation is most commonly carried out using Lawesson's reagent and is a selective process for amides and lactams in the presence of ketones, esters, and lactones.[96] The drawback of using Lawesson's reagent is that the thionation reactions tend to be solvent dependent as the reagent is not soluble in many organic solvents at room temperature, however at elevated temperatures exceeding 110 °C it begins to decompose and polymerise.[96,97]

Thionation of amide ester **31** provided low yields of around 25% at 95 °C in toluene after 24 hours, and 35% when the temperature was increased to 120 °C, noticeably increasing the

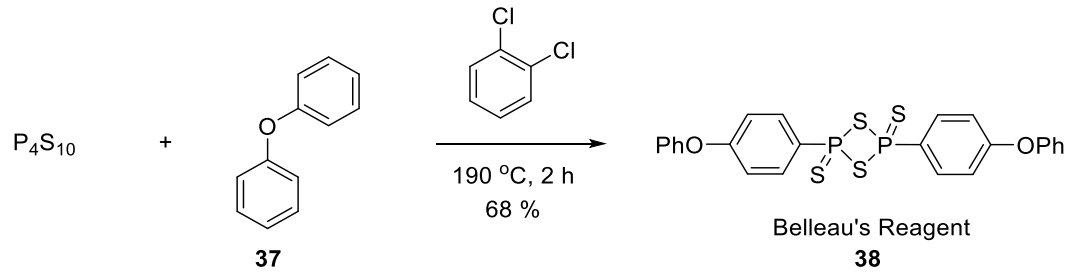
solubility of the reagent (Scheme 6). Significant quantities of starting material were also isolated. Although changing the solvent to dichloromethane (DCM) improved the solubility of the reagent, no reaction occurred suggesting the need for elevated temperatures for amide thionation.



Scheme 6: The reaction conditions used to thionate **31** and subsequently reduce thiolactam **36** to generate amine **33**.

Reduction of the thiolactam (**36**) using Raney nickel was initially carried out at room temperature under an atmosphere of hydrogen (Scheme 6). After two days amine **33** was isolated in 32% yield, but a considerable amount of starting material was still recovered. Any attempt to push the reaction to product formation by increasing the temperature to reflux or the hydrogen pressure up to 3 bars was unsuccessful, either leading to decomposition or failing to improve the yield. Due to the low yields of both the thionation and desulfurization steps, alternative conditions were investigated.

Belleau *et al.* developed a reagent with the same basic structure as Lawesson's reagent, but with diphenyl ether groups flanking the dithiadiphosphetane instead of methoxyphenyl groups.[98] This was synthesised in the hope that the modification would provide improved solubility in organic solvents such as THF, and decrease the temperature required for effective thionation.



Scheme 7: The one step synthesis of Belleau's reagent.[98,99]

Synthesis of the Belleau's reagent (**38**) was achieved by heating diphenyl ether and phosphorous pentasulfide in 1,2-dichlorobenzene (Scheme 7). Initially thionation was carried out in DCM at room temperature however with only partial solubility the reaction did not go to completion and the product could not be separated from Belleau's reagent side-products. The reaction was also carried out in THF which the Belleau's reagent was completely soluble in. After refluxing the reaction mixture overnight, starting material was still present. We then decided to proceed, adding Raney nickel directly to the crude mixture to minimise product loss during thiolactam purification. Unfortunately, this provided a complex mixture which made product isolation challenging and a yield of 29% of amine **33** was obtained which was still very low over the two steps. As a result of the challenges with lactam reduction, an alternative route was required for route optimisation.

3.2.2. Synthetic Route B – Cyanohydrin Formation and *N*-Arylation

Retrosynthetic Analysis

To eliminate the need for selective lactam reduction, a route was envisaged that would initiate from *N*-Boc-protected-3-pyrrolidinone (**40**), enabling functionalisation at the desired C-3 only (Figure 26). This strategy would involve cyanohydrin synthesis to install the tertiary alcohol in the first step (**39**), with nitrile hydrolysis to generate the carbonyl group (**IV**) and *N*-arylation to introduce the desired phenyl group (**II**). This would be followed by derivatisation of intermediate **II** in the same manner previously described (Figure 24B) to generate either amides or ketones.

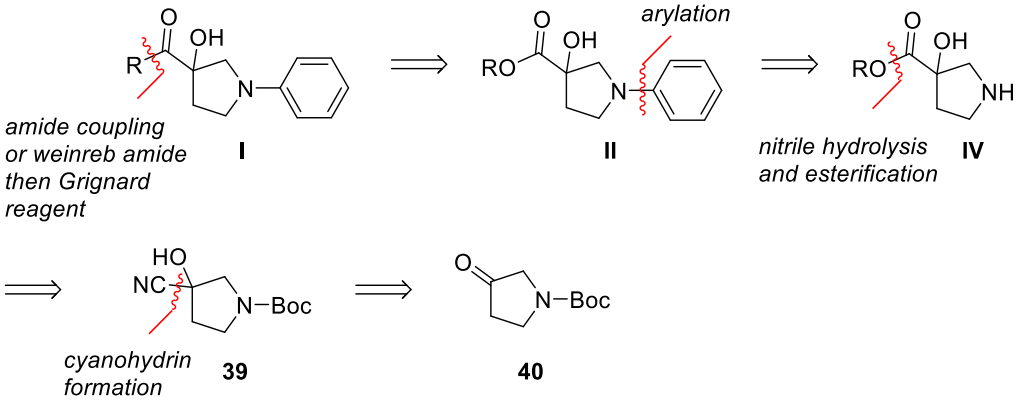
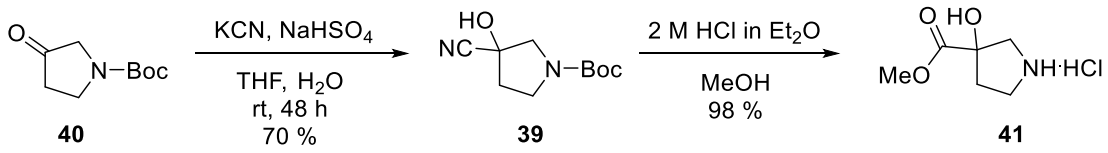


Figure 26: Retrosynthesis starting from *N*-Boc-3-pyrrolidinone.

Cyanohydrin Synthesis and Hydrolysis

Formation of cyanohydrin **39** was found to be solvent and base dependent. When carried out on *tert*-butyl 3-oxopyrrolidine-1-carboxylate **40** using KCN as the cyanide source in a mixture of aqueous sodium bisulfate and diethyl ether as reported by Sherer *et al.*[100], a biphasic mixture was formed seemingly preventing reaction. Alternatively, when a homogeneous mixture of THF and aqueous sodium bisulfite was employed as described by Geoghegan *et al.*[101], no product formation was observed either. It was found that a combination of these conditions in a homogeneous reaction with THF, and aqueous sodium bisulfate led to product formation in good yield (Scheme 8).

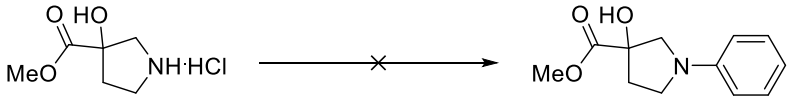


Scheme 8: Formation of cyanohydrin 6 followed by hydrolysis under acidic conditions.

Nitrile hydrolysis was carried out under acidic conditions using methanol as the solvent, effecting Boc group removal concomitantly with methyl ester formation (**41**). This reaction was extremely effective and provided the product in quantitative yield without the need for purification.

Arylation of Pyrrolidine

It was thought that *N*-arylation should be effected at this stage using standard coupling conditions, as further functionalisation of the carbonyl group would be hindered by the presence of the amine hydrochloride which would affect purification and could possibly interfere with future steps. Therefore, a small number of different conditions were utilised to introduce the phenyl group to the hydrochloride amino salt of the pyrrolidine (Table 1).



41 **42**

Coupling Reaction	Reagent	Catalyst	Ligand	Base	Solvent	Temp.
Buchwald-Hartwig	Bromobenzene	$Pd_2(dba)_3$	BINAP	NaO*t*Bu	1,4-dioxane, H_2O	80 °C
Ullmann	Iodobenzene	CuI	N/A	K_2CO_3	DMF	100 °C
Chan Lam	Phenylboronic Acid	$Cu(OAc)_2$	N/A	Pyridine	MeOH	rt

Table 1: A summary of conditions used for *N*-arylation of pyrrolidine **41**.

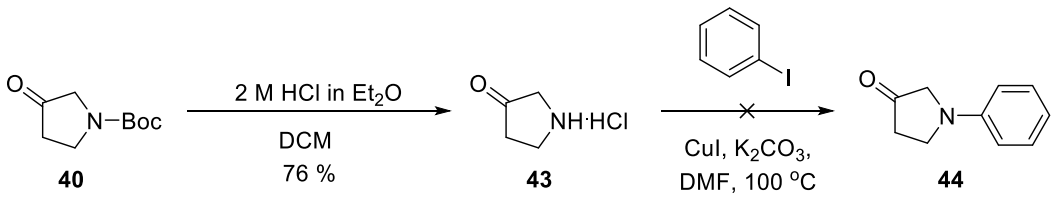
Standard Buchwald-Hartwig amination conditions were first utilised,[102] employing $Pd_2(dba)_3$ as the pre-catalyst with 2,2'-bis(diphenylphosphino)-1,1'-binaphthyl (BINAP) as the ligand, a common choice as bidentate ligands prevent β-hydride elimination by enforcing the *cis* geometry of coupling partners. NaO*t*Bu was chosen as the base as it is commonly used stoichiometrically in catalytic amination reactions because it has been shown to provide fast reaction times, allowing for low catalyst loading. Caution should however be taken when using this base in the presence of some functionalities such as methyl and ethyl esters as these can be converted to amides and *t*-butyl esters.[103] With this in mind, NaO*t*Bu was used in only slight excess with 1.3 equivalents in an attempt to minimise any reaction with the

methyl ester.[104] However, no reaction was observed with bromobenzene after 24 hours at 80°C.

An alternative method for creating new C-N bonds is to use copper catalysis conditions such as those devised by Ullmann *et al.* in the early 1990's.[105] Ullmann-type coupling reactions are advantageous over palladium catalysis because copper is less expensive and the systems are often less sensitive to moisture and air. However the classic Ullmann conditions usually require stoichiometric quantities of copper catalyst as well as highly elevated temperatures.[106,107] Nevertheless, ligand-free conditions employed by B. Wang in a 2015 patent on substrates bearing close structural similarities to that of pyrrolidine ester **41** were used in an attempt to effect arylation.[108] CuI was used as the copper catalyst with 2 equivalents of K_2CO_3 in DMF at 100 °C for 24 hours. However after this time, no reaction was observed and starting materials were recovered.

Finally, arylation of pyrrolidine ester **41** was attempted using Chan Lam coupling conditions described by McCarthy *et al.* in which 1-(*tert*-butyl) 2-methyl (*S*)-piperazine-1,2-dicarboxylate was coupled with phenylboronic acid.[109] Stoichiometric $Cu(OAc)_2$ was used with two equivalents of pyridine in MeOH, in a flask open to the air. Once again, no reaction was observed and only starting materials were isolated.

To determine whether the presence of the α-hydroxy methyl ester has an effect on the outcome of metal catalysed *N*-arylation, an Ullmann-type amination was attempted with pyrrolidin-3-one hydrochloride **43**, generated by removal of the *N*-Boc protecting group of **40** under acidic conditions (Scheme 9). Using the same standard Ullmann conditions as before, no reaction was observed, which suggests that functionality in the 3-pyrrolidine position does not affect metal-catalysed arylation as couplings fail even with a simple pyrrolidinone.



Scheme 9: *N*-Boc deprotection followed by attempted Ullmann-type reaction for introduction of the *N*-phenyl.

In hindsight it was most likely the use of the pyrrolidine as the hydrochloride salt which hindered these coupling reactions, decreasing the nucleophilicity of the pyrrolidine and preventing metal coordination Perhaps if the NaO*t*Bu used in the Buchwald amination had been used in greater excess, this may have provided the free amine allowing for palladium coordination, however the presence of the tertiary alcohol and methyl ester could present possible side reaction problems. For both the Ullmann and Chan Lam couplings, the base was used in excess, however neither reaction yielded product. If carried out again, the introduction of a de-salting step under basic conditions to provide the free amine first would be important as this could potentially facilitate the progression of each coupling reaction.

3.2.3. Synthetic Route C – Amide Derivatives

Retrosynthetic Analysis

As introduction of the *N*-phenyl group to the pyrrolidine proved problematic, it was conceived that a logical alternative would be to synthesise the pyrrolidine ring with the *N*-phenyl group incorporated into the system from the start (Figure 27). This would involve an initial ring closing condensation step with aniline (**48**) and 1,4-dihalobutan-2-ol **47** to generate the *N*-phenyl pyrrolidine with an alcohol in the desired 3-position, which after oxidation to **44** and formation of cyanohydrin **45** would be followed by derivatisation in the same manner as previously described (Figure 24B).

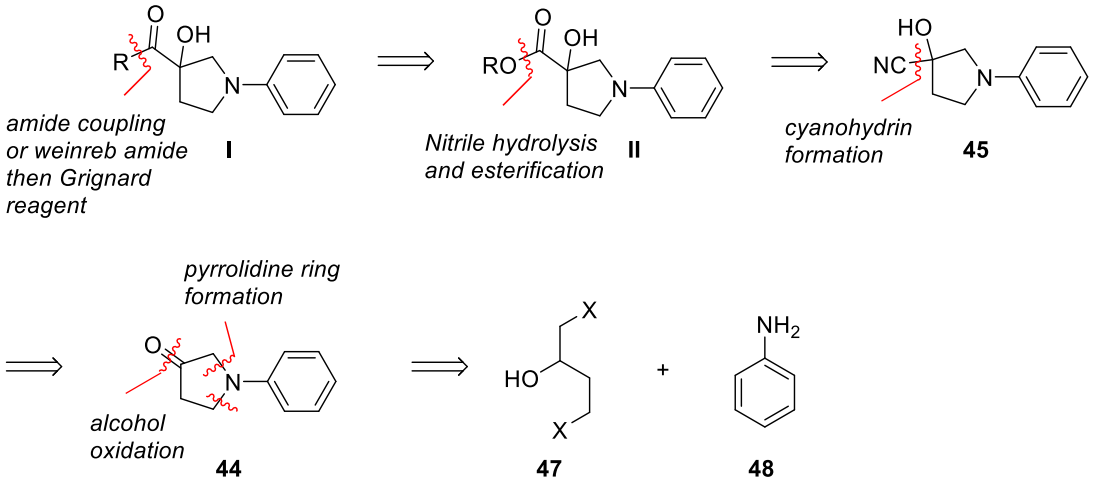
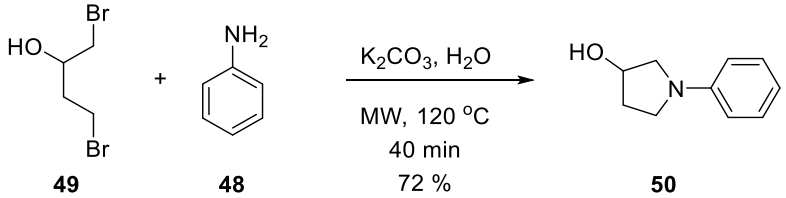


Figure 27: Retrosynthesis starting from the condensation of aniline **48** with 1,4-dihalobutan-2-ol **47**.

Synthesis of (S)-Blebbistatin Amide Derivatives

Synthesis of alcohol **50** was initially attempted using conditions reported by Lihammar *et al.*[110] in which aniline (**48**) and 1,4-dibromobutan-2-ol (**49**) were combined with K_2CO_3 and heated in triethyl phosphate. Although the conversion looked promising by TLC, there appeared to be side-product formation. Another drawback of the procedure was the work-up in which the excess triethyl phosphate had to be removed *in vacuo*. Due to the high boiling point, this proved to be a real challenge, therefore a modified procedure was employed to get around this issue.

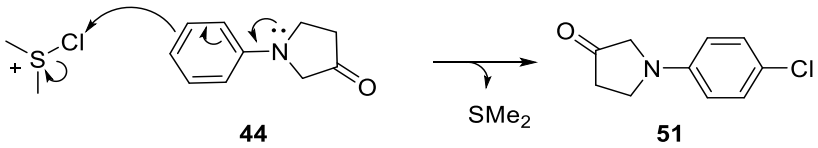
A procedure by Ju *et al.* [111] was followed using water as a solvent instead, and microwave irradiation in order to optimise work-up conditions. The advantage of using water is that, as a good absorber of microwave energy, it can achieve high temperatures (up to 250 ºC) and provides an environmentally clean reaction medium.



Scheme 10: Synthesis of *N*-phenyl pyrrolidine-3-ol **50** from 1,4-dibromobutan-2-ol (**49**) and aniline (**48**).

N-phenyl pyrrolidin-3-ol **50** was obtained in high yield after just 40 minutes, with minimal side-product formation, simple work-up and product isolation (Scheme 10).

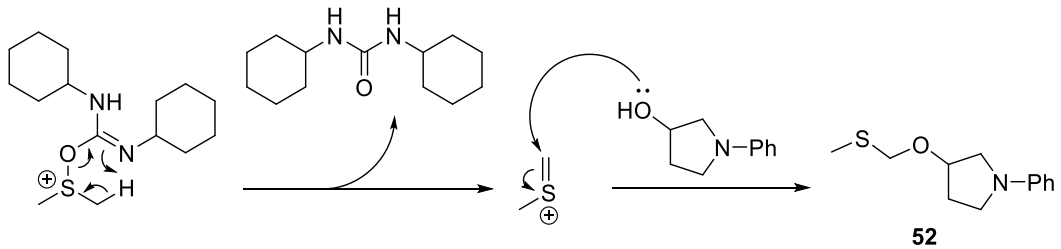
Oxidation of the secondary alcohol of **50** was initially attempted using standard Swern oxidation conditions. This worked to an extent on a small scale, producing yields of around 40%, however when scaled up the major product was the result of a side reaction in which the electron rich phenyl ring attacked the chlorine from the generated chloro(dimethyl)sulfonium chloride, forming the pyrrolidinone with a *para*-chloro substituent, **51** (Figure 28).



44 **51**

Figure 28: Proposed mechanism for the formation of Swern side-product 1-(4-chlorophenyl)pyrrolidin-3-one (**51**), tentatively assigned based on ^{1}H and ^{13}C NMR.

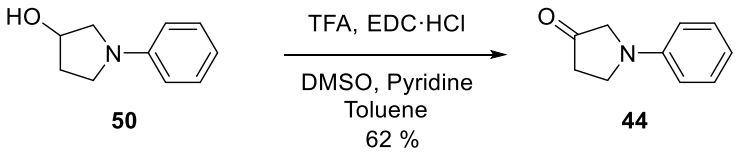
As an alternative, Pfitzner Moffatt oxidation conditions were used as this generates activated DMSO using DCC rather than oxalyl chloride, removing the possibility of electrophilic aromatic substitution of the chlorine. Another advantage of using this method is that it can be carried out at room temperature rather than at -78 °C in the case of the Swern oxidation. Initially, only a 40% yield was achieved and there was a significant side-product. This was the methylthiomethyl ether derivative **52**, formed as a result of elimination of the activated DMSO, generating a highly reactive methyl(methylene)sulfonium species which could easily react with the alcohol (Figure 29).



52

Figure 29: A mechanism to describe the formation of the side-product **52** which results from Pfitzner Moffatt oxidation conditions.[112] **52** has been tentatively assigned based on ^{1}H and ^{13}C NMR.

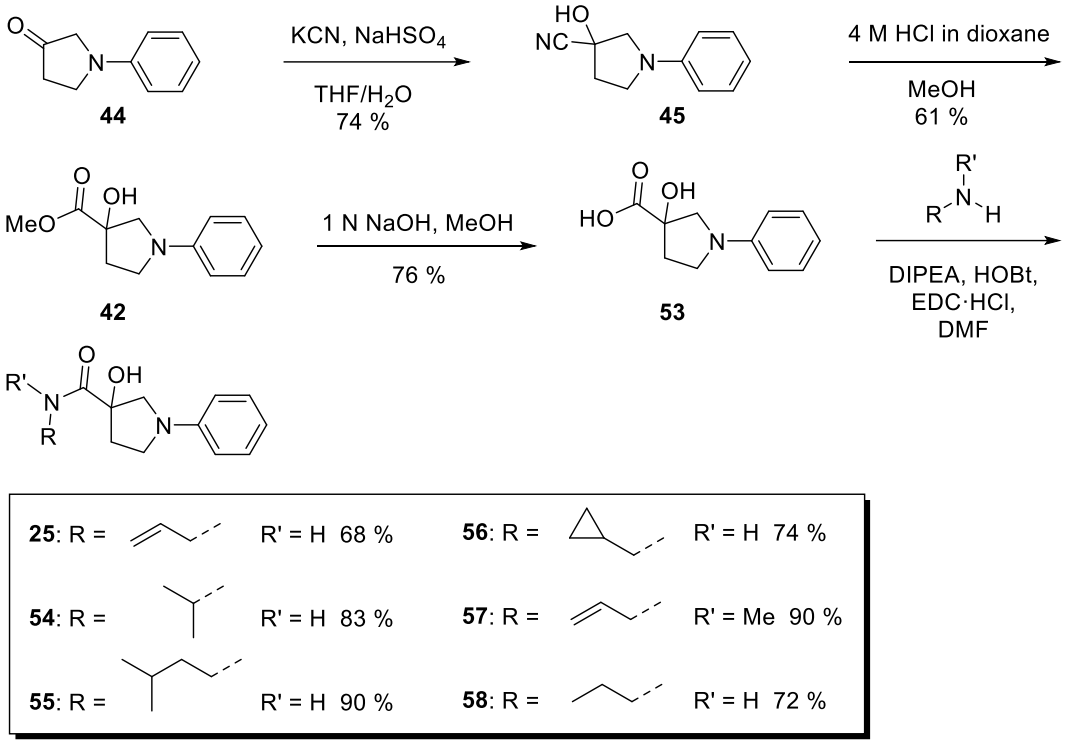
Increasing the equivalents of DCC and DMSO reduced the amount of side-product **52** generated, however this led to an increase in the DCC urea by-product which proved more difficult to remove and decreased the yield. Thus, EDC·HCl was used as a substitute for DCC as the urea by-product generated is water-soluble, simplifying work-up and reducing product loss. Following optimisation, yields were increased to 60% with methylthiomethyl ether formation at 10% of the total (Scheme 11).



Scheme 11: Synthesis of 1-phenylpyrrolidin-3-one using modified Pfitzner Moffatt conditions.

Formation of cyanohydrin **45** was carried out using potassium cyanide and sodium bisulfate in a 2:3 mixture of THF and water respectively. The yield increased with scale, and although the reaction never went to full conversion, NMR analysis of the crude revealed a 9:1 ratio in favour of the desired product which was submitted directly for cyanohydrin hydrolysis (Scheme 12). This was carried out under acidic conditions in methanol, resulting in *in situ* esterification of the carboxylic acid. Methyl ester derivative **42** was obtained, as it was easier to isolate from the reaction mixture than the carboxylic acid. Hydrolysis under basic conditions provided the desired carboxylic acid **53**, which could then be used for the preparation of Bleb amide derivative **25** using standard amide coupling conditions.

Considering the amount of effort required to access this analogue, a small library of closely related amides that produced reasonable docking conformations in the original computational screen were also synthesised. Analogues **54**-**58** were chosen bearing small variations in the chain length and flexibility, with the aim to explore the space in the binding cavity that this part of the molecule is predicted to occupy. Derivative **57** possessing a tertiary amide was also prepared to explore whether the NH hydrogen donor is necessary for activity. These small variations in structure could provide some valuable SAR.

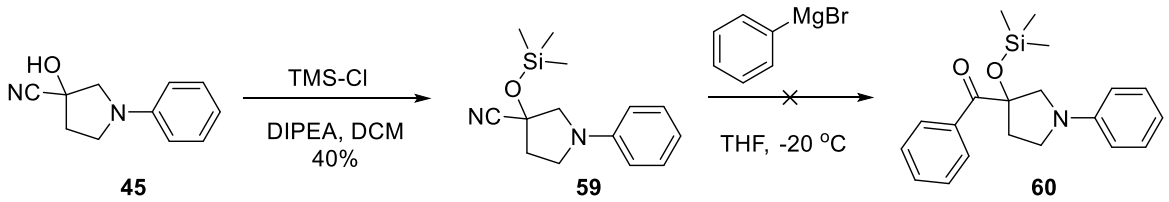


Scheme 12: Route developed for synthesis of amide derivatives of Bleb.

Towards (S)-Blebbistatin Ketone Derivatives: Nitrile Approach

For the synthesis of ketones **26-28** it was envisaged that nucleophilic addition of an appropriate Grignard/organometallic reagent to cyanohydrin **45** could be effective, as this is a well-established method. It is suitable for ketone synthesis as double addition of the organometallic reagent is generally avoided as the reaction proceeds via an imine salt that is hydrolysed to give the ketone product during work-up. This means that any excess organometallic reagent is destroyed at this step and does not have a chance to react with the ketone for a second addition. [113]

Cyanohydrin **45** was protected with a trimethylsilyl (TMS) group (Scheme 13) and phenylmagnesium bromide was added. The reaction was stirred at room temperature overnight, however no reaction was observed. This reaction may be affected by steric hindrance at the quaternary centre due to the presence of the TMS group adjacent to the nitrile group, combined with the bulky phenylmagnesium bromide used.



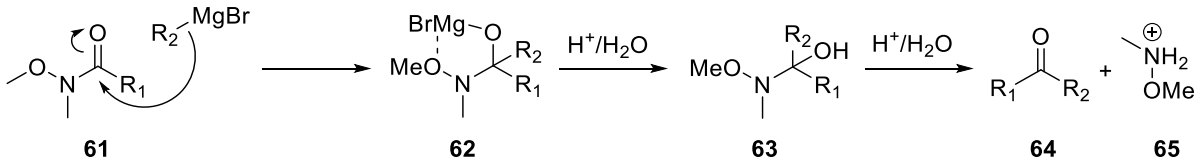
45 **59** **60**

Scheme 13: TMS protection of cyanohydrin **45** followed by attempted nucleophilic acyl substitution using phenylmagnesium bromide.

It has been reported that the use of bulky reactants can often require harsh conditions such as refluxing in high boiling solvents such as toluene, extended reaction times and also excess Grignard reagents.[114] Weiberth *et al.* reported great improvements in yields and shortened reaction times for sterically demanding substrates when the nucleophilic addition was catalysed by a Cu(I) salt. For this reason, sub-stoichiometric CuBr was used in combination with phenylmagnesium bromide to effect nucleophilic addition on protected cyanohydrin **59**. After refluxing overnight in THF, only protected and deprotected starting material were observed.

Towards (S)-Blebbistatin Ketone Derivatives: Weinreb Amide Approach

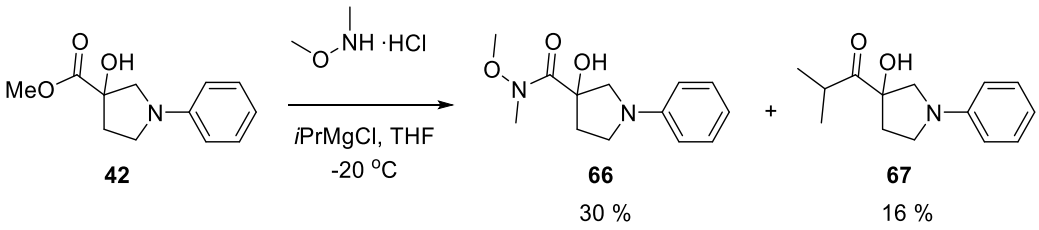
An alternative method of ketone synthesis is to perform nucleophilic acyl substitutions with a Weinreb amide. The advantage of using Weinreb amide derivatives over other carbonyl compounds such as acyl chlorides or esters in reactions involving Grignard reagents is that over-addition will not occur. This is because a stable tetrahedral intermediate (**62**) is formed on addition of the nucleophile, enabling chelation of the metal to the oxygen anion and methoxy group. Due to the stability of this intermediate, an electrophilic carbonyl is not regenerated *in situ* but liberated instead during aqueous work-up (Figure 30).[115]



61 **62** **63** **64** **65**

Figure 30: Mechanism describing the nucleophilic acyl substitution of a Weinreb amide with a Grignard reagent.

Synthesis of Weinreb amide **66** was first attempted using *N*,*O*-dimethylhydroxylamine hydrochloride with *iso*propylmagnesium chloride in DMF (Scheme 14).[116] Initially a yield of 56% was obtained, however following a 4-fold scale-up a significant side reaction occurred generating *iso*propyl ketone **67**. Although unexpected, in some ways this was fortuitous as *iso*propyl ketone **67** is analogous to ketones **26-28** and may be tested for *Pf*MyoA activity. This compound was consequently docked into the SM homology model of *Pf*MyoA and it was not found to preserve the conformation adopted by Bleb in the 1YV3 structure and produced a poor docking score. Therefore, it may be used as a negative control when validating the model experimentally.



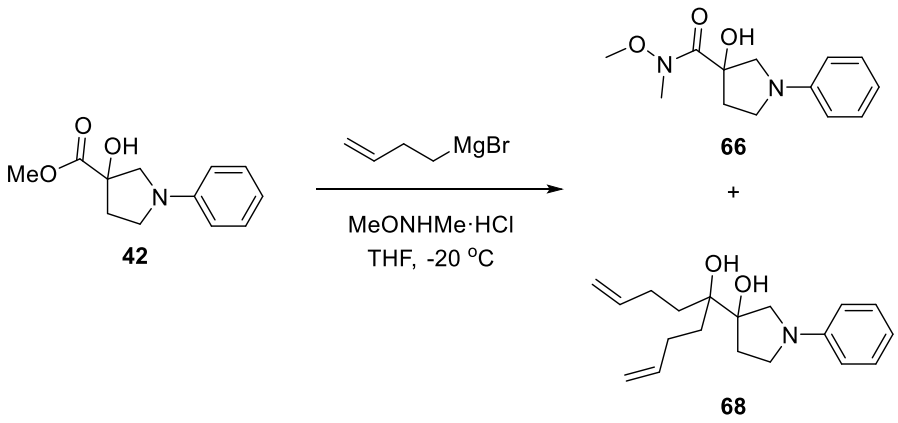
Scheme 14: Synthesis of Weinreb amide **66** on 1.6 mmol scale with side-product *iso*propyl ketone **67** formation.

Formation of this side-product was unexpected as *i*PrMgCl is usually used in this manner as it is a relatively non-nucleophilic Grignard reagent. Two explanations could be possible: either the Grignard reagent is directly attacking the methyl ester (**42**), or it is reacting with the formed Weinreb amide *in situ*. The latter explanation is the most likely as, if nucleophilic addition was occurring on the methyl ester, an uncontrolled reaction would likely occur due to the more electrophilic character of the liberated ketone, causing another addition with the subsequent alcohol formation.

If this was the case, perhaps we could take advantage of this outcome to our benefit. Indeed, a one-pot transformation of esters into ketones via an *in situ* generated Weinreb amide has been reported by Prosser *et al.* in which a less nucleophilic Grignard reagent, such as *i*PrMgCl, is first used to form the Weinreb amide, and then addition of a more reactive Grignard reagent is added in order to generate the desired ketone.[117] They found

that *i*PrMgCl was unreactive towards the forming Weinreb amide, whereas other more nucleophilic Grignard reagents such as methylmagnesium bromide and butylmagnesium bromide were able to form the desired ketone. In our case the *iso*propyl ketone **67** was actually obtained, so if our hypothesis that the Weinreb amide **66** is formed *in situ* and attacked by the excess Grignard reagent is correct, the use of more nucleophilic Grignard reagents should provide the same outcome, furnishing the desired ketones **26-28**.

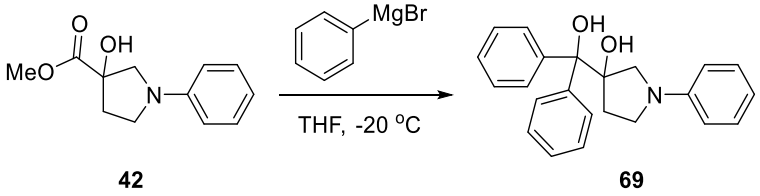
For this reason, a trial reaction following the procedure by Prosser *et al.* was carried out in which methyl ester **42** was combined with *N*,*O*-dimethylhydroxylamine hydrochloride and the nucleophilic Grignard reagent but-3-en-1-ylmagnesium bromide to see if the Weinreb amide would form and react directly with the remaining nucleophile (Scheme 15). After 20 minutes at -20 °C, the Weinreb amide was visible by TLC, and after stirring overnight at room temperature, the starting material had been consumed. Unfortunately, the only products identified were the Weinreb amide **66** and the tertiary alcohol **68** formed as a result of double nucleophilic addition. This suggests that the reaction stopped at the Weinreb amide and the double addition occurred due to excess but-3-en-1-ylmagnesium bromide reacting with unreacted ester, perhaps due to the higher temperature adopted overnight. With better temperature control, this could provide an alternative procedure for Weinreb amide synthesis as it appeared unreactive towards the more nucleophilic Grignard reagent.



Scheme 15: A one-pot procedure used to directly form the desired ketone, which instead lead to double nucleophilic addition generating the tertiary alcohol **68**. Tentative assignment based on ^{1}H and ^{13}C NMR.

This result suggests that the synthesis of *iso*propyl ketone **67** is not occurring as a consequence of amide **66** reacting further with the *i*PrMgCl, but most likely the starting material ester **42** is able to react with the *i*PrMgCl without effecting double addition. Perhaps this is because the first addition of the *iso*propyl group increases steric congestion around the carbonyl carbon, which already has an adjacent quaternary centre, restricting the nucleophilic attack of the second equivalent. This may be coupled with the fact that *i*PrMgCl is a less reactive nucleophile compared to the but-3-en-1-ylmagnesium bromide due to the difference in halide.[118] It was thought that perhaps this reactivity based on steric control could be used to introduce the bulkier phenyl substituent.

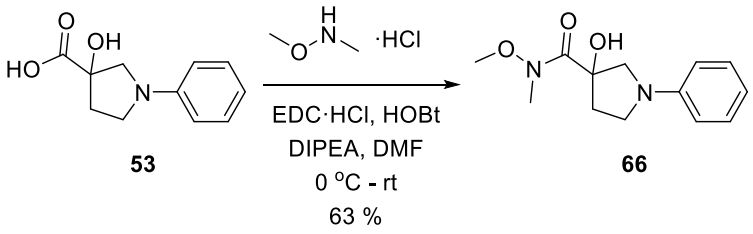
In an attempt to exploit this combination of reactivity and steric control previously observed in the synthesis of *iso*propyl ketone **67**, a reaction was carried out starting from methyl ester **42** and using phenylmagnesium bromide (Scheme 16). The reaction was closely monitored following slow addition of the Grignard reagent at -20 °C and within 12 hours at this temperature the starting material had been consumed, however the major product isolated was the tertiary alcohol **69** formed as a result of double addition. Perhaps the increase in reactivity using the magnesium bromide meant that the steric hindrance following the first addition could be overcome. Alternatively, it could be that the steric effect of the flat phenyl ring is more easily overcome than that of the three-dimensional *iso*propyl group.



Scheme 16: Nucleophilic acyl substitution with phenylmagnesium bromide on ester **42** leading to double addition and formation of tertiary alcohol **69**. Tentative assignment based on ^{1}H and ^{13}C NMR.

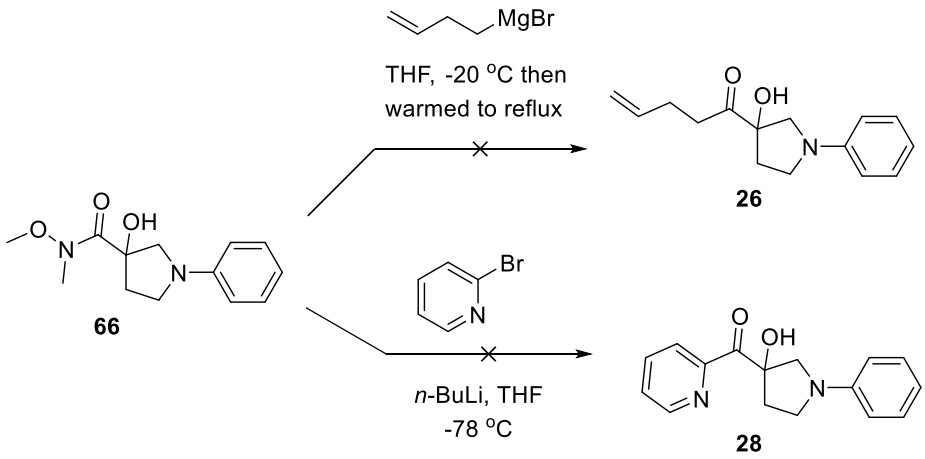
Attention turned quickly back to ways in which the Weinreb amide could be used to effect mono-addition. The use of standard amide coupling conditions from the carboxylic acid **53**

highlighted the superiority of this methodology, since it provided the desired Weinreb amide **66** in good yields (Scheme 17) with no side-product formation.



Scheme 17: Synthesis of Weinreb amide **66** using EDC·HCl amide coupling conditions.

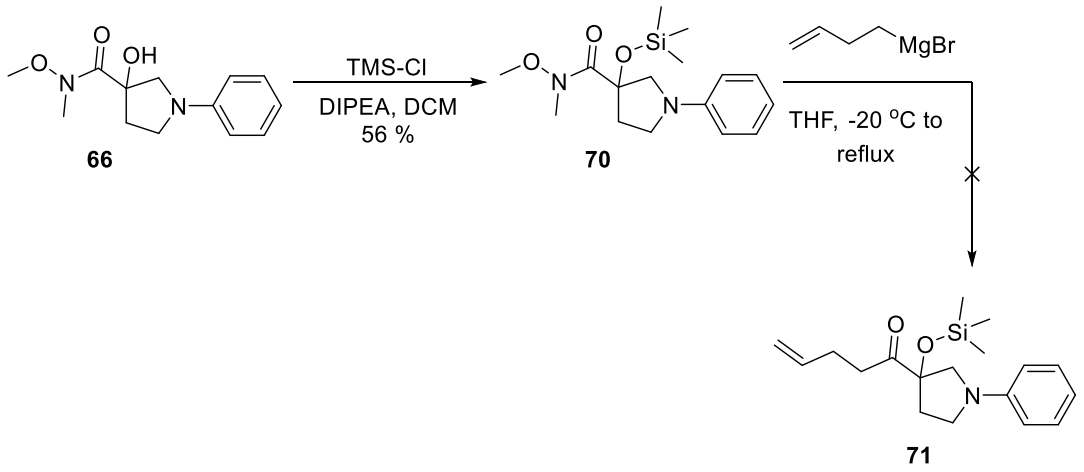
With the Weinreb amide in hand, nucleophilic acyl substitution with but-3-en-1-ylmagnesium bromide was attempted, however only starting material was recovered after refluxing overnight (Scheme 18). This was somewhat expected following the results of the previous experiment in which the Weinreb amide **66** was generated *in situ*. Similarly, when pyridin-2-yllithium (formed via lithium halogen exchange with 2-bromopyridine) was added to Weinreb amide **66**, no reaction was observed and only starting material was isolated. Although it could be argued that in this case this could be due to lithium halogen exchange not occurring, a bright yellow solution was formed during the addition of *n*-BuLi to 2-bromopyridine, suggesting that lithium halogen exchange was indeed happening. Hence it was considered that the nucleophilic addition to the Weinreb amide was the step hampering the reaction instead.



Scheme 18: Attempted nucleophilic acyl substitution of the Weinreb amide **66** to generate ketones **26** and **28**.

This could be because of steric congestion around the carbonyl carbon resulting from the presence of the adjacent quaternary centre and the methylated nitrogen atom. Another possibility is that the basic Grignard/organolithium reagent first deprotonates the tertiary alcohol alpha to the carbonyl, therefore it was decided that the tertiary alcohol should be protected.

A TMS group was chosen as protecting group based on its small size to avoid increasing steric hindrance around the carbonyl carbon, and also the ease of introduction when compared to a more stable but bulkier silyl ether group. Nevertheless, when the TMS-protected alcohol **70** was treated with the corresponding Grignard reagent and allowed to react overnight at room temperature no reaction was observed and forcing the conditions by increasing the temperature only led to deprotection of the silyl group (Scheme 19).



Scheme 19: TMS protection of the tertiary alcohol **(70)** followed by attempted nucleophilic addition of the but-3-en-1-ylmagenesium bromide.

3.2.4. Synthetic Route D – Acyl Anion Equivalents for Ketone Synthesis

Another way in which ketones can be accessed is by temporarily reversing the polarity of the carbonyl group, altering its normal reactivity pattern. This is known as reactivity umpolung and can be used in this case to form acyl anion synthons.[119]

Carbonyls have an electrophilic carbon centre and are therefore susceptible to nucleophilic attack. Reversal of this reactivity is a powerful alternative synthetic strategy to traditional C-C bond-forming methods and is attractive as it enables a whole range of reactions which would be impossible otherwise (Figure 31).[120]

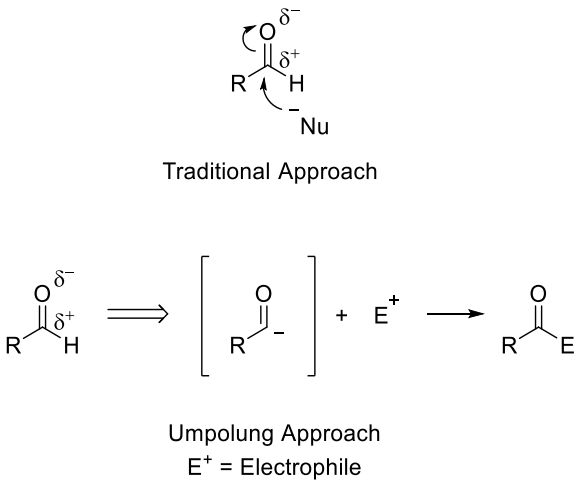


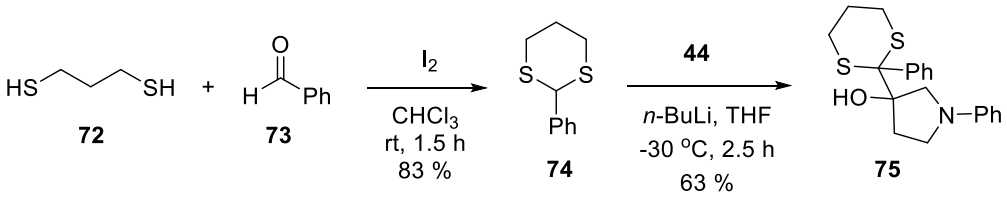
Figure 31: Traditional carbonyl reactivity vs. acyl anion reactivity via the umpolung approach.

Lithiated 1,3-dithiane as Masked Acyl Anion

As acyl anions are known to be unstable, they are traditionally synthesised by functional group manipulation of the corresponding carbonyl compounds followed by stoichiometric deprotonation using strong bases. The best example of this is the Corey-Seebach reaction in which a lithiated 1,3-dithiane is employed as an acyl anion equivalent.[121] These are readily synthesised by deprotonation of the corresponding 1,3-dithianes using an alkyllithium reagent. These lithio-1,3-dithiane derivatives are stabilised by the divalent sulfur atoms

which have greater polarisability compared to oxygen due to increased C-S bond lengths and lower ionisation potential. This also means that the divalent sulfur compounds are more nucleophilic than their oxygen counterparts meaning that they can react with ketones, aldehydes, epoxides, acid derivatives and also alkyl halides without competing elimination reactions.[121]

Therefore, we envisioned the use of the previously synthesised 1-phenylpyrrolidin-3-one **44** as the electrophilic partner for the attack of the corresponding lithio-1,3-dithiane derivative previously prepared from the aldehyde precursor. To this end 2-phenyl-1,3-dithiane (**74**) was selected to be used as a model system for testing this new synthetic route. Thus, synthesis of 1,3-dithiane **74** was achieved starting from propane-1,3-dithiol (**72**) and benzaldehyde (**73**) using catalytic iodine. *In situ* lithiation using stoichiometric *n*-BuLi followed by addition of **44** provided the desired masked ketone **75** in 63% yield (Scheme 20). The final step was to remove the 1,3-dithiane, a crucial and often challenging step due to the stability of dithianes to acids and bases, resulting from the increased nucleophilicity of the sulfur.[119]



Scheme 20: Synthesis of 1,3-dithiane **74** from propane-1,3-dithiol (**72**) and benzaldehyde (**73**), followed by deprotonation with *n*-BuLi and addition of 1-phenylpyrrolidin-3-one (**44**) to generate 1-phenyl-3-(2-phenyl-1,3-dithian-2-yl)pyrrolidin-3-ol (**75**).

Attempted Removal of 1,3-dithiane

There are three general deprotection types which are commonly used in the literature: oxidation, alkylation and metal coordination.[122] There are also many more underdeveloped methods, including protocols based on single-electron transfer (SET)[123] and electro-oxidation.[124] Of these, the most common procedure involves metal coordination with mercury salts, despite the risks to human health and the environment. This method is undesirable as

hydrolysis of the dithiane is the final step towards the desired Bleb analogues, therefore removing all traces of remaining mercury would be paramount for future biological testing which is extremely sensitive to toxic materials. Of most interest were methods which avoided any kind of heavy metal coordination. For this reason, dithiane deprotection was first explored using oxidative conditions.

Oxidative reagents can be used to initially convert a stable sulfide (I) such as that of **75** into a more labile sulfonium ion (**II**) (Figure 32) which, due to the nucleophilicity of the sulfur, can induce ring opening to **III**. This is followed by water-mediated hydrolysis liberating the desired ketone **V**. This mechanism is general for all three methods of dithiane cleavage with the only difference being the type of electrophile used.

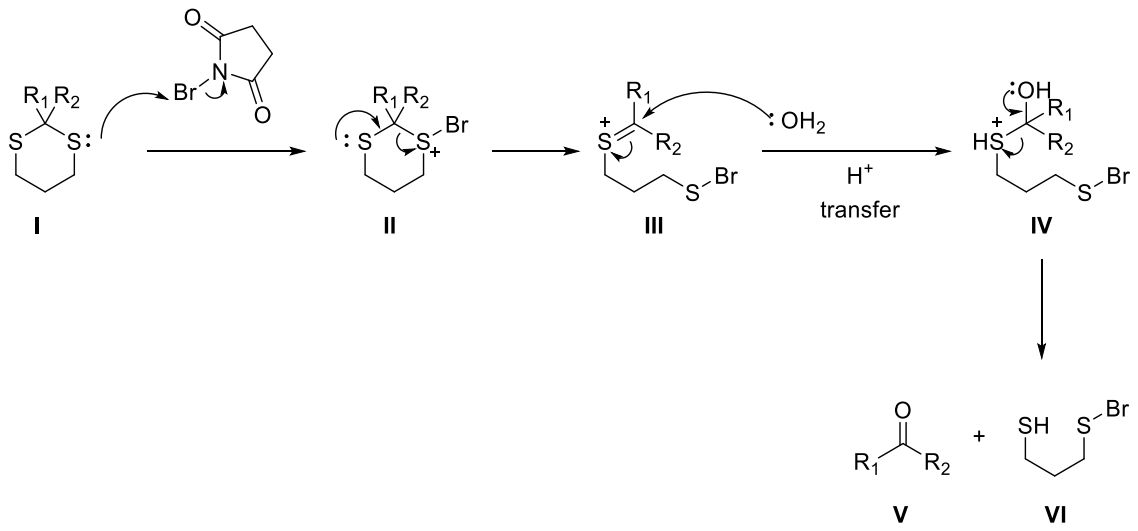
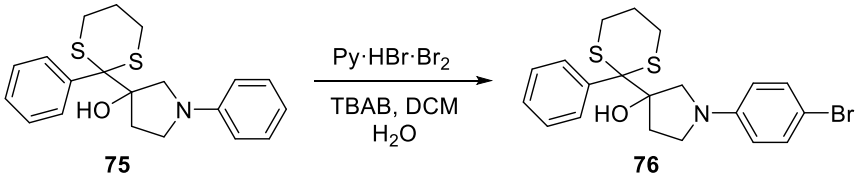


Figure 32: Representative oxidative mechanism for 1,3-dithiane hydrolysis with NBS as the oxidant.

Initially, a solvent-free procedure using *N*-bromosuccinimide (NBS) was attempted, in which the sulfide would be brominated to generate a bromosulfonium intermediate **II** as depicted in Figure 32.[125] The reaction proceeded in a mortar using a pestle to grind together the starting material dithiane **75** with NBS and two drops of water. This appeared to lead to decomposition as the crude ^{1}H NMR showed a complete loss of the *N*-phenyl pyrrolidine signals.

As a milder alternative to this, pyridinium bromide perbromide, a bromine-releasing reagent, was used in a phase transfer reaction in DCM and H_2O in the presence of tetrabutylammonium bromide (TBAB) (Scheme 21).[126] This unexpectedly led to bromination of the *N*-phenyl ring at the *para* position, leaving the dithiane intact (**76**). Unfortunately the same outcome was obtained when iodine was used in the presence of a mild base, leading to exclusive *para* iodination with no apparent reactivity at the dithiane. This could be explained by the increased electron density on the phenyl ring due to the presence of the electron donating nitrogen, as has been observed once before when using Swern conditions to oxidise 1-phenylpyrrolidin-3-ol (**50**) (Figure 28).



75 **76**

Scheme 21: Synthesis of unexpected -*para* substituted side-product **76**. Tentative assignment based on ^{1}H NMR.

Another common method frequently used for dithiane hydrolysis of sensitive substrates is the use of hypervalent iodine reagent, bis(trifluoroacetoxy)iodobenzene (PIFA). In this case, the cleavage would be initiated by nucleophilic attack of the sulfur on the hypervalent iodine and then hydrolysis would occur as previously discussed. This procedure was chosen as it was thought to eliminate the reactivity issue associated with the electron rich aniline moiety, as trifluoroacetic acid (TFA) would be released during the reaction with PIFA, thereby protonating the aniline and protecting the molecule from electrophilic aromatic substitution.[127] However, when the reaction was carried out in a mixture of acetonitrile and water with excess TFA, a complex mixture of products was obtained that discouraged us from further pursuing this method.

To avoid electrophilic halogenating conditions that appeared to be incompatible with the *N*-phenyl group, oxidation of the sulfide bond to the monosulfoxide was attempted using *meta*-chloroperoxybenzoic acid (*m*CPBA) (Figure 33).

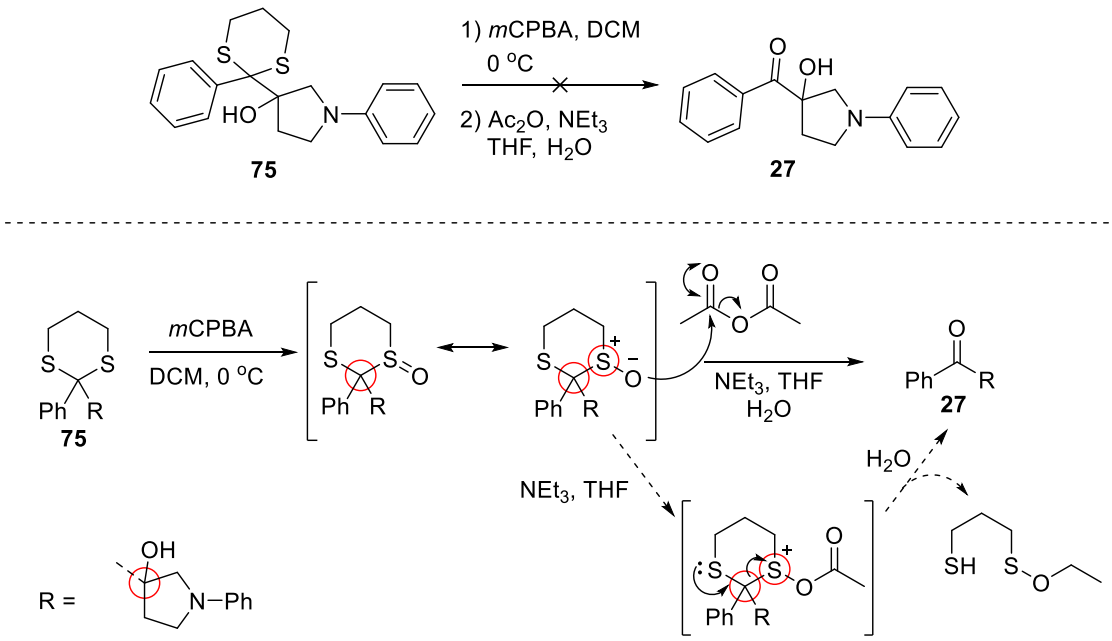
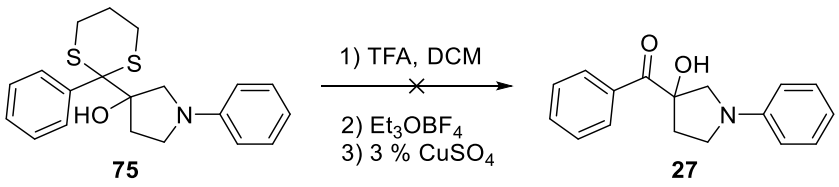


Figure 33: Suggested mechanism for the "Pummerer-like" hydrolysis of dithiane **75**, following sulfide oxidation with *m*CPBA. Stereogenic centres have been highlighted.

Following this, Pummerer-like hydrolysis conditions were employed using acetic acid and triethylamine in THF and water.[128] This resulted in a complex mixture observed from the crude ^{1}H NMR spectrum, which may have been a result of a mixture of intermediate diastereoisomers forming as the reaction progressed. However, no product formation was seen, and some starting material was recovered suggesting that undesired side reactions may be occurring.

In the same way as oxidative hydrolysis, alkylation of the sulfide bond in thioacetals generates sulfonium salts which are good leaving groups and facilitate hydrolysis. The problem with alkylation procedures is the incompatibility of many functional groups prone to alkylation. To prevent *N*-alkylation, the reaction can be carried out in the presence of an acid to initially form a salt. In this case, TFA was used to protonate the amine before the addition of Meerwein's salt, a strong ethylating reagent.[129] Subsequent hydrolysis with copper sulfate and aqueous ammonia was then attempted, however NMR analysis revealed a mixture of products including starting material, but not the desired hydroxy ketone product (Scheme 22).



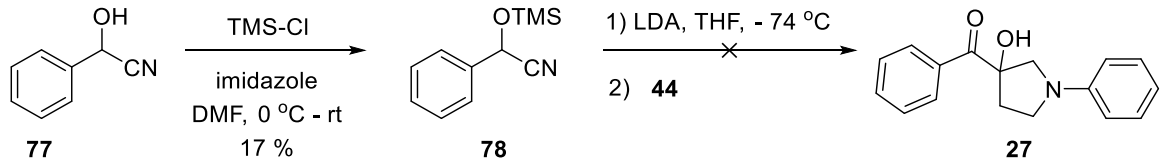
Scheme 22: Dithiane **75** deprotection attempted using alkylation conditions following amine salt formation.

Despite attempts to avoid metal co-ordination methods due to the difficulties with metal removal from final compounds, a method using copper was investigated as copper is far less toxic than mercury, and therefore may be less of an issue for biological assays. A combination reagent made of copper chloride and copper oxide in aqueous acetone was used in an attempt to hydrolyse the 1,3-dithiane moiety.[130] These are mild conditions due to the presence of copper oxide which mediates the reaction preventing an increase in acidity. After several days, no reaction was observed and unreacted starting material was recovered.

Protected Cyanohydrin as Masked Acyl Anion

To avoid the use of dithiane synthesis to generate the acyl anion equivalent, protected cyanohydrins can also be used. In this case the α-carbon of an O-protected cyanohydrin is activated by the presence of the adjacent nitrile group so that when a strong base such as LDA or *n*-BuLi is used, deprotonation can occur generating the desired anion.[131]

Commercially available cyanohydrin **77** was protected with a TMS group with the idea that following generation of the ketone, the alcohol could be deprotected during acidic work-up, followed by cyanide elimination under basic conditions. The protected cyanohydrin **78** was treated with LDA to form the carbanion, before the addition of pyrrolidin-3-one (**44**) and the reaction was kept cold before work-up (Scheme 23). However only starting materials were isolated therefore 1,2-addition did not occur.



Scheme 23: Synthesis of protected cyanohydrin **78** followed by attempted nucleophilic addition of 1-phenylpyrrolidin-3-one (**44**).

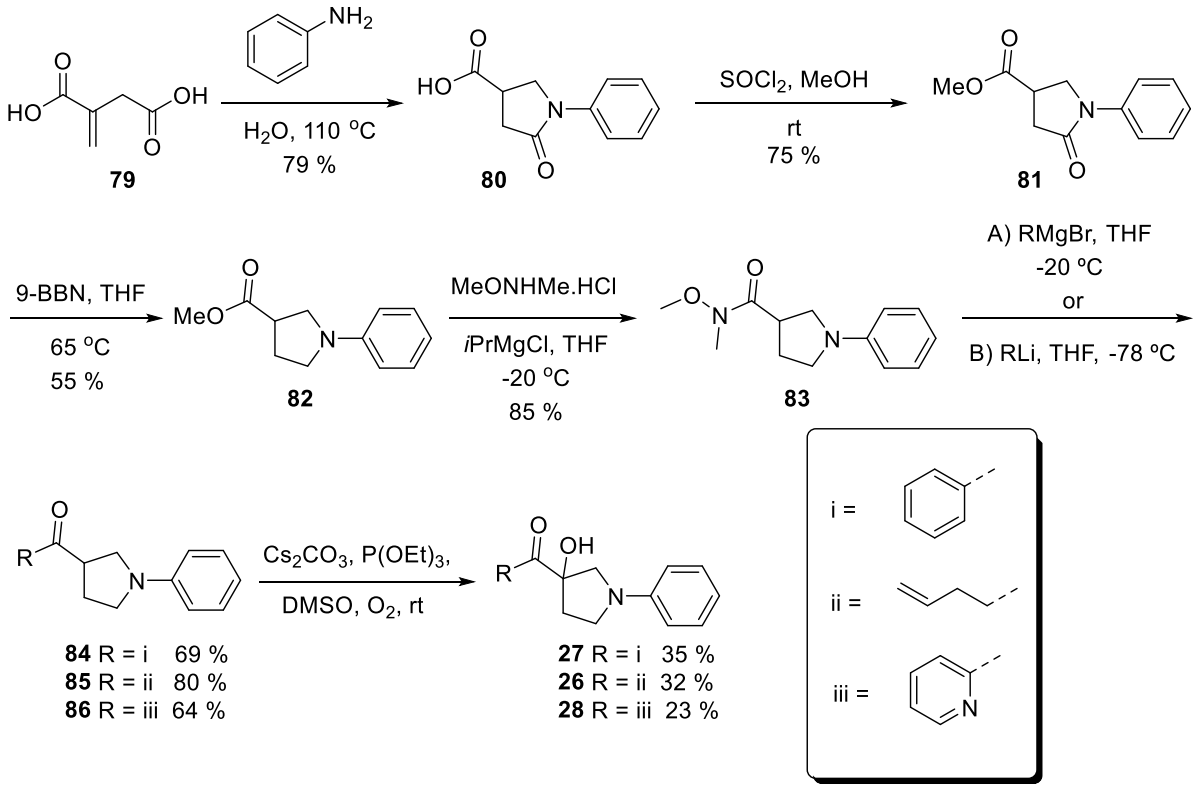
3.2.5. Synthetic Route E - Ketone Derivatives

The next strategy involved evaluating previous methods that had been used and addressing issues that had been unresolved. It was hypothesised that the failings of the Weinreb amide method were due to the steric hindrance around the amide carbonyl as it is flanked by a tertiary alcohol and a methoxylated nitrogen. The alcohol may also be interfering with the Grignard reagents used in the nucleophilic addition, deprotonating and chelating the metal. For these reasons it was decided to synthesise the Weinreb amide without the tertiary alcohol and therefore introduce the alcohol in the final step. It was thought that this may have more success than previous attempts to induce hydroxylation on ester **34** (Scheme 4), due to the higher acidity of the proton alpha to a ketone compared to that of an ester.

Starting from itaconic acid (**79**), the pyrrolidinone ring was formed via condensation with aniline to give carboxylic acid **80**,[132] whose esterification using thionyl chloride in methanol provided methyl ester **81** (Scheme 24). Reduction of the amide using 9-Borabicyclo[3.3.1]nonane (9-BBN) in THF yielded pyrrolidine **82**,[133] which was the necessary precursor for Weinreb amide formation. The use of *i*PrMgCl and *N*,*O*-dimethylhydroxylamine hydrochloride as previously described had far greater success on this substrate without the tertiary alcohol, and generated Weinreb amide **83** in 85% yield.

Nucleophilic addition with the two desired Grignard reagents, and the 2-lithiated pyridine generated by lithium-halogen exchange furnished ketones **84**-**86** in moderate to high yields, validating our hypothesis of the interference of the tertiary alcohol in the reactivity of the Weinreb amide. Final introduction of the tertiary alcohol was achieved using $P(OEt)_3$ with

Cs_2CO_3 in DMSO under an atmosphere of oxygen as previously explored for 1,3-dicarbonyl functionality. These conditions proved effective for the α-hydroxylation of ketones **26**-**28** and provided the desired products as racemic mixtures albeit in low yields.

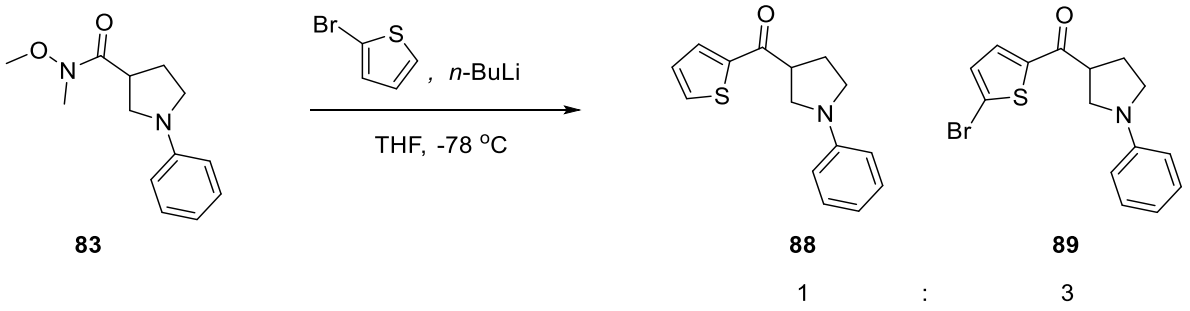


Scheme 24: Synthesis of ketones **26**-**28** from itaconic acid (**79**).

3-Pyridyl and Thiophene Derivatives

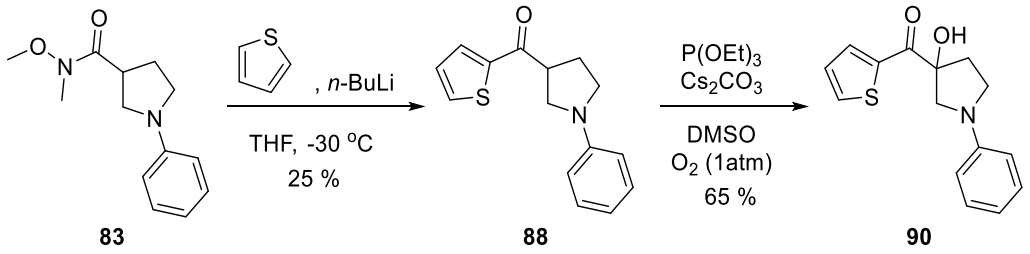
With a straightforward ketone synthesis finally established, we decided to prepare a couple of analogues of the most promising compound to come out of the docking studies, the 2-pyridyl ketone **28**. The 3-pyridyl derivative **87** was envisioned as an interesting derivative, as this would provide a direct comparison to the original 2-pyridyl, keeping the size and hydrogen acceptor the same but varying the nitrogen position on the ring. Additionally, a thiophene ring was selected to replace the pyridyl as it is a smaller heterocycle with a sulfur instead of a nitrogen in the ring. This will be an insightful comparison if the original 2-pyridyl analogue shows activity in the ATPase assay, as this will show whether the nitrogen is necessary as a hydrogen acceptor.

Synthesis of the thiophene analogue was first attempted using 2-bromothiophene with *n*-BuLi to perform lithium-halogen exchange at -78 °C, followed by addition of Weinreb amide **83** as previously reported for derivative **86** (Scheme 25). However the desired thiophene ketone **88** was obtained along with bromothiophene ketone **89** in a 1:3 ratio, indicating that deprotolithiation was favoured when compared to lithium-halogen exchange.



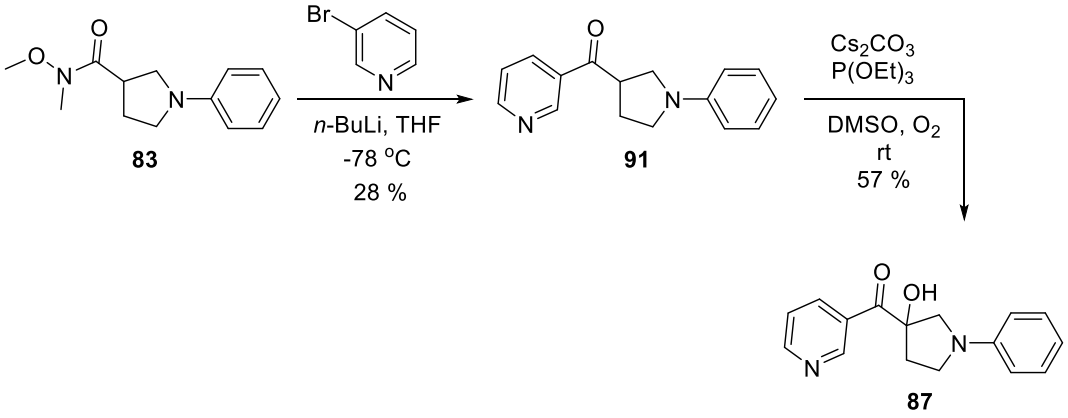
Scheme 25: Synthesis of ketone **88** and side-product **89** when using lithium halogen exchange to introduce thiophene to Weinreb amide **83**.

To overcome this side reaction, the procedure was repeated using thiophene instead, leading to the formation of the pure thiophene ketone **88** (Scheme 26). Although the yield was low, we decided to proceed with the final step since only small amounts of a given compound are needed for biological assessment. α-Hydroxylation was then achieved following previously described conditions to give hydroxylated thiophene ketone **90**.



Scheme 26: Synthesis of thiophene ketone **88** followed by α-hydroxylation.

The 3-pyridyl derivative **87** was prepared successfully using the exact same conditions employed for the synthesis of the 2-pyridyl derivative **28** (Scheme 27).



Scheme 27: Synthesis of 3-pyridyl analogue **87** from Weinreb amide **83**.

3.3. Part 3: Synthesis of 2nd Generation (*S*)-Blebbistatin Analogues

3.3.1. A Structural Biologist's Perspective

While awaiting results from the *Pf*MyoA biochemical assay, a structural biology group headed by Dr Anne Houdusse at the Curie institute was approached. The group has a keen interest in biological motor proteins, with a particular focus on myosin motors.[134–136] In this context, they recently resolved the crystal structure of *Pf*MyoA in the PPS state at a low resolution of 3.45 Å. As a result of this, combined with the fact that these were unpublished results, Dr Houdusse was unable to share the actual structure, but kindly provided us with some structural insights.

She compared our SM model (which had led to the design of the original Bleb derivatives) to the crystal structure of *Pf*MyoA in the PPS state and also the higher resolution structure of MyoVc PPS which has high structural similarity to *Pf*MyoA. She found that the *Pf*MyoA PPS crystal structure was supportive of our initial observation of the SM model that highlighted the smaller binding pocket of *Pf*MyoA compared with MyoII, agreeing that Bleb is too bulky to fit. This was very encouraging since this hypothesis held the rationale for the design of all truncated analogues.

However, one residue was misplaced in the homology model, Phe471. She proposed that this residue is part of a substructure called the switch-II which has a particular conformation in the PPS state. Superimposition of the structure of Bleb bound to *Dd*MyoII with the structure of *Pf*MyoA shows a clash of the Phe471 with a different part of Bleb than previously suggested (Figure 34A). Further support for this hypothesis was obtained as Dr Houdusse compared the structures to that of the PPS of MyoVc which has a tyrosine residue instead of a phenylalanine in this position (Tyr435), and a clash with the pyrrolidine ring of Bleb is also observed (Figure 34B).

Another possible clash may arise from the interaction of Phe270 with the A-ring of Bleb, however in MyoII this residue is a tyrosine that adopts a conformation to avoid the clash when Bleb is bound. Therefore it is likely, since they are both aromatic residues, that the Phe270 of *Pf*MyoA would act in the same way.

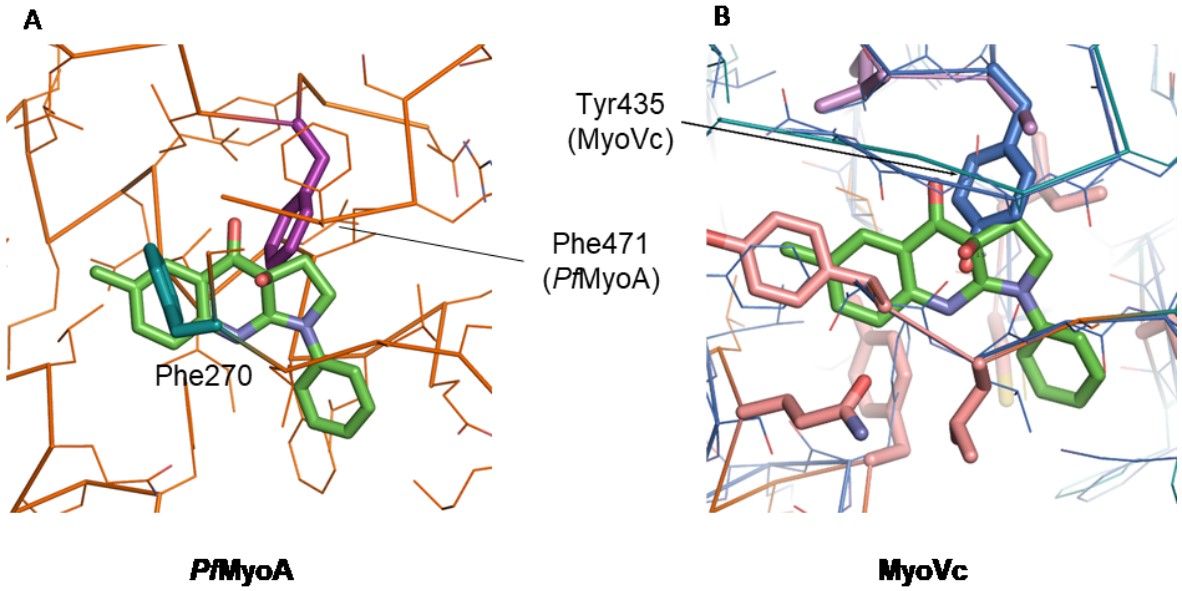


Figure 34A: Structure of Bleb binding site of *Pf*MyoA in PPS state (orange) with Bleb (green) superimposed in 1YV3 conformation with possible problematic residues, Phe471 (purple) and Phe270 (teal) represented as sticks; **B**: Superimposition of *Dd*MyoII bound to Bleb (orange) over the PPS of MyoVc (blue-green). In blue, Tyr435 (the equivalent of Phe471 in PfMyoA) introduces clashes with Bleb and decreases the size of the pocket.

The homology model may have provided an inaccurate representation of the *Pf*MyoA structure as it does not take into account the dynamic nature of the protein and also may not represent the protein in the PPS state. This is important as it is in this state that Bleb is known to trap MyoII at the beginning of the force production event.[137] When carefully studying the homology model, Dr Houdusse noticed that the side chain of the Bleb derivatives is too close to the salt bridge characteristic of the PPS state, and that the phenyl ring occupies a space that would be too close to the γ-phosphate group bound ATP. In order to mimic the way in which Bleb binds to MyoII, the model needs to take into account the conformation of the protein at the time of Bleb binding.

According to these observations, changes should be made to the region of Bleb highlighted in Figure 35. Eliminating this section of the molecule would remove the clash observed between the Phe471 and the tertiary alcohol/ketone moieties. The problem with removing this part of Bleb's structure is that the alcohol and ketone are integral for binding in MyoII, creating key H-bonding interactions. For this reason, instead of simply omitting this part of the molecule, efforts were made to design compounds that were either smaller in size so that they might fit within the smaller *Pf*MyoA cavity, or have greater flexibility to increase the number of possible binding modes.

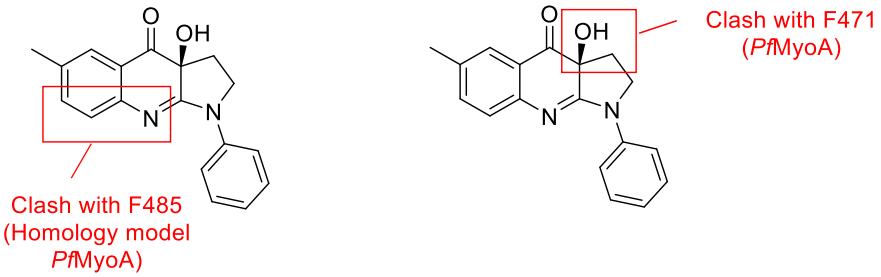


Figure 35: (left) Bleb with the clashes identified with the homology model and (right) Bleb with the clashes identified with the structure of *Pf*MyoA by Anne Houdusse.

Towards this end a 2nd generation of Bleb derivatives were designed (Figure 36). The first group of analogues include molecules that maintain the tricyclic nature of Bleb, but differ due to the size and shape of the D-ring. Smaller aliphatic substituents such as cyclohexyl and cyclopropyl could replace the phenyl group of Bleb to reduce the overall size while maintaining all other important binding interactions. Additionally, phenol **92** in which the middle ring has been opened was envisioned to break the rigidity of the original tricycle. Finally, removal of the *N*-phenylpyrrolidine ring altogether (**93**) could also allow the molecule to fit better in the *Pf*MyoA binding cavity. Synthesis of these compounds was planned to further examine this hypothesis.

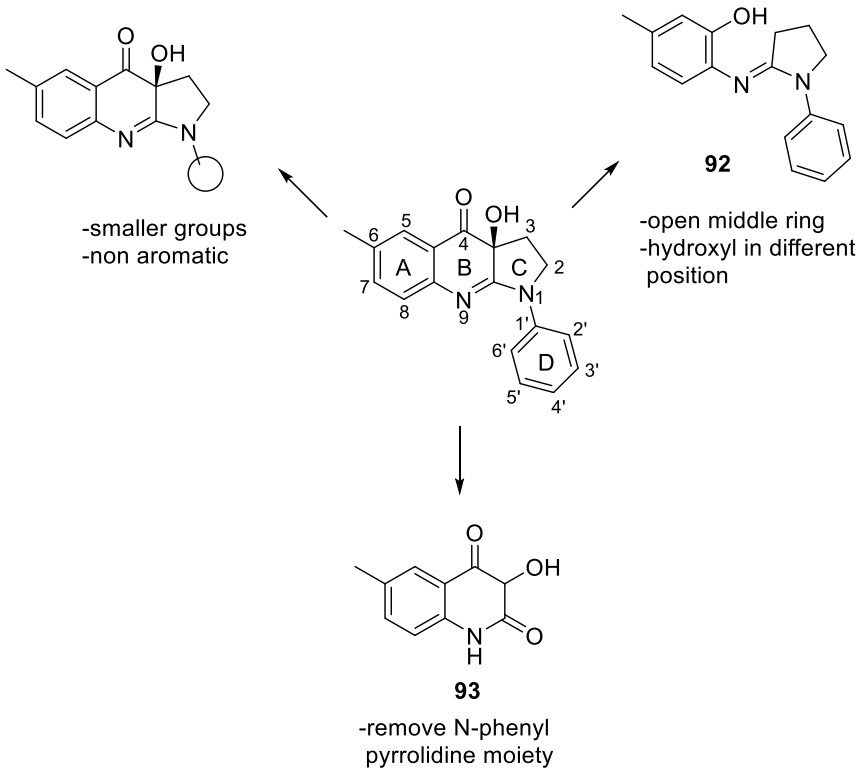


Figure 36: Derivatives of Bleb designed to overcome Bleb clash with Phe471 of *Pf*MyoA proposed by *Pf*MyoA PPS crystal structure.

3.3.2. Synthesis of Derivatives with Smaller Amidine Substituents

Early Stage Derivatisation

Initially, synthesis was focussed on the closest analogues of Bleb with smaller groups attached to the amidine at the N-1 position (Figure 37). The types of groups that were of interest were mostly cyclic aliphatic rings varying in sizes including cyclohexyl, cyclopentyl and cyclopropyl groups as well as *iso*propyl and a simple methyl group.

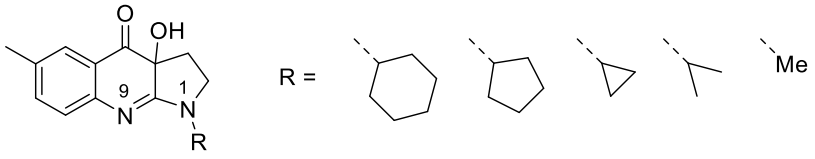
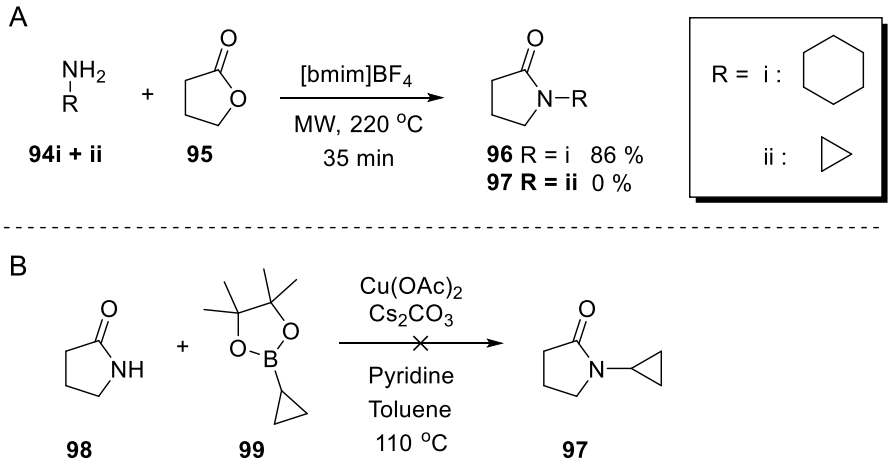


Figure 37: The structure of Bleb with the proposed changes to the N-R group using smaller aliphatic groups.

While there have been a number of publications describing extensions of the Bleb D-ring, very few have explored the synthesis of derivatives with smaller groups at the N-1 position. An exception is the synthesis of Bleb derivatives with varied D-ring heterocycles reported by Lawson *et al.*[63] in which the phenyl ring was replaced with a pyridyl and a thiophene (Figure 11), as well as extensions of the phenyl ring at the 3' and 4' positions. Synthesis of these derivatives involved late stage introduction of the desired heterocycles using coupling conditions optimised for aromatic groups. As there have been no reports on the introduction of aliphatic groups to this position, it was decided to adopt the synthesis route by Lucas-Lopez *et al.*[138] in which construction of the Bleb scaffold started from a building block containing the desired N-1 group.

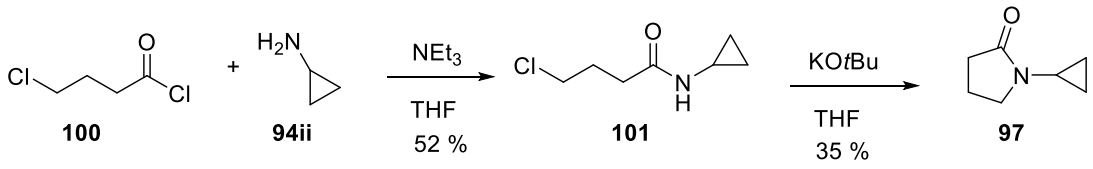
Synthesis of the cyclohexyl pyrrolidinone derivative **96** was achieved by lactamisation of *γ*-butyrolactone (**95**) in an ionic liquid under microwave irradiation (Scheme 28A).[139] This was also attempted using cyclopropylamine, however this led to decomposition. Chan Lam type coupling conditions were also employed in an attempt to achieve N-cyclopropylation (Scheme 28B),[140] however this was also unsuccessful and no product was obtained.



Scheme 28A: Synthesis of 1-cyclohexylpyrrolidin-2-one (**96**) using microwave assisted lactamization conditions from *γ*-butyrolactone (**95**); **B**: Attempted synthesis of 1-cyclopropylpyrrolidin-2-one (**97**) using Chan Lam coupling conditions.

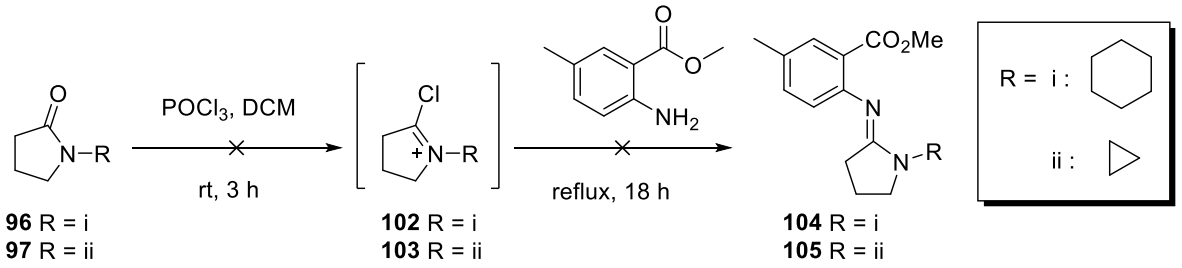
Synthesis of the cyclopropyl intermediate **97** was achieved using a two-step procedure starting from 4-chlorobutanoyl chloride and cyclopropylamine, initially forming amide **101**

under basic conditions (Scheme 29). The ring was closed using potassium *tert*-butoxide to generate 1-cyclopropylpyrrolidin-2-one (**97**) in a yield of 35%.



Scheme 29: Synthesis of 1-cyclopropylpyrrolidin-2-one (**97**) using a 2-step method starting from 4-chlorobutanoyl chloride (**100**).

These pyrrolidinone intermediates **96** and **97** were treated with $POCl_3$ to form Vilsmeier-type intermediates **102** and **103**, and then methyl 2-amino-5-methylbenzoate was added to generate the amidine products (Scheme 30). However, this was unsuccessful for both pyrrolidinone intermediates and only starting materials were recovered. It seemed that either the Vilsmeier-type intermediates were not forming, or the nucleophilic attack of the aniline was not occurring.



Scheme 30: Attempted reaction of pyrrolidinone intermediates **96** and **97** with $POCl_3$ to generate Vilsmeier-type intermediates **102** and **103** that were combined with methyl 2-amino-5-methylbenzoate to form the amidine products (**104** and **105**).

Changes to the reaction procedure were made, including the use of $POCl_3$ in excess rather than stoichiometrically, or the use of a different chlorinated agent such as triphosgene. Additional variations encompassed increasing the length of time of the first step, as well as introducing a base to deprotonate the aniline in the second step. However, all of these modifications were unsuccessful, with only starting materials identified from the reaction mixture.

Previously reported methods for the synthesis of Bleb and analogues thereof, use this approach to introduce the same aniline fragment to the *N*-phenyl-2-pyrrolidinone and the desired amidine is synthesised in moderate to low yields.[138] Verhasselt *et al.* noted that addition of electron withdrawing groups to the aryl amide had a negative effect on the amidine formation yields,[61,63] whereas the use of electron rich 1-(4-methoxyphenyl)pyrrolidin-2-one improved yields significantly, suggesting that electronics of the aryl substituent of the lactam play a significant role in the outcome of the reaction, and perhaps the alkyl amides used were not electron rich enough to allow for the Vilsmeier intermediate to form, or were too unstable as they lacked aryl group stabilisation once formed.

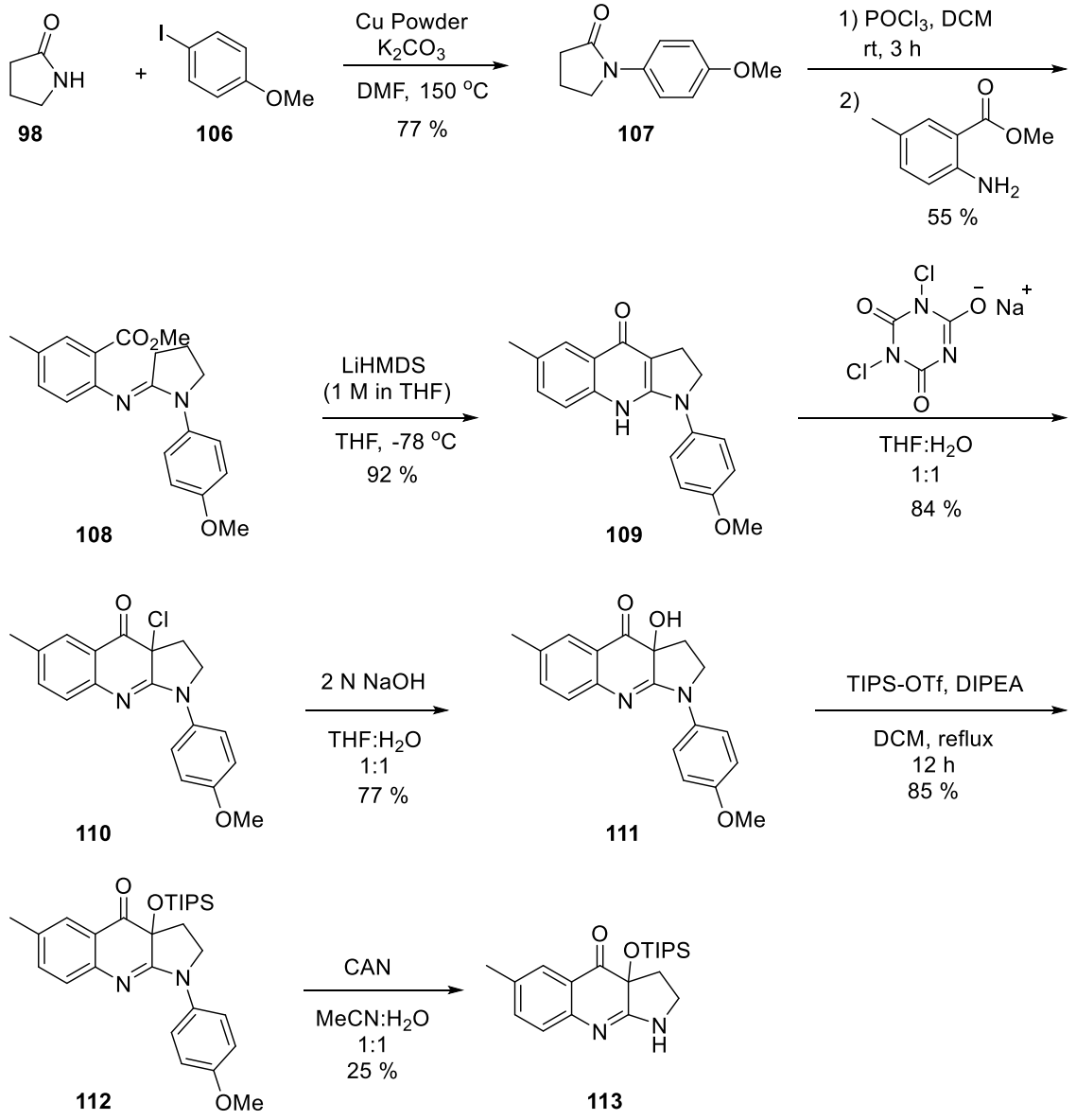
Late Stage Derivatisation

To overcome this issue, the procedure developed by Lawson *et al.* was used, in which a *para*-methoxyphenyl (PMP) group was used to protect the pyrrolidinone nitrogen from the beginning of the synthesis, allowing for late stage PMP removal and subsequent derivatisation of the amidine.[63]

The synthetic route started with a Goldberg coupling of pyrrolidin-2-one (**98**) with 1-iodo-4-methoxybenzene (**106**) to form 1-(4-methoxyphenyl)pyrrolidin-2-one **107** in high yield (Scheme 31).[141,142] Lactam **107** was then reacted with stoichiometric $POCl_3$ to form the Vilsmeier iminium intermediate before the addition of methyl 2-amino-5-methylbenzoate to generate amidine **108**. Cyclisation to quinolone **109** was achieved using excess LiHMDS and α-chlorination was carried out using sodium dichloroisocyanurate. Nucleophilic substitution of the α-chloride with a hydroxyl group using sodium hydroxide generated α-tertiary alcohol **111**, which was protected as a triisopropylsilyl (TIPS) ether (**112**).

Removal of the PMP group using oxidative conditions outlined by Lawson *et al.*[63] proved challenging. They used cerium ammonium nitrate (CAN), which is the most commonly used reagent for effecting this transformation and were able to isolate the desired deprotected amidine **113** in 50% yield. In my hands, consumption of the starting material was observed

after a shorter reaction time and with less equivalents of CAN than reported, however isolation issues led to poor yields of the product, which was often obtained impure despite great purification efforts, with 25% being the highest yield achieved under these conditions.

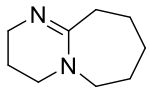


Scheme 31: A 7-step synthesis of amidine intermediate **113** from pyrrolidin-2-one (**98**) and 1-iodo-4-methoxybenzene (**106**) using procedure by Lawson *et al.*[63]

Other methods for removing the PMP group were investigated, including the use of periodic acid with sulfuric acid, and hypervalent iodine reagent $PhI(OAc)_2$, however neither conditions led to PMP group removal.[143] Despite the low yields obtained using CAN, this appeared to be the best method of PMP deprotection for this substrate.

Amidine Alkylation

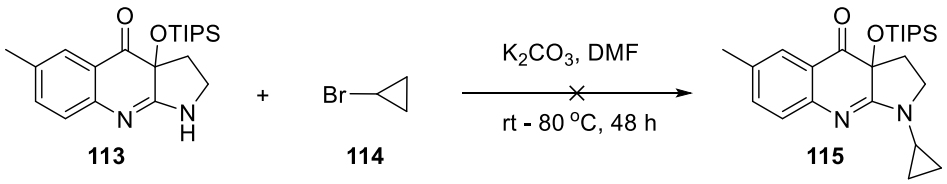
Amidines are the bis-nitrogen analogues of carboxylic acids and esters and are some of the strongest organic bases known with pK_a's above 20. A common amidine base is 1,8-diazabicyclo[5.4.0]undec-7-ene (DBU) (Figure 38) which has a pK_a of 23.9 and is often used due to superior basic properties compared to other types of organic bases.[144] The basicity can be attributed to resonance stability of the protonated forms which are able to delocalise charge over the two nitrogen atoms.[144,145] Due to the high basicity of amidines, there have been limited reports on their nucleophilic potential, and for a long time they were considered non-nucleophilic bases. However more recently, a number of amidines including DBU and closely related guanidines have been used as nucleophilic catalysts in a wide range of transformations including acyl transfer reactions.[144] This shows that some amidines can be strongly basic and nucleophilic in nature.



DBU
pK_a = 23.9 (MeCN)

Figure 38: The structure and pK_a of DBU, a commonly used organic base.

Despite numerous reports on the alkylation of amines, anilines, amides and carbamates, there are very few examples of amidine alkylation. Alkylation of amidine **113** was first attempted by nucleophilic substitution of alkyl halides under basic conditions such as those used for the alkylation of an amine. These types of alkylation conditions have been used with amidines successfully by Wolff *et al.*[146] Initially bromocyclopropane (**114**) was combined with amidine **113** and two equivalents of K_2CO_3 in DMF. After 24 hours at room temperature and then a further 24 hours at 80 °C, the starting material had not reacted and was recovered from the crude mixture (Scheme 32).



Scheme 32: Amidine alkylation reaction using bromocyclopropane with K_2CO_3.

Following this, a stronger base, namely NaH was used to fully deprotonate amidine **113** before addition of the alkyl bromide.[147] Although an immediate change of colour could be observed on addition of NaH, suggesting anion formation, only starting material was recovered after refluxing in the presence of bromocyclopropane (**114**) overnight. It is possible that the anion formed after deprotonation is stabilised by resonance as reported for protonated amidines, making it unreactive as a nucleophile (Figure 39).

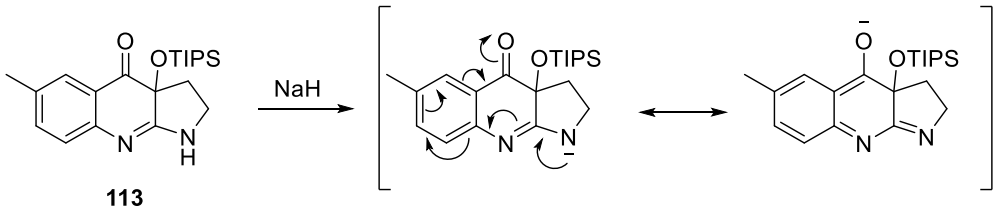
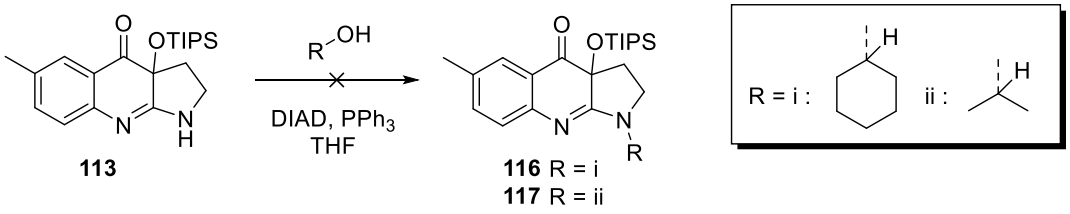


Figure 39: Possible resonance stability of anion formed from deprotonation with NaH.

In a final attempt to push the amidine anion to react with an alkyl halide, MeI, an excellent electrophile was added to amidine **113** after deprotonation. The reaction was then irradiated in a microwave reactor for 10 minutes at 150 °C in a mixture of DMF and THF. After this time, the reaction turned black, and TLC analysis showed mostly starting material with some potential degradation products.

An alternative method for methylation was investigated following a procedure described by Méndez *et al.* in which methylation of an endocyclic amidine was achieved using dimethyl carbonate in the presence of magnesium oxide under microwave irradiation.[148] However when these conditions were employed using amidine **113**, only decomposition of the starting material was observed.

Abarghaz *et al.* reported that alkylation of amidines can be achieved using Mitsunobu conditions.[149] They found that despite the fact that NH amidine systems are relatively less acidic compared to the more explored amide ones, alkylation of primary heterocyclic *N*-acyl amidines can still occur. These conditions have also been used for the alkylation of N,N′-disubstituted formamidines.[150] However, when applied to amidine **113** using either cyclohexanol or *iso*propanol, combined with diisopropyl azodicarboxylate (DIAD) and triphenylphosphine, alkylation was not observed.

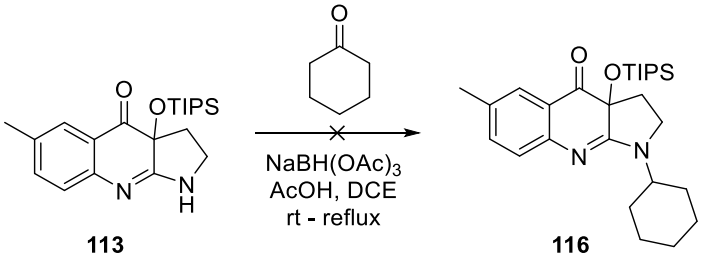


Scheme 33: Attempted alkylation of amidine **113** using Mitsunobu conditions.

Modifications to the procedure were made including preforming the betaine salt, followed by addition of the alcohol and then the amidine. Also, 1,1'-(azodicarbonyl)dipiperidine (ADDP) was used instead of DIAD in order to generate a stronger betaine base to have a better chance of deprotonating the amidine. This has been shown to improve yields for reactions with less acidic nucleophiles.[153] Unfortunately, no reaction was observed in either case and only starting material was isolated.

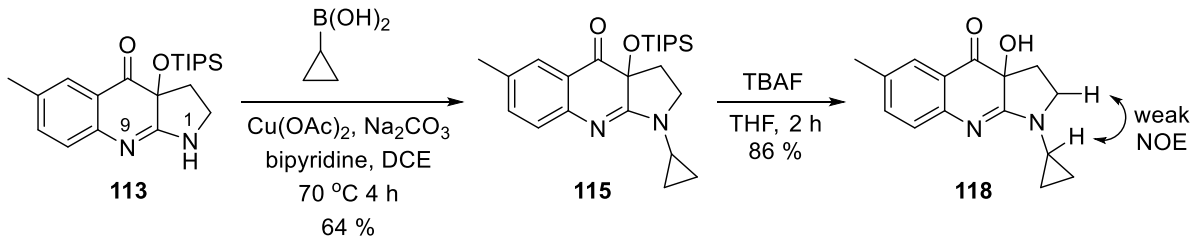
Reductive amination is another common and versatile method for forming C-N bonds, in which an imine is first formed from nucleophilic addition of an amine to a ketone/aldehyde, and this is reduced to produce a new amine. To prevent side reactions with the ketone present in amidine **113**, $NaBH(OAc)_3$ was used as it selectively reduces imines. Reduction of the amidine itself to an aminal was not thought to be an issue as it has been reported that endocyclic amidines are not readily reduced, although experimental data was not provided to explain this.[154] Therefore, following commonly used procedures, cyclohexanone was treated with acetic acid prior to the addition of amidine **113**, and after stirring at room temperature for 30 minutes, the reducing agent was added (Scheme 34). After 12 hours at room

temperature and no observable new product formation, the reaction was heated under reflux for a further 12 hours, however there was no starting material consumption. Due to the high basicity of the amidine, the mildly acidic conditions may have caused protonation, rendering the amidine unreactive as a nucleophile.



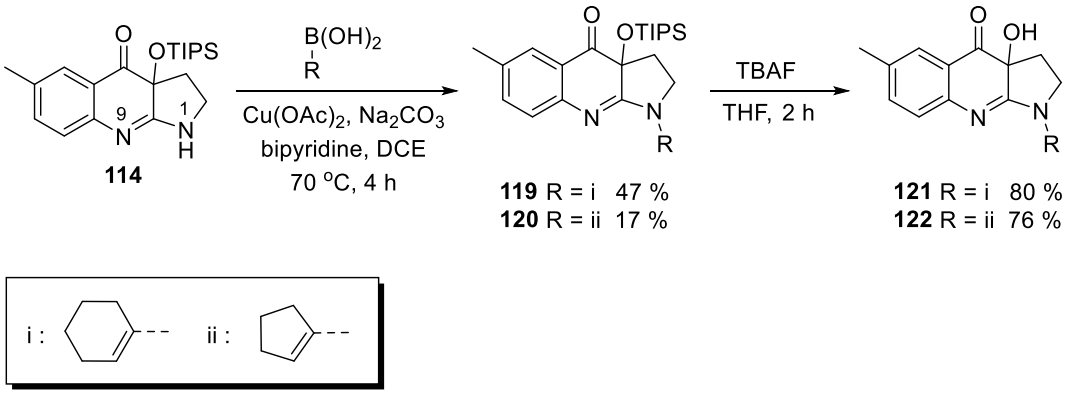
Scheme 34: Alkylation of amidine **113** attempted using reductive amination conditions.

According to Bénard *et al.*, anilines and aliphatic amines can undergo direct N-cyclopropanation using copper promoted Chan Lam conditions.[155] The reactivity of the cyclopropane in this reaction can perhaps be attributed to its highly strained structure, enabling it to behave like a double bond in an alkene, a characteristic sometimes referred to as σ-aromaticity.[156] These conditions were applied to amidine **113** to see if this copper catalysed N-cyclopropanation could be applicable to amidines too (Scheme 35), and fortunately the product (**115**) could be obtained in 64% yield. This was followed by TIPS group removal using tetrabutylammonium fluoride (TBAF) to generate Bleb derivative **118**. The regioselectivity of the N-cyclopropanation reaction was confirmed by NOESY NMR, and the product alkylated at N-1 was the only one observed.



Scheme 35: N-Cyclopropanation of amidine **113** using Chan Lam conditions, followed by TIPS removal using TBAF. Important NOESY correlation has been highlighted.

As the copper catalysed Chan Lam conditions used for the synthesis of cyclopropyl derivative **118** were the only successful conditions found for the alkylation of amidine **113**, we decided to try these conditions while altering the boronic acid to improve chances of successful reaction. An attempted reaction using cyclohexylboronic acid highlighted that alkyl boronic acids are not suitable for the desired transformation, while cyclopropylboronic acid with a sp2-like C-B bond provided the alkylated amidine in good yield. Therefore, we envisioned the use of unsaturated analogues, namely cyclohexenylboronic acid and cyclopentenylboronic acid in the Chan Lam coupling with amidine **113** using the conditions described above. As depicted in Scheme 36, both provided the desired *N*-alkylated amidine products in low to moderate yields. In an attempt to improve the yield, the reaction time was increased but substitution on N-9 was observed instead, complicating the isolation of the desired regioisomer. The TIPS protecting groups were then removed in the same fashion previously described to produce Bleb derivatives **121** and **122**.

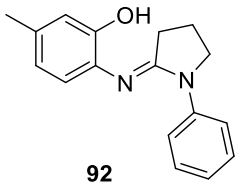


Scheme 36: Synthesis of Bleb analogues **121** and **122** using copper catalysed Chan Lam coupling conditions followed by deprotection of the TIPS protected alcohol.

Although alkene hydrogenation could furnish the target saturated molecules, time constrains, together with the low quantities of the corresponding alkenes obtained hindered any attempt. Nevertheless, since analogues **121** and **122** display the desired structural features for the 2nd generation of Bleb derivatives, they were used anyway.

3.3.3. Synthesis of Open Ring Derivative

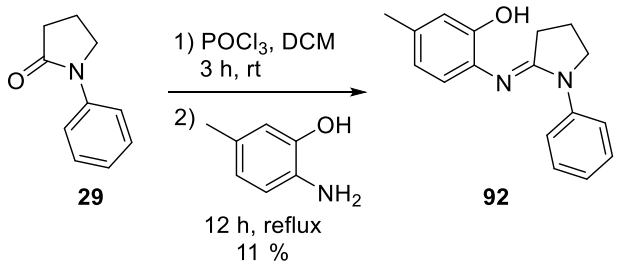
Bleb derivative **92** is of interest as the core amidine structure has been kept intact, while the open middle ring provides the molecule with increased flexibility (Figure 40). Although the carbonyl group that is important for H-bonding of Bleb in MyoII has been removed, a phenol group is present that may provide an alternative interaction point in the MyoA binding site.



92

Figure 40: Structure of Bleb derivative **92**.

Synthesis of Bleb derivative **92** was achieved in a two-step one-pot procedure, starting with *N*-phenyl-2-pyrrolidinone (**29**) forming the chloro-iminium Vilsmeier type intermediate that was then combined with 2-amino-5-methylphenol (Scheme 37).



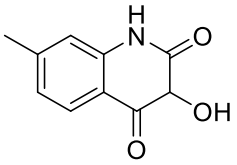
29 **92**

Scheme 37: Synthesis of Bleb intermediate **92** from *N*-phenyl-2-pyrrolidinone and 2-amino-5-methylphenol via a Vilsmeier type chloro-iminium intermediate generated by $POCl_3$.

3.3.4. Synthesis Towards Quinolone Derivative

Bleb derivative **93** was designed to have a much smaller core structure than that of Bleb (Figure 41). While the left-hand side aromatic ring remains intact, the middle ring contains an amide in the place of the amidine and the *N*-phenyl pyrrolidine moiety has been removed

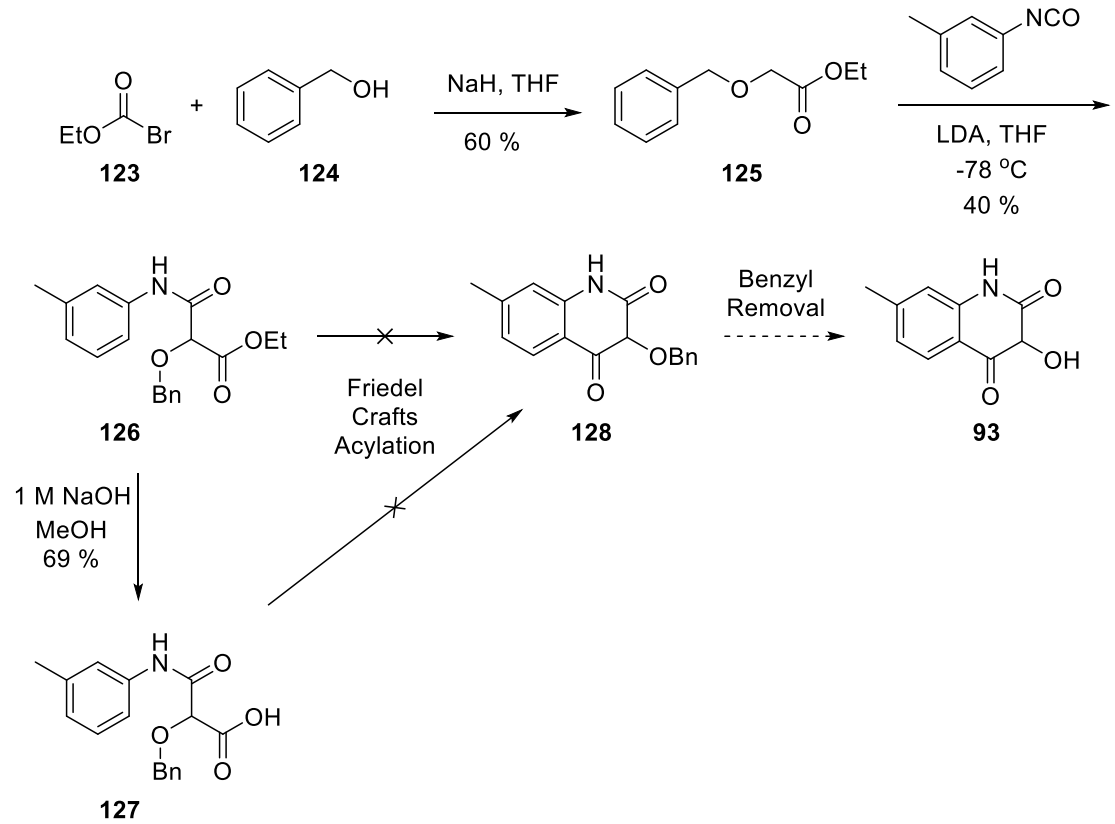
completely. Conversely, the carbonyl group and the adjacent alcohol have been maintained which may provide the key H-bonding interactions for Bleb binding to MyoII.



93

Figure 41: The structure of Bleb derivative **93**.

Synthesis towards Bleb derivative **93** started with the nucleophilic substitution of ethyl carbonobromidate (**123**) with benzyl alcohol (**124**) to form benzyl ether **125**. Under strong basic conditions, the enolate of ester **125** was formed and combined with 1-*iso*cyanato-3-methylbenzene to generate amide ester **126** (Scheme 38).



Scheme 38: Synthesis towards Bleb derivative **93** starting with benzyl protection of ethyl carbonobromidate (**123**), followed by nucleophilic addition to 1-*iso*cyanato-3-methylbenzene. Following successful ring closure, the benzyl group will be removed.

To close the ring, several Friedel Crafts acylation conditions were attempted. Firstly, ester **126** was refluxed in 1,2-dichlorobenzene for 6 hours as described by Yongjun *et al.* for the synthesis of a closely related tetrahydroquinolone with an α-cyano group rather than an α-benzyl ether.[157] Perhaps the failure in this case was due to the presence of the electron donating α-benzyl ether compared to the electron withdrawing cyano group, which could render the ester carbonyl carbon less electrophilic.

Subsequently, conditions employed by Moon *et al.* were used in which Lewis acid $AlCl_3$ was combined with ester **126** to increase the electrophilicity of the ester carbonyl carbon, and the reaction was heated at 120 °C in chlorobenzene. This however lead to decomposition of the starting material.[158] In a last effort, ester **126** was hydrolysed and the resulting carboxylic acid **127** was treated with Eatons's reagent, following a method described by Blackburn *et al.*[159] Unfortunately, decomposition of the starting material was also observed in this case, and due to time constraints, the preparation of derivative **93** couldn't be pursued further. Given more time, the acyl chloride would have been synthesised and combined with a range of Lewis acids known for promoting Friedel-Crafts acylation reactions, and following successful ring closure, cleavage of the benzyl group would be carried out by hydrogenation over a palladium catalyst to generate derivative **93**.

In total, 16 compounds (Figure 42) have been synthesised for assessment of *Pf*MyoA activity and effect on parasite growth and invasion.

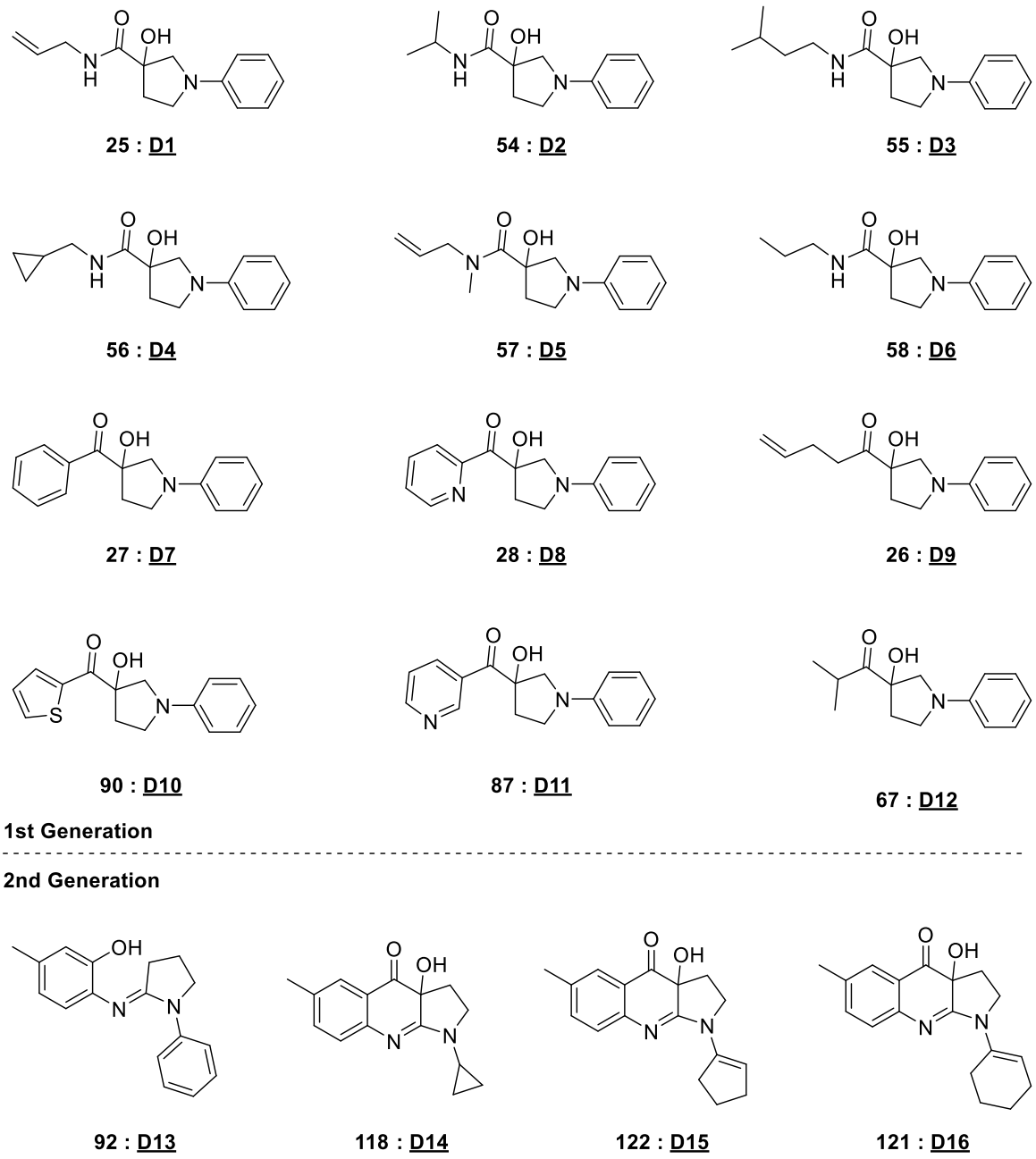


Figure 42: The Bleb derivatives submitted for biological testing to assess their effect on the parasite invasion and growth, and *Pf*MyoA ATpase assay. Numbering system used for biological testing.

3.4. Part 4: Biological Assessment

3.4.1. Invasion and Growth Inhibition Assays

To assess the effect of the Bleb derivatives directly on *P. falciparum* parasite invasion, an invasion inhibition assay (IIA) was initially carried out by Tom Blake of Professor Jake Baum's group at Imperial College. This began with purification of merozoites, the blood-stage invasive form of the parasite, by filtration of ruptured schizonts, from which merozoites were released. They were subsequently added to RBCs in the presence of each drug and left to invade for 40 minutes, followed by quantification of parasitaemia using flow cytometry. This involved staining the infected RBC's with SYBR Green I, a DNA specific fluorescent dye, and flow cytometry data was then collected by fluorescence-activated cell sorting (FACS). As SYBR Green I adheres only to double-stranded DNA, any fluorescence detected was attributable to parasite DNA since mature erythrocytes do not contain DNA or RNA.[160]

Bleb derivatives **D1**-**D16** were tested in this IIA assay and the percentage parasitaemia was compared to treatment with actin inhibitor CytoD, used as a positive control, and a DMSO only negative control. None of the compounds appeared to impede invasion, as parasitaemia was unaffected compared to the negative control (Figure 43A). This suggested that the compounds may not inhibit *Pf*MyoA in parasites, which, for the 1st generation of derivatives (**D1**-**D9**), was not surprising considering the information provided by Dr Houdusse. In one of the experiments, Bleb appeared to increase parasitaemia which contradicts a previous study by Zuccala *et al.* which showed that Bleb has no reproducible effect on merozoites.[47] Since this result was not replicated when Blebbistatin was tested in the second assay, it is likely that this result was an anomaly.

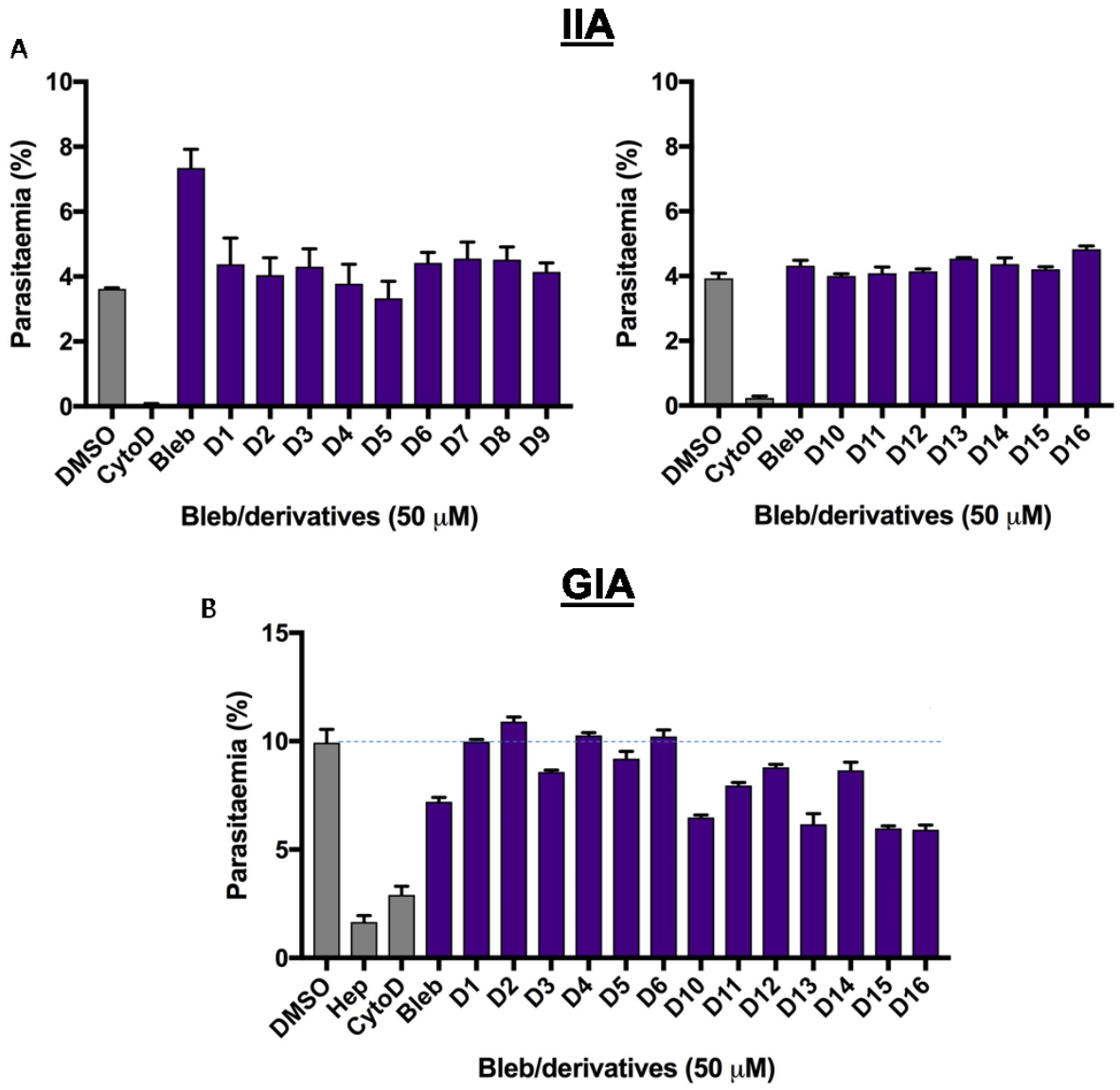


Figure 43**A**: When treated with compounds **D1**-**D16** (50 μM), the invasion of RBC's by purified merozoites is not affected; **B**: Compounds **D1**-**D6** also had no effect on late stage schizonts while compounds **D10**-**D16** appear to cause a growth defect, with **D10**, **D13**, **D15** and **D16** reducing parasitaemia to a greater extent than Bleb. For A and B: Single biological replicates, each with three technical replicates, ± S.D. of technical replicates. (unpublished data by Tom Blake from the Baum group).

To screen for inhibitory effects on parasite replication more generally, including non-invasive processes, a growth inhibition assay (GIA) was also used to test Bleb and thirteen of the derivatives. In this assay, the drugs were added to synchronised late-stage schizonts which were then allowed to invade RBC's for 16 hours. Following this time, the percentage parasitaemia was quantified by flow cytometry as previously described.

Interestingly, this revealed that addition of Bleb to schizonts reduces parasite replication by 50%. This effect appears to be exclusive for this stage, with drug addition to rings and early and late stage trophozoites showing a much lesser effect on replication. (unpublished data by Tom Blake from the Baum group). Compounds **D1**-**D6** did not appear to affect parasitaemia when compared to the DMSO control (Figure 43B), which correlated with the results from the IIA. In contrast, compounds **D10**-**D16**, which are two ketone derivatives of the 1st generation and all of the 2nd generation derivatives, showed some inhibition of parasitaemia at 50μM. Furthermore, four of the compounds affected parasitaemia to a greater extent than Bleb.

Since these compounds do not inhibit parasitaemia in the IIA, a possible explanation for this effect is that these compounds may target a myosin or another off-target protein responsible for processes outside of invasion, that is still essential for parasite development. Additionally, the close structural relationship between these compounds and Bleb may lead to a similar mode of action, and they may cause similar growth defects in late stage schizonts that is not evident in merozoites. In order to confirm whether these compounds do indeed target the invasive motor, a biochemical assay was required to directly assess the effect of these derivatives on *Pf*MyoA.

3.4.2. *Pf*MyoA ATPase Assay

Based on the knowledge that actomyosins require ATP hydrolysis for activation, an ATPase assay was developed by Linda Makhlouf of Professor Jake Baum's group at Imperial College London to screen the Bleb derivatives for *Pf*MyoA activity. This assay is an NADH coupled ATPase assay which means that it provides a readout of oxidised NADH produced when ATP is regenerated following hydrolysis. Briefly, following ATP hydrolysis by actomyosin, a regeneration system uses pyruvate kinase (PK) to convert phosphoenolpyruvate (PEP) and ADP into pyruvate and ATP respectively (Figure 44). Subsequently, lactate dehydrogenase (LDH) converts the pyruvate to lactate which leads to

oxidation of one molecule of NADH. As NADH absorbs light at 340 nm, its decrease over time during an assay can be detected and is proportional to the rate of steady-state ATP hydrolysis. Hence, if the Bleb derivatives inhibit *Pf*MyoA, this process is disrupted and the decrease in NADH absorbance would be slower, correlating with a decrease in ATP hydrolysis and myosin activity.

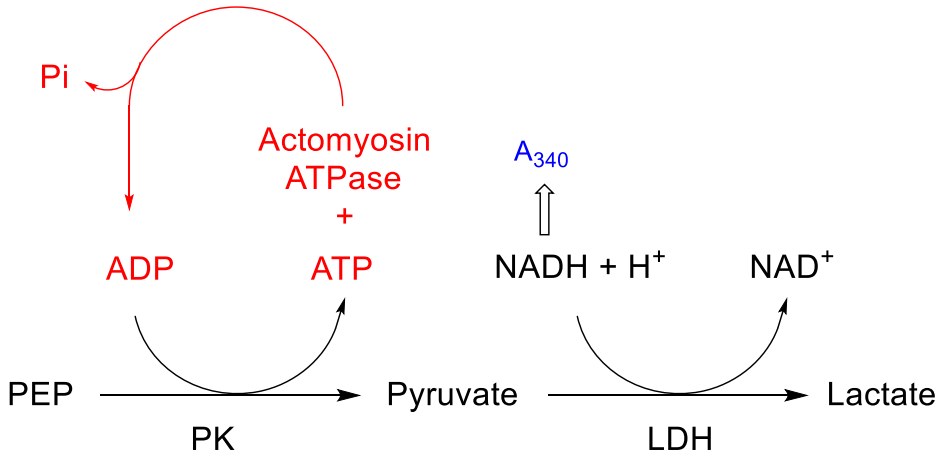


Figure 44: NADH oxidation coupled ATPase assay used to determine actomyosin ATPase activity after treatment with inhibitor.

To quantify the NADH absorbance readings, the Beer-Lambert Law was used to convert, NADH absorbance into concentration which is also the ADP concentration as they are proportional. The increase in ADP concentration (equivalent to the decrease in NADH concentration) was plotted over time and the gradient of the linear fit gave the ATP hydrolysis rate (µM/sec). This value was divided by the concentration of *Pf*MyoA complex per well to give the ATP hydrolysis rate with respect to the enzyme. Normalisation was then carried out to convert the values to relative percentage activity compared to the DMSO only control at 100%.

So far, the ATPase activity with Bleb and derivatives **D1**-**D4** and **D11**-**D16** has been tested, which include six of the 1st generation of derivatives and all of the 2nd generation compounds. Interestingly, and somewhat unexpectedly, Bleb appears to inhibit *Pf*MyoA by almost 50% (Figure 45). This is in contrast with the findings of the IIA in which Bleb does not

inhibit invasion of merozoites (Figure 43A), the form of the parasite where *Pf*MyoA has been shown to play a key role in invasion. In addition, **D1** appears to also inhibit *Pf*MyoA activity to a similar degree as Bleb, while the remaining derivatives do not inhibit *Pf*MyoA compared to the DMSO only control. However, compounds **D14** and **D16** seem to reproducibly activate *Pf*MyoA, with almost double activation compared to the DMSO only control in the case of **D14** (Figure 45). Further studies would be required to investigate this effect such as variation in the drug concentration to generate a dose response.

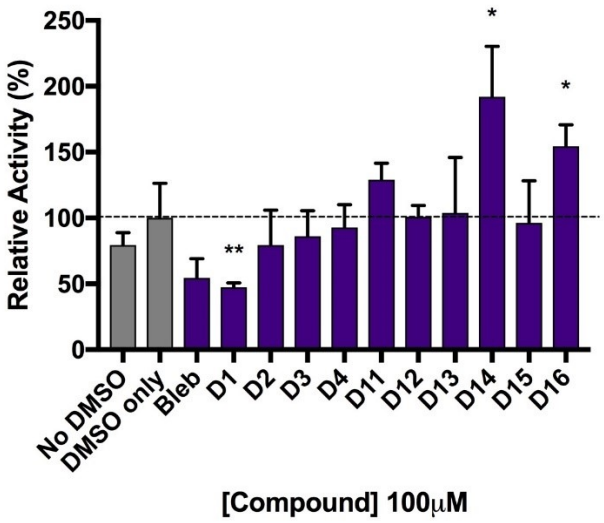


Figure 45: The *Pf*MyoA ATPase activity of Blebbistatin derivatives **D1**-**D4** and **D11**-**D16** (100μM) relative to the DMSO only control. Bleb and compound **D1** appear to inhibit *Pf*MyoA activity, while the remaining compounds show no inhibition of activity. Compounds **D11**, **D14** and **D16** show a significant increase in activity. This assay was carried out in triplicate and the data is representative of the mean ± SEM of triplicates. Statistics: unpaired t-test, *; $p<0.05$, **; $p<0.01$.

Since Bleb has been shown to inhibit the activity of *Pf*MyoA to some extent, but does not inhibit the invasion of merozoites, it is thought that a greater disruption to *Pf*MyoA would be required before the motor fails to support invasion. Derivative **D1** also inhibits *Pf*MyoA activity but does not inhibit parasitaemia in the IIA, therefore a derivative with much greater *Pf*MyoA potency than both these compounds may be needed to affect invasion.

In addition to this, the results of the GIA assay suggest that Bleb may also be acting on a myosin that is responsible for a process outside of invasion but still necessary for blood stage parasite development. This could be parasite egress, early growth or late

development, as the window tested in the GIA means that inhibition must occur in the last few hours of the growth cycle, or the first 24 hours of the next growth cycle (see Figure 3 for blood stage cycle).

It has been postulated that *Pf*MyoE could be sensitive to Bleb. This myosin is primarily expressed in late stage schizonts and has also been suggested to associate with the *Pf*MyoA motor complex, which only assembles in late stage parasites.[161] This aligns with the stage of parasite development in which Bleb and several derivatives have been shown to inhibit growth. Furthermore, *Pf*MyoE is significantly upregulated in parasites presented in patients with severe malaria, suggesting that it may have a role in severe disease pathogenesis.[162]

In order to rationalise this hypothesis, the structural models of the six *Plasmodium* myosins were created by the Baum group and the putative Bleb-binding sites were compared with that of Bleb-sensitive MyoII and Bleb-resistant MyoV. It was found that the resistance of Bleb to MyoV could be rationalised by the presence of a bulky aromatic tyrosine residue in the Switch II in the place of a small serine residue in MyoII. All but one of the *Plasmodium* myosins also have bulky aromatic residues in this position, while *Pf*MyoE has a small *iso*leucine residue (V. Chapman, unpublished data). It has been postulated that as a result of structural similarities between *Pf*MyoE and MyoII and divergence from the structures of other *Plasmodium* myosins, that *Pf*MyoE may be Bleb-sensitive, and therefore closely related Bleb derivatives may inhibit this myosin too. Hence this could also explain the GIA inhibitory effect of structurally similar 2nd generation compounds **D13-D16**. 1st generation ketone derivatives **D10-D12** also show exclusive inhibition of parasitaemia in the GIA. Since these were the only ketone derivatives of the 1st generation tested in the GIA, it would be interesting to see if ketones **D7-D9** show similar inhibition of parasitaemia, as this could indicate a trend in favour of this functional group, over compounds with the amide in this position (**D1-D6**).

3.5. Conclusions and Future Work

Using structure guided design, inhibitors of *Plasmodium* invasion motor, *Pf*MyoA, were designed, initially based on a homology model and then based on knowledge of the crystal structure. In total, 16 compounds were synthesised, and were tested for *Pf*MyoA activity and effects on parasite growth and invasion. In contrast to the original hypothesis of Bleb-resistance in *Pf*MyoA, it was found that Bleb, as well as one synthesised compound, **D1**, were the only compounds to inhibit *Pf*MyoA activity. With neither compound showing any effect on merozoite invasion, it is suggested that greater *Pf*MyoA potency may be required to disrupt the sophisticated invasion motor.

These moderate affinity *Pf*MyoA inhibitors, Bleb and compound **D1** could be further assessed to obtain dose response curves and IC_{50} values. Since a biochemical assay has now been developed and the crystal structure will soon be available, these compounds could be optimised iteratively based on acquired SAR, or co-crystallised with *Pf*MyoA for more rational structure-based drug development.

Interestingly, Bleb and the 2nd generation derivatives cause a growth defect when added to late stage schizonts. It is therefore hypothesised that they may inhibit *Pf*MyoE a myosin predicted to bear structural similarities to Bleb-sensitive MyoII. While there is currently no available data on the specific function of *Pf*MyoE, from these studies it is thought that it may have a role outside of invasion, essential for parasite growth or replication. From a drug development viewpoint this may provide a suitable new target for drugs that are based on the structure of Bleb.

More studies would be required to elucidate the mode of action of Bleb and the derivatives, followed by the development of a *Pf*MyoE biochemical assay if this myosin is identified as the target. Furthermore, to address the selectivity of the derivatives, assessment of their MyoII activity would be required. Future approaches may include iterative structural changes

of these derivatives for optimisation of the growth defect observed in late stage schizonts, coupled with modifications designed to minimise inhibition of MyoII.

PART 2

Synthesis of Fluoroquinolone Derivatives as Inhibitors of RSK4 for a Novel Therapeutic Treatment of Lung Cancer

4. Introduction

4.1. Lung Cancer

Cancer is a disease caused by an uncontrolled division of abnormal cells in any part of the body. These cells can spread to and invade surrounding tissue, as well as travel to distant parts of the body via the blood stream or lymph system (metastasis), leading to widespread tumour growth. Globally, nearly 1 in 6 deaths are caused by cancer which in 2015, equated to 8.8 million people. There are more than 100 different types of cancer, and each is distinguished by the type of cell that is originally affected.[163]

Lung cancer is responsible for the majority of global cancer deaths. In 2015, it had a 20 % mortality rate amongst cancer patients in the UK and studies have shown that it is the second most common cancer for both men and women, exceeded only by prostate and breast cancer.[164] Over the last 40 years the number of lung cancer cases have declined, however the mortality rate has remained almost constant with only 1 in 3 patients surviving for one year following diagnosis and as few as 5 % surviving for 10 years.

There are two major histological subtypes of lung cancer as classified by the WHO: non-small cell carcinoma (NSCLC) which is the most common type of lung cancer with an incidence rate of 80 - 85 %, and small cell carcinoma (SCLC) with a much lower incidence rate of 10-15 %.[165] NSCLC is further subdivided into three classes which include large cell and squamous cell carcinoma which occur in the lining of the bronchi and develop from epithelial cells, and adenocarcinomas which develop from glandular tissue in the outlying areas of the lung and make up around 40 % of lung cancers.[166] SCLC may be less common but it can spread more quickly to other parts of the body, therefore has a higher mortality rate than NSCLC.

A major challenge facing physicians is the generally asymptomatic nature of lung cancer in the early stages of the disease. This means that by the time the patient has a diagnosis, only

18 % of primary tumours will not have metastasised to other parts of the body.[165] Poor prognosis is common due to late diagnosis resulting in the disease having already progressed past the point of possible surgical intervention. Additionally, resistance of cancer cells to conventional chemotherapeutic treatments is another challenge facing cancer research today and contributes to the lack of success in treating lung cancer patients.[167]

4.1.1. Lung Cancer Pathogenesis

Tumorigenesis can be characterised by a multistep process in which normal cells undergo genetic mutations which lead to violation of tissue homeostasis, enabling the formation of a malignant tumour.[168] These mutations can result in: independent control of growth signals, immunity to anti-growth signals, uncontrolled cell proliferation, resistance to programmed cell death known as apoptosis, angiogenesis and invasion of surrounding tissue and metastasis to other parts of the body.[169] A combination of genetic and epigenetic processes occurring in the respiratory epithelium leads to lung cancer of which there are many potentially responsible risk factors classed as either behavioural, environmental or genetic.[166]

There have been numerous studies of the specific genes and signalling pathways involved in the pathogenesis of lung cancer and these have shown that multiple (more than 20 per tumour) epigenetic and genetic alterations are strongly implicated.[170] Some of the main signalling pathways identified include growth promoting networks such as the epidermal growth factor receptor (EGFR) pathway made up of receptor tyrosine kinases (RTKs) which are linked to the Ras/mitogen-activated kinase-like protein kinase (MAPK)/extracellular-signal-regulated kinase (ERK) pathway, the janus kinase (JAK)/signal transducer and activator of transcription (STAT) pathway, as well as the phosphatidylinositol-3-kinase (PI3K)/Akt pathway (Figure 46A). When signalling abnormalities arise, each of these networks are known to result in either cell proliferation, angiogenesis or evasion of programmed cell death.[171,172]

Alterations of tumour growth inhibitory pathways such as the p53 network and its downstream effectors, cyclin-dependent kinases (CDK), and the retinoblastoma gene product (Rb) are also some of the most commonly found in lung cancer.[173] This is because they are closely associated with cell cycle regulation, as the phosphorylation state of Rb determines whether a cell should remain in cycle arrest (G0-G1 stage) or progress to the synthesis stage (S stage) of the cell cycle. Mis-regulation of Rb can result in disruption of the G1 checkpoint control leading to uncontrolled cell cycle entry.[174]

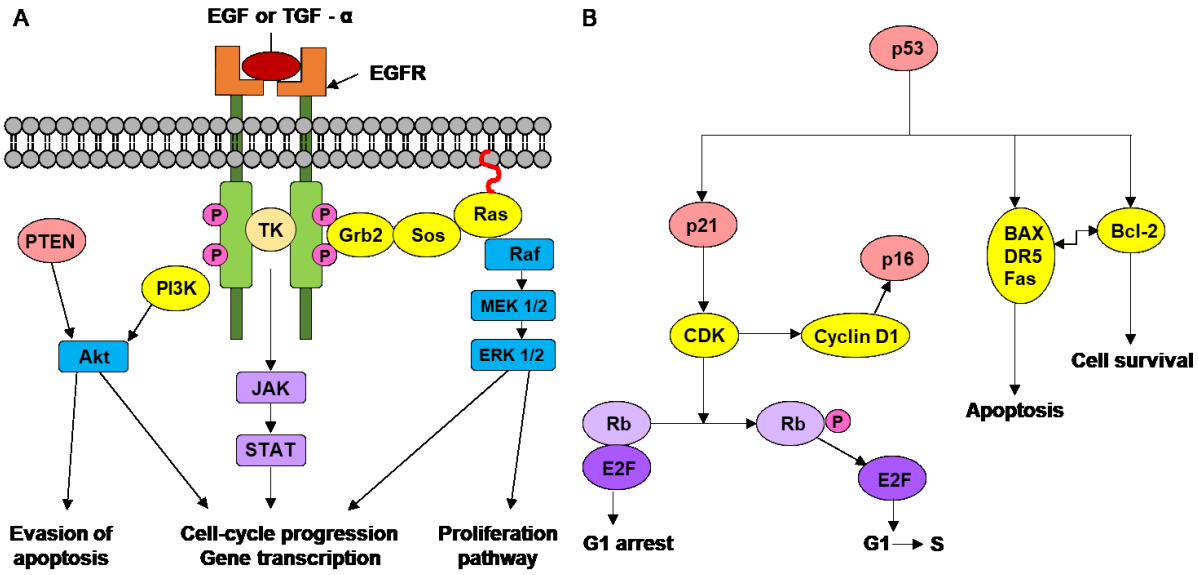


Figure 46A: EGFR signalling pathway. Growth factors such as EGF or transforming growth factor (TGF)-α bind to the hetero- and homodimer kinase domain (TK) and cause activation and receptor transphosphorylation of the Ras/ERK, PI3K/Akt and JAK/STAT pathways; **B**: The p53 signalling pathway, stimulated by cell stress signals. The downstream pathways control cell cycle arrest, and susceptibility to programmed cell death. Adapted from Brambilla *et al.*[170]

Malignant tumours are also known to employ mechanisms of cell proliferation and growth to evade apoptosis. Modifications to the mitochondrial apoptosis genes Bax (pro-apoptotic) and Bcl-2 (anti-apoptotic) are implicated in this mechanism of action. Moreover, when members of the tumour necrosis factor receptor (TNF) family, including the tumour necrosis factor receptor-like apoptosis inducing ligand death receptor 5 (TRAIL-DR5) and Fas, are downregulated, they are able to resist mechanisms of mitochondrial and death receptor-controlled apoptosis (Figure 46B).[168,173,175]

Many of the oncogenic pathways involve participation of protein kinases. They provide protein function regulation by catalysing the transfer of the terminal phosphate of ATP to substrates containing serine, threonine or tyrosine residues (Figure 47).[176] This can influence protein stability and activity as well as formation of recognition sites for protein recruitment and even programming for cell death.[177] As they are intrinsic in almost all aspects of cellular physiology, mis-regulation can lead to cancer, amongst a myriad of other diseases.[178] For this reason protein kinases are important therapeutic targets.

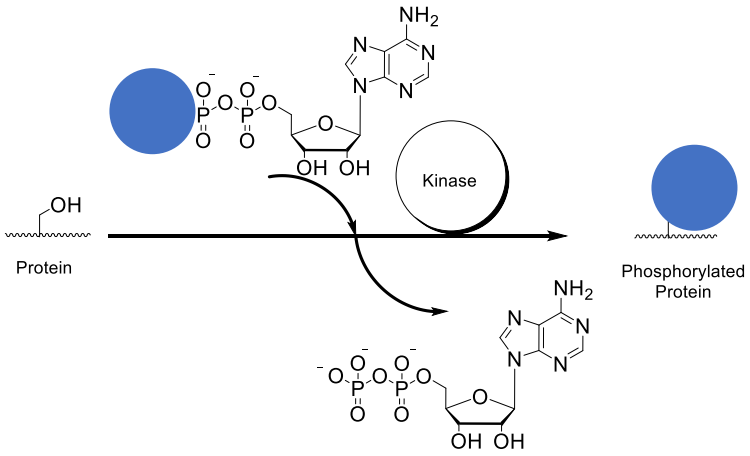


Figure 47: Protein phosphorylation by ATP hydrolysis, catalysed by a protein kinase.

4.1.2. Current Treatments of NSCLC

For NSCLC diagnosed at an early stage (I-IIIa), surgery is recommended as first-line treatment if the patient can tolerate it. This is often followed by adjuvant therapy which is usually chemotherapy, but can also be radiotherapy or targeted therapy, in order to destroy any remaining cancer cells remaining after surgical resection.[179]

As the early stages of lung cancer development can be asymptomatic, approximately 40 % of newly diagnosed patients present with stage IV progression. At this point the first-line treatment is cytotoxic combination chemotherapy which usually involves a platinum based drug, either cisplatin or carboplatin, combined with gemcitabine (Gemzar), vinorelbine (Navelbine), pemetrexed (Alimta), irinotecan (Campto) paclitaxel (Taxol), or a close relative

docetaxel (Taxotere) (Figure 48).[180] Although often effective for killing cancer cells, these therapies tend to also produce adverse side effects on the body due to the destruction of healthy cells.[179]

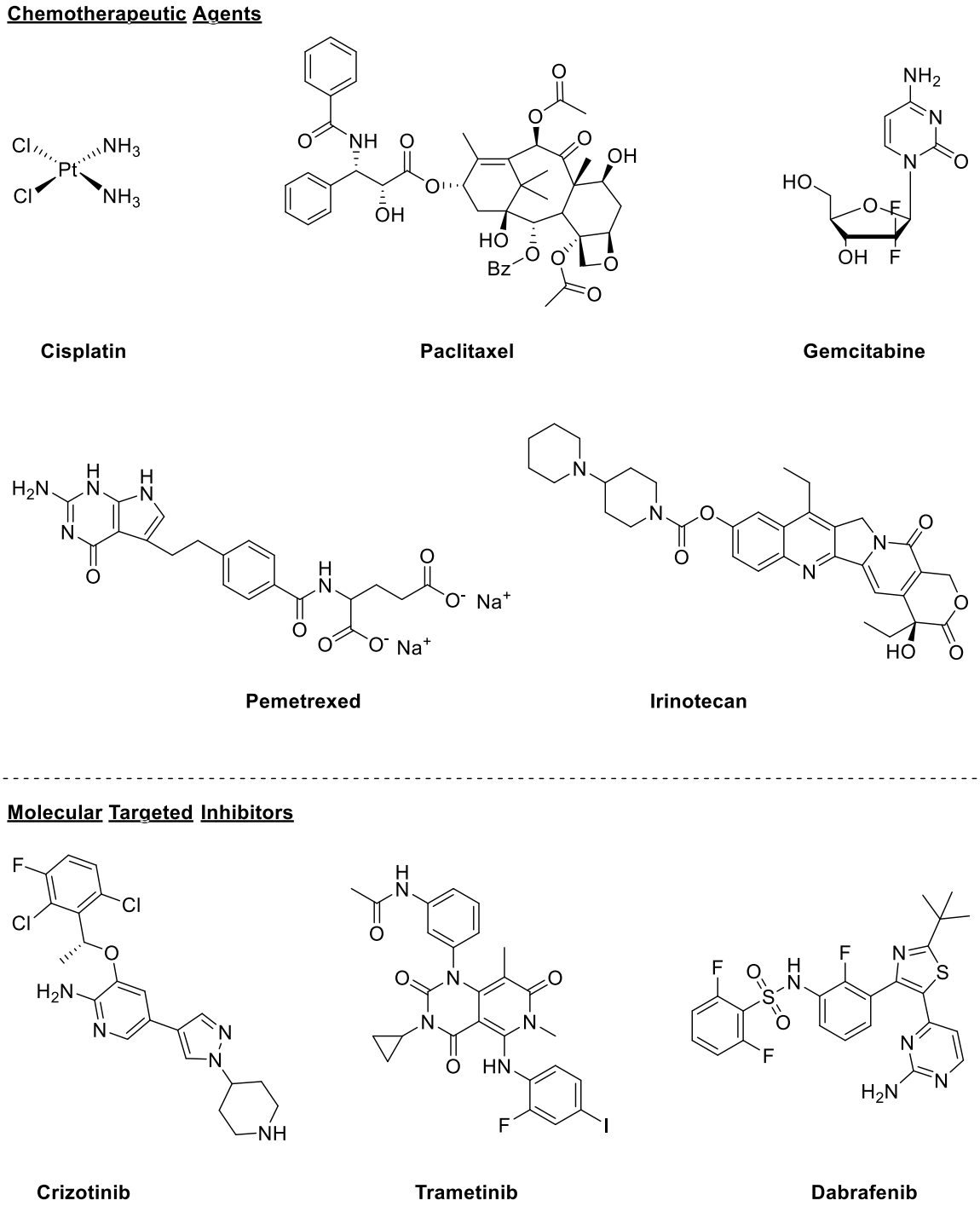


Figure 48: The structures of commonly used chemotherapeutic agents and drugs designed to inhibit target oncological pathways/genes.

For treatment of advanced NSCLC, immunotherapy, a method by which the body's own immune system is harnessed to target cancer cells can be used to help improve patient survival.[179] Another increasingly successful strategy is to use molecular targeted therapy. This is because in almost 70 % of patients there is a potentially controllable molecular target.[181] For example gefitinib and erlotinib (Figure 48) are both reversible, competitive inhibitors of the TK domain of EGFR, a target for which characteristic mutations can be identified from patient genome screens and these are known as biomarkers.[182] Other targeted drugs include crizotinib (Xalkori) designed to inhibit receptor tyrosine kinases that result from echinoderm microtubule-associated protein-like 4-anaplastic lymphoma kinase (EML4-ALK) fusions caused by chromosomal translocation.[170] This rearrangement is present in 3-7 % of patients with NSCLC and is usually seen in younger non-smoking adults.[179]

Most recently, the combination of a MAP or ERK Kinase (MEK) inhibitor called trametinib, and a B-Raf inhibitor called dabrafenib was FDA approved for the treatment of NSCLC with the B-Raf V600E mutation. MEK and B-Raf are part of the Ras/Raf/MEK pathway which plays an important role in the EGFR growth promoting network.[183]

Over the last 10 years there has been great advances in the treatment of NSCLC with the introduction of personalised oncological therapy and immunotherapy, as well as the overall decline in cigarette smoking. As lung cancer is still the deadliest cancer to date, more must be done to identify new oncological targets for novel treatments.

4.2. The Ribosomal S6 Kinase Family

4.2.1. RSK Structure and Function

The 90-kDa ribosomal S6 kinases (RSKs) are a family of highly conserved threonine/serine protein kinases which include four homologous isoforms found in humans, RSK1-4.[184] RSKs are structurally unique, possessing two functionally distinct kinase domains separated by a linker region on the same polypeptide chain. These are the amino-terminal kinase domain (NTKD) which is closely related to the protein kinase AGC family, and the carbon-terminal kinase domain (CTKD), homologous to the calmodulin-dependent protein kinase (CAMPK).[185,186] The NTKD controls downstream substrate phosphorylation, while the CTKD appears to only provide autophosphorylation of the NTKD.[187]

The RSKs are downstream regulators of the Ras/Raf/MEK pathway, a network important for the activation of intracellular proteins responsible for cellular responses such as proliferation, apoptosis, differentiation and cell growth.[185,188] This protein kinase cascade is triggered by extracellular signalling molecules such as cytokine and growth factors, as well as neurotransmitters and peptide hormones,[188] causing stimulation of cell-surface growth factor receptors. These bind to the hetero- and homodimer TK domain, enabling activation and receptor transphosphorylation (Figure 49). This leads to the formation of docking sites for growth factor receptor-bound protein-2 (Grb2) and the guanine nucleotide-exchange factor son of sevenless (Sos), which stimulate Ras. Subsequent activation proceeds via a series of kinase phosphorylations with activation of Raf isoforms (A-C) by Ras which in turn activates MEK 1/2.[189] Activation of ERK 1/2 follows, and these are capable of phosphorylating and directly activating multiple substrates including the RSKs.[185]

RSK is activated by several phosphorylations at 6 or 7 serine and threonine residues. Using RSK1 as an example (Figure 49), activation is initiated by docking of ERK 1/2 at the CTKD followed by phosphorylation of Thr573 in the activation loop of the CTKD, as well as Thr359 and Ser363 present in the linker region. Activation of the CTKD leads to autophosphorylation

of the Ser380 located in a hydrophobic motif of the linker enabling subsequent formation of a phosphoinositide-dependent kinase (PDK) docking site in the activation loop of the NTKD. Phosphorylation of Ser221 of the NTKD leads to full activation of RSK1, followed by autophosphorylation of Ser737 and subsequent dissociation of ERK 1/2.[186]

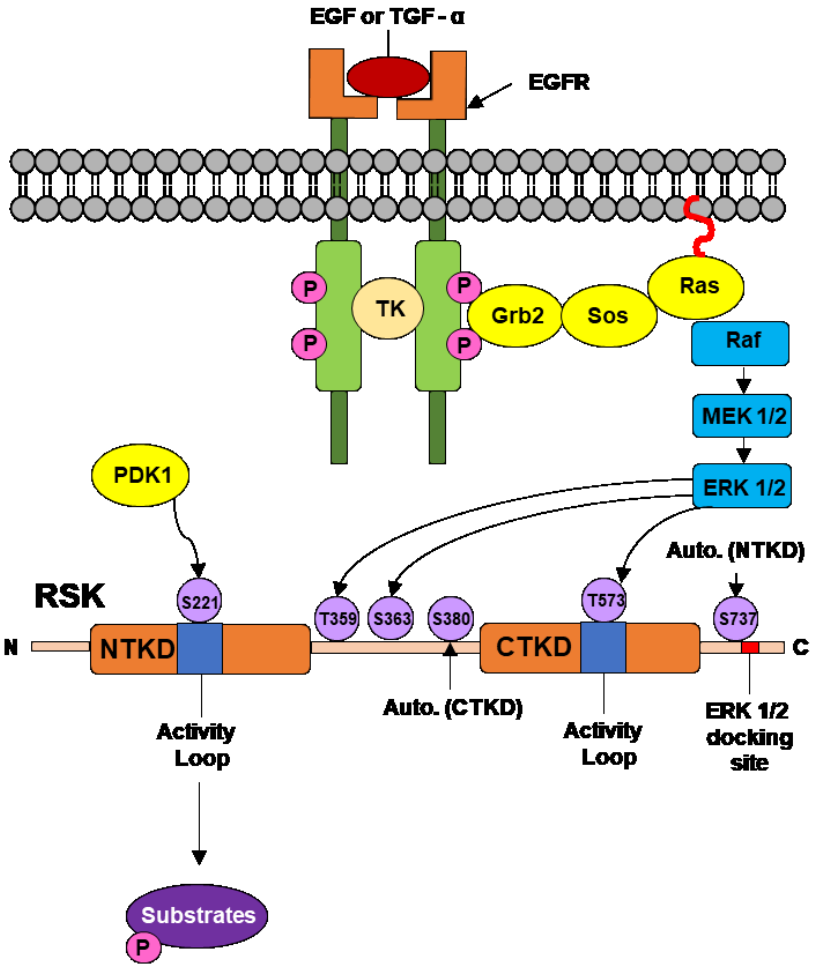


Figure 49: The Ras/ERK/RSK signalling cascade. RSK is activated by ERK 1/2, in the presence of PDK1. The residue numbering refers to RSK1. Adapted from Brambilla *et al.*[170] and Ikuta *et al.*[186]

The RSKs have been implicated in cell cycle regulation through phosphorylation of substrates likely to participate in growth control such as glycogen synthase kinase 3 (GSK3) an important regulator of multiple signalling networks,[190] cAMP response element-binding protein (CREB),[191] CBP/p300 coactivator family,[192] estrogen receptor α (ERα),[193] IκBα/NFκB and c-Fos.[194] The RSKs also participate in the inhibition of Myt1 (Myelin transcription factor 1) which is a $p34^{cdc2}$ inhibitory kinase that induces meiosis I entry.[195]

As the Ras/ERK signalling network is important for regulating cell survival, the RSKs are downstream effectors which directly influence the fate of a cell. For example, RSK1 and RSK2 phosphorylation of proapoptotic Bcl-2/Bcl-XL-associated death promoter (BAD)[196] and death-associated protein kinase (DAPK) regulates apoptosis by inactivation.[197] Uncontrolled regulation of the Ras/ERK/RSK pathway can therefore cause a range of diseases including cancers.

4.2.2. RSKs in Cancer

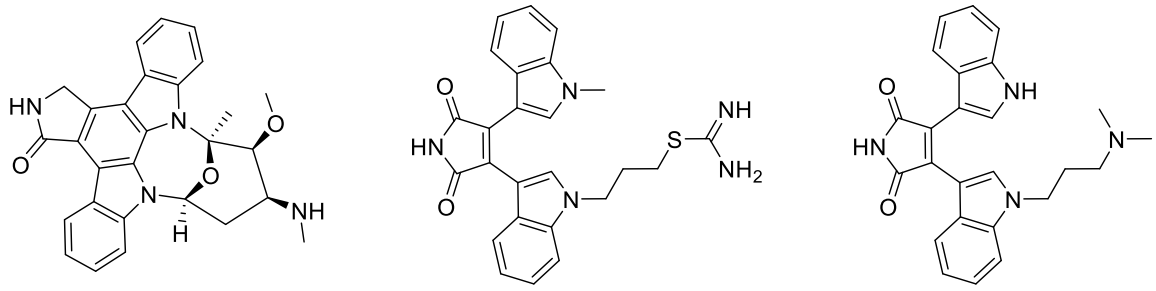
Currently there are limited reports on the specific and shared functions of the individual RSK isoforms, however the divergence in function is most apparent in cancer due to variance in expression. While the expression of RSK1 and RSK2 in tumour cells is generally associated with increased tumour growth and survival, expression of RSK3 and RSK4 is linked to tumour growth suppression.[198] Over-expression or over-activation of RSK1 and RSK2 has been observed in a number of cancer types suggesting that they may be associated with oncogenesis. These include; breast cancer[199], prostate cancer[200], head and neck squamous cell carcinoma (HNSCC),[201] leukemia,[202] melanoma,[203] glioblastoma,[204] multiple myeloma,[189] and lung cancer. In contrast, RSK3 expression in ovarian tumours leads to a decrease in proliferation rates suggesting that it is a tumour suppressor,[205] while RSK4 overexpression in breast cancer also leads to a decrease in cancer cell proliferation.[206]

Interestingly, Lara *et al.* found that RSK1 is a repressor of NSCLC metastasis, as down-regulation increases the metastatic ability of a tumour *in vitro* and *in vivo*.[207] By contrast, a report by Larrea *et al.*[208] suggested that over-expression of RSK1 leads to an increase in migration in melanoma. Due to a number of conflicting reports on the roles of RSK in various cancers, further studies must be done to elucidate the roles that the individual RSK isoforms play in tumorigenesis.

4.2.3. RSK Inhibitors

Due to the presence of two catalytic kinase domains each containing a non-identical ATP-binding site, RSKs present two logical sites for potential inhibition, either at the CTKD or the NTKD.[209] A few small molecule inhibitors have been developed however very few are RSK selective and some are active against other kinases.

Staurosporine (Figure 50) is a non-specific bisindoylmaleimide inhibitor with one of the highest potencies measured for a RSK small molecule inhibitor with a RSK1 IC_{50} of 0.3-1 nM. However it lacks selectivity for RSKs alone and is active against a broad range of protein kinases.[209] Both Ro31-8220 and GF109203x are potent derivatives of Staurosporine with IC_{50} values for the inhibition of RSK2 at 36 nM and 310 nM respectively. Similar inhibition is observed for the other RSK isoforms as well as slightly greater inhibition of protein kinase C (PKC). It was postulated that the two compounds bind to the RSK2 NTKD ATP pocket as it has been found to be structurally similar to PKC.



Staurosporine
RSK1 IC_{50} : 0.3 - 1 nM
PKA IC_{50} : 8.2 nM
CK1 IC_{50} : 164 µM

Ro31-8220
RSK1 IC_{50} : 200 nM
RSK2 IC_{50} : 36 nM
RSK3 IC_{50} : 5 nM
PKC : 4 - 8 nM

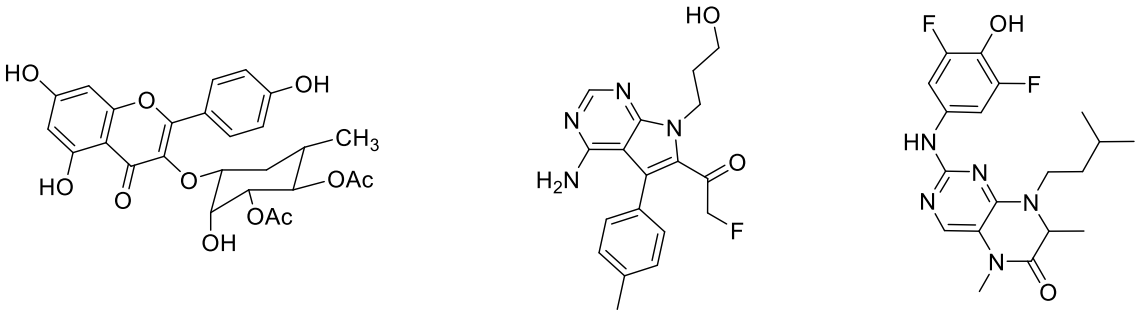
GF109203x
RSK1 IC_{50} : 610 nM
RSK2 IC_{50} : 310 nM
RSK3 IC_{50} : 120 nM
PKC : 8 - 12 nM

Figure 50: The structures of several non-specific RSK inhibitors and their selectivity between RSK isoforms and other kinases. Protein kinase A (PKA), casein kinase 1 (CK1).[209]

Compound SL0101 is flavonol rhamnoside natural product extracted from the tropical plant *Fosteronia refracta* and was the first RSK specific inhibitor to be identified. It inhibits RSK2 with an IC_{50} of 50-100 nM and also RSK1 (Figure 51), but not related kinases such as MSK1 and p70S6K1 or unrelated related kinases. SL0101 binds at the NTKD ATP- binding site and

inhibits RSK2 activity competitively, affecting downstream substrates of RSK.[209] In cells however, it has a relatively poor EC_{50} of 50 μM, indicating that either there is inadequate cellular inhibition, issues with cellular permeability or metabolism, or that the drug has some off-target effects. Moreover, despite inhibition of breast cancer cell growth by treatment of SL0101 derivatives, they have also been shown to promote tumour growth in NSCLC.[198] Due in part to concerns about off-target effects, there has been reduced development of flavonol rhamnosides as specific-RSK inhibitors.

1-[4-Amino-7-(3-hydroxypropyl)-5-(4-methylphenyl)-7H-pyrrolo(2,3-d) pyrimidin-6-yl]-2-fluoroethanone (FMK) contains a pyrrolopyrimidine moiety (Figure 51) and is an irreversible RSK1 and RSK2 specific inhibitor with a RSK2 IC_{50} of 15 nM and an EC_{50} value of 200 nM *in vitro*, though FMK also shows inhibition of RSK1 and RSK4.[210,211] The selectivity of FMK for RSKs is largely due to the stereoelectronic configuration of the molecule in the CTKD ATP-binding pocket. FMK functions by binding to the CTKD ATP-binding site and inhibiting autophosphorylation at important regulatory residue Ser386. As the CTKD is not always necessary for RSK activation,[212] and the drug only functions when the kinase is inactive, the usefulness of FMK is limited.



SL0101
RSK1 : 77 % inhibition at 10 μM
RSK2 IC_{50} : 50 - 100 nM

FMK
RSK2 IC_{50} : 15 nM

BI-D1870
RSK1 IC_{50} : 10 nM
RSK2 IC_{50} : 20 nM

Figure 51: The structure of several RSK specific inhibitors and the levels of inhibition of RSK1 and RSK2 achieved.[209]

BI-D1870 is an ATP-competitive pan-RSK inhibitor with high RSK1-4 potency of 15-30 nM *in vitro*, depending on the isoform and complete RSK inhibition is possible at 10 μM (Figure

51). As a dihydropteridinone, BI-D1870 binds to the NTKD ATP-binding site and functions by affecting the phosphorylation of RSK substrates rather than targeting upstream ERK signalling.[209] It is most active against RSK3 and RSK4, suggesting that there is some differences in structure between the RSK isoforms. Despite some selectivity over other ACG kinases, BI-D1870 also inhibits Aurora B, PIM3, MST2, PLK1, GSK3β and MELK.[211] Furthermore, it has a short plasma half-life and low drug stability which means that its pharmacokinetic profile is poor.[213,214]

While a number of pan-RSK inhibitors have been developed over the years, there are still no isoform specific inhibitors. This would be key to avoiding off-target effects, especially as different RSK isoforms sometimes appear to have opposing roles in disease.

4.2.4. The RSK4 Isoform

Although the RSK isoforms exhibit high sequence identity of 73-80 %[215], RSK4 is functionally distinct from RSK1-3 in a number of ways. Firstly, RSK4 is constitutively activated in serum-deprived cells and in the absence of growth factor, a requirement for activation of RSKs1-3.[216] This is caused by maximal phosphorylation of three RSK4 activating sites, Ser232, Ser372 and Ser389 (Figure 52), which are phosphorylated at the same level in both serum starved and growth factor stimulated cells. An explanation of this constitutive activity is the fact that RSK4 expression is 10-20 times lower in most cells compared with RSK1-3.[38] This means that the basal activity of highly expressed kinases such as ERK is high enough to effect maximal RSK4 phosphorylation, of which ERK has been shown to induce at least 50 % phosphorylation by constitutively activating Ser372 and Thr581. Maximally phosphorylated residues Ser232 and Ser389 function together to stabilise the NTKD in the active conformation, leading to activation of RSK4 by about 80 %. The remaining 50 % ERK-independent RSK4 activity is derived from autophosphorylation of Ser232 and Ser389 by the NTKD and CTKD respectively, as unlike the other RSK isoforms, PDK1 is not required for phosphorylation of Ser232 present in the NTKD activation loop.[216]

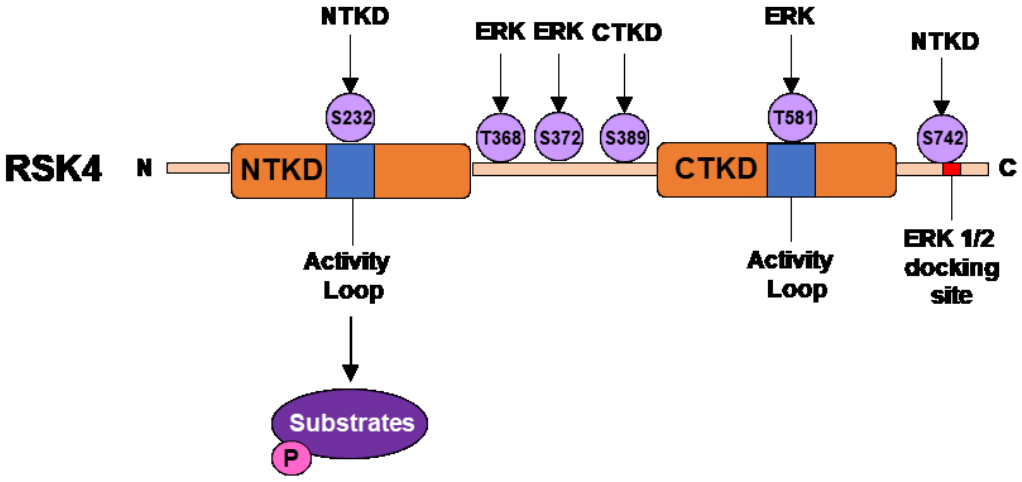


Figure 52: The structure of RSK4, characterised by the presence of an NTKD and CTKD. RSK4 is activated by ERK 1/2, independent of PDK1 via multiple phosphorylations of serine/threonine residues. The residue numbering refers to RSK4.

RSK4 is characterised as a predominantly cytosolic protein and has unique cellular functions compared with RSK1-3 isoforms. While some studies suggest RSK4 is a tumour suppressor gene, others have reported that it promotes tumour growth. For example, it has been demonstrated by Berns *et al.*[217] and Dümmler *et al.*[216] that RSK4 is a mediator of p53-induced growth arrest as RSK4 silencing leads to loss of p53 dependent G_1 cell cycle arrest.

Moreover, it was shown that knock-down of RSK4 suppressed the mRNA expression for CDK inhibitor $p21^{cip1}$ which is an important part of the p53 antiproliferation response (Figure 46B). It has therefore been hypothesised that RSK4 indirectly mediates p53 by phosphorylating its downstream effectors in a growth factor-independent manner. Furthermore, a report by Lopez-Vicente *et al*. has shown that RSK4 is involved in cell senescence regulation through p21. This is a mechanism that cancer cells are able to override in order to achieve immortality and transformation, therefore is has been suggested that down-regulation of RSK4 could provide a proliferative advantage for cancer cells.[194] RSK4 also has an anti-invasive and anti-metastatic effect when overexpressed in breast cancer cells,[206] while downregulation of RSK4 mRNA in renal and colon cancer confers accelerated growth and is further evidence of RSK4's role as a tumour suppressor.[218]

In contrast, a study by Bender and Ullrich showed that overexpression of RSK4 is linked with resistance of tyrosine kinase inhibitor sunitinib in renal cell carcinoma (RCC) cell lines, suggesting its role as a tumour growth promotor.[219] In addition to this, Fan *et al*. have shown that due to RSK4 overexpression in RCC cell lines, it could be a promotor of tumour invasion and migration, as well as cell cycle progression.[220]

Clearly there is some disparity over the cellular functions of RSK4 with respect to its role in cancer. A possible explanation for these contrasting findings is that depending on the context or disease, RSK4 may act as a tumour suppressor or promotor. Another plausible explanation could be the presence of different RSK4 splice variants, which were first identified by Sun *et al*., with different or even opposite functions.[221]

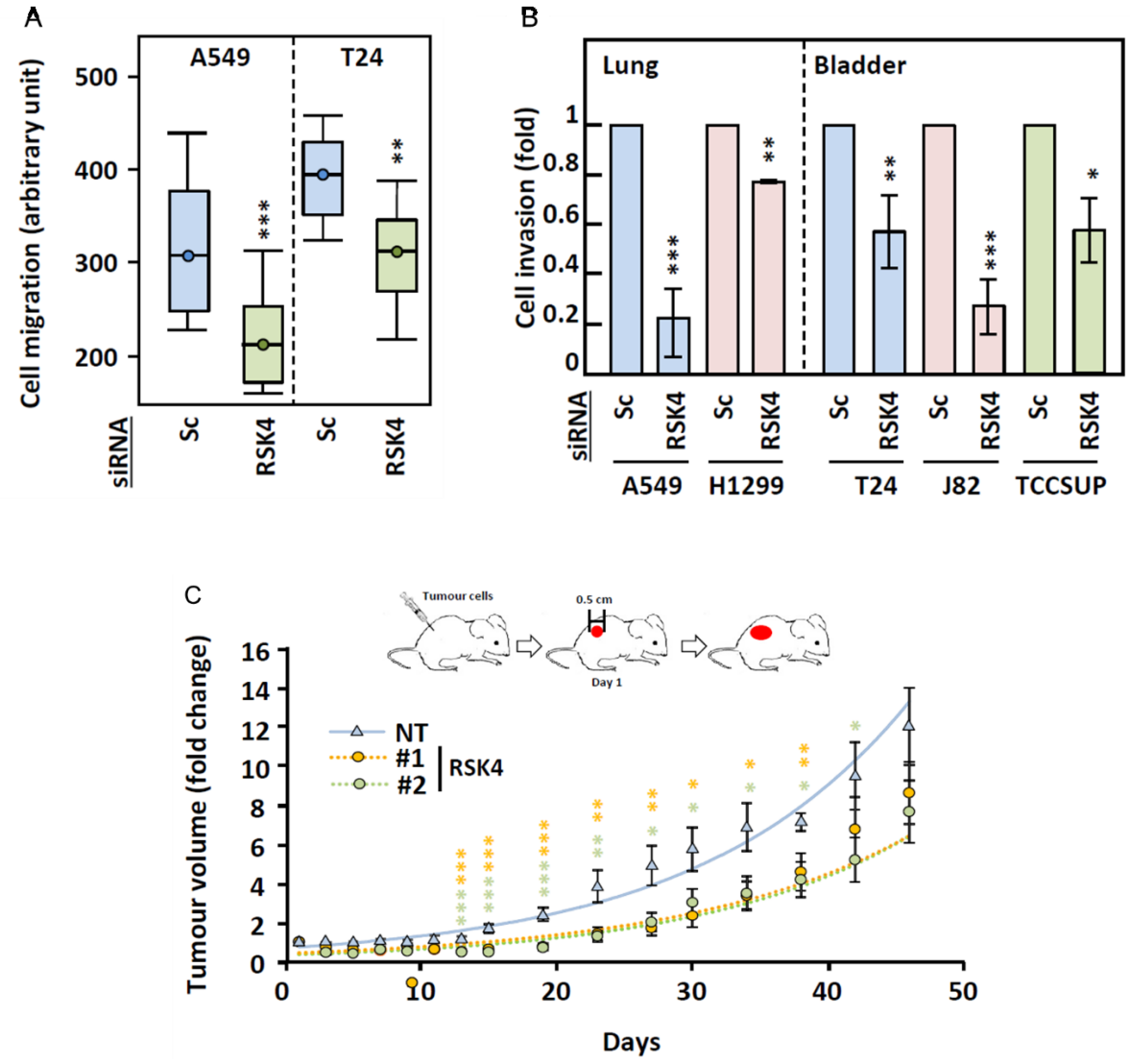
4.2.5. RSK4 vs. RSK1 in Lung Cancer: Discovery of a Novel Therapeutic Target

A biology group at Imperial College lead by Dr Olivier Pardo and Professor Michael Seckl have identified RSK4 as a tumour promotor and regulator of chemotherapy resistance in NSCLC adenocarcinoma as well as in bladder cancer, while RSK2 and RSK3 appeared to have no impact on tumorigenesis (Chrysostomou *et al*., submitted manuscript). As previously mentioned, studies within the same research group have shown that RSK1 acts in the opposite manner and is a tumour suppressor with respect to lung cancer.[207]

Micro-arrays of lung cancer tissue showed that RSK4 is overexpressed in almost 60 % of primary lung cancer samples, while in normal lung specimens, RSK4 is undetectable. Using lung cancer datasets that were publicly available, this was shown to correlate with poor patient prognosis. In contrast, it was shown that RSK1 is highly expressed within normal lung epithelial cells but is poorly expressed in adenocarcinoma human alveolar basal epithelial (A549) cells.

Moreover, silencing of RSK4 using RNA interference (RNAi) or a CRISPR-mediated knock-out clone suppressed invasion and migration in A549 cells *in vitro*, as well as several other

lung cancer cell lines and a few bladder cancer cell lines (Figure 53A and B). Interestingly, previous studies with RSK1 showed the opposite effect, with migration and invasion increasing in A549 cells with down-regulation *in vitro*.[207] In addition, the effect of RSK4 silencing on anoikis, a type of programmed cell death that targets circulating cells, was observed and this resulted in cell-death, an event not observed for RSK1 and non-targeting siRNAs. This has been shown to be associated with NFκB activity which is downregulated when RSK4 is silenced. In contrast, overexpression of RSK4 appears to have the opposite effect. Collectively, these studies indicate that RSK4 is an important regulator of lung cancer metastasis.



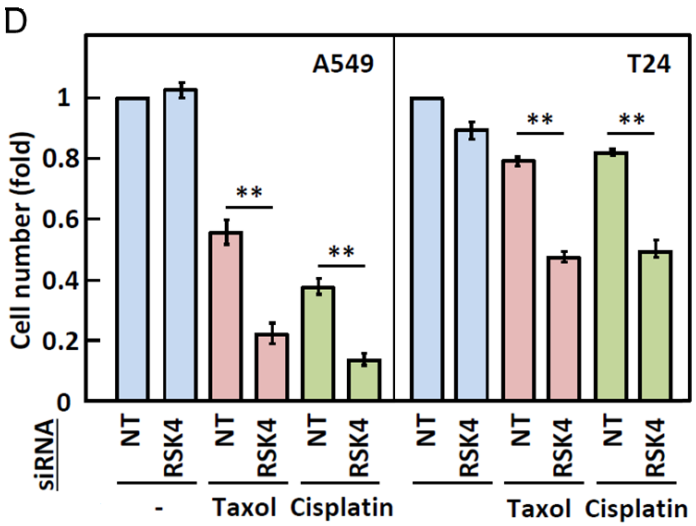


Figure 53A: Downregulation of RSK4 in A549 lung cancer cells of T24 bladder cancer cells reduces cell migration. A549 and T24 cells were transfected with or without RSK4 and scrambled (Sc) siRNAs for 48 hr prior to a random walk assay. The cell speed was determined by analysis of the resulting cell track;. **B**: Downregulation of RSK4 in multiple lung cancer and bladder cancer cell lines reduces cell invasion. A549 and H1299 lung cancer cells and T24, J82 and TCCSUP bladder cancer cells were transfected with or without RSK4 and scrambled (Sc) siRNAs for 48 hr. A chemo-attractive gradient was provided for the cells by coverage with a collagen I matrix overlaid with EGF. The cells were fixed and stained 48 hrs later using Sytox Green and the extent of cell invasion was measured using confocal imaging. Bar graphs represent the mean ± SEM of 36 fields of view per condition. Both A and B experiments were carried out in triplicate; **C**: Downregulation of RSK4 hinders lung adenocarcinoma xenograft growth. RSK4-CRISPR-mediated knock-out clones or A549 non-targeting (NT) were injected into *nude* mice and the tumour growth rate was measured without chemotherapeutic treatment; **D**: Downregulation of RSK4 increases sensitivity of lung and bladder cancer cell lines to chemotherapy. RSK4 was silenced in A549 or T24 cells using siRNA knock-down and treated with either cisplatin (12.5 μM for A549 cells and 3.5 μM for T24 cells) or taxol (40 nM for T24 cells and 58 nM for A549 cells). Determination of the cell number using crystal violet staining was carried out with normalisation to the related control condition. This experiment was carried out in triplicate and the data is representative of the mean ± SEM of quadruplicates. (Statistics: ANOVA (A, C and D), t-test (B) and *; $p<0.05$, **; $p<0.01$, ***; $p<0.001$. (Chrysostomou *et al.*, submitted manuscript)

These results were corroborated by studies carried out *in vivo*. When the A549 RSK4 knock-out clone was injected into *nude* mice, the tumour growth progression over 48 days was much slower compared with non-targeted A549 cells (Figure 53C). Furthermore, the effect of RSK4 silencing on metastasis was also addressed *in vivo*, with A549 RSK4 knock-out clones shown as less able to disseminate within the lungs of injected mice. Conversely, silencing RSK1 in A549 cells within zebrafish using RNAi appeared to enhance metastasis.[207]

Knock-out of RSK4 using RNAi and RSK4-CRISPR clones has also been shown to sensitise lung and bladder cancer cells to chemotherapeutic drugs, cisplatin and taxol, while overexpression of RSK4 leads to resistance of A549 cells to chemotherapy (Figure 53D). This is linked to an increase in DNA damage and apoptosis during RSK4 downregulation, mediated by a decrease in expression of anti-apoptotic proteins; cellular inhibitor of apoptosis protein 1 (clAP1) and B-cell lymphoma 2 (BCL2). Conversely, when RSK1 is silenced in lung and bladder cancer cells, the opposite outcome is observed with resistance to chemotherapeutic drugs, cisplatin and taxol.

From these studies, it is clear that RSK4 is a tumour promotor of lung adenocarcinoma as overexpression leads to increased metastasis, drug resistance and poor patient prognosis, while silencing RSK4 has been shown to reverse these traits. Therefore, a RSK4 inhibitor could be therapeutically beneficial for the treatment of lung adenocarcinoma. RSK1 is also a regulator of lung cancer, however it has been shown to influence the disease in a completely converse way suggesting its role as a tumour suppressor. In addition, the pan-inhibitor SL0101 has been shown to effect a similar increase in invasion of A549 cells, indicating RSK1 inhibition over RSK4. For this reason, a selective inhibitor of RSK4 over other RSK isoforms is desirable to avoid loss of anti-cancer activity and to avoid toxicity resulting from high RSK1 expression in normal lung epithelial cells.

4.2.6. Inhibitors of RSK4: The Fluoroquinolones

The fluoroquinolones are a family of antibiotics that are either based on a quinolone or naphthyridine core structure. The first quinolone antibacterial agent, nalidixic acid, was identified in the 1960s and was a by-product of the antimalarial agent chloroquine.[222] Since then numerous modifications have been made to the structure to improve pharmacokinetic properties and increase the activity against both Gram positive and Gram negative bacteria, as well as anaerobic bacteria (Figure 54).[223]

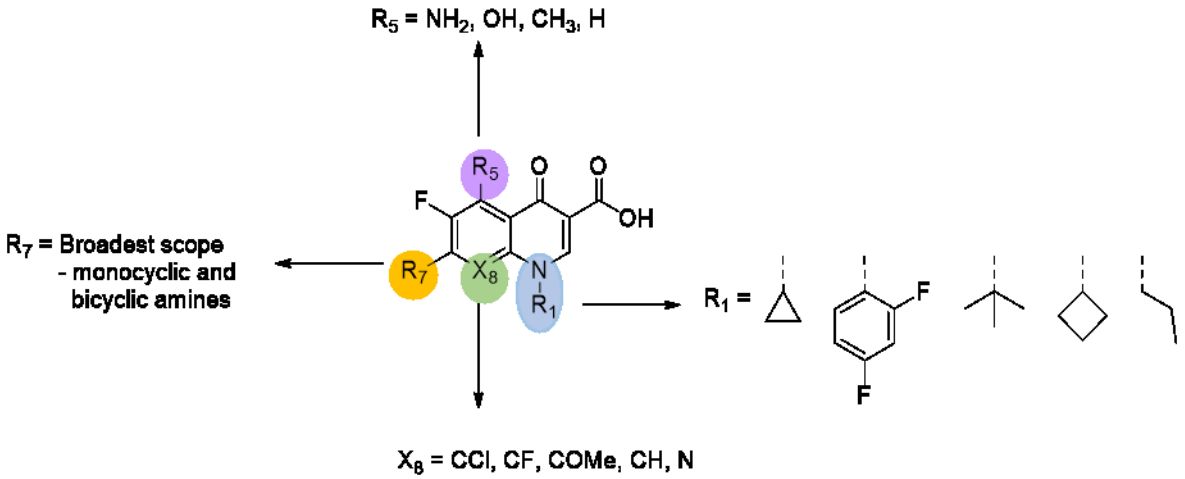


Figure 54: General structure of fluoroquinolone antibiotics with the key points of variation highlighted to show some of the key modifications made to improve properties.

Fluoroquinolones function as antibiotics by accumulating within bacteria via passive diffusion and inhibiting two targets, both of which are type II topoisomerases that are required for bacterial survival. The first is DNA gyrase which is responsible for negative super-coiling of double-stranded DNA and is therefore essential for DNA replication.[224] The second is topoisomerase IV which controls DNA relaxation and decatenation, and during DNA replication it separates the replicating daughter chromosomes or plasmids in bacteria.[225] Inhibition of these enzymes occur due to the formation of a stable ternary complex comprised of the fluoroquinolone, the enzyme and DNA. The drug forms pi-pi stacking interactions with DNA through its aromatic system, and also binds to it via the substituent at quinolone position 1. The presence of the carboxylic acid at position 3 and the carbonyl group at position 4 enables hydrogen bonding to DNA, while the fluoro substituent at position 7 provides interactions with the enzyme.[222]

In the search for a RSK4 selective inhibitor, Chrysostomou *et al*. performed a high through-put homogenous time resolved fluorescence (HTRF)-based assay which identified molecules that interfered with ERK dependent RSK4 activation. This method was used to exploit the differences in RSK activation, as unlike RSK4, the other isoforms require activation by PDK1. The group had confidence that a RSK4 selective inhibitor could be identified due to the increased expression in A549 lung cancer cells compared to very low

expression in normal lung tissues and most other human tissue.[215] In order to avoid finding ATP competitive inhibitors that could target many kinases, non-ATP competitive inhibitors were identified following dephosphorylation of recombinant RSK4 prior to incubation with test molecules, followed by reactivation by ERK2.

From a known drug library of 1675 compounds, 12 were identified as non-competitive ATP inhibitors of RSK4 with inhibition of >75% at 30μM. Of these compounds, Moxifloxacin (Moxi), a fluoroquinolone antibiotic was shown to inhibit RSK4 reversibly with a pIC_{50} of 5.20, while not interfering with ERK2 activity. Moreover, the efficiency of Moxi was unchanged with increasing RSK4 concentration, indicating that the molecule is not causing an effect by degrading RSK4. It is also selective for RSK4 over RSK1 as tested in cells, therefore providing the desired inhibitor profile at this early stage.

Further analysis of fluoroquinolone antibiotics in the context of RSK4 activation using the previously mentioned HTRF assay identified several additional inhibitors which were Trovafloxacin (Trova), Marbofloxacin (**129**), Rufloxacin (**130**) and Tosufloxacin (**131**). A few other floxacins were shown to be inactive, including Ciprofloxacin (**132**), Danofloxacin (**133**) and Piromidic acid (**134**), however despite these differences in RSK4 activity, no clear SAR could be deduced (Figure 55). Importantly, only RSK4 inhibitors appeared to sensitise A549 cells to cisplatin and taxol with superior results exhibited by Trova (Figure 56). This drug and others identified as RSK4 inhibitors including Moxi and **133** were able to reproduce previous RSK4 silencing results with inhibition of A549 cell migration and invasion.

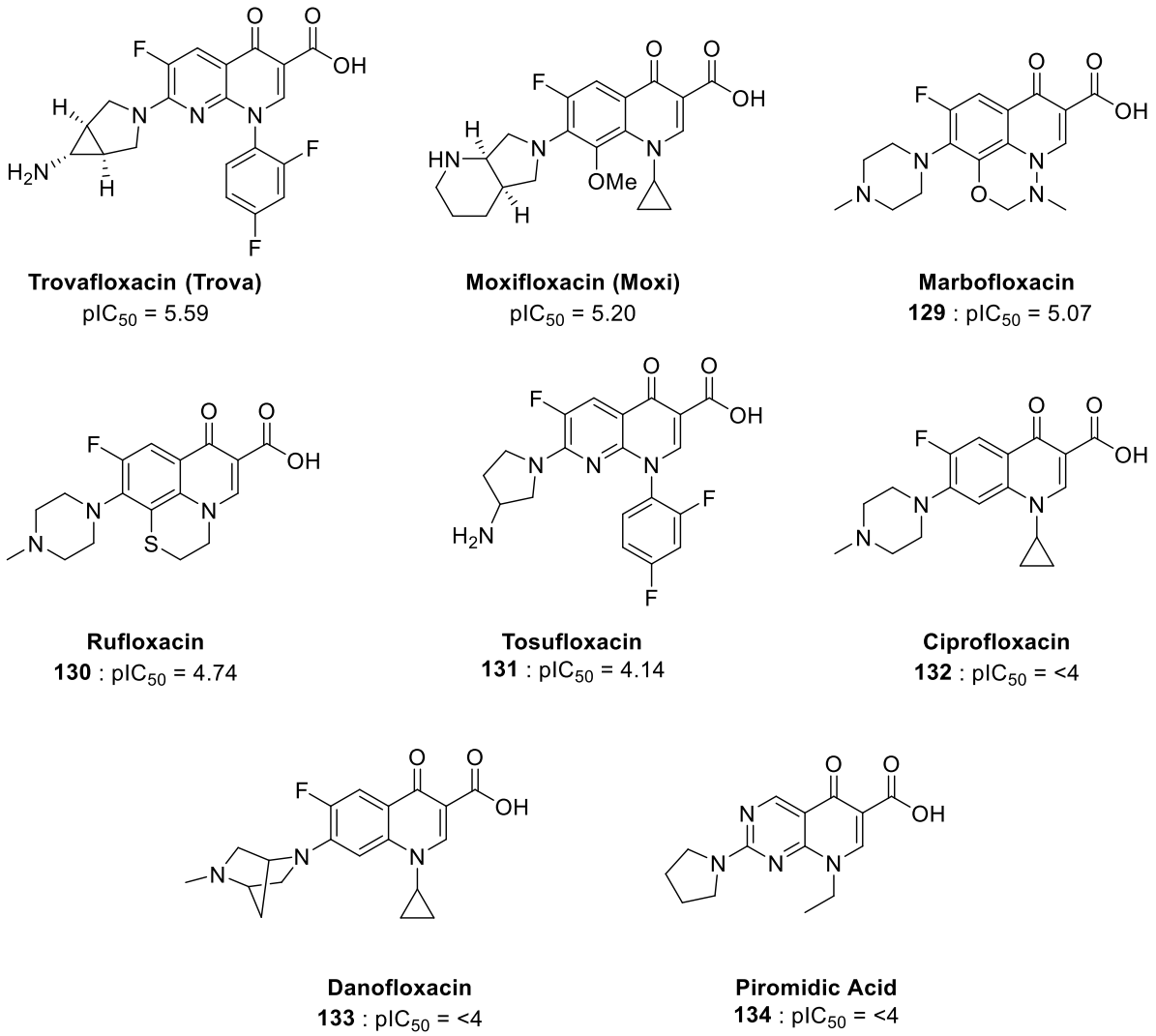


Figure 55: A sample of Floxacin antibiotics that were tested in the RSK4s HTRF assay, and their pIC_{50} values obtained.

Furthermore, administration of Trova to *nude* mice which had been injected with Luciferase-encoding A549 cells led to a major decrease in tumour growth compared to control animals and sensitised the cells to cisplatin response. Chrysostomou *et al*. also demonstrated that Trova binds to the inactive NTKD of RSK4, suggesting that the RSK4 inhibitors function by allosterically activating the NTKD, although this would need to be confirmed using co-crystallisation of the drug bound to RSK4.

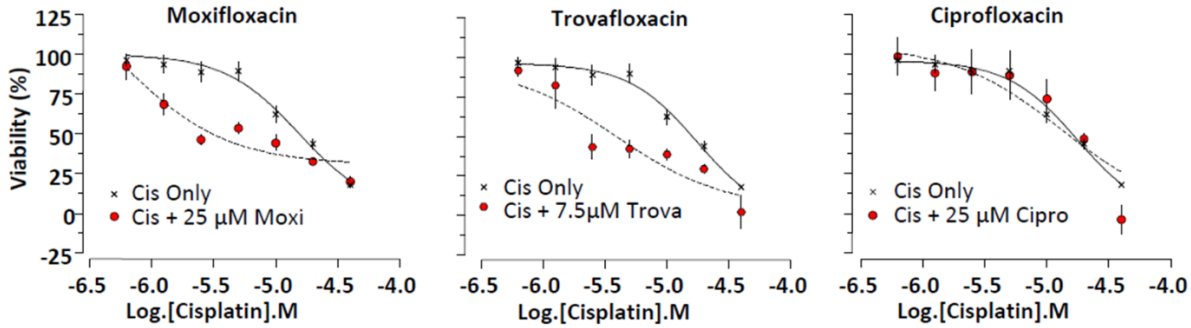


Figure 56: RSK4 inhibitor Trova is best able to sensitise A549 cells for cisplatin treatment. Prior to cisplatin treatment, either Moxi, Trova or Ciprofloxacin were added to A549 cells at the stated concentrations. Cell viability was determined after 72 h using an Alamar Blue assay. Trova treated A549 cells are more readily sensitised than those treated with Moxi, while Ciprofloxacin shows no activity. Experiment was carried out in triplicate. Each data point represents the mean of quadruplicates ± SEM. (Chrysostomou *et al*., submitted manuscript)

4.3. Project Aims

RSK4 has been identified as a significant mediator of lung adenocarcinoma metastasis and chemotherapeutic resistance *in vitro* and *in vivo* and therefore presents an attractive novel therapeutic target for the treatment of lung cancer. A family of fluoroquinolone antibiotics have been shown to inhibit RSK4 and reproduce the results of previous investigations involving RSK4 knock-out. In particular, Moxi and Trova exhibit the highest potency amongst the floxacins and provide the greatest potentiation of chemotherapeutic response *in vivo*. This project will address the relatively low (μM) RSK4 activity of these repurposed compounds by establishing a medicinal chemistry programme which will be used to develop more potent and selective inhibitors of RSK4. To do this the structures of Moxi and Trova will be altered iteratively to generate SAR which will be used to differentiate functionality required for RSK4 activity and antibiotic activity. The overall goal of this project is to identify at least one novel lead compound which has optimised RSK4 bioactivity as well as enhanced pharmacokinetic properties which could have potential clinical application for the treatment of lung cancer in the future.

5. Results and Discussion

5.1. Part 1: Synthesis of Moxi/Trovafloxacin Derivatives

5.1.1. Combinational Derivative Design

Based on preliminary data that identified the family of fluoroquinolone antibiotics as RSK4 inhibitors, synthesis of compounds closely related in structure was desired in order to develop some structure activity relationships (SAR) and ideally improve the potency against RSK4.

Trova and Moxi were identified as the most potent RSK4 inhibitors from a small molecule screen measuring ERK2 induced RSK4 activation (see section 4.2.6.). These two drugs differ in structure, with Trova containing a 1,8-naphthyridine core while Moxi is based on a 4-quinolone core structure with a methoxy group in the C-8 position (Figure 57). They also incorporate different side chains at the C-7 position. Trova has an amino-substituted 3-azabicyclo[3.1.0]-hexane while Moxi has (4a*S*,7a*S*)-octahydro-1*H*-pyrrolo[3,4-*b*]pyridine substituted in this position. A final comparison is that the N-1 of Trova has a 2,4-difluorobenzene substituent while the same position in Moxi contains a cyclopropane substituent.

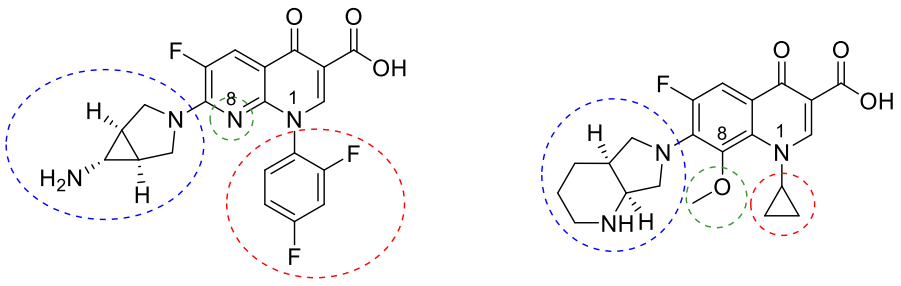


Figure 57: The structure of Trova (left) and Moxi (right) with the key parts of the molecule highlighted to show points of diversification

Due to the differences in structure, the fact that both had a pIC_{50} value greater than 5 and were therefore worth pursuing, and also the ease at which these parts of the molecules could be diversified, initial synthetic efforts were aimed at synthesising compounds which

combined the key elements of these structures, probing the importance of each for RSK4 activity.

The two core structures were divided between myself and another PhD student, Luiza Dos Reis Cruz. My objective was to explore the SAR based around the Moxi quinolone core, while Luiza would synthesise derivatives based on the Trova naphthyridine core. Initial diversification for both series would start with alteration of the amino group in the C-7 position. Various amines would be used to explore the tolerance of divergent size, shape, basicity and H-bond donor/acceptors (Figure 58).

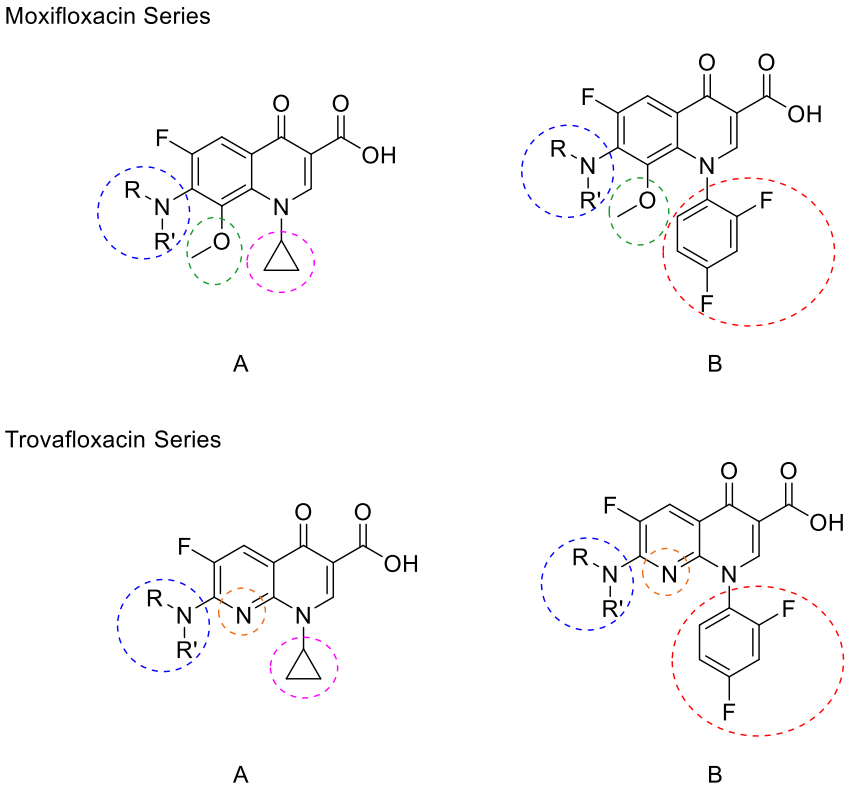


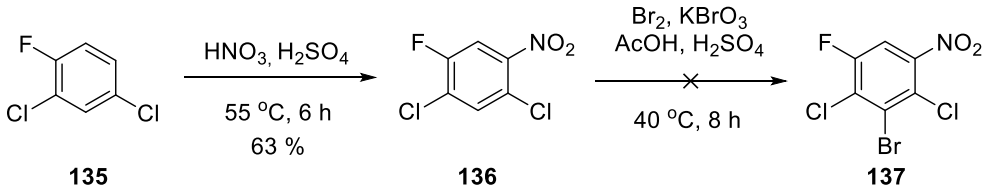
Figure 58: Four series of Moxi/Trova derivatives that were pursued with highlighting to show which parts of the molecules were altered and which were kept constant. Trova-derived molecule were synthesised by another PhD student, Luiza Dos Reis Cruz.

The original Trova amine (amino-substituted 3-azabicyclo[3.1.0]-hexane) would also be incorporated into the Moxi core structure to see if combining these key structural elements maintained RSK4 activity.

5.1.2. Synthesis of Moxifloxacin Derivatives

Formation of the 8-Methoxy-4-quinolone Core

Synthesis was initiated following a patent procedure by Wang *et al.* in which a series of functionalisation steps were employed to generate the 8-methoxy-4-quinolone core of Moxi, starting from 2,4-dichlorofluorobenzene.[226] This was a suitable synthetic route as the starting material was commercially available and inexpensive, and even though it consisted of 9 steps the patent quoted consistently high yields for each. This procedure was initiated with selective nitration at the C-5 position of 2,4-dichlorofluorobenzene (**135**), directed by chloro-substituents in the *ortho* and *para* positions (Scheme 39).



135 **136** **137**

Scheme 39: Selective nitration of 2,4-dichlorofluorobenzene followed by attempted bromination using conditions by Wang *et al*.

Subsequent C-3 bromination was more challenging due to the presence of multiple deactivating groups. The first conditions investigated were those described in the patent in which **136** was treated with a combination of bromine and potassium bromate in acetic acid and sulfuric acid under reflux (Scheme 39), however no reaction was observed. A paper by Groweiss *et al.* described a similar reaction with $NaBrO_3$ and it was noted that bromination did not occur in highly deactivated nitro systems such as 1,3-dinitrobenzene and *m*-nitrobenzoic acid. It was also observed that in each of these cases an excess of bromine gas was released which was also detected in this case.[227]

Rajesh *et al*. reported the effective bromination of highly deactivated aromatics containing at least two electron withdrawing substituents using NBS and concentrated sulfuric acid at 100ºC.[228] This procedure had more success in our system, however incomplete conversion

coupled with difficulties in separating the product from the starting material meant that better bromination conditions were still desired.

Alternative conditions reported by Derbyshire *et al.* in which bromination was achieved using bromine and silver sulfate in sulfuric acid.[229] The purpose of the silver sulfate in the reaction is that it can react with bromide anions in aqueous solution that are released during bromine hydrolysis. This forms silver bromide, promoting the equilibrium to proceed in the forward direction (Figure 59).

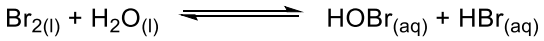
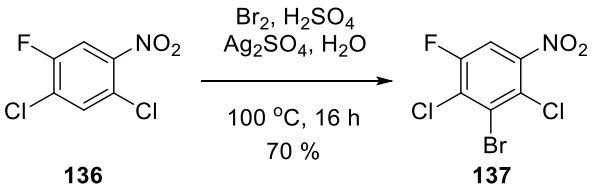


Figure 59: Equation to show the equilibrium reaction during bromine hydrolysis.

Consequently, bromide cations are steadily produced which can react with an electron deficient aromatic system such as ours, while the resulting by-product silver bromide precipitates out of solution. This method was favoured over others as 90% conversion was achieved with a yield of 70% for bromide **137** (Scheme 40).



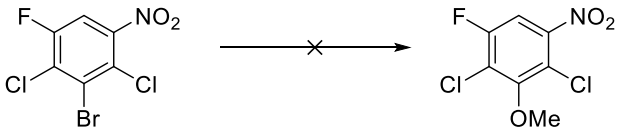
Scheme 40: Bromination of 1,5-dichloro-2-fluoro-4-nitrobenzene **136** using bromine, sulfuric acid and silver sulfate in water.

Following the outlined route by Wang *et al*., nucleophilic aromatic substitution to replace the bromo- substituent with a methoxide group *ortho* to both chloro- substituents (**138**) was the next expected step (Table 2).[226] The method described using sodium methoxide in methanol proved problematic in our hands as the fluoride was preferentially displaced rather than the expected bromide. This may be due to the high reactivity of fluorine towards nucleophilic aromatic substitution, compared with other halides, due to its superior inductive effect. This

leads to acceleration of the addition step and stabilisation of the resulting anionic intermediate.[230]

Alternative conditions were investigated, including those described by Aalten *et al.* in which an Ullmann-type reaction was used to promote nucleophilic aromatic substitution on bromo- and iodo- substituted aromatics, by exploiting the fact that they have larger atomic radii and are therefore more polarisable, these substituents can facilitate complex formation and subsequent electron transfer steps.[231,232] Nevertheless, displacement of the fluoride was still favoured over the bromide.

Palladium catalysis was also employed in an attempt to achieve C-O cross coupling. As bromine is more reactive than fluorine or chlorine towards oxidative addition, it was thought that this could occur selectively in our system. However observation of the crude ^{1}H NMR revealed that the fluorine had once again been preferentially displaced, possibly due to competing nucleophilic aromatic substitution which was known to work well at the fluoro-position.



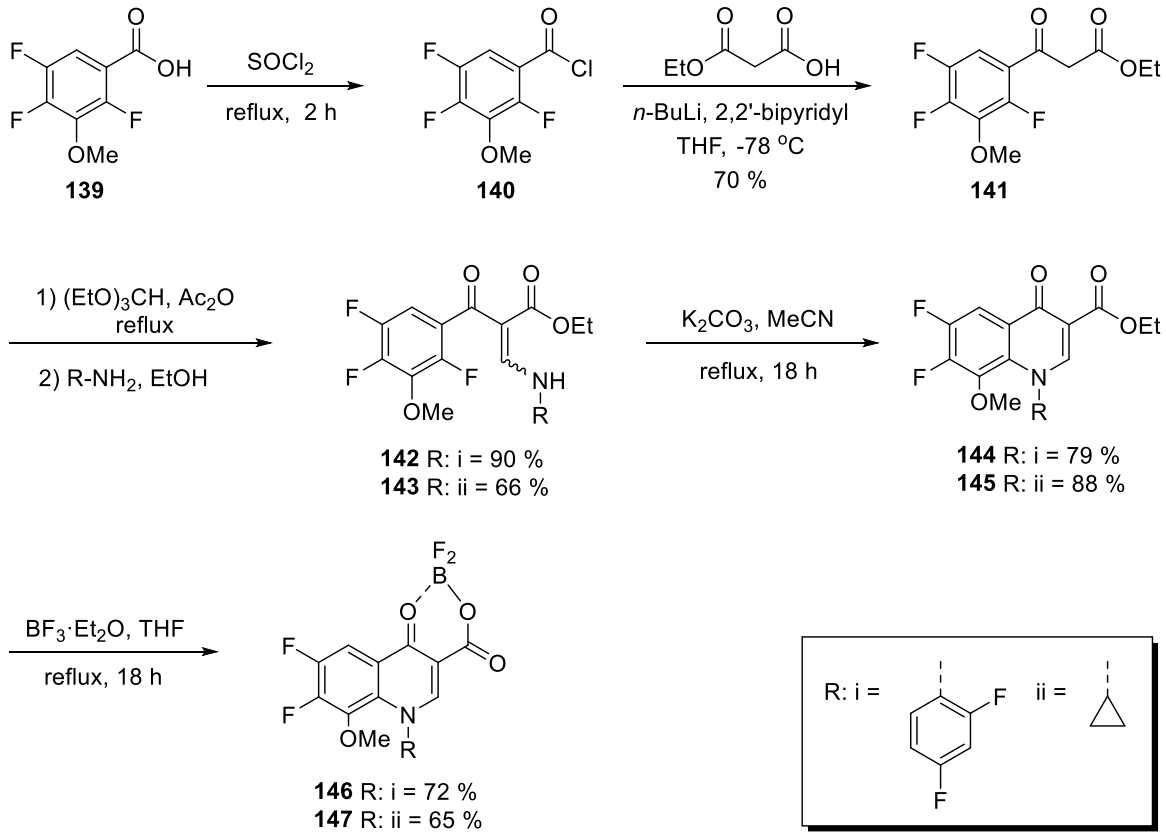
137 **138**

Conditions	Outcome
S_NAr: NaOMe, NaOH, MeOH, 60 °C	Fluoride displacement favoured over bromide
Ullmann: NaOMe, CuBr, EtOAc, MeOH, MW 120 °C, 30 min	
Buchwald: $Pd(OAc)_2$, Cs_2CO_3, *t*-BuXPhos, MeOH, PhMe, 80 °C, 2 h	

Table 2: A summary of the conditions used to displace the bromide.

As the experimental results and observations of reactivity could not be reconciled with the consistently high yields quoted in the patent, a different approach to the synthesis of the 8-methoxy-4-quinolone core was sought. A shorter synthesis consisting of 5 steps reported by

Sanchez *et al*. for the synthesis of 8-alkyoxy quinolones was identified starting from 2,4,5-trifluoro-3-methoxybenzoic acid (**139**) (Scheme 41).[233] Synthesis began with conversion of the acid **139** to the acyl chloride **140** using oxalyl chloride in the presence of catalytic quantities of DMF, to generate a more reactive chlorinating species, an imidoyl chloride. However this method was not optimal on a large scale due to the high boiling point of DMF, therefore oxalyl chloride was replaced with thionyl chloride, negating the requirement for DMF activation. Acyl chloride **140** was used to acylate mono-ethyl malonate using *n*-BuLi and 2,2'-bipyridyl in THF, followed by decarboxylation to generate keto-ester **141** as an inseparable mixture of the keto and enol form.



Scheme 41: Synthesis of 8-methoxy-4-quinoline core with 2,4-difluorobenzene and cyclopropane substituted at N-1 position following a 5 step synthesis.

Keto-ester **141** was then treated with triethylorthoformate in acetic anhydride generating an ethyl vinyl ether intermediate, to which either 2,4-difluoroaniline or cyclopropylamine was added in ethanol, enabling formation of enamines **142** and **143** as mixtures of the *E* and *Z*

isomers which were not separated (Scheme 41). Subsequent intramolecular cyclisation by nucleophilic aromatic substitution of the 5-fluoro substituent generated quinolone esters **144** and **145**. Initially NaH was used to effect this transformation however this led to low yields of less than 20% for cyclopropyl derivative **145**. The reason for this may be that these strong basic conditions invoke competing cyclopropyl ring opening due to the irreversible generation of a nitrogen anion. Consequently, potassium carbonate, a milder base was used which vastly improved the yields for both the cyclopropyl and the 2,4-difluorobenzene derivatives.

Ester hydrolysis using Lewis acid boron trifluoride lead to the formation of boron difluoride chelates **146** and **147**. The function of this chelate is to facilitate nucleophilic aromatic substitution of the 7-fluoro substituent by withdrawing electron density thereby activating the ring towards nucleophilic attack (Figure 60A). Without the boron chelate this reaction is much harder to achieve.[233] Formation of the boron difluoride chelate is not necessary in the case of the naphthyridone core as it contains a pyridine-like ring allowing for delocalisation of electron density onto the nitrogen atom during substitution (Figure 60B).

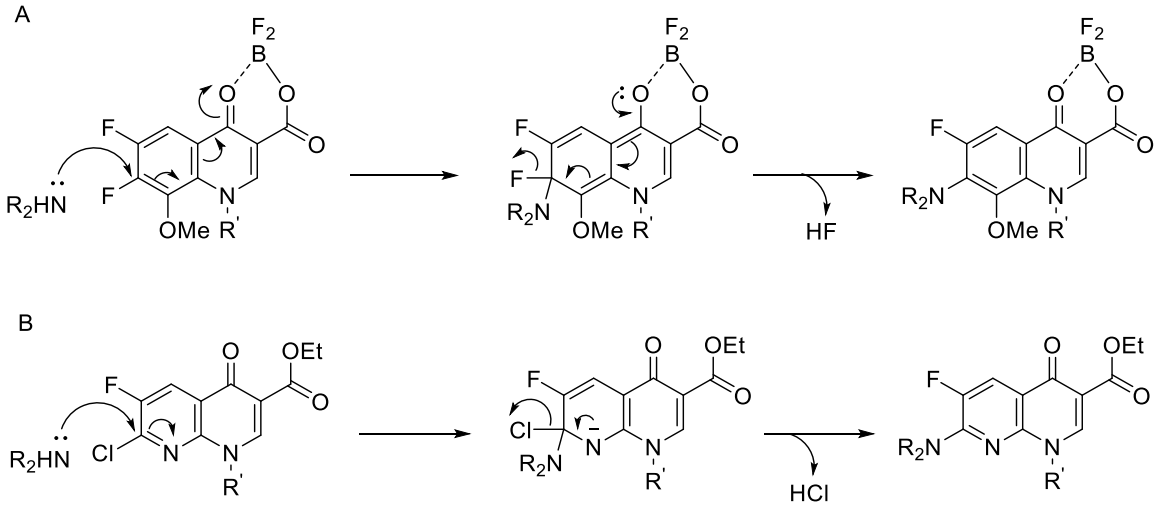
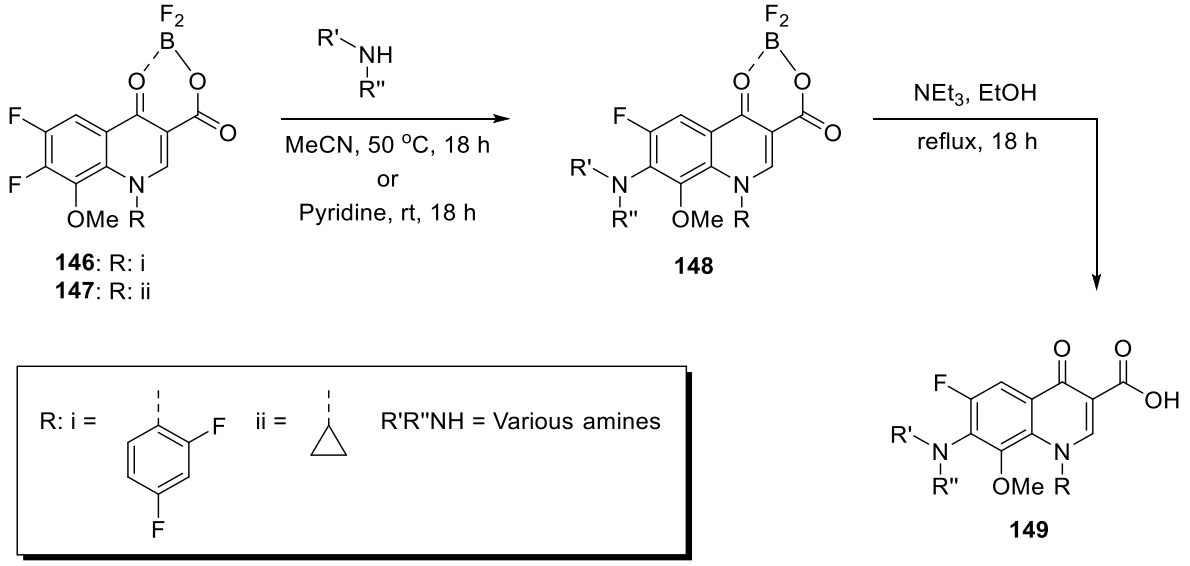


Figure 60A: The boron difluoride chelate used to activate the ring towards nucleophilic aromatic substitution; **B**: Delocalisation of electrons onto the nitrogen of Trova during nucleophilic aromatic substitution.

Synthesis of Analogues Via S_NAr of 7-Fluoro Substituent

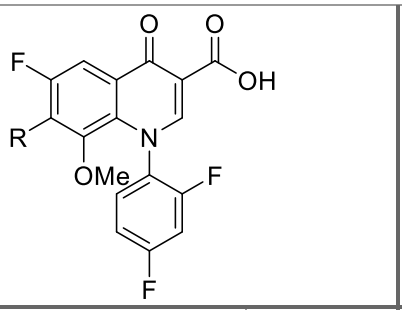
Subsequent substitution of the 7-fluoro substituent of **146** and **147** with various amines was initially carried out in acetonitrile at 50 °C. This was followed by hydrolysis of the boron difluoride chelate **148**, achieved by refluxing in triethylamine and ethanol (Scheme 42). Purification was accomplished by suspending the crude residue in water and adjusting the pH to firstly remove impurities insoluble at high pH, then precipitate the product at low pH. These were well documented conditions used for the synthesis of Moxi and analogues thereof.[233, 234]

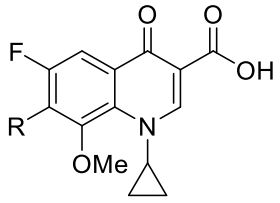


Scheme 42: General scheme showing introduction of amines in the C-7 position by S_NAr followed by hydrolysis of hydrolysis of the boron difluoride chelate to generate 8-methoxy-4-quinoline derivatives.

It was found that for some analogues, particularly those containing the 2,4-difluorobenzene moiety, nucleophilic aromatic substitution produced the desired products in poor yields and contained major impurities, including unreacted starting materials which were difficult to remove using acid-base precipitation. Due to the zwitterionic nature of these compounds, other methods of purification such as column chromatography were difficult, therefore full conversion was desired to facilitate acid/base precipitation. A reason for the poor reactivity of some amines towards S_NAr was perhaps poor solubility of the amine or the 7-fluoro boron difluoride chelate derivative in MeCN. For this reason, S_NAr was tested in both DMSO and

pyridine to see if either produced a better yield than the reaction in MeCN. The advantage of using DMSO was that the reaction could be heated to higher temperatures, however removal of the solvent during the work-up was difficult due to its high boiling point. Although the reactions carried out in both solvents provided the product in higher yields than when run in MeCN, pyridine was the solvent of choice as the reaction could be carried out at room temperature, presumably since pyridine can also act as a base. These mild conditions, and the fact that the 7-fluoro boron difluoride chelate derivative exhibited high solubility in pyridine would hopefully limit side reactions and improve starting material consumption, especially when using excess amine.





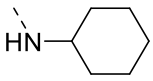
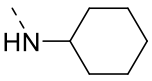
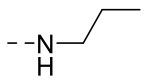
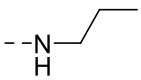
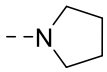
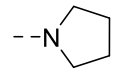
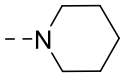
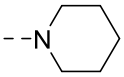
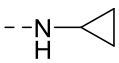
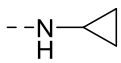
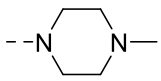
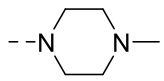
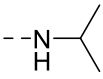
No.	R	Yield %	No.	R	Yield %
150		52	**157**		87
151		52	**158**		89
152		95	**159**		71
153		90	**160**		98
154		65	**161**		70
155		51	**162**		87
156		77	**163**		30
			164		88

Table 3: Initial Moxi-Trova analogues synthesised via S_NAr of 7-fluoro substituent.

Initially a series of simplistic amines **150**-**164** were incorporated into each quinolone core, starting from methylamine, and increasing in alkyl chain length and aliphatic ring size (Table 3). These small one-point changes in the structures will enable meaningful SAR to be obtained from the biological data and will prove whether bulky bicyclic amines like those of both Trova and Moxi are necessary for RSK4 activity.

Synthesis of (1α,5α,6α)-6-tert-Butyloxycarbonylamino-3-azabicyclo[3.1.0]hexane

The amino-substituted 3-azabicyclo[3.1.0]-hexane substituent of Trova was synthesised in order to generate the two 8-methoxy-4-quinolone analogues of Trova, with the cyclopropyl and 2,4-difluorobenzene N-1 substituents.

Synthesis of (1α,5α,6α)-6-*tert*-Butyloxycarbonylamino-3-azabicyclo[3.1.0]hexane (**170**) was carried out based on a reported procedure by Sun *et al*, starting from *N*-benzylmaleimide (**165**) which underwent cyclopropanation using bromonitromethane and K_2CO_3 generating intermediate **166** (Scheme 43).[235] The average yield for this reaction was low at around 30 %, which appeared to decrease with increasing scale. This was a result of undesired side reactions of both the *N*-benzylmaleimide and the bromonitromethane with the base, leading to tar formation. Formation of the desired *exo*-stereoisomer was confirmed by observation of the ^{1}H NMR. The vicinal H-H coupling constant between the proton alpha to the nitro group, and the two protons of the bridge is very low at 1.6 Hz, consistent with the *trans* configuration. If the *endo*-product had been isolated, this coupling constant would have been much higher at around 7-13 Hz, representative of the *cis* configuration.[236] Formation of the *exo*-stereoisomer is favoured due to steric hindrance of the puckered bicyclic system with the nitro group in the *endo*-product, a clash that is alleviated when the protons of the cyclopropane are *trans* to each other (Figure 61).

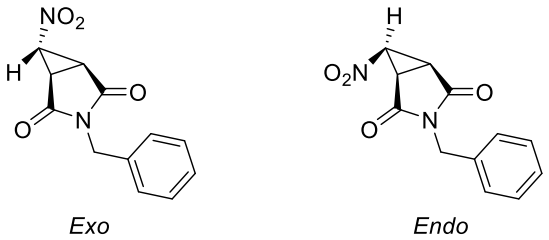
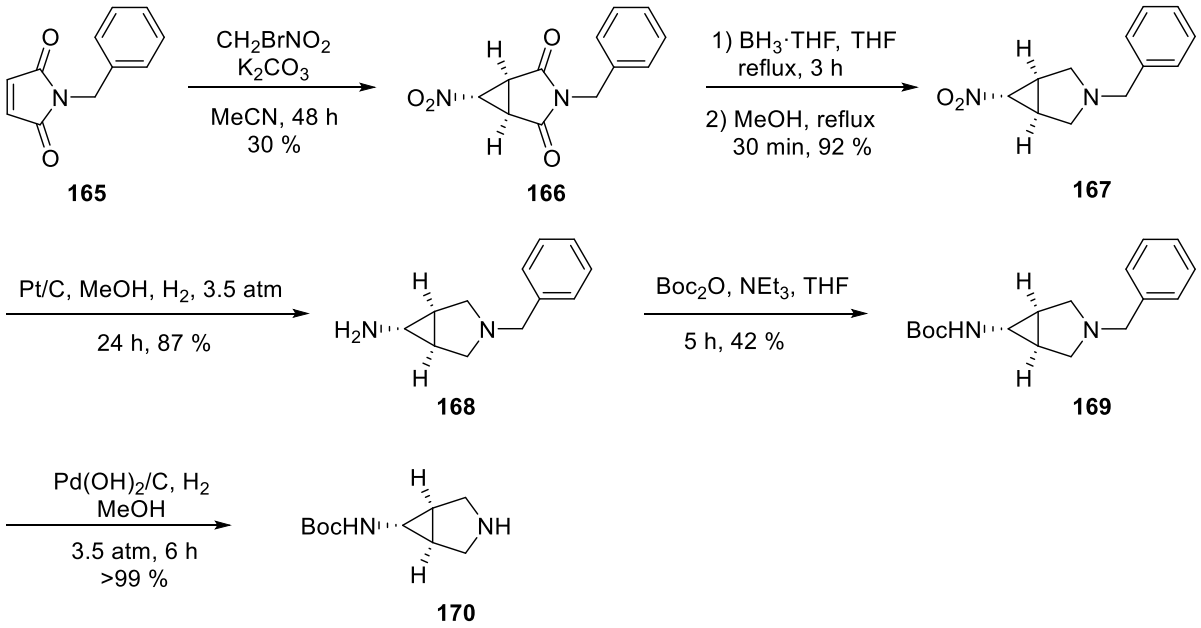


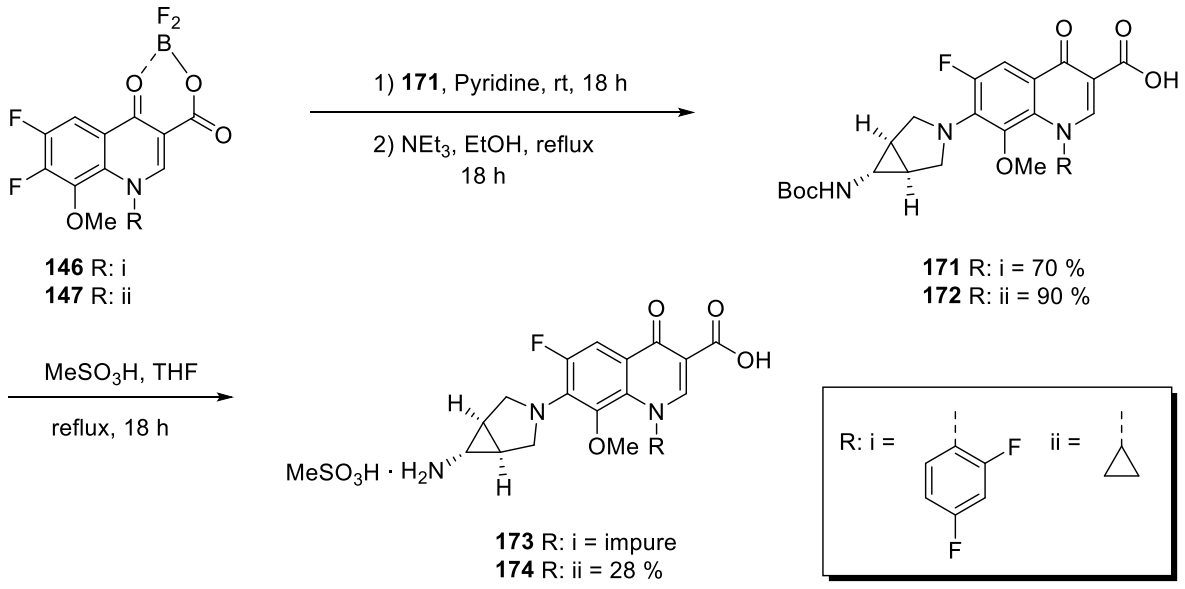
Figure 61: The structures of the *endo*- and *exo*-stereoisomers of 3-azabicyclo[3.1.0]hexane **167**.

This was followed by amide reduction of 3-azabicyclo[3.1.0]hexane **166** using BH_3-THF and selective reduction of the nitro group by hydrogenation over a platinum on carbon catalyst (Scheme 43).[237] Initially this was carried out at 3.5 atm however this led to decomposition of the cyclopropyl ring. The pressure was consequently reduced to 3 atm, providing the desired primary amine **168** in 90% yield. Amine **168** was then protected with a Boc group using di-*tert*-butyl dicarbonate under basic conditions and the benzyl group was reduced by hydrogenation over a palladium on carbon catalyst generating (1α,5α,6α)-6-*tert*-butyloxycarbonylamino-3-azabicyclo[3.1.0]hexane **170** in almost quantitative yield.



Scheme 43: Synthesis of (1α,5α,6α)-6-*tert*-Butyloxycarbonylamino-3-azabicyclo[3.1.0]hexane (**170**).

S_NAr using Boc-protected amine **170** with 2,4-difluorobenzene intermediate **146** and cyclopropyl intermediate **147** were carried out using conditions previously described (Scheme 44), and high yields were achieved for each. This was followed by removal of the Boc group under acidic conditions, and formation of an amine salt. When using HCl in diethyl ether, the product precipitated out of solution, however for both derivatives, impurities were present that could not be removed with trituration in various solvents, or by column chromatography. For this reason, methanesulfonic acid was selected to deprotect the primary amine in milder conditions using two equivalents of acid in THF. This worked well for cyclopropylamine intermediate **172** and the desired mesylate salt **174** was generated in 28% after product precipitation. When this procedure was used for 2,4-difluorobenzene intermediate **171**, the product **173** was observed by ^{1}H NMR, however there was again significant impurities present. Several methods for purification were attempted, including preparative HPLC, however none were successful, and the product obtained was not pure enough for biological testing.



Scheme 44: Nucleophilic aromatic substitution of the 7-fluoro substituent using Boc protected amino-substituted 3-azabicyclo[3.1.0]-hexane **170** and subsequent Boc deprotection to generate amine salts **173** and **174**.

Improving Derivative Solubility

An issue with fluoroquinolones is that they often have poor water solubility which can result in low bioavailability. A reason for this is that they are amphoteric, containing both basic and acidic groups which can both be ionised to varying degrees depending on the pH. This can affect the solubility and lipophilicity of fluoroquinolones, which are crucial parameters in determining the availability of drug molecules to enter biological membranes. [238] As a result fluoroquinolone antibiotics have been known to cause drug precipitation in the body which can lead to deposits in sites such as the cornea and in the kidneys.[239,240]

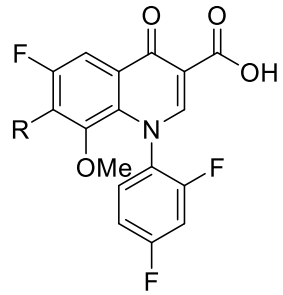
There are a number of ways in which the water solubility of a drug molecule can be improved, including reducing hydrophobicity, introducing soluble appendages and the formation of salts with pharmaceutically acceptable counterions.[241,242] With the aim to improve solubility, amines were selected for S_NAr of the 7-fluoro substituent which either contained ionisable groups that could readily form salts under acidic or basic conditions or oxygen containing groups such as hydroxyl groups. These can form hydrogen bonds with water and have been reported as being effective solubilising appendages,[241] especially in the cases of sugars such as glucose.

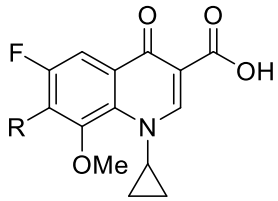
A summary of all compounds synthesised, including salt formations can be found in Table 4. Amines such as piperazine and piperidin-4-amine with basic free amines had to be introduced in their Boc-protected forms and were then deprotected under acidic conditions to generate the appropriate salt. Some derivatives have been synthesised as the HCl salt and/or the mesylate salt. Both forms are commonly used in the pharmaceutical industry with HCl anionic salts the most widely used as chloride ions exist in gastric and intestinal fluids therefore the salt will not induce toxicity.[242] Mesylate salts of fluoroquinolone antibiotics have been made in the past and have shown improvements in solubility, including for Trova.[243]

Efforts were made to generate anionic amine salts of previously synthesised analogues shown in Table 3 under acidic conditions, however the neutral compounds were always

recovered. Using a predictive pKa programme (ilab.cds.rcs.org) it was observed that the pKa's for the protonated amines of these intermediates which contained one nitrogen were between -1 and 1, therefore even under strongly acidic conditions, the amines may not be protonated. For this reason, the cationic salts of a few derivatives were synthesised due to the presence of the carboxylic acid. Sodium hydroxide was added to a solution of the derivative in ethanol and the sodium salt was isolated by filtration following precipitation. With both neutral compounds and cationic salts of the same derivatives in hand, a direct comparison to assess which formation was more soluble could be carried out.

In total 33 compounds were synthesised varying the substituent at the C-7 position of the 8-methoxy-4-quinolone core with different amines for the purpose of generating meaningful SAR about the size and shape tolerated in this position, and to also assess the solubility by including solubilising groups and forming the anionic and cationic salts. In general, compounds baring the 2,4-difluorobenzene moiety at the N-1 position were less soluble in DMSO or H_2O than those with a cyclopropyl group in this position. Furthermore, compounds isolated as the mesylate salts were much more soluble than sodium salts which were almost impossible to solubilise. Introduction of small acyclic amines such as methylamine and propylamine provided compounds with greater solubility than those with cyclic groups such as pyrrolidine and piperidine. However cyclic amines with ionisable groups attached, including hydroxyl and amino groups had superior solubility as expected.





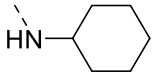
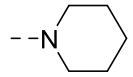
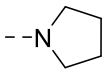
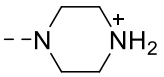
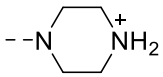
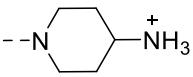
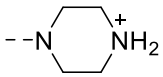
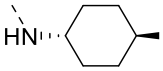
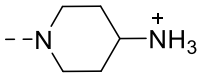
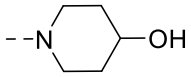
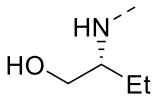
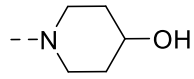
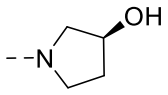
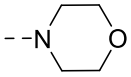
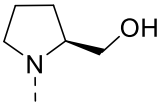
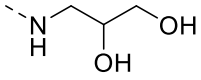
No.	R	Counter-ion	Yield %	No.	R	Counter-ion	Yield %
175		Na^+	64[a]	**184**		Na^+	47[a]
176		Na^+	68[a]	**185**		HCl	1) 65[b] 2) >99
177		HCl	1) 75[b] 2) >99	**186**		HCl	1) 99[b] 2) 98
178		$MeSO_3^-$	1) 75[b] 2) 98	**187**		N/A	91
179		$MeSO_3^-$	1) 78[b] 2) 92	**188**		N/A	70
180		N/A	90	**189**		N/A	40
181		N/A	75	**190**		N/A	30
182		N/A	85	**191**		N/A	70
183		N/A	84				

Table 4: Moxi-Trova analogues synthesised in order to improve solubility. [a] Yield for salt formation only, as S_NAr yield has been quoted in Table 3. [b] Yield for S_NAr and for salt formation included.

5.2. Part 2: Biological Assessment

5.2.1. RSK4 Biochemical Assay

The initial plan for biological assessment of the synthesised Moxi and Trova derivatives was to employ the HTRF assay used to identify the original hit compounds, measuring interference of ERK2 mediated RSK4 activation by each derivative. However, due to limited availability of resources, this assay could not be carried out.

As an alternative Luiza Dos Reis Cruz, another chemist from our group, worked within a biology group with RSK expertise at Vanderbilt University led by Dr Deborah Lannigan, to develop a RSK4 activity assay. This assay differed from the original in that the readout was obtained from phosphorylation of ERα, a downstream substrate of the RSK family,[244] rather than activation of RSK4 itself. However, the recombinant RSK4 produced for this assay was in its fully phosphorylated form. Since the fluoroquinolone compounds have been shown to function by preventing RSK4 phosphorylation, and do not bind to fully phosphorylated RSK4 (Chrysostomou *et al*., submitted manuscript), inhibition of RSK4 with these compounds could not be assessed. For use in evaluating the activity of the fluoroquinolone derivatives, this assay would require further optimisation with phosphatase treatments of RSK4 to provide the inactivated form of the protein.

5.2.2. RSK4 Cell-based Assay

Instead, a cell-based assay was developed by Luiza in order to assess the degree of RSK4 phosphorylation following treatment of a cell-line overexpressing RSK4 with the Moxi and Trova derivatives. If the derivatives do inhibit RSK4 activation, a decrease in phosphorylation will be observed compared to untreated cells in which RSK4 will be constitutively activated.

To observe changes in RSK4 phosphorylation, GFP tagged RSK4 was engineered into HEK293 cells and the cells were then incubated for 2 h with either 50 μM inhibitors, DMSO (negative control) or 10 μM UO126, an ERK inhibitor (positive control). Only derivatives

soluble at 50 mM DMSO were used therefore, of the 33 Moxi-analogues synthesised, 16 were tested. EGF was then added at the end of the incubation period at a final concentration of 20 nM to trigger activation of the upstream signalling pathway. The cells were then lysed and the resulting lysates were analysed using immunoblotting with phospho-RSK (pRSK) specific antibodies to detect phosphorylated RSK4, shown as two bands on the western-blot (Figure 63A). The lower band represents phosphorylation of the endogenous RSK1-4 while the upper band corresponds to the engineered GFP-tagged RSK4. The results were normalised against total GFP (and therefore exogenous RSK4) detected using a GFP specific antibody. To quantify the bands of the Western blots, ImageJ was used and the exogenous pRSK and exogenous pRSK4 values were plotted (Figure 63B).

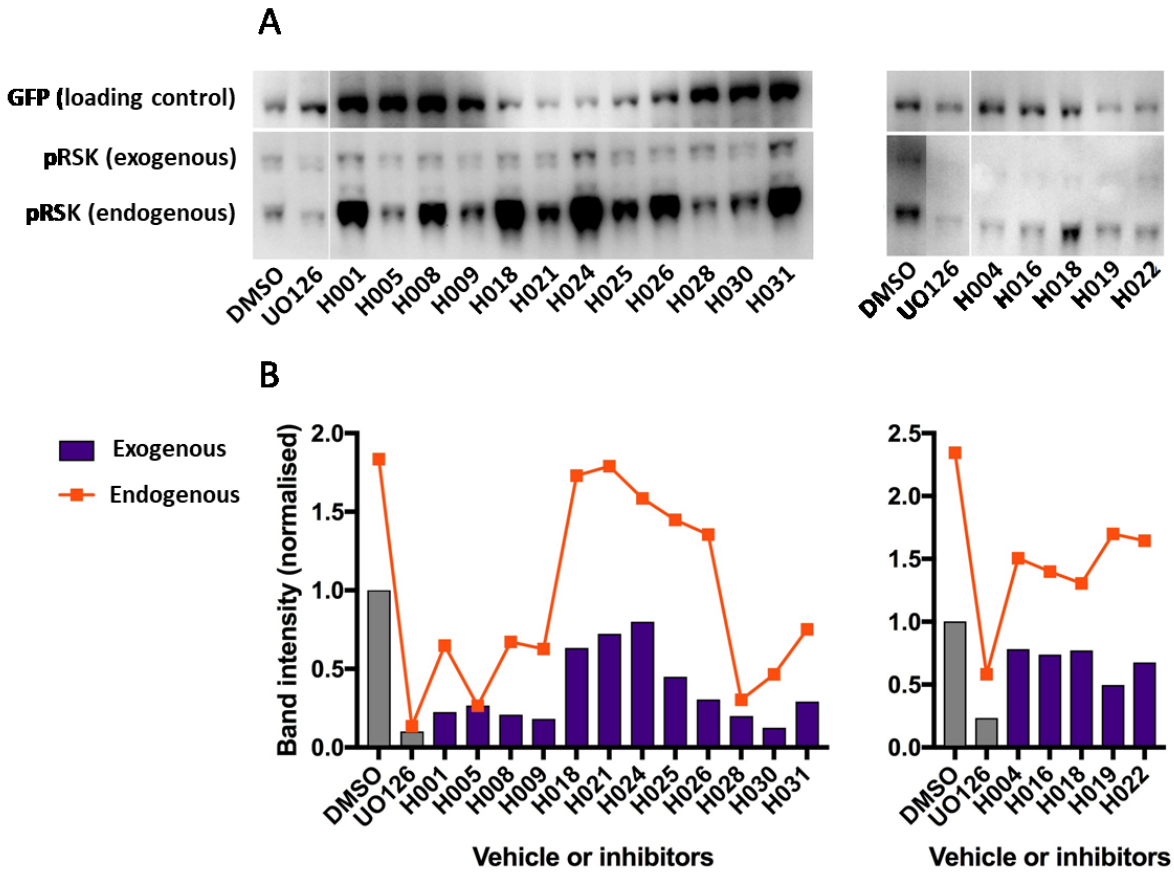


Figure 63A: Western blots showing detection of endogenous pRSK (lower band) and exogenous pRSK4 (upper band) following treatment with 16 Moxi-derivatives at 50 μM, DMSO (negative control) or UO126 at 10 μM (positive control), using a GFP loading control; **B**: Band intensity as quantified from western blots and normalised to the DMSO control, in which the exogenous pRSK4 and endogenous pRSK is represented as bars and lines respectively. Data generated by Luiza Dos Reis Cruz.

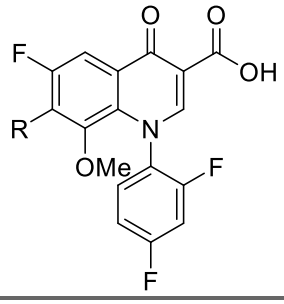
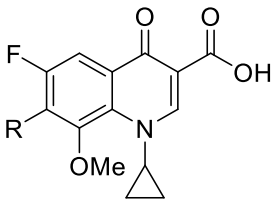
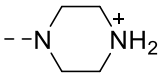
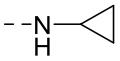
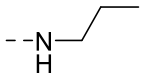
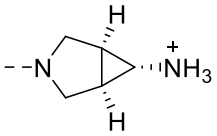
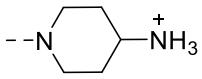
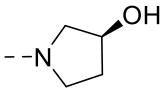
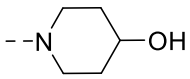
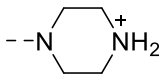
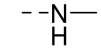
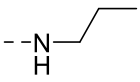
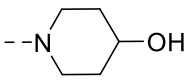
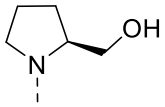
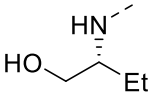
					
> 50% Inhibition of pRSK4					
No.	**R**	**Counter-ion**	**No.**	**R**	**Counter-ion**
H001 (178)		$MeSO_3^-$	**H019** (162)		N/A
H005 (152)		N/A	**H025** (187)		N/A
H008 (180)		N/A	**H026** (174)		$MeSO_3^-$
H009 (179)		$MeSO_3^-$	**H030** (190)		N/A
H028 (181)		N/A	**H031** (185)		HCl
< 50% Inhibition of pRSK4					
H004 (151)		N/A	**H016** (158)		N/A
			H018 (159)		N/A
			H021 (188)		N/A
			H022 (191)		N/A
			H024 (189)		N/A

Table 5: The structures of Moxi-derivatives that were soluble in 50 mM DMSO and were therefore tested in cell-based assay. The compounds are grouped into those that inhibited pRSK4 by more or less than 50% compared to the negative control. Numbering system used for biological testing.

From this data, it appears that 10 of the 16 compounds tested show at least 50% inhibition of RSK4 phosphorylation as quantified from the exogenous pRSK4 bands. A reduction in endogenous pRSK is also observed for these 10 compounds though this represents phosphorylation of all the RSK isoforms and is not specific for pRSK4, as a non-RSK specific antibody was used to run the gels.

Although a greater number of derivatives with a cyclopropyl group at the N-1 position were tested due to better solubility, a greater percentage of the compounds with a 2,4-difluorophenyl group at the N-1 position showed more than 50% pRSK4 inhibition (Table 5). In addition, those baring a 2,4-difluorophenyl group generally showed greater percentage inhibition compared to inhibitors with a cyclopropyl group. This suggests that this group may be important for RSK4 inhibition. Moreover, the best inhibitors appear to have a hydrogen donor on the C-7 side chain, either in the form of a hydroxyl group, or a primary or secondary amine. These features are clearly important for solubility but may also prove valuable for RSK4 inhibition.

Alongside these compounds, a closely related series based on the Trova naphthyridine core was synthesised by Luiza in which the C-7 group was varied in the same manner. The most soluble of these have also been tested using this cell-based assay and the results suggest that there is a similar trend in which compounds baring a 2,4-difluorophenyl group produce the highest percentage inhibition of RSK4 phosphorylation.

To validate these findings, the assay would need to be repeated to obtain statistically significant data and carried out using different concentrations of inhibitor to generate a dose response. Furthermore, to confirm that the phosphorylation detected using immunoblotting is in fact from pRSK4, proteomics could be employed to identify the phosphorylation state of key residues of RSK4, depending on the treatment of cells.

5.3. Conclusions and Future Work

A large number of compounds have been synthesised for the inhibition of RSK4, a lung cancer promotor, based on hit antibiotics, Moxi and Trova. With the aim to improve potency, compounds were initially designed to combine core structural features of both Moxi and Trova, while providing diversity at the C-7 position. As the solubility of these compounds were an issue and could limit their biological application, alternative salt formations were investigated, as well as introduction of solubilising groups in the C-7 position. The most soluble derivatives across both series were tested in a cell-based assay measuring the levels of exogenous RSK4 phosphorylation, and 17 of the 28 tested compounds showed at least 50% inhibition with a moderate structural trend. This was a promising result and could provide a foundation for future SAR investigations following a more iterative approach, with variations to different parts of the molecule.

Validation of the cell-based assay would be required before testing of new compounds to ensure that the readout is detection of RSK4 phosphorylation. It would also be useful to test Moxi and Trova in this assay to evaluate whether the derivatives have improved RSK4 inhibition. A limitation of the cell-based assay at this early stage of drug development is that it is hard to say whether the compounds that do not show inhibition are inactive or simply impeded by poor cell membrane permeability. Therefore, it may be useful in the future to use a biochemical assay to initially test for RSK4 inhibition as this can be easily adapted for testing many compounds at once, and the activity of a drug can be assessed, regardless of its pharmacokinetic properties.

The most promising compounds could then be tested in a lung cancer cell chemo-sensitisation assay to assess whether they maintain the synergistic effect with cisplatin and taxol shown by Moxi and Trova. Furthermore, these compounds could be tested in the context of lung cancer cell migration and invasion, processes which if successfully repressed, could lead to a novel anti-metastatic treatment.

6. Final Remarks

While both projects have yielded positive results, with compounds synthesised having either a desired phenotypic effect or inhibition of the desired target, development to an advanced stage has been hindered by a number of challenges. These include difficulties in assay development and limited availability of resources required for assays to be carried out at the frequency needed for drug development. Nevertheless, both projects have been advanced to a stage which will provide a valuable foundation for future work.

7. Experimentals

7.1. General Methods

All reagents were obtained from commercial sources and were used as purchased from the manufacturers unless stated otherwise. Anhydrous solvents used were freshly distilled under N_2 from calcium hydride (DCM, NEt_3 and pyridine), sodium benzophenone (THF, Et_2O and PhMe) and magnesium (MeOH). Use of H_2O refers to redistilled H_2O. Organometallic reagents were titrated using no-deuterium proton NMR spectroscopy described by Hoye *et al.*[245] Reactions requiring anhydrous conditions were conducted in oven-dried glassware under a flow of dry N_2. Room temperature (rt) conditions refer to ambient temperature without external heating or cooling. Temperatures at 0 °C are achieved using an ice/salt bath.

Reactions were monitored by analytical thin-layer chromatography (TLC) carried out on pre-coated aluminium backed plates with Merck Kiesegel 60 F254 (230–400 mesh). The plates were visualised under UV light (254 nm) and were stained with either $KMnO_4$ (aq. potassium permanganate), ninhydrin solution or PMA (phosphomolybdic acid solution). Column chromatography was carried out with Fluorochem 60 silica gel (230–400 mesh, 40-63 μm). Hydrogenation reactions at higher pressures than atmospheric were carried out in a 3911 Parr shaker hydrogenator at rt. Microwave irradiation was carried out using a Discoverer SP system (CEM Technology).

^1H, ^{13}C and ^{19}F NMR spectra were obtained using a Bruker Advance 400 spectrometer at 400 MHz, 101 and 377 MHz respectively. For some compounds, ^{13}C NMR spectra were obtained using a Bruker Advance 500 spectrophotometer at 126 MHz. For ^1H NMR spectra chemical shifts are quoted in parts per million (ppm) written as δ values to the nearest 0.01 ppm. Coupling constants are quoted as *J* values measured in Hertz (Hz) to the nearest 0.1 Hz. ^1H NMR spectra are reported as follows: chemical shift, signal splitting (singlet (s), doublet (d), t (triplet), q (quartet), m (multiplet) or as a combination of these), coupling

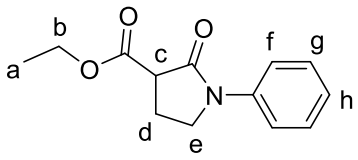
constant, integration, assignment). ^{13}C NMR spectra were recorded with broadband proton spin decoupling and chemical shifts are quoted to the nearest 0.1 ppm with ^{13}C - ^{19}F coupling constants reported to the nearest 0.1 Hz. ^{19}F NMR spectra were recorded with proton decoupling and chemical shifts are quoted to the nearest 0.1 Hz with coupling constants reported to the nearest 0.1 Hz. All chemical shifts are referenced to the residual solvent signals: $CDCl_3$ in ^1H spectra (δH) = 7.26, ^{13}C spectra (δC) = 77.00; CD_3OD (δH) = 3.34, (δC) = 49.00; d_6-DMSO(δH) = 2.50, (δC) = 77.00; d_3-MeCN(δH) = 1.96, (δC) = 118.95, 1.00.

High and low resolution mass spectra (HRMS, EI, ES) were recorded by the Imperial College London Department of Chemistry Mass Spectroscopy Service on a Micromass Platform II and Micromass AutoSpeq-Q spectrometers. Melting points were determined using a Stuart SMP11 machine with a maximum temperature of 250 °C and the values are uncorrected. Infrared spectra were recorded either neat on a Perkin Elmer Spectrum 100 fitted with a universal ATR accessory.

For purity analysis, analytical LC-MS was carried out by the Imperial College London Department of Chemistry Mass Spectroscopy Service using a Waters Aquity UPLC I-CLASS instrument. A Waters BEH Acquity C18 column (50mm x 2.1mm) was used with an injection volume of 10 µL, a flow rate of 0.5 mL/min and a column temperature of 40 °C. Each run lasted 4 minutes starting with a solvent system consisting of 95 % solvent A (99.9% water, 0.1% formic acid) and 5 % solvent B (99.9% acetonitrile, 0.1% formic acid), and linearly adjusting to 5 % solvent A and 95 % solvent B at 3.2 minutes. At 3.5 minutes the solvent system returned to the original composition and the purity was assessed using the UV trace, measured by a photodiode array detector (210 -280 nm). HPLC grade solvents were used obtained from either Sigma Aldrich or Thermo Fisher. Optical rotations were recorded on a Perkin-Elmer 241 Polarimeter with a path length of 0.5 dm. Concentrations (c) are quoted in g/100 mL.

7.2. Synthetic Procedures: Part 1

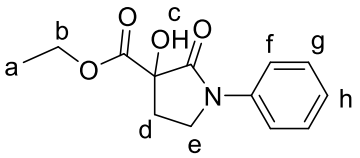
(±)-Ethyl 2-oxo-1-phenylpyrrolidine-3-carboxylate - 30



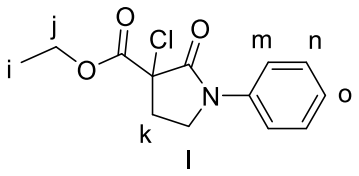
Based on reported procedure by Lui *et al.*[246] To a solution of diisopropylamine (2.70 mL, 15.5 mmol) in dry THF (8 mL) was added *n*-BuLi (2.9 M in hexanes, 5.35 mL) dropwise at -78 °C under N_2. The solution was stirred at 0 °C for 20 min before the dropwise addition of a solution of *N*-phenylpyrrolidinone (0.50 g, 6.2 mmol) in dry THF (8 mL) at -40 °C. The reaction was stirred for 30 min at this temperature followed by the addition of a solution of diethyl carbonate (1.90 mL, 15.5 mmol) in dry THF (9 mL). The reaction was stirred at -40 °C for 2 h and then for 16 h at rt. The reaction mixture was quenched with saturated aq. NH_4Cl at 0 °C and the aqueous phase was extracted with DCM (50 mL x 3). The combined organic phases were combined, dried over Na_2SO_4 and purified by flash column chromatography (30 % EtOAc in pentane) giving phenylpyrrolidine **30** as an off-white solid (1.27 g, 88 %).

^{1}H NMR (400 MHz, $CDCl_3$) δ 7.63 – 7.58 (m, 2H, 2 x CH-*f*), 7.40 – 7.32 (m, 2H, 2 x CH-*g*), 7.19 – 7.13 (m, 1H, CH-*h*), 4.30 – 4.21 (m, 2H, CH_2-*b*), 3.98 (ddd, *J* = 9.2, 8.6, 5.2 Hz, 1H, CH-*e*), 3.84 (ddd, *J* = 9.2, 8.1, 6.2 Hz, 1H, CH-*e*), 3.63 (dd, *J* = 9.2, 7.0 Hz, 1H, CH-*c*), 2.54 (dddd, *J* = 13.1, 8.4, 7.0, 6.2 Hz, 1H, CH-*d*), 2.39 (dddd, *J* = 13.1, 9.2, 8.1, 5.2, 1H, CH-*d*), 1.31 (t, *J* = 7.1 Hz, 3H, CH_3-*a*); **^{13}C NMR** (101 MHz, $CDCl_3$) δ 170.0, 169.0, 139.0, 129.0 (2C), 125.1, 120.3 (2C), 61.9, 50.1, 47.4, 22.3, 14.3; **HRMS (ES+)** Calculated for $C_{13}H_{16}NO_3$ ($M+H^+$): 234.1130; found: 234.1129. These spectroscopic data correspond to previously reported data.[247]

<u>Method 1</u> (±)-Ethyl 3-hydroxy-2-oxo-1-phenylpyrrolidine-3-carboxylate (31) and (±)-Ethyl 3-chloro-2-oxo-1-phenylpyrrolidine-3-carboxylate (32)



31



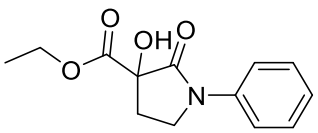
32

Based on a procedure by Sherer *et al.*[100] To a solution of phenylpyrrolidine **30** (100 mg, 0.43 mmol) in *iso*propanol (3 mL) was added $CeCl_3 \cdot 7H_2O$ (65 mg, 0.17 mmol) and O_2 gas was bubbled through the solution at rt for 15 min. The reaction was then stirred under O_2 (1 atm) for 16 h, then concentrated under rotary evaporation and purified by flash column chromatography (30 % EtOAc in pentane) to give hydroxy-phenylpyrrolidine **31** as an off-white solid (38 mg, 35 %) and chloro-phenylpyrrolidine **32** as a yellow oil (33 mg, 29 %).

31: **IR V_{max} / cm^{-1}**: 3388, 2982, 1744, 1692, 1406, 1300, 1155; **^{1}H NMR** (400 MHz, $CDCl_3$) δ 7.68 – 7.62 (m, 2H, 2 x CH-*f*), 7.44 – 7.37 (m, 2H, 2 x CH-*g*), 7.24 – 7.18 (m, 1H, CH-*h*), 4.36 – 4.22 (m, 2H, CH_2-*b*), 4.04 – 3.96 (m, 2H, CH-*e* + OH-*c*), 3.89 (td, *J* = 9.2, 2.7 Hz, 1H, CH-*e*), 2.72 (ddd, *J* = 13.3, 7.4, 2.7 Hz, 1H, CH-*d*), 2.36 (ddd, *J* = 13.3, 9.2, 8.1 Hz, 1H, CH-*d*), 1.30 (t, *J* = 7.1 Hz, 3H, CH_3-*a*); **^{13}C NMR** (101 MHz, $CDCl_3$) δ 171.4, 170.0, 138.9, 129.2 (2C), 125.6, 120.2 (2C), 78.9, 63.0, 45.4, 30.5, 14.2; **HRMS (ES+)** Calculated for $C_{13}H_{16}NO_4$ ($M+H^+$): 250.1079; found: 250.1078. These spectroscopic data correspond to previously reported data.[247]

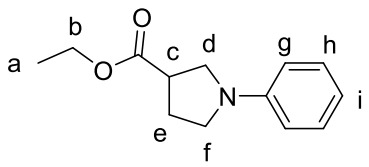
32: **IR V_{max} / cm^{-1}**: 2983, 1757, 1706, 1399, 1302, 1252; **^{1}H NMR** (400 MHz, $CDCl_3$) δ 7.67 – 7.61 (m, 2H, 2 x CH-*m*), 7.44 – 7.36 (m, 2H, 2 x CH-*n*), 7.25 – 7.19 (m, 1H, CH-*o*), 4.35 (q, *J* = 7.1 Hz, 2H, CH_2-*j*), 4.06 – 3.90 (m, 2H, CH_2-*l*), 3.10 (ddd, *J* = 13.8, 7.7, 7.0 Hz, 1H, CH-*k*), 2.59 (ddd, *J* = 13.8, 7.0, 4.0 Hz, 1H, CH-*k*), 1.35 (t, *J* = 7.1 Hz, 3H, CH_3-*i*); **^{13}C NMR** (101 MHz, $CDCl_3$) δ 166.7, 166.4, 138.5, 129.1 (2C), 125.7, 120.3 (2C), 69.0, 63.6, 45.7, 34.2, 14.0; **HRMS (ES+)** Calculated for $C_{13}H_{15}ClNO_3$ ($M+H^+$): 268.0740; found: 268.0738.

<u>Method 2</u> (±)-Ethyl 3-hydroxy-2-oxo-1-phenylpyrrolidine-3-carboxylate - 31



Based on a procedure by Liang *et al.*[88] To a solution of phenylpyrrolidine **30** (1.1 g, 4.9 mmol) in DMSO (10 mL) was added $P(OEt)_3$ (1.7 mL, 9.8 mmol) and Cs_2CO_3 (0.32 g, 0.98 mmol) under O_2 (1 atm) and the reaction was stirred at rt for 2 h. The reaction was diluted with brine (30 mL), extracted with EtOAc (3 × 40 mL) and washed with brine (3 × 50 mL). The solution was dried over Na_2SO_4, concentrated under rotary evaporation then purified by flash column chromatography (30 % EtOAc in pentane) to give hydroxy-phenylpyrrolidine **31** as a white solid (0.88 g, 72 %). All data corresponded with data collected from method 1.

(±)-Ethyl 1-phenylpyrrolidine-3-carboxylate - 34

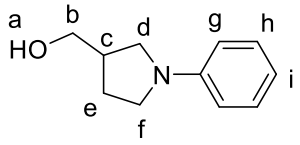


To a solution of phenylpyrrolidine **30** (0.10 g, 0.43 mmol) in THF (2 mL) was added BH_3·THF (0.64 mL, 1 M in THF) and the reaction was stirred under N_2 at rt for 16 h. MeOH (1 mL) was then added, then water (10 mL) and the aqueous phase was extracted with EtOAc (3 x 10 mL). The combined organic phases were washed with brine (20 mL), dried over Na2SO4, filtered and concentrated under rotary evaporation. The resulting residue was purified by flash column chromatography (30 % EtOAc in pentane) to give phenylpyrrolidine ester **34** as a colourless oil (15 mg, 16 %).

IR Vmax / cm^{-1}: 2850, 1732, 1599, 1507, 1371, 1185, 748; **^{1}H NMR** (400 MHz, $CDCl_3$) δ 7.28 – 7.20 (m, 2H, 2 x CH-*g*), 6.73 – 6.67 (m, 1H, CH-*i*), 6.61 – 6.54 (m, 2H, 2 x CH-*h*), 4.18 (q, J = 7.1 Hz, 2H, CH_2-*b*), 3.61 – 3.49 (m, 2H, CH-*d* + CH-*f*), 3.47 – 3.39 (m, 1H, CH-*f*), 3.38

– 3.30 (m, 1H, CH-*d*), 3.24 – 3.15 (m, 1H, CH-*c*), 2.34 – 2.23 (m, 2H, CH_2-*e*), 1.28 (t, *J* = 7.1 Hz, 3H, CH_3-*a*); **^{13}C NMR** (101 MHz, $CDCl_3$) δ 173.8, 147.7, 129.3 (2C), 116.3, 112.0 (2C), 61.0, 50.23, 47.4, 43.3, 28.7, 14.4.

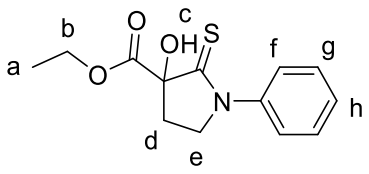
(±)-(1-Phenylpyrrolidin-3-yl)methanol - 35



To a solution of phenylpyrrolidine **30** (0.20 g, 0.86 mmol) in THF (4 mL) was added BH_3·THF (2.1 mL, 1 M in THF) and the reaction was heated to reflux under N_2 for 16 h. MeOH was then added (2 mL), then water (10 mL) and the aqueous phase was extracted with EtOAc (3 x 10 mL). The combined organic phases were then washed with brine (20 mL), dried over Na_2SO_4, filtered and concentrated under rotary evaporation. The resulting residue was purified by flash column chromatography (30 % EtOAc in Pentane) to give primary alcohol **35** as a purple oil (97 mg, 64 %).

IR Vmax / cm^{-1}: 3339, 2925, 1598, 1507, 1372, 747; **^{1}H NMR** (400 MHz, $CDCl_3$) δ 7.26 – 7.20 (m, 2H, 2 x CH-*g*), 6.74 – 6.68 (m, 1H, CH-*i*), 6.63 – 6.57 (m, 2H, 2 x CH-*h*), 3.71 (qd, *J* = 10.4, 6.9 Hz, 2H, CH_2-*b*), 3.46 (dd, *J* = 9.3, 7.4 Hz 1H, CH-*d*), 3.44 – 3.38 (m, 1H, CH-*f*), 3.33 (dt, *J* = 9.1, 7.4, CH*f*), 3.16 (dd, J = 9.3, 6.1 Hz, 1H, CH-*d*), 2.66 – 2.52 (m, 1H, CH-*c*), 2.17 (dtd, *J* = 12.3, 7.4, 4.9 Hz, 1H, CH-*e*), 1.85 (ddd, *J* = 15.1, 12.3, 7.4 Hz, 1H, CH-*e*), 1.62 (s, 1H, OH-*a*); **^{13}C NMR** (101 MHz, $CDCl_3$) δ 148.0, 129.3 (2C), 115.9, 111.9 (2C), 65.5, 50.7, 47.2, 41.0, 28.0.

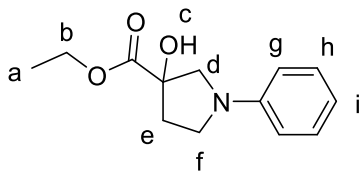
(±)-Ethyl 3-hydroxy-1-phenyl-2-sulfanylidenepyrrolidine-3-carboxylate - 36



Based on reported procedure by Banerjee *et al.*[248] To a solution of hydroxy-phenylpyrrolidine **31** (0.10 g, 0.40 mmol) in dry toluene (4 mL) was added Lawesson's reagent (0.34 g, 0.60 mmol) and the resulting suspension was heated to 120 °C for 16 h. The reaction was concentrated under rotary evaporation and the resulting residue was purified by flash column chromatography (20 % EtOAc in pentane) to give thiolactam **36** as a white solid (38 mg, 35 %).

IR V_{max} / cm^{-1}: 3453, 2980, 1743, 1497, 1433, 1296, 1165; **^{1}H NMR** (400 MHz, $CDCl_3$) δ 7.56 – 7.45 (m, 4H, 2 x CH-*f* + 2 x CH-*g*), 7.41 – 7.34 (m, 1H, CH-*h*), 4.36 – 4.25 (m, 3H, CH_2-*b* + CH-*e*), 4.24 (s, 1H, OH-*c*), 4.11 – 4.03 (m, 1H, CH-*e*), 2.84 (ddd, *J* = 13.2, 7.2, 2.1 Hz, 1H, CH-*d*), 2.40 (dt, *J* = 13.2, 9.2 Hz, 1H, CH-*d*), 1.35 (t, *J* = 7.1 Hz, 3H); **^{13}C NMR** (101 MHz, $CDCl_3$) δ 200.3, 171.0, 140.3, 129.6 (2C), 128.5, 124.6 (2C), 85.9, 62.8, 55.5, 32.2, 14.2; **HRMS (ES+)** Calculated for $C_{13}H_{16}NO_3S$ ($M+H^+$): 266.0851; found: 266.0856.

(±)-Ethyl 3-hydroxy-1-phenylpyrrolidine-3-carboxylate - 33

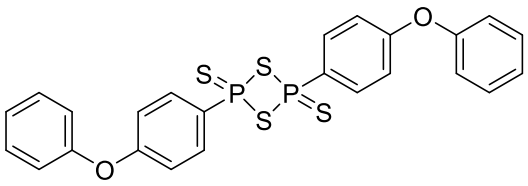


To a solution of thiolactam **36** (42 mg, 0.16 mmol) in THF (1.6 mL) and EtOH (0.4 mL) was added Raney Nickel slurry in water (20 % by weight, 10 mg) and the reaction was stirred vigorously under H_2 (1 atm) for 48 h. The reaction was filtered through Celite® washing with EtOH (10 mL) and the filtrate was concentrated under rotary evaporation. The resulting

residue was dissolved in $CHCl_3$ (5 mL) and passed through a Biotage phase separation funnel then concentrated under rotary evaporation and purified by flash column chromatography (20 % EtOAc in pentane) to give hydroxy-phenylpyrrolidine **33** as a yellow oil (12 mg, 32 %).

^{1}H NMR (400 MHz, $CDCl_3$) δ 7.26 – 7.20 (m, 2H, 2 x CH-*g*), 6.71 (t, J = 7.3 Hz, 1H, CH-*i*), 6.55 (d, J = 7.8 Hz, 2H, 2 x CH-*h*), 4.37 – 4.24 (m, 2H, CH_2-*b*), 3.77 (d, J = 10.1 Hz, 1H, CH-*d*), 3.61 – 3.49 (m, 2H, CH_2-*f*), 3.41 (m, 2H, CH-*d* + OH-*c*), 2.48 (dt, J = 12.8, 8.7 Hz, 1H, CH-*e*), 2.19 (dddd, J = 12.8, 6.5, 3.5, 0.9 Hz, 1H, CH-*e*), 1.32 (t, J = 7.1 Hz, 3H, CH_3-*a*); **^{13}C NMR** (101 MHz, $CDCl_3$) δ 174.9, 147.5, 129.3 (2C), 116.4, 112.0 (2C), 79.8, 62.6, 59.3, 46.9, 37.7, 14.3.

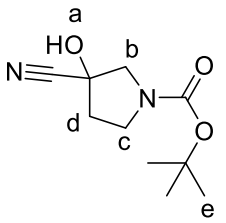
2,4-Bis(4-phenoxyphenyl)-1,3,2,4-dithiadiphosphetane 2,4-disulfide (Belleau's Reagent) - 38



Phosphorous pentasulfide (5.0 g, 11 mmol) and phenyl ether (13.4 mL, 85.5 mmol) in 1,2-dichlorobenzene (80 mL) were heated to 190 °C until H_2S evolution was no longer observed. The reaction was cooled to rt and a yellow solid crashed out which was collected by filtration, washing with Et_2O. The solid was recrystallized from PhMe and dried under high vacuum to yield Belleau's Reagent (**38**) as pale yellow solid (2.67 g, 45 %).

Mp ($CHCl_3$) 190°C (lit.[98] mp 187-190 °C); **IR Vmax / cm^{-1}**: 2824 (br), 2277 (br), 1585, 1490, 1195, 1141, 1010, 944, 839, 693.

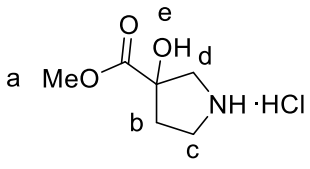
(±)-*Tert*-butyl 3-cyano-3-hydroxypyrrolidine-1-carboxylate - 39



Based on a procedure by Sherer *et al.*[100] To a solution of *tert*-butyl 3-oxopyrrolidine-1-carboxylate (1.0 g, 5.4 mmol) in THF (10 mL) and water (15 mL) was added $NaHSO_4$ monohydrate (1.8 g, 13 mmol) at 0 °C and the resulting mixture was stirred at 0 °C for 15 min before the addition of KCN (970 mg, 15.0 mmol). After stirring at rt for 24 h the reaction was diluted with EtOAc (20 mL) and washed with H_2O (4 x 50 mL). The organic phase was dried over Na_2SO_4, filtered and purified by flash column chromatography (2 % MeOH in DCM) to yield cyanohydrin **39** as a yellow solid (0.75 g, 65 %).

^{1}H NMR (400 MHz, $CDCl_3$) δ 4.55 (br s, 1H, OH-*a*), 3.81 – 3.47 (m, 4H, CH-*b* + CH_2-*c*), 2.37 – 2.29 (m, 2H, CH_2-*d*), 1.46 (s, 9H, $(CH_3)_3$-*e*); **^{13}C NMR** (101 MHz, $CDCl_3$) δ 154.6, 119.6, 80.9, 69.9, 57.5, 44.0, 38.7, 28.6 (3C); **HRMS (ES-)** Calculated for $C_{10}H_{16}ClN_2O_3$ ($M+Cl^-$): 247.0849; found: 247.0845; Calculated for $C_{11}H_{17}N_2O_5$ ($M-H^+ + HCO_2H$): 257.1137; found: 257.1140. These spectroscopic data correspond to previously reported data.[101]

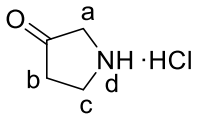
(±)-3-Hydroxy-3-(methoxycarbonyl)pyrrolidin-1-ium chloride - 41



To a solution of cyanohydrin **39** (100 mg, 0.47 mmol) in MeOH (2.5 mL) was added HCl (2 M in Et_2O, 2 mL) at 0 °C and the resulting mixture was stirred at rt for 24 h. The solvent was then removed by rotary evaporation to yield methylester **41** as a brown solid (80 mg, 93 %).

^{1}H NMR (400 MHz, MeOD) δ 3.66 – 3.42 (m, 3H, CH_2-*d* + CH-*c*), 3.42 – 3.21 (m, 4H, CH_3-*a* + CH-*c*), 2.43 – 2.30 (m, 1H, CH-*b*), 2.27 – 2.11 (m, 1H, CH-*b*); **^{13}C NMR** (101 MHz, MeOD) δ 173.0, 80.5, 56.0, 53.6, 45.8, 37.7.

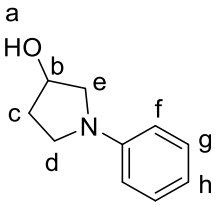
3-Oxopyrrolidin-1-ium chloride - 43



To a solution of *tert*-butyl 3-oxopyrrolidine-1-carboxylate (1.0 g, 5.4 mmol) in DCM (10 mL) was added HCl (2 M in Et_2O, 13.5 mL) and the reaction was stirred at rt for 48 h. The resulting solid was filtered and washed with Et_2O (20 mL) and DCM (20 mL) and then dried under high vacuum to yield pyrrolidinone **43** as a light brown solid (0.50 g, 76 %).

^{1}H NMR (400 MHz, DMSO) δ 10.02 (s, 2H, NH_2-*d*), 3.65 – 3.48 (m, 4H, CH_2-*a* + CH_2-*c*), 2.56 – 2.51 (m, 2H, CH_2-*b*); **^{13}C NMR** (101 MHz, DMSO) δ 208.3, 49.1, 42.4, 34.5.

(±)-1-Phenylpyrrolidin-3-ol - 50

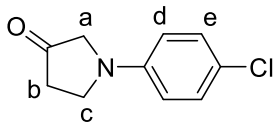


Based on a procedure by Ju and Varma.[111] To a 10 mL microwave vial was added aniline (0.10 mL, 1.1 mmol), 2,4-dibromobutan-1-ol (0.20 mL, 1.7 mmol), K_2CO_3 (0.41 g, 3.2 mmol) and H_2O (2 mL) and the vial was sealed and irradiated in a microwave for 40 min at 120 °C. The reaction was diluted with H_2O (20 mL) and the aqueous phase was then extracted using EtOAc (3 x 10 mL) and the combined organic phases were dried over Na_2SO_4 and the solvent was removed under rotary evaporation. This was followed by purification by flash

chromatography (20 % EtOAc in pentane) to yield pyrrolidinol **50** as a white solid (0.12 g, 70 %).

^{1}H NMR (400 MHz, $CDCl_3$) δ 7.31 – 7.24 (m, 2H, CH-*g*), 6.74 (t, *J* = 7.3 Hz, 1H, CH-*h*), 6.61 (dd, *J* = 8.6, 0.8 Hz, 2H, CH-*f*), 4.59 (dq, *J* = 7.2, 2.5 Hz, 1H, CH-*b*), 3.56 – 3.46 (m, 2H, CH_2-*d*), 3.37 (td, *J* = 8.9, 3.6 Hz, 1H, CH-*e*), 3.31 – 3.24 (m, 1H, CH-*e*), 2.25 – 2.13 (m, 1H, CH-*c*), 2.11 – 1.97 (m, 2H, CH-*c* + OH-*a*); **^{13}C NMR** (101 MHz, $CDCl_3$) δ 147.9, 129.3 (2C), 116.2, 112.0 (2C), 71.4, 56.4, 45.7, 34.3; **HRMS (ES+)** Calculated for $C_{10}H_{14}NO$ ($M+H^+$): 164.1075; found: 164.1073. These spectroscopic data correspond to previously reported data.[111]

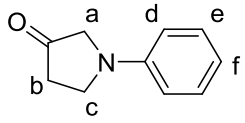
1-(4-chlorophenyl)pyrrolidin-3-one - 51



A solution of oxalyl chloride (73 µL, 0.61 mmol) in DCM (3 mL) was cooled to -78 °C under an atmosphere of N_2 before the dropwise addition of DMSO (122 µL, 1.72 mmol). After 15 min of stirring, a solution of 1-phenylpyrrolidin-3-ol (**50**) (100 mg, 0.61 mmol) in DCM (2 mL) was added, followed by the addition of NEt_3 (370 µL, 2.65 mmol). The reaction mixture was allowed to warm to rt overnight and was then diluted with DCM (20 mL) and H_2O (40 mL) and the aqueous phase was extracted with DCM (4 x 50 mL). The combined organic phases were then washed thoroughly with H_2O (5 x 100 mL) and brine (80 mL), dried over Na_2SO_4, filtered and purified by flash column chromatography (10 % EtOAc in pentane) to yield pyrrolidinone **51** as a white solid (0.52 g, 44 %).

^{1}H NMR (400 MHz, $CDCl_3$) δ 7.26 – 7.20 (m, 2H, 2 x CH-*e*), 6.60 – 6.53 (m, 2H, 2 x CH-*d*), 3.70 – 3.61 (m, 4H, CH_2-*a* + CH_2-*c*), 2.72 (t, *J* = 7.4 Hz, 2H, CH_2-*b*); **^{13}C NMR** (101 MHz, $CDCl_3$) δ 211.6, 146.3, 129.3 (2C), 123.1, 113.7 (2C), 55.4, 45.1, 37.2.

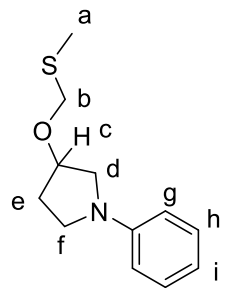
1-Phenylpyrrolidin-3-one - 44



To a solution of 1-phenylpyrrolidin-3-ol (**50**) (1.6 g, 9.6 mmol) in PhMe (60 mL) under N_2 was added DMSO (6.8 mL, 96 mmol) followed by EDC·HCl (5.5 g, 29 mmol) and pyridine (1.6 mL, 19 mmol). TFA (0.37 mL, 4.8 mmol) was added slowly at 0 °C and the reaction was stirred at this temperature for 1 h and then at rt for 2 h. Most of the solvent was removed by rotary evaporation and the resulting residue was diluted with DCM (50 mL) and H_2O (100 mL) and the aqueous phase was extracted with DCM (4 x 50 mL). The combined organic phases were then washed thoroughly with H_2O (5 x 100 mL) and brine (80 mL), dried over Na_2SO_4, filtered and purified by flash column chromatography (5 % EtOAc in pentane) to yield pyrrolidinone **44** as an orange solid (0.96 g, 62 %).

^{1}H NMR (400 MHz, $CDCl_3$) δ 7.35 – 7.27 (m, 2H, 2 x CH-*e*), 6.84 (t, *J* = 7.3 Hz, 1H, CH-*f*), 6.68 (dd, *J* = 8.6, 0.8 Hz, 2H, 2 x CH-*d*), 3.73 – 3.67 (m, 4H, CH_2-*a* + CH_2-*c*), 2.73 (t, *J* = 7.4 Hz, 2H, CH_2-*b*); **^{13}C NMR** (101 MHz, $CDCl_3$) δ 212.3, 147.8, 129.6 (2C), 118.3, 112.7 (2C), 55.5, 45.1, 37.3; **HRMS (ES+)** Calculated for $C_{10}H_{12}NO$ ($M+H^+$): 162.0919; found: 162.0917.

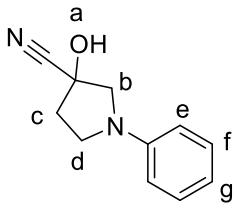
(±)-3-((methylthio)methoxy)-1-phenylpyrrolidine - 52



Formed as a minor side product during the procedure described for the synthesis of pyrrolidinone **44**.

^{1}H NMR (400 MHz, $CDCl_3$) δ 7.28 – 7.19 (m, 2H, 2 x CH-*h*), 6.69 (t, *J* = 7.3 Hz, 1H, CH-*i*), 6.57 (d, *J* = 7.8 Hz, 2H, 2 x CH-*g*), 4.67 (s, 2H, CH_2-*b*), 4.57 (ddd, *J* = 8.7, 5.0, 2.8 Hz, 1H, CH-*c*), 3.53 (dd, *J* = 10.4, 5.2 Hz, 1H, CH-*d*), 3.47 – 3.30 (m, 3H, CH-*d* + CH_2-*f*), 2.20 – 2.09 (m, 5H, CH_2-*e* + CH_3-*a*); **^{13}C NMR** (101 MHz, $CDCl_3$) δ 147.9, 129.3 (2C), 116.1, 111.9 (2C), 75.6, 73.4, 53.3, 45.9, 31.3, 14.0.

(±)-3-Hydroxy-1-phenylpyrrolidine-3-carbonitrile - 45

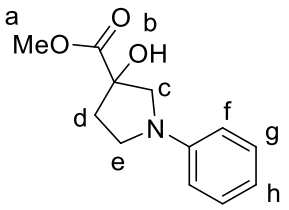


Based on a procedure by Sherer *et al.*[100] To a solution of pyrrolidinone **44** (0.14 g, 0.87 mmol) in THF (3 mL) and H_2O (4.5 mL) was added $NaHSO_4$ monohydrate (0.29 g, 2.1 mmol) at 0 °C and the resulting mixture was stirred at this temperature for 15 min before the addition of KCN (0.16 g, 2.4 mmol). After stirring at rt for 24 h the reaction was diluted with EtOAc (20 mL) and the organic phase was washed with H_2O (4 x 30 mL), dried over

Na_2SO_4, filtered and concentrated under rotary evaporation to yield cyanohydrin **45** as an orange solid (0.13 g with 10 % starting material, 74 %) which was used directly in the next step.

IR Vmax / cm^{-1}: 3433, 2855, 2246 (CN), 1601, 1509, 1379, 1255, 941, 750, 696; **^{1}H NMR** (400 MHz, $CDCl_3$) δ 7.30 – 7.23 (m, 2H, 2 x CH-*f*), 6.78 (t, *J* = 7.3 Hz, 1H, CH-*g*), 6.56 (d, *J* = 7.9 Hz, 2H, 2 x CH-*e*), 3.84 (d, *J* = 10.5 Hz, 1H, CH-*b*), 3.61 – 3.49 (m, 3H, CH-*b* + CH-*d*), 3.17 (br s, 1H, OH-*a*), 2.62 – 2.34 (m, 2H, CH-*c*); **^{13}C NMR** (101 MHz, $CDCl_3$) δ 146.7, 129.4 (2C), 120.0, 117.5, 112.2 (2C), 71.2, 60.1, 45.7, 39.0; **HRMS (ES+)** Calculated for $C_{11}H_{13}N_2O$ ($M+H^+$): 189.1028; found: 189.1020.

(±)-Methyl 3-hydroxy-1-phenylpyrrolidine-3-carboxylate - 42

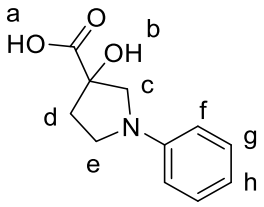


To a solution of cyanohydrin **45** (0.13 g, 0.67 mmol) in MeOH (2 mL) was added HCl (4 M in dioxane, 1.7 mL) dropwise at 0 °C and the reaction was stirred at rt for 16 h. The solvent was removed by rotary evaporation and resulting residue was diluted with EtOAc (20 mL) and H_2O (50 mL) and the aqueous phase was extracted with EtOAc (4 x 20 mL). The combined organic phases were then washed with H_2O (50 mL) and brine (30 mL), dried over Na_2SO_4, filtered and purified by flash column chromatography (20 % EtOAc in petroleum ether) to yield methylester **42** as a yellow oil (91 mg, 61 %).

IR Vmax / cm^{-1}: 3462, 2855, 1734, 1599, 1609, 1372, 1280, 1217, 1128, 750, 693; **^{1}H NMR** (400 MHz, $CDCl_3$) δ 7.28 – 7.20 (m, 2H, 2 x CH-*g*), 6.71 (t, *J* = 7.3 Hz, 1H, CH-*h*), 6.55 (d, *J* = 8.5 Hz, 2H, 2 x CH-*f*), 3.85 (s, 3H, CH_3-*a*), 3.78 (d, *J* = 10.1 Hz, 1H, CH-*c*), 3.61 – 3.49 (m, 2H, CH_2-*e*), 3.42 (d, *J* = 10.1 Hz, 1H, CH-*c*), 3.33 (s, 1H, OH-*b*), 2.49 (dt, *J* = 12.8, 8.6 Hz,

1H, CH-*d*), 2.26 – 2.15 (m, 1H, CH-*d*); **^{13}C NMR** (101 MHz, $CDCl_3$) δ 175.3, 147.5, 129.3 (2C), 116.5, 112.0 (2C), 79.8, 59.3, 53.4, 46.8, 37.7; **HRMS (ES+)** Calculated for $C_{12}H_{16}NO_3$ ($M+H^+$): 222.1130; found: 222.1130.

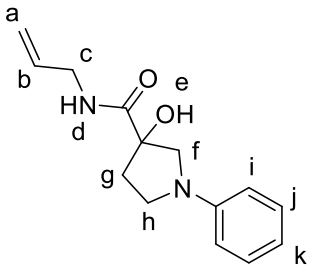
(±)-3-Hydroxy-1-phenylpyrrolidine-3-carboxylic acid - 53



To a solution of methylester **42** (0.37 g, 1.7 mmol) in MeOH (15 mL) was added NaOH (1 M, 3.3 mL) and the reaction was stirred at rt for 2 h. The solvent was removed under rotary evaporation then H_2O (20 mL) was added and the solution was acidified to pH 3 (1 M HCl). The aqueous phase was extracted using EtOAc (3 x 30 mL) and the combined organic phases were washed with brine (30 mL) and dried over Na_2SO_4. After filtration the solvent was removed by rotary evaporation to obtain the carboxylic acid **53** as a yellow solid (0.26 g, 76 %).

IR Vmax / cm^{-1}: 3405, 2923, 2853, 1720, 1599, 1507, 1372, 749, 692; **^{1}H NMR** (400 MHz, $CDCl_3$) δ 7.32 – 7.21 (m, 2H, 2 x CH-*g*), 6.79 (t, *J* = 7.3 Hz, 1H, CH-*h*), 6.63 (d, *J* = 8.0 Hz, 2H, 2 x CH-*f*), 5.73 (br. s, 2H, OH-*a* + OH-*b*), 3.83 (d, *J* = 10.1 Hz, 1H, CH-*c*), 3.57 (dd, *J* = 8.3, 5.4 Hz, 2H, CH_2-*e*), 3.46 (d, *J* = 10.1 Hz, 1H, CH-*c*), 2.56 (dt, *J* = 12.9, 8.5 Hz, 1H, CH-*d*), 2.31 – 2.20 (m, 1H, CH-*d*); **^{13}C NMR** (101 MHz, $CDCl_3$) δ 178.2, 147.1, 129.5 (2C), 117.8, 112.9 (2C), 79.6, 59.5, 47.5, 37.6; **HRMS (EI+)** Calculated for $C_{11}H_{14}NO_3$ ($M+H^+$): 207.0895; found: 207.0905.

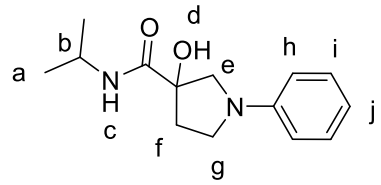
(±)-*N*-Allyl-3-hydroxy-1-phenylpyrrolidine-3-carboxamide - 25



Based on a procedure by Bull *et al.*[249] To a solution of carboxylic acid **53** (50 mg, 0.24 mmol) in DMF (3 mL) was added allylamine (20 µL, 0.27 mmol), HOBt (33 mg, 0.24 mmol) and DIPEA (20 µL, 0.12 mmol) at 0 °C. EDC·HCl (56 mg, 0.29 mmol) was then added and the reaction was stirred at 0 °C for 30 min before warming to rt for 16 h. The reaction was diluted with EtOAc (20 mL) and H_2O (20 mL) and the aqueous phase was extracted with EtOAc (2 x 10 mL). The combined organic phases were washed thoroughly with H_2O (3 x 20 mL), dried over Na_2SO_4, filtered and then purified by flash column chromatography (50 % EtOAc in hexane) to obtain amide **25** as a brown oil (40 mg, 68 %) with purity of ≥95 % by LC-MS analysis.

IR Vmax / cm^{-1}: 3344, 2855, 1642, 1598, 1531, 1506, 1480, 1369, 747, 693 **^{1}H NMR** (400 MHz, CD_3CN) δ 7.42 (s, 1H, NH-*d*), 7.24 – 7.13 (m, 2H, 2 x CH-*j*), 6.64 (tt, *J* = 7.3, 0.9 Hz, 1H, CH-*k*), 6.56 (dd, *J* = 8.7, 0.9 Hz, 2H, 2 x CH-*i*), 5.88 (ddt, *J* = 17.2, 10.3, 5.2 Hz, 1H, CH-*b*), 5.20 (dq, *J* = 17.2, 1.7 Hz, 1H, CH-*a*), 5.13 (dq, *J* = 10.3, 1.7 Hz, 1H, CH-*a*), 4.02 (s, 1H, OH-*e*), 3.85 (ddt, *J* = 6.9, 5.2, 1.6 Hz, 2H, CH_2-*c*), 3.68 (d, *J* = 10.3 Hz, 1H, CH-*f*), 3.52 – 3.40 (m, 2H, CH_2-*h*), 3.28 (dd, *J* = 10.3, 1.4 Hz, 1H, CH-*f*), 2.54 – 2.43 (m, 1H, CH-*g*), 2.02 (dddd, *J* = 13.0, 6.1, 2.9, 1.4 Hz, 1H, CH-*g*); **^{13}C NMR** (101 MHz, CD_3CN) δ 174.0, 148.9, 136.0, 130.0 (2C), 116.7, 115.5, 112.7 (2C), 81.8, 60.3, 47.4, 42.0, 38.2; **HRMS (ES+)** Calculated for $C_{14}H_{19}N_2O_2$ ($M+H^+$): 247.1447; found: 247.1441.

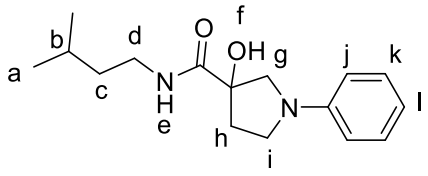
(±)-3-Hydroxy-*N*-*iso*propyl-1-phenylpyrrolidine-3-carboxamide - 54



Following the procedure described for the preparation of amide **25**, the title compound was prepared from carboxylic acid **53** (30 mg, 0.15 mmol), *iso*propylamine (14 µL, 0.16 mmol), HOBt (20 mg, 0.15 mmol), DIPEA (13 µL, 0.072 mmol) and EDC·HCl (33 mg, 0.17 mmol) in DMF (2 mL). Purification was carried out using preparative LC-MS (H_2O (+0.1% formic acid)/MeCN (+0.1% formic acid) 1:1 – 100 % H_2O) to obtain amide **54** as a colourless oil (30 mg, 83 %) with purity of ≥95 % by LC-MS analysis.

IR Vmax / cm^{-1}: 3357, 2973, 2928, 2862, 1652, 1601, 1506, 1369, 1134, 747, 693; **^{1}H NMR** (400 MHz, CD_3CN) δ 7.22 – 7.15 (m, 2H, 2 x CH-*i*), 7.05 (s, 1H, NH-*c*), 6.63 (t, *J* = 7.3 Hz, 1H, CH-*j*), 6.58 (dd, *J* = 8.7, 0.9 Hz, 2H, 2 x CH-*h*), 4.06 – 3.92 (m, 2H, OH-*d* + CH-*b*), 3.67 (d, *J* = 10.3 Hz, 1H, CH-*e*), 3.51 – 3.39 (m, 2H, CH_2-*g*), 3.24 (dd, *J* = 10.3, 1.3 Hz, 1H, CH-*e*), 2.47 (dt, *J* = 12.9, 9.5 Hz, 1H, CH-*f*), 2.03 – 1.95 (m, 1H, CH-*f*), 1.15 (d, *J* = 6.6 Hz, 6H, 2 x CH_3-*a*); **^{13}C NMR** (101 MHz, CD_3CN) δ 173.1, 148.9, 130.0 (2C), 116.7, 112.7 (2C), 81.7, 60.3, 47.4, 42.1, 38.2, 22.7 (2C); **HRMS (ES+)** Calculated for $C_{14}H_{21}N_2O_2$ ($M+H^+$): 249.1603; found: 249.1595.

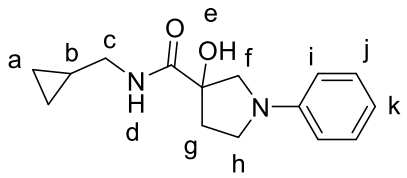
(±)-3-Hydroxy-*N*-*iso*pentyl-1-phenylpyrrolidine-3-carboxamide - 55



Following the procedure described for the preparation of amide **25**, the title compound was prepared from carboxylic acid **53** (30 mg, 0.15 mmol), 3-methylbutan-1-amine (18 µL, 0.16 mmol), HOBt (20 mg, 0.15 mmol), DIPEA (13 µL, 0.072 mmol) and EDC·HCl (33 mg, 0.17 mmol) in DMF (2 mL). Purification was carried out using preparative LC-MS (H_2O (+0.1% formic acid)/MeCN (+0.1% formic acid) 1:1 – 100 % H_2O) to obtain amide **55** as a white solid (36 mg, 90 %) with purity of ≥95 % by LC-MS analysis.

IR Vmax / cm^{-1}: 3338, 2960, 2932, 2868, 1649, 1599, 1538, 1506, 1480, 1372, 750, 693; **^{1}H NMR** (400 MHz, CD_3CN) δ 7.32 – 7.14 (m, 3H, NH-e + 2 x CH-k), 6.63 (tt, *J* = 7.3, 0.9 Hz, 1H, CH-l), 6.55 (dd, *J* = 8.7, 0.9 Hz, 2H, 2 x CH-*j*), 3.99 (s, 1H, OH-*f*), 3.66 (d, *J* = 10.2 Hz, 1H, CH-*g*), 3.51 – 3.39 (m, 2H, CH_2-*i*), 3.29 – 3.19 (m, 3H, CH-*g* + CH_2-*d*), 2.47 (dt, *J* = 12.9, 9.5 Hz, 1H, CH-*h*), 1.99 (dddd, *J* = 12.9, 5.9, 2.7, 1.3 Hz, 1H, CH-*h*), 1.61 (dp, *J* = 13.4, 6.6 Hz, 1H, CH-*b*), 1.39 (dt, *J* = 8.4, 7.1 Hz, 2H, CH_2-*c*), 0.92 (d, *J* = 6.6 Hz, 6H, 2 x CH_3-*a*); **^{13}C NMR** (101 MHz, CD_3CN) δ 173.8, 148.9, 130.0 (2C), 116.7, 112.7 (2C), 81.8, 60.2, 47.4, 39.3, 38.2, 26.5, 22.8 (2C); **HRMS (ES+)** Calculated for $C_{16}H_{25}N_2O_2$ ($M+H^+$): 277.1916; found: 277.1921.

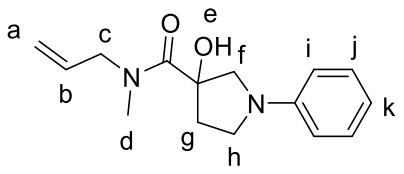
(±)-*N*-(Cyclopropylmethyl)-3-hydroxy-1-phenylpyrrolidine-3-carboxamide - 56



Following the procedure described for the preparation of amide **25**, the title compound was prepared from carboxylic acid **53** (30 mg, 0.15 mmol), cyclopropylmethanamine (14 µL, 0.16 mmol), HOBt (20 mg, 0.15 mmol), DIPEA (13 µL, 0.072 mmol) and EDC·HCl (33 mg, 0.17 mmol) in DMF (2 mL). Purification was carried out using preparative LC-MS (H_2O (+0.1% formic acid)/MeCN (+0.1% formic acid) 1:1 – 100 % H_2O) to obtain amide **56** as a white solid (28 mg, 74 %) with purity of ≥95 % by LC-MS analysis.

IR Vmax / cm^{-1}: 3328, 2925, 2859, 1649, 1601, 1534, 1509, 1480, 1369, 747, 693; **^{1}H NMR** (400 MHz, CD_3CN) δ 7.36 (s, 1H, NH-*d*), 7.24 – 7.13 (m, 2H, 2 x CH-*j*), 6.63 (t, J = 7.3 Hz, 1H, CH-*k*), 6.55 (d, J = 7.9 Hz, 2H, 2 x CH-*i*), 4.04 (s, 1H, OH-*e*), 3.67 (d, J = 10.2 Hz, 1H, CH-*f*), 3.51 – 3.41 (m, 2H, CH_2-*h*), 3.26 (dd, J = 10.2, 1.2 Hz, 1H, CH-*f*), 3.13 – 3.05 (t, J = 6.4 Hz, 2H, CH_2-*c*), 2.48 (dt, J = 12.9, 9.5 Hz, 1H, CH-*g*), 2.00 (dddd, J = 12.9, 6.0, 2.8, 1.2 Hz, 2H, CH-*g*), 1.06 – 0.90 (m, 1H, CH-*b*), 0.54 – 0.37 (m, 2H, CH_2-*a*), 0.27 – 0.14 (m, 2H, CH_2-*a*); **^{13}C NMR** (101 MHz, CD_3CN) δ 173.9, 148.9, 130.0 (2C), 116.7, 112.7 (2C), 81.8, 60.3, 47.4, 44.3, 38.2, 11.6, 3.6 (2C); **HRMS (ES+)** Calculated for $C_{15}H_{21}N_2O_2$ ($M+H^+$): 261.1603; found: 261.1602.

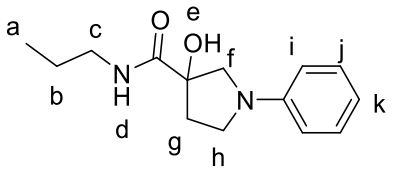
(±)-*N*-Allyl-3-hydroxy-*N*-methyl-1-phenylpyrrolidine-3-carboxamide - 57



Following the procedure described for the preparation of amide **25**, the title compound was prepared from carboxylic acid **53** (30 mg, 0.15 mmol), *N*-allylmethylamine (16 µL, 0.16 mmol), HOBt (20 mg, 0.15 mmol), DIPEA (13 µL, 0.072 mmol) and EDC·HCl (33 mg, 0.17 mmol) in DMF (2 mL). Purification was carried out using preparative LC-MS (H_2O (+0.1% formic acid)/MeCN (+0.1% formic acid) 1:1 – 100 % H_2O) to obtain amide **57** as a colourless oil (34 mg, 90 %) with purity of ≥95 % by LC-MS analysis.

IR Vmax / cm^{-1}: 3357, 2932, 2859, 1614, 1509, 1484, 1372, 750, 696; **^{1}H NMR** (500 MHz, CD_3CN at 333K) δ 7.33 – 7.28 (m, 2H, 2 x CH-*j*), 6.76 (tt, *J* = 7.3, 0.9 Hz, 1H, CH-*k*), 6.71 (dd, *J* = 8.7, 0.9 Hz, 2H, 2 x CH-*i*), 6.02 – 5.88 (m, 1H, CH-*b*), 5.34 – 5.24 (m, 2H, CH_2-*a*), 4.31 – 4.07 (m, 3H, CH_2-*c* + OH-*e*), 3.98 (d, *J* = 10.5 Hz, 1H, CH-*f*), 3.54 (dtd, *J* = 15.8, 8.9, 5.0 Hz, 2H, CH_2-*h*), 3.43 (dd, *J* = 10.5, 0.6 Hz, 1H, CH-*f*), 3.15 (br s, 3H, CH-*d*), 2.70 (dt, *J* = 13.1, 8.9 Hz, 1H, CH-*g*), 2.27 – 2.20 (m, 1H, CH-*g*); **^{13}C NMR** (126 MHz, CD_3CN at 333k) δ 173.2, 149.4, 130.3 (2C), 118.6, 117.5, 117.3, 113.3 (2C), 82.4, 60.3, 52.9, 47.5, 38.6, 30.5; **HRMS (ES+)** Calculated for $C_{15}H_{21}N_2O_2$ ($M+H^+$): 261.1603; found: 261.1613.

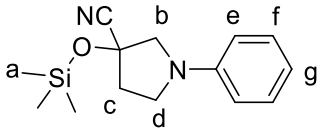
(±)-3-Hydroxy-1-phenyl-*N*-propylpyrrolidine-3-carboxamide - 58



Following the procedure described for the preparation of amide **25**, the title compound was prepared from carboxylic acid **53** (30 mg, 0.15 mmol), *n*-propylamine (16 µL, 0.13 mmol), HOBt (20 mg, 0.15 mmol), DIPEA (13 µL, 0.072 mmol) and EDC·HCl (33 mg, 0.17 mmol) in DMF (2 mL). Purification was carried out using preparative LC-MS (H2O (+0.1% formic acid)/MeCN (+0.1% formic acid) 1:1 – 100 % H_2O) to obtain amide **58** as a white solid (26 mg, 72 %) with purity of ≥95 % by LC-MS analysis.

IR Vmax / cm^{-1}: 3351, 2960, 2932, 2862, 1652, 1601, 1538, 1509, 1372, 750, 693; **^{1}H NMR** (400 MHz, CD_3CN) δ 7.30 (s, 1H, NH-*d*), 7.23 – 7.15 (m, 2H, 2 x CH-*j*), 6.63 (tt, *J* = 7.3, 0.9 Hz, 1H, CH-*k*), 6.55 (dd, *J* = 8.6, 0.9 Hz, 2H, 2 x CH-*i*), 4.03 (s, 1H, OH-*e*), 3.67 (d, *J* = 10.2 Hz, 1H, CH-*f*), 3.52 – 3.38 (m, 2H, CH_2-*h*), 3.25 (dd, *J* = 10.2, 1.3 Hz, 1H, CH-*f*), 3.22 – 3.14 (m, 2H, CH_2-*c*), 2.47 (dt, *J* = 12.9, 9.5 Hz, 1H, CH-*g*), 1.99 (dddd, *J* = 12.9, 6.2, 2.7, 1.3 Hz, 1H, CH-*g*), 1.51 (apparent sext, 2H, CH_2-*b*), 0.90 (t, *J* = 7.4 Hz, 3H, CH_3-*a*); **^{13}C NMR** (101 MHz, CD_3CN) δ 174.0, 148.9, 130.0 (2C), 116.7, 112.7 (2C), 81.8, 60.3, 47.4, 41.6, 38.2, 23.6, 11.6; **HRMS (ES+)** Calculated for $C_{14}H_{21}N_2O_2$ ($M+H^+$): 249.1603; found: 249.1614.

(±)-1-Phenyl-3-((trimethylsilyl)oxy)pyrrolidine-3-carbonitrile - 59

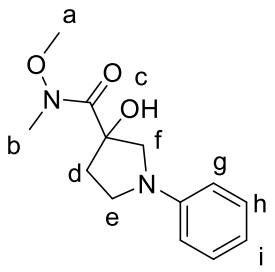


To a solution of cyanohydrin **45** (46 mg, 0.24 mmol) in anhydrous DCM (2 mL) was added DIPEA (170 µL, 0.98 mmol) followed by TMSCl (93 µL, 0.73 mmol) and the reaction was

heated under reflux for 3 h and then cooled and quenched with saturated aq. NH_4Cl (20 mL). The aqueous phase was extracted with DCM (3 x 10 mL) and the combined organic phases were dried over Na_2SO_4 and filtered. Purification was carried out using column chromatography (5 % EtOAc in pentane) to obtain the TMS-protected cyanohydrin **59** as a yellow oil (10 mg, 17 %).

^{1}H NMR (400 MHz, $CDCl_3$) δ 7.29 – 7.22 (m, 2H, 2 x CH-*f*), 6.75 (t, *J* = 7.3 Hz, 1H, CH-*g*), 6.54 (d, *J* = 7.8 Hz, 2H, CH-*e*), 3.85 (d, *J* = 10.0 Hz, 1H, CH-*b*), 3.57 – 3.45 (m, 3H, CH_2-*d* + CH-*b*), 2.57 – 2.47 (m, 1H, CH-*c*), 2.43 – 2.34 (m, 1H, CH-*c*), 0.30 (s, 9H, CH-*a*); **^{13}C NMR** (101 MHz, $CDCl_3$) δ 146.79, 129.48 (2C), 120.76, 117.12, 111.89 (2C), 72.24, 60.38, 45.52, 40.02, 29.85 (grease), 1.18 (3C).

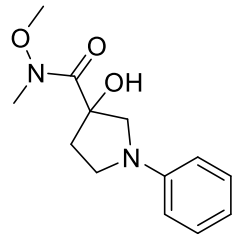
<u>Method 1</u>: (±)-3-Hydroxy-*N*-methoxy-*N*-methyl-1-phenylpyrrolidine-3-carboxamide - 66



Based on a procedure by Iriarte *et al.*[116] To a solution of methylester **42** (91 mg, 0.41 mmol) in anhydrous THF (3 mL) under N_2 was added *N,O*-dimethylhydroxylamine hydrochloride (60 mg, 0.62 mmol) followed by the dropwise addition of *i*PrMgCl (2 M in THF, 0.82 mL) at -20 °C. The reaction was allowed to warm to rt for 16 h and then was quenched with saturated aq. NH_4Cl (20 mL) and the aqueous phase was extracted with EtOAc (3 x 20 mL). The combined organic phases were dried over Na_2SO_4, filtered then purified by flash column chromatography (30 % EtOAc in pentane) to obtain the desired amide **66** as an off-white oil (58 mg, 56 %).

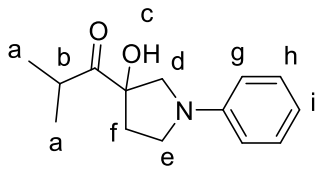
IR Vmax / cm^{-1}: 3363, 2928, 2852, 1639, 1601, 1506, 1372, 1001, 750, 693; **^{1}H NMR** (400 MHz, $CDCl_3$) δ 7.28 – 7.20 (m, 2H, 2 x CH-*h*), 6.73 (tt, *J* = 7.3, 0.9 Hz, 1H, CH-*i*), 6.58 (dd, *J* = 8.6, 0.9 Hz, 2H, 2 x CH-*g*), 3.92 (s, 1H, OH-*c*), 3.85 (d, *J* = 10.4 Hz, 1H, CH-*f*), 3.75 (s, 3H, CH_3-*a*), 3.59 – 3.47 (m, 2H, CH_2-*e*), 3.40 (dd, *J* = 10.4, 0.9 Hz, 1H, CH-*f*), 3.31 (s, 3H, CH_3-*b*), 2.61 (dt, *J* = 12.9, 9.1 Hz, 1H, CH-*d*), 2.17 (dddd, *J* = 12.9, 6.4, 2.9, 1.0 Hz, 1H, CH-*d*); **^{13}C NMR** (101 MHz, $CDCl_3$) δ 173.5, 147.8, 129.3 (2C), 116.4, 112.1 (2C), 80.9, 61.4, 59.0, 46.6, 36.9, 33.9; **HRMS (EI+)** Calculated for $C_{13}H_{19}N_2O_3$ ($M+H^+$): 251.1396; found: 251.1396.

<u>Method 2</u>: (±)-3-Hydroxy-*N*-methoxy-*N*-methyl-1-phenylpyrrolidine-3-carboxamide - 66



Following the procedure described for the preparation of amide **25**, the title compound was prepared from carboxylic acid **53** (500 mg, 2.41 mmol), *N,O*-dimethylhydroxylamine hydrochloride (247 mg, 2.53 mmol), HOBt (326 mg, 2.41 mmol), DIPEA (840 µL, 4.82 mmol) and EDC·HCl (508 mg, 2.65 mmol) in DMF (20 mL). The crude was purified by flash column chromatography (40 % EtOAc in pentane) to obtain amide **66** as an off-white oil (380 mg, 63 %). All data corresponded with data collected from method 1.

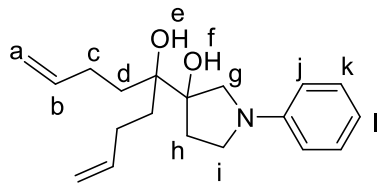
(±)-1-(3-Hydroxy-1-phenylpyrrolidin-3-yl)-2-methylpropan-1-one - 67



To a solution of methylester **42** (91 mg, 0.41 mmol) in anhydrous THF (3 mL) under N_2 was added *N,O*-dimethylhydroxylamine hydrochloride (60 mg, 0.62 mmol) followed by the dropwise addition of *i*PrMgCl (2 M in THF, 0.82 mL) at -20 °C. The reaction was allowed to warm to rt for 16 h and then was quenched with saturated aq. NH_4Cl (20 mL) and the aqueous phase was extracted with EtOAc (3 x 20 mL). The combined organic phases were dried over Na_2SO_4, filtered then purified by flash column chromatography (30 % EtOAc in pentane) to obtain *iso*propyl ketone **67** as a white solid (15 mg, 16 %).

IR Vmax / cm^{-1}: 3468, 2986, 2906, 2846, 1725, 1601, 1509, 1379, 1245, 1217, 1137, 1106, 744, 687; **^{1}H NMR** (400 MHz, $CDCl_3$) δ 7.30 – 7.22 (m, 2H, 2 x CH-*h*), 6.75 (tt, *J* = 7.3, 0.9 Hz, 1H, CH-*i*), 6.58 (dd, *J* = 8.7, 0.9 Hz, 2H, 2 x CH-*g*), 5.16 (hept, *J* = 6.3 Hz, 1H, CH-*b*), 3.77 (d, *J* = 10.1 Hz, 1H, CH-*d*), 3.62 – 3.46 (m, 3H, CH_2-*e* + OH-*c*), 3.43 (dd, *J* = 10.1, 0.9 Hz, 1H, CH-*d*), 2.48 (dt, *J* = 12.6, 8.7 Hz, 1H, CH-*f*), 2.19 (dddd, *J* = 12.6, 6.6, 3.5, 0.9 Hz, 1H, CH-*f*), 1.31 (t, *J* = 6.3 Hz, 6H, 2 x CH_3-*a*); **^{13}C NMR** (101 MHz, $CDCl_3$) δ 174.4, 147.5, 129.3 (2C), 116.4, 112.0 (2C), 79.7, 70.5, 59.3, 46.9, 37.7, 21.8 (2C); **HRMS (ES+)** Calculated for $C_{14}H_{20}NO_2$ ($M+H^+$): 234.1494; found: 234.1491; purity is ≥95 % by LC-MS analysis.

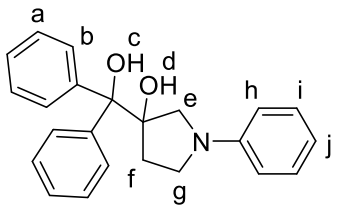
(±)-3-(5-Hydroxynona-1,8-dien-5-yl)-1-phenylpyrrolidin-3-ol - 68



To a solution of methylester **42** (100 mg, 0.45 mmol) in anhydrous THF (5 mL) under N_2 was added *N,O*-dimethylhydroxylamine hydrochloride (33 mg, 0.54 mmol) followed by the dropwise addition of but-3-en-1-ylmagnesium bromide (0.33 M solution in THF, 6.16 mL) at -20 °C. The reaction was allowed to warm to rt for 16 h and then was quenched with saturated aq. NH_4Cl (20 mL) and the aqueous phase was extracted with DCM (3 x 20 mL). The combined organic phases were dried over Na_2SO_4, filtered and concentrated under rotary evaporation. The crude material was analysed and the ^1H and ^{13}C NMR were tentatively assigned.

^{1}H NMR (400 MHz, $CDCl_3$) δ 7.30 – 7.18 (m, 2H, 2 x CH-*k*), 6.71 (t, *J* = 7.3 Hz, 1H, CH-*l*), 6.58 (d, *J* = 7.8 Hz, 2H, 2 x CH-*j*), 5.86 (ddtd, *J* = 10.1, 7.3, 6.5, 0.7 Hz, 2H, 2 x CH-*b*), 5.14 – 5.04 (m, 2H, CH_2-*a*), 5.00 (dd, *J* = 10.1, 1.6 Hz, 2H, CH_2-*a*), 3.58 (d, *J* = 10.3 Hz, 1H, CH-*g*), 3.52 (td, *J* = 9.3, 6.9 Hz, 1H, CH-*i*), 3.42 (td, *J* = 9.3, 1.6 Hz, 1H, CH-*i*), 3.20 (dd, *J* = 10.3, 1.2 Hz, 1H, CH-*g*), 2.34 – 2.16 (m, 6H, OH-*e*, 2 x CH_2-*c*, CH-*h*), 2.03 (s, 1H, OH-*f*), 1.94 (ddt, *J* = 13.1, 6.9, 1.6 Hz, 1H, CH-*h*), 1.88 – 1.69 (m, 4H, 2 x CH_2-*d*); **^{13}C NMR** (101 MHz, $CDCl_3$) δ 147.7, 138.8, 138.9, 129.4 (2C), 117.2, 115.0 (2C), 112.5 (2C), 85.8, 76.4, 57.4, 47.0, 38.0, 34.9, 34.5, 28.8, 28.7.

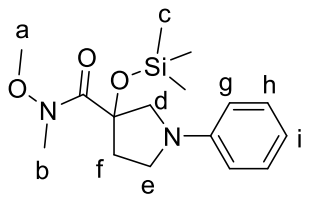
(±)-3-(Hydroxydiphenylmethyl)-1-phenylpyrrolidin-3-ol - 69



To a solution of ester **42** (0.10 g, 0.45 mmol) in THF (2 mL) was added PhMgBr (2.26 M in THF, 0.24 mL) dropwise at -20 °C under N_2. The reaction was stirred at this temperature for 12 h and was then quenched with saturated aq. NH_4Cl (5 mL) and the aqueous phase was extracted with EtOAc (2 x 10 mL). The combined organic phases were dried over Na_2SO_4, filtered and concentrated under rotary evaporation. The crude material was analysed and the ^1H and ^{13}C NMR were tentatively assigned.

^{1}H NMR (400 MHz, CD_3CN) δ 7.74 – 7.68 (m, 2H, 2 x CH-*b*), 7.66 – 7.60 (m, 2H, 2 x CH-*b*), 7.36 – 7.24 (m, 6H, 6 x CH-*a*), 7.20 – 7.11 (m, 2H, 2 x CH-*i*), 6.60 (tt, *J* = 7.2, 1.0 Hz, 1H, CH-*j*), 6.49 (dd, *J* = 8.7, 1.0 Hz, 2H, 2 x CH-*h*), 4.03 (s, *J* = 15.7 Hz, 1H, OH-*c*), 3.80 (d, *J* = 10.5 Hz, 1H, CH-*e*), 3.40 – 3.30 (m, 2H, CH_2-*g*), 3.22 (s, 1H, OH-*d*), 3.14 (dd, *J* = 10.5, 0.9 Hz, 1H, CH-*e*), 2.60 (dt, *J* = 13.3, 9.6 Hz, 1H, CH-*f*), 1.79 (dt, *J* = 13.3, 4.1 Hz, 1H, CH-*f*); **^{13}C NMR** (101 MHz, CD_3CN) δ 149.2, 146.6, 146.1, 130.0 (2C), 129.1 (2C), 128.9 (2C), 128.6 (2C), 128.4 (2C), 127.9, 127.8, 116.5, 112.6 (2C), 86.5, 81.0, 58.8, 47.1, 35.8.

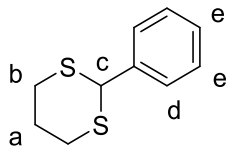
(±)-*N*-Methoxy-*N*-methyl-1-phenyl-3-((trimethylsilyl)oxy)pyrrolidine-3-carboxamide - 70



To a solution of amide **66** (61 mg, 0.24 mmol) in anhydrous DCM (3 mL) was added DIPEA (170 µL, 0.97 mmol) followed by TMSCl (90 µL, 0.73 mmol) and the reaction was stirred at rt for 16 h. After this time, some starting material was still present therefore the reaction mixture was heated under reflux for 1 h and then cooled and quenched with saturated aq. NH_4Cl (20 mL) and the aqueous phase was extracted with DCM (3 x 10 mL). The combined organic phases were dried over Na_2SO_4, filtered and purified by column chromatography (10 % EtOAc in pentane) to obtain TMS-protected amide **70** as an orange oil (44 mg, 56 %).

^{1}H NMR (400 MHz, $CDCl_3$) δ 7.29 – 7.20 (m, 2H, 2 x CH-*h*), 6.69 (t, *J* = 7.3 Hz, 1H, CH-*i*), 6.56 (d, *J* = 7.9 Hz, 2H, 2 x CH-*g*), 3.81 – 3.73 (m, 4H, CH_3-*a* + CH-*d*), 3.57 (d, *J* = 10.8 Hz, 1H, CH-*d*), 3.*51* – 3.37 (m, 2H, CH_2-e), 3.30 (br. s, 3H, CH_3-*b* broad due to rotomers), 2.59 (dt, *J* = 13.2, 8.7 Hz, 1H, CH-*f*), 2.37 – 2.26 (m, 1H, CH-*f*), 0.14 (s, 9H, 3 x CH_3-*c*); **^{13}C NMR** (101 MHz, $CDCl_3$) δ 147.7, 129.3 (2C), 116.1, 111.7 (2C), 83.6, 61.1, 58.5, 46.0, 36.5, 1.8 (3C) *N*-methyl carbon and carbonyl carbon not seen due to rotamers.

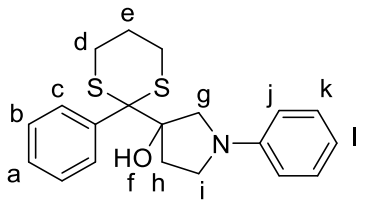
2-Phenyl-1,3-dithiane - 74



Synthesis according to Yu *et al.*[250] To solution of benzaldehyde (0.48 mL, 4.7 mmol) in $CHCl_3$ (20 mL) was added propane-1,3-dithiol (0.52 mL, 5.2 mmol) followed by iodine (0.12 g, 0.47 mmol) and the reaction was stirred at rt for 1.5 h. The reaction was quenched with 10 % aq. sodium thiosulfate (18 mL) and the aqueous phase was extracted with DCM (3 x 20 mL). The combined organic phases were then washed with 5 % NaOH (20 mL) and brine (2 x 30 mL), dried over $MgSO_4$ and concentrated under rotary evaporation. The crude was purified by flash column chromatography (5 % EtOAc in pentane) to afford dithiane **74** as a white solid (0.85 g, 83 %).

^{1}H NMR (400 MHz, $CDCl_3$) δ 7.51 – 7.44 (m, 2H, 2 x CH-*d*), 7.38 – 7.27 (m, 3H, 3 x CH-*e*), 5.17 (s, 1H, CH-*c*), 3.15 – 3.01 (m, 2H, CH_2-*b*), 2.98 – 2.85 (m, 2H, CH-*b*), 2.24 – 2.12 (m, 1H, CH-*a*), 2.01 – 1.86 (m, 1H, CH-*a*); **^{13}C NMR** (101 MHz, $CDCl_3$) δ 139.3, 128.9 (2C), 128.6, 127.9 (2C), 51.6, 32.3 (2C), 25.3; **HRMS (EI+)** Calculated for $C_{10}H_{13}S_2$ ($M+H^+$): 196.0380; found: 196.0385. These spectroscopic data correspond to previously reported data.[250]

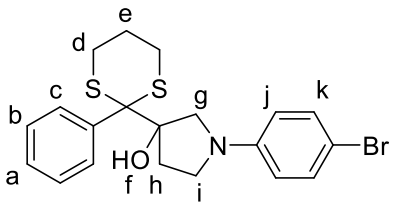
(±)-1-Phenyl-3-(2-phenyl-1,3-dithian-2-yl)pyrrolidin-3-ol - 75



To a solution of dithiane **74** (0.20 g, 1.0 mmol) in dry THF (5 mL) was added *n*-BuLi (2.5 M in hexanes, 0.41 mL) dropwise at -30 °C and the reaction was stirred at this temperature for 1 h. *N*-phenyl-3-pyrrolidinone (0.18 g, 1.1 mmol) in dry THF (2 mL) was then added dropwise and the temperature was allowed to warm to -20 °C. The reaction was stirred between -10 °C and -5 °C for 2.5 h and then was quenched with saturated aq. NH_4Cl and the aqueous phase was extracted with DCM (3 x 10 mL). The combined organic phases were dried over Na_2SO_4, filtered, concentrated under rotary evaporation and purified by flash column chromatography (10 % EtOAc in pentane) to afford dithiane **75** as a white solid (0.20 g, 55 %).

IR Vmax / cm^{-1}: 3401, 2938, 2849, 1601, 1506, 1445, 1372, 1322, 1280, 1055, 1033, 947, 747, 718, 693; **^{1}H NMR** (400 MHz, $CDCl_3$) δ 8.16 – 8.10 (m, 2H, 2 x CH-*c*), 7.50 – 7.42 (m, 2H, 2 x CH-*b*), 7.37 – 7.28 (m, 1H, CH-*a*), 7.23 – 7.16 (m, 2H, 2 x CH-*k*), 6.66 (dd, *J* = 15.2, 7.9 Hz, 1H, CH-*l*), 6.51 (d, *J* = 7.9 Hz, 2H, 2 x CH-*j*), 4.05 (d, *J* = 10.6 Hz, 1H, CH-*g*), 3.70 (m, 1H, OH-*f*), 3.46 – 3.33 (m, 2H, CH_2-*i*), 3.16 (dd, *J* = 10.6, 1.0 Hz, 1H, CH-*g*), 2.78 – 2.62 (m, 4H, 2 x CH_2-*d*), 2.62 – 2.51 (m, 1H, CH-*h*), 1.96 – 1.85 (m, 2H, CH_2-*e*), 1.78 (dd, *J* = 13.0, 5.9 Hz, 1H, CH-*h*); **^{13}C NMR** (101 MHz, $CDCl_3$) δ 147.7, 137.6, 131.1 (2C), 129.2 (2C), 129.0 (2C), 127.9, 116.0, 111.7 (2C), 85.1, 67.5, 57.3, 46.3, 34.3, 27.8 (2C), 24.9; **HRMS (ES+)** Calculated for $C_{20}H_{24}NOS_2$ ($M+H^+$): 358.1299; found: 358.1308.

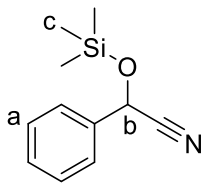
(±)-1-(4-Bromophenyl)-3-(2-phenyl-1,3-dithian-2-yl)pyrrolidin-3-ol - 76



To a solution of dithiane **75** (50 mg, 0.14 mmol) in DCM (3 mL) and H_2O (1 mL) was added pyridinium bromide perbromide (89 mg, 0.28 mmol) and TBAB (5 mg, 0.016 mmol) and the reaction was stirred at rt for 8 h. The aqueous phase was then extracted with DCM (2 x 20 mL) and the combined organic phases were dried over Na_2SO_4, filtered and concentrated under rotary evaporation. The crude material was analysed and the ^{1}H NMR was tentatively assigned.

^{1}H NMR (400 MHz, $CDCl_3$) δ 8.16 – 8.06 (m, 2H, 2 x CH-*c*), 7.49 – 7.39 (m, 4H, 2 x CH-*b* + 2 x CH-*k*), 7.37 – 7.31 (m, 1H, CH-*a*), 6.35 – 6.18 (m, 2H, 2 x CH-*j*), 4.02 (d, *J* = 10.7 Hz, 1H, CH-*g*), 3.42 – 3.26 (m, 2H, CH_2-*i*), 3.12 (d, *J* = 10.7 Hz, 1H, CH-*g*), 2.78 – 2.60 (m, 4H, 2 x CH_2-*d*), 2.56 (ddd, *J* = 13.0, 10.5, 9.0 Hz, 1H, CH-*h*), 1.97 – 1.82 (m, 2H, CH_2-*e*), 1.75 (dd, *J* = 13.0, 6.0 Hz, 1H, CH-*h*);

(±)-2-Phenyl-2-((trimethylsilyl)oxy)acetonitrile - 78

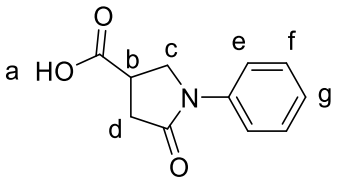


Synthesis according to Toukoniitty *et al.*[251] To a solution of imidazole (1.02 g, 15.0 mmol) in DMF (15 mL) was added TMSCl (1.4 mL, 11 mmol) dropwise at 0 °C under N_2. The reaction was stirred at this temperature for 15 min before the dropwise addition of 2-hydroxy-2-phenylacetonitrile (1.0 g, 7.5 mmol). The reaction was stirred at rt for 1 h before quenching

with H_2O (50 mL) and then the aqueous phase was extracted with EtOAc (2 x 30 mL). The combined organic phases were washed thoroughly with H_2O (3 x 50 mL), dried over Na_2SO_4, filtered and then purified by flash column chromatography (0.5 - 1 % EtOAc in pentane) to obtain TMS-protected cyanohydrin **78** as a yellow oil (254 mg, 17 %).

^{1}H NMR (400 MHz, $CDCl_3$) δ 7.51 – 7.35 (m, 5H, 5 x CH-*a*), 5.50 (s, 1H, CH-*b*), 0.25 – 0.22 (m, 9H, 3 x CH_3-*c*). These spectroscopic data correspond to previously reported data.[252]

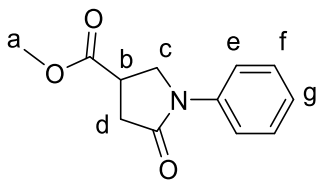
(±)-5-Oxo-1-phenylpyrrolidine-3-carboxylic acid - 80



Synthesis according to Griffioen *et al.*[253] A mixture of aniline (0.98 mL, 11 mmol), itaconic acid (1.68 g, 12.9 mmol) in H_2O (4 mL) was heated in a sealed tube at 110 °C for 18 h. The reaction was cooled to rt and NaOH (6 M, 4 mL) was added and the resulting precipitate was filtered. To the filtrate was added HCl (6 M) until pH 1 and the resulting precipitate was filtered, washed with water and dried under high vacuum to yield carboxylic acid **80** as a white solid which required no further purification (1.75 g, 79 %).

^{1}H NMR (400 MHz, DMSO) δ 12.79 (s, 1H, OH-*a*), 7.64 (d, *J* = 8.2 Hz, 2H, 2 x CH-*e*), 7.37 (t, *J* = 7.9 Hz, 2H, 2 x CH-*f*), 7.14 (t, *J* = 7.4 Hz, 1H, CH-*g*), 4.09 – 4.00 (m, 1H, CH-*c*), 3.96 (dd, *J* = 9.8, 5.7 Hz, 1H, CH-*c*), 3.44 – 3.22 (m, 1H, CH-*b*), 2.74 (qd, *J* = 17.0, 8.1 Hz, 2H, CH-*d*); **^{13}C NMR** (101 MHz, DMSO) δ 174.2, 171.8, 139.1, 128.7 (2C), 124.1, 119.5 (2C), 49.9, 35.2, 35.2; **HRMS (ES+)** Calculated for $C_{11}H_{11}NO_3$ ($M+H^+$): 206.0817; found: 206.0809; Calculated for $C_{13}H_{15}N_2O_3$ ($M+MeCN+H^+$): 247.1083; found: 247.1094. These spectroscopic data correspond to previously reported data.[133]

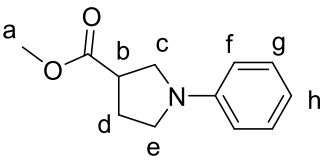
(±)-Methyl 5-oxo-1-phenylpyrrolidine-3-carboxylate - 81



Synthesis according to Jones *et al.*[133] To a suspension of carboxylic acid **80** (1.74 g, 8.5 mmol) in dry MeOH (20 mL) was added $SOCl_2$ (0.66 mL, 9.0 mmol) dropwise at 0 °C under N_2. The reaction warmed to rt and was stirred for 18 h. The resulting solution was concentrated under rotary evaporation and the residue was dissolved in DCM (20 mL), washed with water (3 x 50 mL) and dried over $MgSO_4$. The crude material was purified by flash column chromatography (20 % EtOAC in pentane) to yield methylester **81** as a white solid (1.39 g, 75 %).

^{1}H NMR (400 MHz, $CDCl_3$) δ 7.61 – 7.54 (m, 2H, 2 x CH-*e*), 7.41 – 7.33 (m, 2H, 2 x CH-*f*), 7.20 – 7.13 (m, 1H, CH-*g*), 4.08 (ddd, *J* = 18.5, 9.9, 7.7 Hz, 2H, CH_2-*c*), 3.77 (s, 3H, CH_3-*a*), 3.42 – 3.30 (m, 1H, CH-*b*), 2.90 (qd, *J* = 17.3, 8.7 Hz, 2H, CH_2-*d*); **^{13}C NMR** (101 MHz, $CDCl_3$) δ 173.0, 171.6, 138.9, 129.1 (2C), 125.1, 120.3 (2C), 52.7, 50.5, 36.0, 35.6; **HRMS (ES+)** Calculated for $C_{12}H_{14}NO_3$ ($M+H^+$): 220.0974; found: 220.0981.

(±)-Methyl 1-phenylpyrrolidine-3-carboxylate - 82

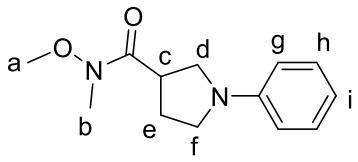


Synthesis according to Griffioen *et al.*[253] To a solution of methylester **81** (1.1 g, 5.0 mmol) in THF (20 mL) under an N_2 was added 9-BBN (0.5 M in THF, 22.1 mL) and the reaction was stirred at 65 °C for 2 h. The reaction was cooled to rt and ethanolamine (0.67 mL, 11 mmol)

was added. The reaction mixture was then concentrated under rotary evaporation and the residue was triturated with pentane and cooled to -20 °C for 1 h. Following filtration through Celite®, the filtrate was concentrated under rotary evaporation and the crude material was purified by flash column chromatography (3 % EtOAc in Pentane) to yield phenylpyrrolidine **82** as a yellow oil (0.57 g, 55 %).

^{1}H NMR (400 MHz, $CDCl_3$) δ 7.28 – 7.21 (m, 2H, 2 x CH-*g*), 6.74 – 6.68 (m, 1H, CH-*h*), 6.61 – 6.56 (m, 2H, 2 x CH-*f*), 3.74 (s, 3H, CH_3-*a*), 3.62 – 3.50 (m, 2H, CH_2-*c*), 3.44 (ddd, *J* = 9.0, 7.4, 5.5 Hz, 1H, CH-*e*), 3.35 (dt, *J* = 9.0, 7.3 Hz, 1H, CH-*e*), 3.27 – 3.17 (m, 1H, CH-*b*), 2.37 – 2.23 (m, 2H, CH_2-*d*); **^{13}C NMR** (101 MHz, $CDCl_3$) δ 174.2, 147.6, 129.3 (2C), 116.3, 112.0 (2C), 52.2, 50.2, 47.3, 43.1, 28.6; **HRMS (ES+)** Calculated for $C_{12}H_{16}NO_2$ ($M+H^+$): 206.1181; found: 206.1188. These spectroscopic data correspond to previously reported data.[253]

(±)-*N*-Methoxy-*N*-methyl-1-phenylpyrrolidine-3-carboxamide - 83

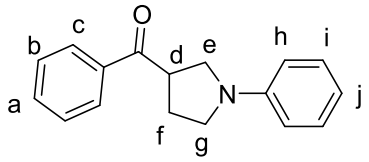


Based on a procedure by Iriarte *et al.*[116] To a solution of phenylpyrrolidine **82** (0.52 g, 2.6 mmol) and *N,O*-dimethylhydroxylamine hydrochloride (0.34 g, 3.8 mmol) in THF (12 mL) was added *i*PrMgCl (2 M solution in THF, 5.1 mL) dropwise at -20 °C under N_2. The reaction was stirred at rt for 2.5 h and was quenched with saturated aq. NH_4Cl (10 mL) and the aqueous phase was extracted with EtOAc (2 x 20 mL). The combined organic phases were dried over Na_2SO_4, filtered and concentrated under rotary evaporation. The crude material was purified by flash column chromatography (30 % EtOAC in pentane) to yield amide **83** as a yellow oil (0.51 g, 85 %).

IR Vmax / cm^{-1}: 3335, 2935, 1661, 1601, 1506, 1376, 1176, 753, 696; **^{1}H NMR** (400 MHz, $CDCl_3$) δ 7.27 – 7.19 (m, 2H, 2 x CH-*h*), 6.69 (t, *J* = 7.3 Hz, 1H, CH-*i*), 6.58 (dd, *J* = 8.7, 0.9

Hz, 2H, 2 x CH-*g*), 3.74 (s, 3H, CH_3-*a*), 3.63 – 3.42 (m, 4H, CH_2-*d* + CH_2-*f*), 3.41 – 3.32 (m, 1H, CH-*c*), 3.23 (s, 3H, CH_3-*b*), 2.39 – 2.16 (m, 2H, CH_2-*e*); **^{13}C NMR** (101 MHz, CDCl3) δ 174.3, 147.7, 129.2 (2C), 116.1, 112.0 (2C), 61.6, 50.6, 47.6, 40.2, 32.5, 28.7; **HRMS (ES+)** Calculated for $C_{13}H_{19}N_2O_2$ ($M+H^+$): 235.1447; found: 235.1450.

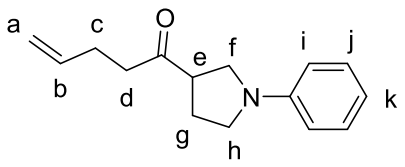
(±)-Phenyl(1-phenylpyrrolidin-3-yl)methanone - 84



To a solution of amide **83** (0.10 g, 0.43 mmol) in THF (2 mL) was added PhMgBr (2.26 M in THF, 0.57 mL) dropwise at -20 °C under N_2. The reaction was stirred at 0 °C for 3 h and was then quenched with saturated aq. NH_4Cl (5 mL) and the aqueous phase was extracted with EtOAc (2 x 10 mL). The combined organic phases were dried over Na_2SO_4, filtered and concentrated under rotary evaporation before purification by flash column chromatography (5 % EtOAC in pentane) to yield phenyl ketone **84** as a yellow solid (74 mg, 69 %).

IR Vmax / cm^{-1}: 3059, 2963, 2903, 2865, 1677, 1595, 1512, 1372, 1271, 1236, 1223, 1166, 753, 690; **^{1}H NMR** (400 MHz, $CDCl_3$) δ 8.04 – 7.97 (m, 2H, 2 x CH-*c*), 7.64 – 7.58 (m, 1H, CH-*a*), 7.55 – 7.48 (m, 2H, 2 x CH-*b*), 7.27 – 7.20 (m, 2H, 2 x CH-*i*), 6.70 (t, J = 7.3 Hz, 1H, CH-*j*), 6.59 (d, J = 7.8 Hz, 2H, 2 x CH-*h*), 4.20 – 4.09 (m, 1H, CH-*d*), 3.71 – 3.56 (m, 2H, CH_2-*e*), 3.52 – 3.40 (m, 2H, CH_2-*g*), 2.48 – 2.28 (m, 2H, CH_2- *f*); **^{13}C NMR** (101 MHz, $CDCl_3$) δ 199.7, 147.8, 136.4, 133.5, 129.3 (2C), 128.9 (2C), 128.6 (2C), 116.3, 112.2 (2C), 50.5, 47.6, 45.7, 28.9; **HRMS (ES+)** Calculated for $C_{17}H_{18}NO$ ($M+H^+$): 252.1388; found: 252.1393.

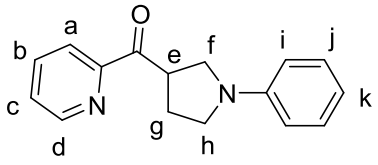
(±)-1-(1-Phenylpyrrolidin-3-yl)pent-4-en-1-one - 85



Following the procedure described for the preparation of phenyl ketone **84**, the title compound was prepared from amide **83** (0.10 g, 0.43 mmol) and but-3-en-1-ylmagnesium bromide (0.33 M solution in THF, 3.88 mL) in THF (2 mL). Purification was carried out using column chromatography (5 % EtOAc in pentane) to obtain the pentene ketone **85** as a white solid (79 mg, 80 %).

IR Vmax / cm^{-1}: 3084, 3059, 2979, 2839, 1703, 1595, 1509, 1344, 1188, 998, 906, 747, 690; **^{1}H NMR** (400 MHz, $CDCl_3$) δ 7.30 – 7.22 (m, 2H, 2 x CH-*j*), 6.73 (tt, *J* = 7.3, 0.9 Hz, 1H, CH-*k*), 6.60 (dd, *J* = 8.7, 0.9 Hz, 2H, 2 x CH-*i*), 5.85 (ddt, J = 17.0, 10.2, 6.5 Hz, 1H, CH-*b*), 5.09 (ddd, *J* = 17.0, 3.2, 1.6 Hz, 1H, CH-*a*), 5.04 (ddd, *J* = 10.2, 2.8, 1.3 Hz, 1H, CH-*a*) 3.55 – 3.49 (m, 2H, CH_2-*f*), 3.47 – 3.26 (m, 3H, CH-*e* + CH_2-*h*), 2.75 – 2.57 (m, 2H, CH_2-*d*), 2.46 – 2.35 (m, 2H, CH_2-*c*), 2.34 – 2.15 (m, 2H, CH_2-*g*); **^{13}C NMR** (101 MHz, $CDCl_3$) δ 209.2, 147.7, 137.1, 129.3 (2C), 116.3, 115.6, 112.1 (2C), 50.4, 49.3, 47.5, 40.8, 28.1, 27.7; **HRMS (ES+)** Calculated for $C_{15}H_{20}NO$ ($M+H^+$): 230.1545; found: 230.1546.

(±)-(1-Phenylpyrrolidin-3-yl)(pyridin-2-yl)methanone - 86

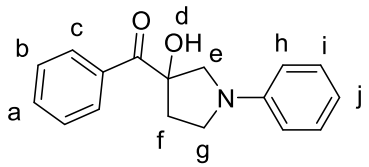


To a solution of 2-bromopyridine (81 µL, 0.85 mmol) in THF (2 mL) was added *n*-BuLi (2.5 M in hexanes, 340 µL) dropwise at -78 °C under N_2. The reaction was stirred at -78 °C for 30 min before the dropwise addition of amide **83** (100 mg, 0.43 mmol) in THF (2 mL). The

reaction was stirred at rt for 1 h and was then quenched with saturated aq. NH_4Cl (5 mL) and the aqueous phase was extracted with EtOAc (2 x 10 mL). The combined organic phases were dried over Na_2SO_4, filtered and concentrated under rotary evaporation before purification by flash column chromatography (10 % EtOAc in pentane) to yield 2-pyridyl ketone **86** as a yellow solid (69 mg, 64 %).

IR Vmax / cm^{-1}: 3068, 2928, 2865, 2824, 1693, 1598, 1582, 1506, 1480, 1369, 1331, 1226, 1179, 995, 741, 690: **^{1}H NMR** (400 MHz, $CDCl_3$) δ 8.72 (ddd, *J* = 4.8, 1.7, 0.9 Hz, 1H, CH-*d*), 8.09 (dt, *J* = 7.9, 1.1 Hz, 1H, CH-*a*), 7.86 (td, *J* = 7.7, 1.7 Hz, 1H, CH-*b*), 7.50 (ddd, *J* = 7.7, 4.8, 1.1 Hz, 1H, CH-*c*), 7.26 – 7.19 (m, 2H, 2 x CH-*j*), 6.68 (tt, *J* = 7.3, 1.0 Hz, 1H, CH-*k*), 6.60 (dd, *J* = 8.7, 1.0 Hz, 2H, 2 x CH-*i*), 4.71 – 4.58 (m, 1H, CH-*e*), 3.74 (dd, *J* = 9.5, 8.4 Hz, 1H, CH-*f*), 3.57 (dd, *J* = 9.5, 6.7 Hz, 1H, CH-*f*), 3.53 – 3.39 (m, 2H, CH_2-*h*), 2.47 – 2.29 (m, 2H, CH_2-*g*); **^{13}C NMR** (101 MHz, $CDCl_3$) δ 201.2, 153.0, 149.2, 147.9, 137.1, 129.2 (2C), 127.4, 122.7, 116.0, 112.1 (2C), 50.3, 47.7, 44.9, 28.5; **HRMS (ES+)** Calculated for $C_{16}H_{17}N_2O$ (M+H$^+$): 253.1341; found: 253.1346.

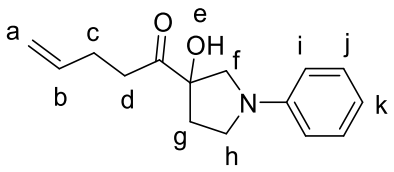
(±)-(3-Hydroxy-1-phenylpyrrolidin-3-yl)(phenyl)methanone - 27



To a solution of phenyl ketone **84** (30 mg, 0.12 mmol) in DMSO (1 mL) was added $P(OEt)_3$ (40 µL, 0.23 mmol) and Cs_2CO_3 (8 mg, 0.02 mmol) under O_2 (1 atm) and the reaction was stirred at rt for 16 h. The reaction was diluted with brine (10 mL) and the aqueous phase was extracted with EtOAc (3 × 10 mL). The combined organic phases were washed with brine (3 × 15 mL), dried over Na_2SO_4, filtered and concentrated under rotary evaporation before purification by flash column chromatography (10 % EtOAc in pentane) to give hydroxy-ketone **27** as a yellow oil (12 mg, 35 %) with purity of ≥95 % by LC-MS analysis.

IR Vmax / cm^{-1}: 3351, 3065, 2925, 2855, 1680, 1601, 1509, 1372, 1271, 753, 696; **^{1}H NMR** (400 MHz, $CDCl_3$) δ 8.19 – 8.10 (m, 2H, 2 x CH-*c*), 7.62 – 7.56 (m, 1H, CH-*a*), 7.50 – 7.43 (m, 2H, 2 x CH-*b*), 7.32 – 7.24 (m, 2H, 2 x CH-*i*), 6.80 (t, *J* = 7.3 Hz, 1H, CH-*j*), 6.68 (d, *J* = 7.8 Hz, 2H, 2 x CH-*h*), 4.39 (s, 1H, OH-*d*), 4.27 (d, *J* = 11.0 Hz, 1H, CH-*e*), 3.84 (td, *J* = 8.7, 1.5 Hz, 1H, CH-*g*), 3.58 (ddd, *J* = 10.3, 9.0, 6.7 Hz, 1H, CH-*g*), 3.42 (d, *J* = 11.0 Hz, 1H, CH-*e*), 2.81 (ddd, *J* = 13.4, 10.4, 8.7 Hz, 1H, CH-*f*), 2.28 – 2.19 (m, 1H, CH-*f*); **^{13}C NMR** (101 MHz, $CDCl_3$) δ 200.7, 147.9, 133.8, 132.6, 130.1 (2C), 129.4 (2C), 128.9 (2C), 117.5, 113.2 (2C), 84.5, 61.3, 47.5, 40.2; **HRMS (ES+)** Calculated for $C_{17}H_{18}NO_2$ ($M+H^+$): 268.1338; found: 268.1342.

(±)-1-(3-Hydroxy-1-phenylpyrrolidin-3-yl)pent-4-en-1-one - 26

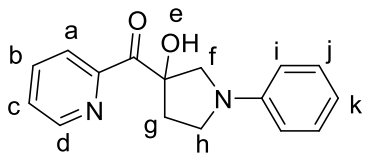


Following the procedure described for the preparation of hydroxy-ketone **27**, the title compound was prepared from pentene ketone **85** (79 mg, 0.34 mmol), Cs_2CO_3 (22 mg, 0.069 mmol), $P(OEt)_3$ (120 µL, 0.69 mmol) in DMSO (2 mL) under O_2 (1 atm). Purification was carried out using column chromatography (10 % EtOAc in pentane) to obtain the hydroxy-ketone **26** as a yellow oil (27 mg, 32 %) with purity of ≥95 % by LC-MS analysis.

^{1}H NMR (400 MHz, CD_3CN) δ 7.23 – 7.15 (m, 2H, 2 x CH-*j*), 6.65 (t, *J* = 7.3 Hz, 1H, CH-*k*), 6.56 (dd, *J* = 8.8, 1.0 Hz, 2H, 2 x CH-*i*), 5.86 (ddt, *J* = 16.9, 10.2, 6.5 Hz, 1H, CH-*b*), 5.01 (dddd, J = 29.3, 10.2, 3.3, 1.5 Hz, 2H, CH_2-*a*), 4.04 (s, 1H, OH-*e*), 3.65 (d, *J* = 10.5 Hz, 1H, CH-*f*), 3.50 – 3.39 (m, 2H, CH_2-*h*), 3.21 (dd, *J* = 10.5, 1.1 Hz, 1H, CH-*f*), 2.85 – 2.77 (m, 2H, CH_2-*d*), 2.42 – 2.27 (m, 3H, CH_2-*c* + CH-*g*), 2.02 (dddd, *J* = 11.2, 5.8, 3.9, 1.1 Hz, 1H, CH-*g*); **^{13}C NMR** (101 MHz, CD_3CN) δ 212.1, 148.7, 138.5, 130.0 (2C), 116.8, 115.5, 112.7 (2C),

85.6, 58.9, 47.3, 37.2, 36.9, 28.2; **HRMS (ES+)** Calculated for $C_{15}H_{20}NO_2$ ($M+H^+$): 246.1494; found: 246.1493

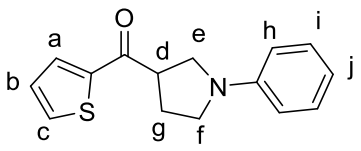
(±)-(3-Hydroxy-1-phenylpyrrolidin-3-yl)(pyridin-2-yl)methanone - 28



Following the procedure described for the preparation of hydroxy-ketone **27**, the title compound was prepared from 2-pyridyl ketone **86** (66 mg, 0.26 mmol), Cs_2CO_3 (17 mg, 0.052 mmol), $P(OEt)_3$ (90 µL, 0.52 mmol) in DMSO (2 mL) under O_2 (1 atm). Purification was carried out using column chromatography (20 % EtOAc in pentane) to obtain the hydroxy-ketone **28** as a yellow solid (16 mg, 23 %) with purity of ≥95 % by LC-MS analysis.

IR Vmax / cm^{-1}: 3268, 3065, 2925, 2843, 1703, 1601, 1509, 1372, 1239, 1220, 1185, 956, 747, 680; **^{1}H NMR** (400 MHz, $CDCl_3$) δ 8.65 (ddd, *J* = 4.8, 1.5, 0.8 Hz, 1H, CH-*d*), 8.19 – 8.12 (m, 1H, CH-*a*), 7.97 (td, *J* = 7.8, 1.5 Hz, 1H, CH-*b*), 7.57 (ddd, *J* = 7.8, 4.8, 1.2 Hz, 1H, CH-*c*), 7.25 – 7.19 (m, 2H, 2 x CH-*j*), 6.69 (t, *J* = 7.3 Hz, 1H, CH-*k*), 6.58 (d, *J* = 7.8 Hz, 2H, 2 x CH-*i*), 6.40 (s, 1H, CH-*e*), 3.93 (d, *J* = 10.5 Hz, 1H, CH-*f*), 3.67 – 3.59 (m, 2H, CH-*f* + CH-*h*), 3.54 (td, *J* = 8.3, 3.9 Hz, 1H, CH-*h*), 2.72 (dt, *J* = 12.9, 8.3 Hz, 1H, CH-*g*), 2.38 – 2.28 (m, 1H, CH-*g*); **^{13}C NMR** (101 MHz, $CDCl_3$) δ 196.9, 152.3, 148.0, 147.8, 138.4, 129.2 (2C), 127.9, 124.3, 116.1, 112.0 (2C), 85.9, 59.0, 46.7, 36.2; **HRMS (ES+)** Calculated for $C_{16}H_{17}N_2O_2$ ($M+H^+$): 269.1290; found: 269.1290.

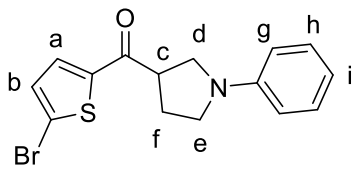
(±)-(1-Phenylpyrrolidin-3-yl)(thiophen-2-yl)methanone - 88



To a solution of thiophene (34 µL, 0.43 mmol) in THF (2 mL) was added *n*-BuLi (2.5 M in hexanes, 170 µL) dropwise at -30 °C under a under N_2. The reaction was warmed to 0 °C and then stirred at this temperature for 40 min until a bright yellow solution was observed. The reaction was cooled to -30 °C and amide **83** (100 mg, 0.43 mmol) in THF (1 mL) was added dropwise. The reaction was warmed to rt and stirred for 1 h before being quenched with saturated aq. NH_4Cl (5 mL) and the aqueous phase was extracted with EtOAc (2 x 10 mL). The combined organic phases were dried over Na_2SO_4, filtered and concentrated under rotary evaporation before purification by flash column chromatography (3 % EtOAc in pentane) to yield thiophene ketone **88** as an orange solid (27 mg, 25 %).

IR Vmax / cm^{-1}: 3090, 2852, 1658, 1599, 1506, 1414, 1366, 1230, 750, 696; **^{1}H NMR** (400 MHz, $CDCl_3$) δ 7.79 (dd, *J* = 3.8, 0.8 Hz, 1H, CH-*a*), 7.69 (dd, *J* = 4.8, 0.8 Hz, 1H, CH-*c*), 7.28 – 7.20 (m, 2H, 2 x CH-*i*), 7.18 (dd, *J* = 4.8, 3.8 Hz, 1H, CH-*b*), 6.71 (t, *J* = 7.3 Hz, 1H, CH-*j*), 6.59 (d, *J* = 8.0 Hz, 2H, 2 x CH-*h*), 4.00 (p, *J* = 7.7 Hz, 1H, CH-*d*), 3.72 – 3.58 (m, 2H, CH_2-*e*), 3.54 – 3.39 (m, 2H, CH_2-*f*), 2.52 – 2.26 (m, 2H, CH_2-*g*); **^{13}C NMR** (101 MHz, $CDCl_3$) δ 192.6, 147.7, 143.9, 134.3, 132.2, 129.3 (2C), 128.4, 116.4, 112.2 (2C), 50.8, 47.7, 47.0, 29.2; **HRMS (ES+)** Calculated for $C_{15}H_{16}NOS$ ($M+H^+$): 258.0953; found: 258.0951.

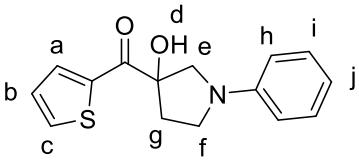
(±)-(5-Bromothiophen-2-yl)(1-phenylpyrrolidin-3-yl)methanone – 89



Following the procedure described for the preparation of 2-pyridyl ketone **86**, the title compound was prepared from 2-bromothiophene (41 µL, 0.43 mmol), amide **83** (50 mg, 0.21 mmol) and *n*-BuLi (2.5 M in hexanes, 85 µL) in THF (3 mL) under N_2. Purification was carried out using column chromatography (10 % EtOAc in pentane) to obtain bromothiophene ketone **89** as a yellow solid (32 mg, 45 %).

^{1}H NMR (400 MHz, $CDCl_3$) δ 7.52 (d, *J* = 4.0 Hz, 1H, CH-*a*), 7.28 – 7.20 (m, 2H, 2 x CH-*h*), 7.15 (d, *J* = 4.0 Hz, 1H, CH-*b*), 6.71 (t, *J* = 7.3 Hz, 1H, CH-*i*), 6.59 (d, *J* = 8.0 Hz, 2H, 2 x CH-*g*), 3.91 (p, *J* = 7.7 Hz, 1H, CH-*c*), 3.70 – 3.54 (m, 2H, CH_2-*d*), 3.54 – 3.37 (m, 2H, CH_2-*e*), 2.48 – 2.26 (m, 2H, CH_2-*f*); **^{13}C NMR** (101 MHz, $CDCl_3$) δ 191.6, 147.6, 145.2, 132.3, 131.5, 129.3 (2C), 123.4, 116.5, 112.2 (2C), 50.7, 47.7, 46.3, 29.2; **HRMS (ES+)** Calculated for $C_{15}H_{15}BrNOS$ ($M+H^+$): (^{79}Br) 336.0058; found: 336.0056 and (^{81}Br) 338.0032; found: 338.0054.

(±)-(3-Hydroxy-1-phenylpyrrolidin-3-yl)(thiophen-2-yl)methanone - 90

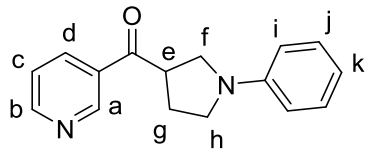


To a solution of thiophene ketone **88** (27 mg, 0.10 mmol) in DMSO (1 mL) was added $P(OEt)_3$ (36 µL, 0.21 mmol) and Cs_2CO_3 (7 mg, 0.02 mmol) under O_2 (1 atm) and the reaction was stirred at rt for 16 h and then at 50 °C for 1 h. The reaction was cooled and diluted with brine (10 mL) and the aqueous phase was extracted with EtOAc (3 × 10 mL).

The combined organic phases were washed with brine (3 × 15 mL), dried over Na_2SO_4, filtered and concentrated under rotary evaporation before purification by flash column chromatography (10 % EtOAc in pentane) to give hydroxy-ketone **90** as a yellow oil (19 mg, 65 %) with purity of ≥95 % by LC-MS analysis.

IR Vmax / cm^{-1}: 3417, 2855, 1649, 1601, 1506, 1411, 1357, 1261, 1036, 734, 693; **^{1}H NMR** (400 MHz, $CDCl_3$) δ 8.01 (dd, *J* = 4.0, 0.9 Hz, 1H, CH-*a*), 7.72 (dd, *J* = 4.9, 0.9 Hz, 1H, CH-*c*), 7.32 – 7.22 (m, 2H, 2 x CH-*i*), 7.14 (dd, *J* = 4.9, 4.0 Hz, 1H, CH-*b*), 6.79 (t, *J* = 7.3 Hz, 1H, CH-*j*), 6.67 (d, *J* = 7.9 Hz, 2H, 2 x CH-*h*), 4.19 (d, *J* = 10.9 Hz, 2H, CH-*e* + OH-*d*), 3.78 (td, *J* = 8.8, 1.6 Hz, 1H, CH-*f*), 3.63 – 3.53 (m, 1H, CH-*f*), 3.44 (d, *J* = 10.9 Hz, 1H, CH-*e*), 2.77 (ddd, *J* = 13.4, 10.1, 8.8 Hz, 1H, CH-*g*), 2.26 (dd, *J* = 13.4, 6.0 Hz, 1H, CH-*g*); **^{13}C NMR** (101 MHz, CD_3CN) δ 194.4, 148.9, 141.2, 136.1, 135.9, 130.1 (2C), 129.3, 117.0, 112.9 (2C), 85.9, 60.2, 47.4, 38.4; **HRMS (ESI)** Calculated for $C_{15}H_{16}NO_2S$ ($M+H^+$): 274.0902; found: 274.0915

(±)-(1-Phenylpyrrolidin-3-yl)(pyridin-3-yl)methanone - 91

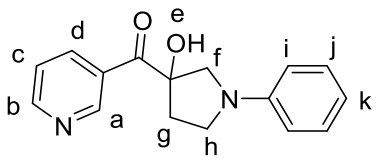


To a solution of 3-bromopyridine (82 µL, 0.85 mmol) in THF (2 mL) was added *n*-BuLi (2.5 M in hexanes, 340 µL) dropwise at -78 °C under N_2. The reaction was stirred at this temperature for 30 min and a dark blue colour was observed. After this time, amide **83** (100 mg, 0.43 mmol) in THF (1 mL) was added dropwise and the reaction was slowly warmed to rt and stirred for 1 h. The reaction was then quenched with saturated aq. NH_4Cl (5 mL) and the aqueous phase was extracted with EtOAc (2 x 10 mL). The combined organic phases were dried over Na_2SO_4, filtered and concentrated under rotary evaporation before

purification by flash column chromatography (40 % EtOAc in pentane) to yield 3-pyridyl ketone **91** as a yellow oil (27 mg, 28 %).

IR Vmax / cm^{-1}: 2925, 2859, 1687, 1598, 1509, 1369, 1236, 753, 696; **^{1}H NMR** (400 MHz, $CDCl_3$) δ 9.22 (d, *J* = 1.8 Hz, 1H, CH-*a*), 8.82 (dd, *J* = 4.8, 1.6 Hz, 1H, CH-*b*), 8.28 (dt, *J* = 8.0, 1.6 Hz, 1H, CH-*d*), 7.47 (dd, *J* = 8.0, 4.8 Hz, 1H, CH-*c*), 7.29 – 7.18 (m, 2H, 2 x CH-*j*), 6.71 (t, *J* = 7.3 Hz, 1H, CH-*k*), 6.59 (d, *J* = 7.9 Hz, 2H, 2 x CH-*i*), 4.18 – 4.04 (m, 1H, CH-*e*), 3.73 – 3.57 (m, 2H, CH_2-*f*), 3.54 – 3.39 (m, 2H, CH_2-*h*), 2.48 – 2.31 (m, 2H, CH_2-*g*); **^{13}C NMR** (101 MHz, $CDCl_3$) δ 198.5, 153.89, 150.0, 147.6, 136.0, 131.6, 129.3 (2C), 124.0, 116.6, 112.3 (2C), 50.1, 47.6, 46.0, 28.6; **HRMS (ES+)** Calculated for $C_{16}H_{17}N_2O$ ($M+H^+$): 253.1341; found: 253.1337.

(±)-(3-Hydroxy-1-phenylpyrrolidin-3-yl)(pyridin-3-yl)methanone - 87

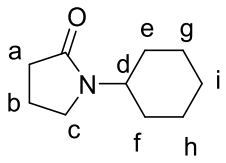


Following the procedure described for the preparation of hydroxy-ketone **27**, the title compound was prepared from 3-pyridyl ketone **91** (40 mg, 0.16 mmol), Cs_2CO_3 (10 mg, 0.032 mmol), $P(OEt)_3$ (54 µL, 0.32 mmol) in DMSO (1 mL) under O_2 (1 atm). Purification was carried out using column chromatography (30 - 40 % EtOAc in pentane) to obtain hydroxy-ketone **87** as a yellow oil (10 mg, 24 %) with purity of ≥95 % by LC-MS analysis.

IR Vmax / cm^{-1}: 3259, 2925, 1690, 1598, 1509, 1372, 1271, 1030, 750, 693; **^{1}H NMR** (400 MHz, CD_3CN) δ 9.26 (dd, *J* = 2.2, 0.9 Hz, 1H, CH-*a*), 8.74 (dd, *J* = 4.8, 1.7 Hz, 1H, CH-*b*), 8.44 (ddd, *J* = 8.0, 2.2, 1.7 Hz, 1H, CH-*d*), 7.47 (ddd, *J* = 8.0, 4.8, 0.9 Hz, 1H, CH-*c*), 7.24 – 7.17 (m, 2H, 2 x CH-*j*), 6.67 (tt, *J* = 7.3, 1.0 Hz, 1H, CH-*k*), 6.63 – 6.58 (m, 2H, 2 x CH-*i*), 4.32 (s, 1H, OH-*e*), 3.90 (d, *J* = 10.6 Hz, 1H, CH-*f*), 3.56 – 3.45 (m, 3H, CH_2-*h* + CH-*f*), 2.65 (dt, J = 13.0, 8.6 Hz, 1H, CH-*g*), 2.27 (dddd, *J* = 13.0, 6.5, 3.8, 1.1 Hz, 1H, CH-*g*). **^{13}C NMR**

(101 MHz, CD_3CN) δ 200.9, 154.0, 151.7, 148.8, 138.1, 130.0 (2C), 126.4, 124.3, 117.0, 112.9 (2C), 86.0, 59.6, 47.2, 37.8; **HRMS (ES+)** Calculated for $C_{16}H_{17}N_2O_2$ ($M+H^+$): 269.1290; found: 269.1295.

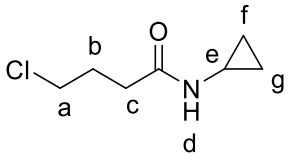
1-Cyclohexylpyrrolidin-2-one - 96



Synthesis according to Orrling *et al.*[139] A mixture of *γ*-butyrolactone (0.15 mL, 2.0 mmol), cyclohexylamine (0.69 mL, 6.0 mmol) and 1-butyl-3-methylimidazolium tetrafluoroborate (0.37 mL, 2.0 mmol) was vigorously stirred in a sealed microwave vial for 20 s prior to microwave irradiation at 220 °C for 35 min. Once cooled the reaction mixture was diluted with EtOAc (50 mL) and the organic phase was washed with saturated aq. NH_4Cl (2 x 70 mL), dried over Na_2SO_4, filtered and concentrated under rotary evaporation. The crude product was purified by flash column chromatography (60 % EtOAc in pentane) to yield lactam **96** as a yellow oil (0.22 g, 86 %).

^{1}H NMR (400 MHz, $CDCl_3$) δ 3.98 – 3.79 (m, 1H, CH-*d*), 3.30 (t, *J* = 7.0 Hz, 2H, CH_2-*c*), 2.33 (t, *J* = 8.1 Hz, 2H, CH_2-*a*), 1.99 – 1.88 (m, 2H, CH_2-*b*), 1.81 – 1.54 (m, 5H, CH_2-*e*, CH_2-*f*, CH-*i*), 1.42 – 1.22 (m, 4H, CH_2-*g*, CH_2-*h*), 1.14 – 0.94 (m, 1H, CH-*i*); **^{13}C NMR** (101 MHz, $CDCl_3$) δ 174.3, 50.5, 42.9, 31.7, 30.3 (2C), 25.5, 25.5 (2C), 18.2. These spectroscopic data correspond to previously reported data.[139]

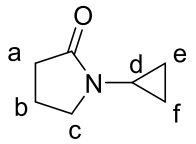
4-Chloro-*N*-cyclopropylbutanamide - 101



Based on a procedure by Takao *et al.*[254] To a solution of cyclopropylamine (0.10 mL, 1.4 mmol) in dry THF (2 mL) under N_2 was added NEt_3 (0.20 mL, 1.4 mmol) and the mixture was cooled at 0 °C. With vigorous stirring, 4-chlorobutyryl chloride (0.16 mL, 1.4 mmol) was added dropwise and the reaction was stirred at 0 °C for 2 h. The precipitate formed was removed by filtration and was washed with THF (2 x 10 mL). The filtrate was concentrated under rotary evaporation and the resulting residue was dissolved in EtOAc (20 mL), washed with HCl (1 M, 10 mL), then brine (2 x 10 mL) and the organic phase was dried over Na_2SO_4, filtered and concentrated under rotary evaporation to yield amide **101** as a white solid (118 mg, 52 %).

IR Vmax / cm^{-1}: 3322, 3246, 3068, 2970, 2925, 1639, 1547, 1531, 1423, 1268, 1023; **^{1}H NMR** (400 MHz, $CDCl_3$) δ 5.68 (s, 1H, NH-*d*), 3.60 (t, *J* = 6.2 Hz, 2H, CH_2-*a*), 2.76 – 2.66 (m, 1H, CH-*e*), 2.31 (t, *J* = 7.1 Hz, 2H, CH_2-*c*), 2.16 – 2.05 (m, 2H, CH_2-*b*), 0.80 – 0.73 (m, 2H, CH_2-*f*), 0.52 – 0.45 (m, 2H, CH_2-*g*); **^{13}C NMR** (101 MHz, $CDCl_3$) δ 173.2, 44.7, 33.1, 28.2, 22.8, 6.8 (2C); **HRMS (ES+)** Calculated for $C_7H_{13}ClNO$ ($M+H^+$): (^{35}Cl) 162.0686; found: 162.0681 and (^{37}Cl) 164.0651; found: 164.0658.

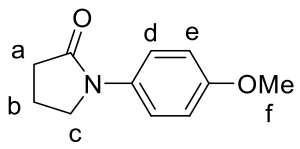
1-Cyclopropylpyrrolidin-2-one - 97



Based on a procedure by Takao *et al.*[254] Potassium *tert*-butoxide (80 mg, 0.71 mmol) was suspended in dry THF (1.5 mL) under nitrogen and the mixture was cooled at 0 ˚C. Amide **101** (113 mg, 0.70 mmol) in dry THF (0.5 mL) was added dropwise with vigorous stirring. The reaction was stirred at 0 °C for an additional 2 h and was then diluted with EtOAc (15 mL) and washed with brine (3 x 10 mL). The organic phase was dried over Na_2SO_4, filtered and concentrated under rotary evaporation before purification by flash column chromatography (70 % EtOAc in pentane with 1 % NEt_3) to yield lactam **97** as an orange oil (31 mg, 35 %).

^{1}H NMR (400 MHz, $CDCl_3$) δ 3.28 – 3.20 (m, 2H, CH_2-*c*), 2.60 – 2.51 (m, 1H, CH-*d*), 2.30 (t, *J* = 8.1 Hz, 2H, CH_2-*a*), 1.96 – 1.84 (m, 2H, CH_2-*b*), 0.73 – 0.57 (m, 4H, CH_2-*e* + CH_2-*f*); **^{13}C NMR** (101 MHz, $CDCl_3$) δ 176.3, 47.5, 31.9, 25.2, 18.1, 4.9 (2C); **HRMS (ES+)** Calculated for $C_7H_{12}NO$ ($M+H^+$): 126.0919; found: 126.0923.

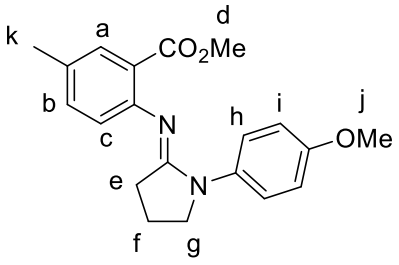
1-(4-Methoxyphenyl)pyrrolidin-2-one - 107



Synthesis according to Guazzelli *et al.*[142] To a solution of pyrrolidin-2-one (4.5 mL, 59 mmol) in DMF (15 mL) was added copper powder (2.5 g, 39 mmol), K_2CO_3 (2.7 g, 20 mmol) and 1-iodo-4-methoxybenzene (4.6 g, 20 mmol) and the reaction was heated to 150 °C for 18 h. The reaction was cooled and filtered through Celite®, washing with DCM (3 x 20 mL). The filtrate was concentrated under rotary evaporation yielding pyrrolidinone **107** as an off-white solid (2.9 g, 77%) which was used without purification.

^{1}H NMR (400 MHz, $CDCl_3$) δ 7.52 – 7.45 (m, 2H, 2 x CH-*d*), 6.93 – 6.86 (m, 2H, 2 x CH-*e*), 3.85 – 3.77 (m, 5H, CH_2-*c* + CH_3-*f*), 2.58 (t, *J* = 8.1 Hz, 2H, CH_2-*a*), 2.19 – 2.08 (m, 2H, CH_2-*b*); **^{13}C NMR** (101 MHz, $CDCl_3$) δ 174.0, 156.6, 132.7, 121.9 (2C), 114.1 (2C), 55.6, 49.3, 32.6, 18.1; **HRMS (ES+)** Calculated for $C_{11}H_{14}NO_2$ ($M+H^+$): 192.1025; found: 192.1025. These spectroscopic data correspond to previously reported data.[142]

Methyl 2-((2-(4-methoxyphenyl)cyclopentylidene)amino)-5-methylbenzoate - 108

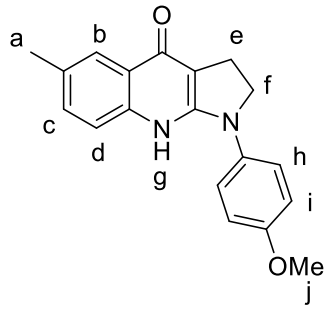


Synthesis according to Lawson *et al.*[63] To a solution of pyrrolidinone **107** (2.9 g, 15 mmol) in dry DCM (30 mL) under nitrogen was added $POCl_3$ (1.4 mL, 15 mmol) and the reaction was stirred at rt for 3 h. A solution of methyl 2-amino-5-methylbenzoate (2.1 g, 13 mmol) in DCM

(5 mL) was then added to the reaction mixture and then heated under reflux (40 °C) for 18 h. The reaction was cooled to rt, diluted with DCM (50 mL) and washed with saturated aq. $NaHCO_3$ (3 x 70 mL). The organic phase was dried over Na_2SO_4, filtered and concentrated under rotary evaporation and the crude product was purified by flash column chromatography (20 % EtOAc in pentane with 1 % NEt_3) to yield amidine **108** as a yellow oil (2.33 g, 55 %).

^{1}H NMR (400 MHz, $CDCl_3$) δ 7.69 (d, *J* = 9.0 Hz, 2H, 2 x CH_2-*h*), 7.64 (d, *J* = 1.0 Hz, 1H, CH-*a*), 7.16 (dd, *J* = 8.1, 1.5 Hz, 1H, CH-*b*), 6.94 – 6.85 (m, 2H, 2 x CH_2-*h*), 6.70 (d, *J* = 8.1 Hz, 1H, CH-*c*), 3.86 – 3.80 (m, 5H, CH_2-*g* + CH_3-*d*), 3.78 (s, 3H, CH_3-*j*), 2.43 (t, *J* = 7.8 Hz, 2H, CH_2-*e*), 2.31 (s, 3H, CH_3-*k*), 2.03 (p, *J* = 7.3 Hz, 2H, CH_2-*f*); **^{13}C NMR** (101 MHz, $CDCl_3$) δ 168.0, 160.0, 155.8, 151.1, 135.0, 133.6, 131.1, 130.9, 123.5, 122.5 (2C), 122.3, 114.1 (2C), 55.6, 51.8, 51.2, 29.1, 20.7, 20.0; **HRMS (ES+)** Calculated for $C_{20}H_{23}N_2O_3$ ($M+H^+$): 339.1709; found: 339.1703. These spectroscopic data correspond to previously reported data.[63]

1-(4-Methoxyphenyl)-6-methyl-1,2,3,9-tetrahydro-4*H*-pyrrolo[2,3-*b*]quinolin-4-one - 109

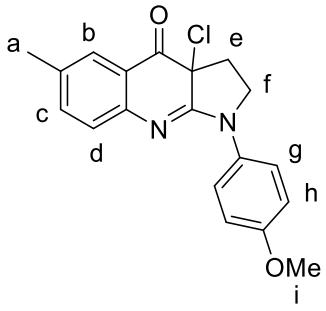


Synthesis according to Lawson *et al.*[63] To a solution of amidine **108** (2.3 g, 6.8 mmol) in dry THF (10 mL) under nitrogen was added LiHMDS (1M in THF, 17.1 mL) at -78 °C. The reaction was warmed to 0 °C over 3 h and was quenched at this temperature with saturated aq. NH_4Cl (50 mL). The resulting mixture was allowed to warm to rt for 1 h and the

precipitate was filtered, washed with ice cold ethyl acetate (10 mL) and dried extensively under vacuum to yield quinolone **109** as a cream solid (1.84 g, 92 %).

^{1}H NMR (400 MHz, DMSO) δ 8.29 – 7.54 (m, 4H, NH-*g*, CH-*b*, 2 x CH-*h*), 7.44 (d, *J* = 8.2 Hz, 1H, CH-*c*), 7.27 (d, *J* = 8.2 Hz, 1H, CH-*d*), 6.97 (d, *J* = 8.7 Hz, 2H, 2 x CH-*i*), 4.00 (t, *J* = 7.8 Hz, 2H, CH_2-*f*), 3.75 (s, 3H, CH_3-*j*), 3.20-2.98 (m, 2H, CH_2-*e*), 2.39 (s, 3H, CH_3-*a*); **^{13}C NMR** (126 MHz, DMSO) δ 164.9, 159.2, 154.0, 146.5, 135.7, 130.3 (2C), 125.7, 120.8, 119.0, 113.9 (2C), 106.0, 55.2, 48.4, 22.2, 20.9; **HRMS (ES+)** Calculated for $C_{19}H_{19}N_2O_2$ ($M+H^+$): 307.1447; found: 307.1458. These spectroscopic data correspond to previously reported data.[63]

(±)-3a-Chloro-1-(4-methoxyphenyl)-6-methyl-1,2,3,3a-tetrahydro-4*H*-pyrrolo[2,3-*b*]quinolin-4-one - 110

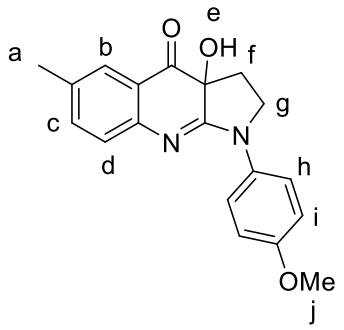


Synthesis according to Lawson *et al.*[63] A 1:1 mixture of THF and H_2O (30 mL) was added to quinolone **109** (1.85 g, 6.33 mmol) and to this mixture was added sodium dichloroisocyanurate (0.70 g, 3.2 mmol). The reaction was stirred at rt for 4 h and the resulting precipitate was filtered, washed with ice cold THF:H_2O (1:1) (5 mL) and dried extensively under vacuum to yield chloro-quinolone **110** as a red solid (1.55 g, 72 %).

^{1}H NMR (400 MHz, DMSO) δ 11.18 (s, 1H), 8.00 – 7.91 (m, 2H, 2 x CH-*g*), 7.60 (d, *J* = 1.9 Hz, 1H, CH-*b*), 7.42 (dd, *J* = 8.3, 1.9 Hz, 1H, CH-*c*), 7.13 (d, *J* = 8.3 Hz, 1H, CH-*d*), 7.05 – 6.99 (m, 2H, 2 x CH-*h*), 4.22 – 3.96 (m, 2H, CH_2-*f*), 3.78 (s, 3H, CH_3-*i*), 2.80 (dt, *J* = 14.2, 8.4 Hz, 1H, CH-*e*), 2.58 (dd, *J* = 14.2, 5.2 Hz, 1H, CH-*e*), 2.31 (s, 3H, CH_3-*a*); **^{13}C NMR** (101

MHz, DMSO) δ 188.7, 161.9, 156.0, 150.0, 148.8, 137.3, 133.3, 132.7, 126.6, 126.0, 121.7 (2C), 119.8, 114.0 (2C), 63.0, 55.3, 47.8, 30.0, 20.2; **HRMS (ES+)** Calculated for $C_{19}H_{18}ClN_2O_2$ ($M+H^+$): (^{35}Cl) 341.1057; found: 341.1052 and (^{37}Cl) 343.1022; found: 343.1006 . These spectroscopic data correspond to previously reported data.[63]

(±)-3a-Hydroxy-1-(4-methoxyphenyl)-6-methyl-1,2,3,3a-tetrahydro-4*H*-pyrrolo[2,3-*b*]quinolin-4-one - 111

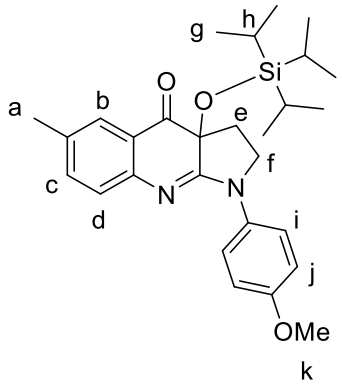


Synthesis according to Lawson *et al.*[63] A 1:1 mixture of THF and H_2O (15 mL) was added to chloro-quinolone **110** (1.53 g, 4.49 mmol) and to this mixture was added NaOH (2 M, 4.15 mL). The reaction was stirred at rt for 18 h and was then diluted with DCM (50 mL) and washed with saturated aq. NH_4Cl (3 x 30 mL). The organic phase was dried over Na_2SO_4, filtered and concentrated under rotary evaporation before purification by flash column chromatography (30 % EtOAc in pentane) to yield hydroxy-quinolone **111** as an orange solid (1.12 g, 77 %).

^{1}H NMR (400 MHz, $CDCl_3$) δ 7.77 – 7.70 (m, 2H, 2 x CH-*h*), 7.60 (d, *J* = 1.7 Hz, 1H, CH-*b*), 7.21 (dd, *J* = 8.2, 1.7 Hz, 1H, CH-*c*), 7.04 (d, *J* = 8.2 Hz, 1H, CH-*d*), 6.97 – 6.91 (m, 2H, 2 x CH-*i*), 4.03 – 3.93 (m, 1H, CH-*g*), 3.85 – 3.73 (m, 4H, CH_3-*j* + CH-*g*), 2.41 (dd, *J* = 13.7, 5.6 Hz, 1H, CH-*f*), 2.31 (s, 3H, CH_3-*a*), 2.29 – 2.16 (m, 1H, CH-*f*), 1.63 (s, 1H, OH-*e*); **^{13}C NMR** (101 MHz, $CDCl_3$) δ 194.6, 164.6, 156.7, 149.2, 137.5, 133.3, 133.2, 127.4, 126.1, 122.1 (2C), 120.2, 114.2, 73.82, 55.7, 48.7, 29.2, 20.8; **HRMS (ES+)** Calculated for $C_{19}H_{19}N_2O_3$

(M+H$^+$): 323.1396; found: 323.1399. These spectroscopic data correspond to previously reported data.[63]

(±)-1-(4-Methoxyphenyl)-6-methyl-3a-((triisopropylsilyl)oxy)-1,2,3,3a-tetrahydro-4*H*-pyrrolo[2,3-*b*]quinolin-4-one - 112

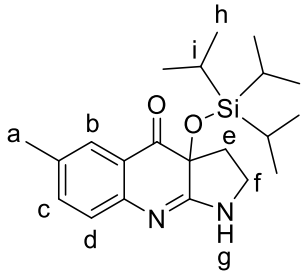


Synthesis according to Lawson *et al.*[63] To a suspension of hydroxy-quinolone **111** (1.30 g, 4.03 mmol) in dry DCM (23 mL) under N_2 was added dry DIPEA (2.81 mL, 16.1 mmol) followed by TIPSOTf (3.26 mL, 12.1 mmol) and the reaction was heated under reflux for 18 h. The reaction was cooled to rt and quenched with saturated aq. NH_4Cl (60 mL) and the aqueous phase was extracted with DCM (3 x 50 mL). The combined organic phases were dried over Na_2SO_4, concentrated under rotary evaporation before purification by flash column chromatography (10 % EtOAc in pentane) to yield TIPS-protected quinolone **112** as an orange solid (1.64 g, 85 %).

^{1}H NMR (400 MHz, $CDCl_3$) δ 7.86 – 7.78 (m, 2H, 2 x CH-*i*), 7.60 (d, *J* = 1.8 Hz, 1H, CH-*b*), 7.29 (dd, *J* = 8.1, 1.8 Hz, 1H, CH-*c*), 7.13 (d, *J* = 8.1 Hz, 1H, CH-*d*), 6.98 – 6.91 (m, 2H, 2 x CH-*j*), 4.12 (td, *J* = 9.7, 5.6 Hz, 1H, CH-*f*), 3.93 – 3.85 (m, 1H, CH-*f*), 3.82 (s, 3H, CH_3-*k*), 2.47 (dd, *J* = 13.8, 5.6 Hz, 1H, CH-*e*), 2.35 – 2.24 (m, 4H, CH_3-*a* + CH-*e*), 0.93 – 0.81 (m, 21H, 6 x CH_3-*g* + 3 x CH-*h*); **^{13}C NMR** (101 MHz, $CDCl_3$) δ 195.2, 165.1, 156.5, 150.0, 137.2, 133.9, 132.8, 127.2, 126.2, 122.1 (2C), 121.7, 114.3 (2C), 75.5, 55.7, 48.6, 30.6, 20.8, 18.0

(d, J = 9.8 Hz, 3C), 13.3 (6C); **HRMS (ES+)** Calculated for $C_{28}H_{39}N_2O_3Si_3$ ($M+H^+$): 479.2730; found: 479.2731. These spectroscopic data correspond to previously reported data.[63]

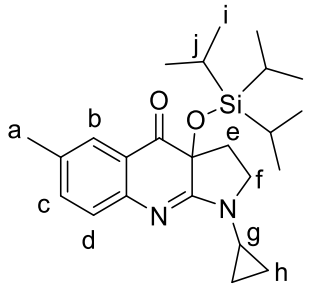
(±)-6-Methyl-3a-((triisopropylsilyl)oxy)-1,2,3,3a-tetrahydro-4*H*-pyrrolo[2,3-*b*]quinolin-4-one - 113



Based on a procedure by Lawson *et al.*[63] A 1:1 mixture of MeCN and H_2O (80 mL) was added to TIPS-protected quinolone **112** (1.32 g, 2.76 mmol) and the resulting suspension was cooled to 0 °C and CAN (5.14 g, 9.38 mmol) was added portion-wise over 4 h until the starting material had been consumed by TLC. The solvent was lyophilized and the resulting residue was purified by flash column chromatography (0.5 – 4 % (1% NH_4OH in MeOH) in $CHCl_3$) to yield amidine **113** as a yellow solid (0.25 g, 25 %).

^{1}H NMR (400 MHz, MeOD) δ 7.54 (d, *J* = 1.1 Hz, 1H, CH-*b*), 7.31 (dd, *J* = 8.3, 1.8 Hz, 1H, CH-*c*), 6.91 (d, *J* = 8.3 Hz, 1H, CH-*d*), 3.84 – 3.65 (m, 2H, CH_2-*f*), 2.41 – 2.20 (m, 5H, CH_3-*a* + CH_2-*e*), 0.98 – 0.82 (m, 21H, 6 x CH_3-*h* + 3 x CH-*i*); **^{13}C NMR** (126 MHz, MeOD) δ 194.24, 168.24, 145.89, 137.95, 132.27, 128.77, 121.25, 119.55, 33.25, 20.44, 18.31 (d, J = 9.1 Hz, 3C), 14.36 (6C); **HRMS (ES+)** Calculated for $C_{21}H_{33}N_2O_2Si$ ($M+H^+$): 373.2311; found: 373.2313. These spectroscopic data correspond to previously reported data.[63]

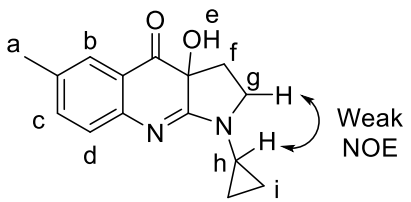
(±)-1-Cyclopropyl-6-methyl-3a-((triisopropylsilyl)oxy)-1,2,3,3a-tetrahydro-4*H*-pyrrolo[2,3-*b*]quinolin-4-one - 115



Based on a procedure by Bénard *et al.*[155] To a suspension of amidine **113** (20 mg, 0.054 mmol), cyclopropyl boronic acid (9 mg, 0.1 mmol) and Na_2CO_3 (11 mg, 0.11 mmol) in DCE (0.5 mL) was added a suspension of $Cu(OAc)_2$ (10 mg, 0.054 mmol) and bipyridine (9 mg, 0.05 mmol) in hot DCE (1.3 mL). The reaction was heated to 70 °C for 4 h before cooling to rt and quenching with 25 % aq. NH_4OH (10 mL). The aqueous phase was extracted with DCM (3 x 15 mL) and the combined organic phases were washed with brine (20 mL), dried over Na_2SO_4 and concentrated under rotary evaporation before purification by flash column chromatography (30 % EtOAc in pentane) to yield cyclopropyl amidine **115** as a yellow solid (12 mg, 54 % calculated with 32 % bipyridine impurity).

IR Vmax / cm^{-1}: 2932, 2871, 1690, 1626, 1607, 1484, 1461, 1134, 1039, 887; **^{1}H NMR** (400 MHz, $CDCl_3$) δ 7.53 (d, *J* = 1.7 Hz, 1H, CH-*b*), 7.29 – 7.22 (m, 1H, CH-*c* (overlapping with $CDCl_3$)), 7.11 (d, *J* = 8.1 Hz, 1H, CH-*d*), 3.62 (td, *J* = 9.6, 5.7 Hz, 1H, CH-*f*), 3.41 – 3.32 (m, 1H, CH-*f*), 2.99 – 2.90 (m, 1H, CH-*g*), 2.33 – 2.25 (m, 4H, CH_3-*a* + CH-*e*), 2.22 – 2.11 (m, 1H, CH-*e*), 0.91 – 0.81 (m, 25H, 6 x CH_3-*I* + 3 x CH-*j* + 2 x CH_2-*h*); **^{13}C NMR** (101 MHz, $CDCl_3$) δ 195.5, 168.3, 149.4, 137.2, 131.9, 127.2, 125.7, 121.8, 75.5, 47.0, 30.9, 26.9, 20.7, 18.0 (d, *J* = 11.4 Hz, 3C), 13.3 (6C), 6.1, 5.6; **HRMS (ES+)** Calculated for $C_{24}H_{37}N_2O_2Si$ ($M+H^+$): 413.2624; found: 413.2627.

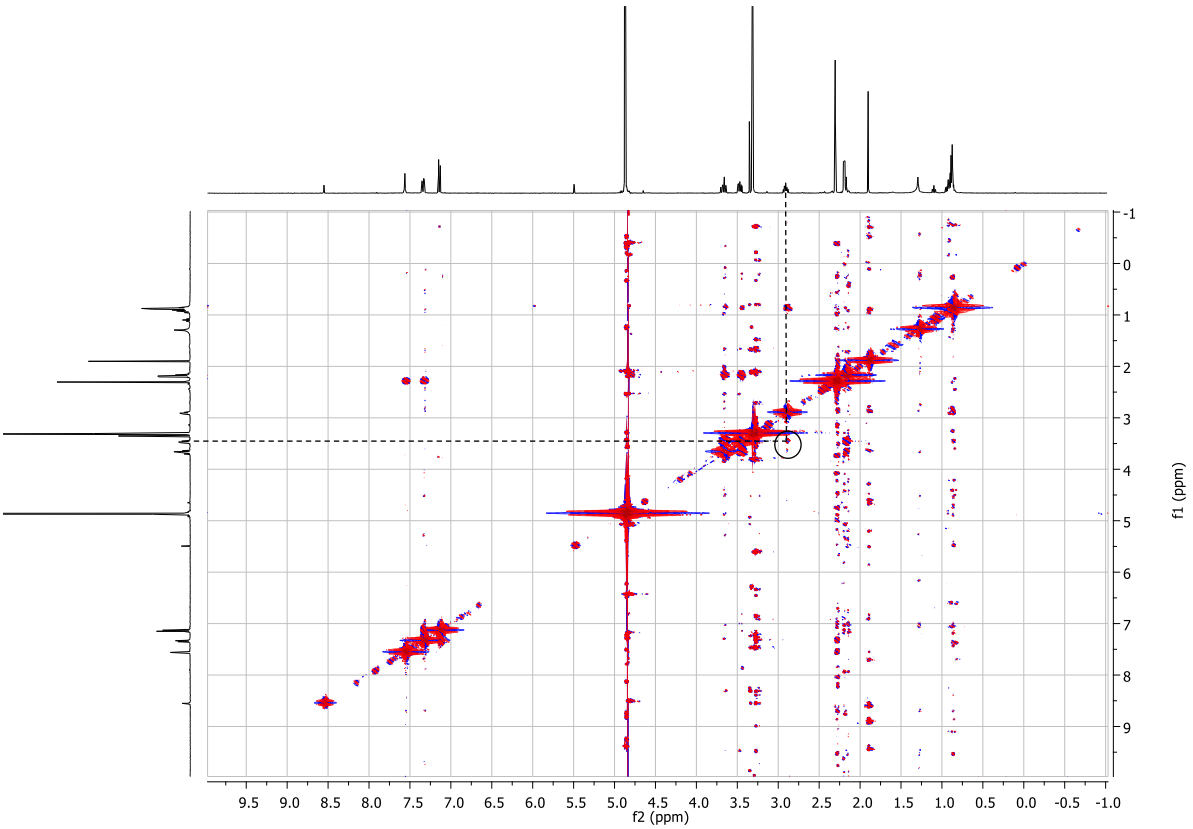
(±)-1-Cyclopropyl-3a-hydroxy-6-methyl-1,2,3,3a-tetrahydro-4*H*-pyrrolo[2,3-*b*]quinolin-4-one - 118



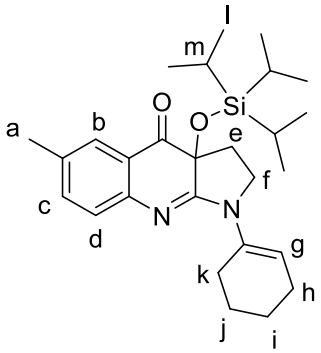
Based on a procedure by Lawson *et al.*[63] To a solution of cyclopropyl amidine **115** (12 mg, 0.029 mmol) in dry THF (0.5 mL) under N_2 was added TBAF (1 M in THF, 87 µL) dropwise at 0 °C and the reaction was stirred at rt for 2 h. The solvent was then removed under reduced pressure and the resulting residue was purified by flash column chromatography (2 % MeOH in DCM) to yield hydroxyl-amidine **118** as a yellow solid (6 mg, 80 %) with purity of ≥95 % by LC-MS analysis.

IR Vmax / cm^{-1}: 2928, 1690, 1607, 1484, 1290, 1220; **^{1}H NMR** (400 MHz, CD_3CN) δ 7.50 (d, *J* = 1.9 Hz, 1H, CH-*b*), 7.29 (dd, *J* = 8.1, 1.9 Hz, 1H, CH-*c*), 6.98 (d, *J* = 8.1 Hz, 1H, CH-*d*), 4.34 (s, 1H, OH-*e*), 3.62 – 3.51 (m, 1H, CH-*g*), 3.38 – 3.30 (m, 1H, CH-*g*), 2.96 – 2.87 (m, 1H, CH-*h*), 2.28 (s, 3H, CH_3-*a*), 2.12 – 2.08 (m, 1H, CH-*f* (overlapping with H_2O)), 1.97 – 1.94 (m, 1H, CH-*f* (overlapping with CD_3CN)), 0.86 – 0.73 (m, 4H, 2 x CH_2-*i*); **^{13}C NMR** (101 MHz, CD_3CN) δ 196.1, 168.9, 151.8, 137.7, 132.4, 127.5, 126.1, 122.0, 74.3, 46.9, 30.1, 27.5, 20.5, 5.6, 5.3; **HRMS (ES+)** Calculated for $C_{15}H_{17}N_2O_2$ ($M+H^+$): 257.1290; found: 257.1297.

NOESY NMR (400 MHz MeOD)



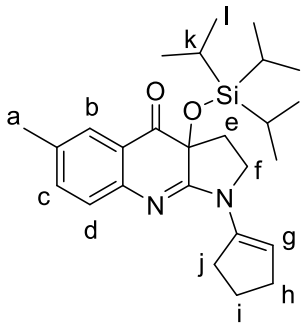
(±)-1-(Cyclohex-1-en-1-yl)-6-methyl-3a-((triisopropylsilyl)oxy)-1,2,3,3a-tetrahydro-4*H*-pyrrolo[2,3-*b*]quinolin-4-one - 119



Following the procedure described for the preparation of cyclopropyl amidine **115**, the title compound was prepared from amidine **113** (28 mg, 0.075 mmol) with cyclohex-1-en-1-ylboronic acid (19 mg, 0.15 mmol), Na_2CO_3 (16 mg, 0.15 mmol), $Cu(OAc)_2$ (14 mg, 0.075 mmol), bipyridine (12 mg, 0.075 mmol) in DCE (2 mL). Purification was carried out by flash column chromatography (5 % EtOAc in pentane) to yield cyclohexene amidine **119** as a yellow solid (16 mg, 47 %).

IR Vmax / cm^{-1}: 2928, 2865, 1690, 1604, 1477, 1290, 1258, 1131, 1039, 883; **^{1}H NMR** (400 MHz, $CDCl_3$) δ 7.54 (d, *J* = 1.3 Hz, 1H, CH-*b*), 7.24 (dd, *J* = 8.2, 1.9 Hz, 1H, CH-*c*), 7.05 (d, *J* = 8.2 Hz, 1H, CH-*d*), 5.92 – 5.85 (m, 1H, CH-*g*), 3.84 (td, *J* = 9.8, 5.7 Hz, 1H, CH-*f*), 3.69 – 3.61 (m, 1H, CH-*f*), 2.61 – 2.46 (m, 2H, CH_2-*k*), 2.38 – 2.26 (m, 4H, CH_3-*a* + CH-*e*), 2.24 – 2.10 (m, 3H, CH-*e* + CH_2-*h*), 1.79 – 1.71 (m, 2H, CH_2-*j*), 1.66 – 1.59 (m, 2H, CH_2-*i*), 0.94 – 0.80 (m, 21H, 6 x CH_3-*l* + 3 x CH-*m*); **^{13}C NMR** (101 MHz, $CDCl_3$) δ 195.5, 165.4, 150.4, 137.3, 137.1, 132.2, 127.1, 126.0, 121.6, 117.6, 75.5, 48.3, 30.5, 26.9, 24.6, 22.9, 22.0, 20.7, 18.0 (d, *J* = 10.7 Hz, 3C), 13.33 (6C); **HRMS (ES+)** Calculated for $C_{27}H_{41}N_2O_2Si$ ($M+H^+$): 453.2937; found: 453.2927.

(±)-1-(Cyclopent-1-en-1-yl)-6-methyl-3a-((triisopropylsilyl)oxy)-1,2,3,3a-tetrahydro-4*H*-pyrrolo[2,3-*b*]quinolin-4-one - 120

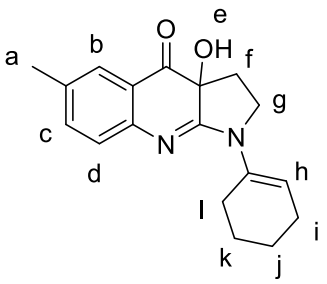


Following the procedure described for the preparation of cyclopropyl amidine **115**, the title compound was prepared from amidine **113** (38 mg, 0.10 mmol) with cyclopent-1-en-1-ylboronic acid (23 mg, 0.20 mmol), Na_2CO_3 (22 mg, 0.20 mmol), $Cu(OAc)_2$ (19 mg, 0.10 mmol), bipyridine (16 mg, 0.10 mmol) in DCE (2 mL). Purification was carried out by flash column chromatography (2.5 % EtOAc in pentane) to yield cyclopentene amidine **120** as a yellow/orange solid (16 mg, 47 %).

IR Vmax / cm^{-1}: 2944, 2932, 2868, 1693, 1633, 1607, 1480, 1128, 1042; **^{1}H NMR** (400 MHz, $CDCl_3$) δ 7.57 (d, *J* = 1.6 Hz, 1H, CH-*b*), 7.29 – 7.24 (m, 1H, CH-*c* overlapping with $CDCl_3$), 7.08 (d, *J* = 8.1 Hz, 1H, CH-*d*), 5.79 – 5.74 (m, 1H, CH-*g*), 3.86 (td, *J* = 9.9, 5.8 Hz, 1H, CH-*f*), 3.76 – 3.66 (m, 1H, CH-*f*), 3.05 – 2.83 (m, 2H, CH_2-*j*), 2.50 – 2.40 (m, 2H, CH_2-*h*), 2.36

(dd, *J* = 13.9, 5.8 Hz, 1H, CH-*e*), 2.30 (s, 3H, CH_3-*a*), 2.27 – 2.14 (m, 1H, CH-*e*), 1.99 – 1.88 (m, 2H, CH-*i*), 0.91 – 0.81 (m, 21H, 6 x CH_3-*l* + 3 x CH-*k*); **^{13}C NMR** (101 MHz, $CDCl_3$) δ 195.2, 164.7, 149.9, 140.6, 137.10, 132.8, 127.2, 126.3, 121.6, 112.2, 75.0, 48.0, 33.0, 30.6, 30.5, 22.3, 20.8, 18.0 (d, *J* = 7.7 Hz, 3C), 13.3 (6C); **HRMS (ES+)** Calculated for $C_{21}H_{33}N_2O_2Si$ ($M+H^+$ without cyclopentene): 373.2311; found: 373.2311.

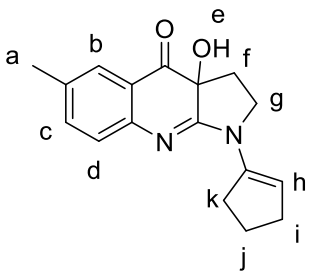
(±)-1-(Cyclohex-1-en-1-yl)-3a-hydroxy-6-methyl-1,2,3,3a-tetrahydro-4*H*-pyrrolo[2,3-*b*]quinolin-4-one - 121



Following the procedure described for the preparation of hydroxyl-amidine **118**, the title compound was prepared from cyclohexene amidine **119** (15 mg, 0.033 mmol) with TBAF (1 M in THF, 100 µL) in THF (0.5 mL). Purification was carried out by flash column chromatography (25 – 30 % EtOAc in pentane) to yield hydroxyl-amidine **121** as a yellow solid (8 mg, 80 %) with purity of ≥95 % by LC-MS analysis.

^{1}H NMR (400 MHz, $CDCl_3$) δ 7.58 (d, *J* = 1.6 Hz, 1H, CH-*b*), 7.18 (dd, *J* = 8.1, 1.6 Hz, 1H, CH-*c*), 6.98 (d, *J* = 8.1 Hz, 1H, CH-*d*), 5.62 – 5.56 (m, 1H, CH-*h*), 3.93 (td, *J* = 9.8, 5.7 Hz, 1H, CH-*g*), 3.55 (dd, *J* = 9.8, 8.6 Hz, 1H, CH-*g*), 2.73 – 2.61 (m, 1H, CH-*l*), 2.36 (dd, *J* = 13.5, 5.7 Hz, 1H, CH-*f*), 2.28 (s, 3H, CH_3-*a*), 2.24 – 2.05 (m, 4H, CH-*l* + CH-*f*+ CH_2-*i*), 1.79 – 1.65 (m, 1H, CH-*k*), 1.65 – 1.46 (m, 3H, CH-*k* + CH_2-*j*); **^{13}C NMR** (101 MHz, $CDCl_3$) δ 194.8, 165.2, 149.4, 137.3, 137.1, 132.5, 127.4, 125.8, 120.3, 117.6, 73.8, 48.8, 29.6, 26.9, 24.6, 22.8, 21.9, 20.70; **HRMS (ES+)** Calculated for $C_{18}H_{21}N_2O_2$ ($M+H^+$): 297.1603; found: 297.1608.

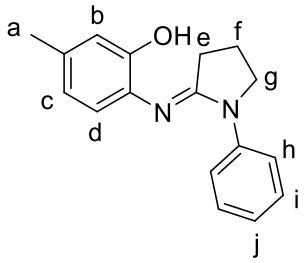
(±)-1-(Cyclopent-1-en-1-yl)-3a-hydroxy-6-methyl-1,2,3,3a-tetrahydro-4*H*-pyrrolo[2,3-*b*]quinolin-4-one - 122



Following the procedure described for the preparation of hydroxyl-amidine **118**, the title compound was prepared from cyclopentene amidine **120** (7 mg, 0.02 mmol) with TBAF (1 M in THF, 50 µL) in THF (300 µL). Purification was carried out by flash column chromatography (20 % EtOAc in pentane) to yield hydroxyl-amidine **122** as a yellow solid (3 mg, 76 %) with purity of ≥95 % by LC-MS analysis.

IR Vmax / cm^{-1}: 2927, 2851, 1698, 1634, 1606, 1482, 1296; **^{1}H NMR** (400 MHz, $CDCl_3$) δ 7.61 (dd, *J* = 1.6, 0.5 Hz, 1H, CH-*b*), 7.29 – 7.24 (m, 1H, CH-*c* overlapping with $CDCl_3$), 7.09 (d, *J* = 8.1 Hz, 1H, CH-*d*), 5.80 – 5.76 (m, 1H, CH-*h*), 3.94 (td, *J* = 10.0, 5.9 Hz, 1H, CH-*g*), 3.75 – 3.67 (m, 1H, CH-*g*), 2.98 – 2.78 (m, 2H, CH_2-*k*), 2.48 – 2.32 (m, 3H, CH_2-*l* + CH-*f*), 2.31 (s, 3H, CH_3-*a*), 2.20 (ddd, *J* = 13.8, 9.9, 8.7 Hz, 1H, CH-*f*), 1.98 – 1.85 (m, 2H, CH_2-*j*); **^{13}C NMR** (101 MHz, $CDCl_3$) δ 194.7, 164.2, 149.3, 140.3, 137.5, 133.3, 127.4, 126.4, 120.3, 113.3, 73.5, 48.1, 33.0, 30.5, 29.1, 22.3, 20.8; **HRMS (ES+)** Calculated for $C_{17}H_{19}N_2O_2$ ($M+H^+$): 283.1447; found: 283.1448.

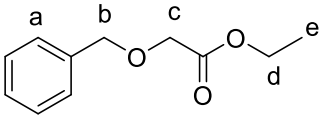
5-Methyl-2-((1-phenylpyrrolidin-2-ylidene)amino)phenol - 92



Following the procedure described for the preparation of amidine **108**, the title compound was prepared from 1-phenylpyrrolidin-2-one (200 mg, 1.2 mmol) and 2-amino-5-methylphenol (130 mg, 1.0 mmol) with $POCl_3$ (120 µL, 1.2 mmol), in DCM (3 mL). Purification was carried out by flash column chromatography (20 % EtOAc in pentane with 1 % NEt_3) to yield amidine **92** as a colourless oil (30 mg, 11 %) with purity of ≥95 % by LC-MS analysis.

IR Vmax / cm^{-1}: 3421, 3344, 3055, 2925, 2871, 1604, 1576, 1509, 1480, 1318, 1261, 1115, 817, 744, 690; **^{1}H NMR** (400 MHz, $CDCl_3$) δ 7.54 (d, *J* = 8.1 Hz, 1H, CH-*d*), 7.30 – 7.27 (m, 1H, CH-*b*), 7.20 – 7.10 (m, 3H, CH-*c* + 2 x CH-*i*), 6.70 (tt, *J* = 7.4, 1.0 Hz, 1H, CH-*j*), 6.63 – 6.59 (m, 2H, 2 x CH-*h*), 3.29 (t, *J* = 6.8 Hz, 2H, CH_2-*g*), 3.04 (t, *J* = 7.3 Hz, 2H, CH_2-*e*), 2.48 (s, 3H, CH_3-*a*), 2.20 (p, *J* = 7.1 Hz, 2H, CH_2-*f*); **^{13}C NMR** (101 MHz, $CDCl_3$) δ 166.1, 151.2, 148.2, 139.2, 135.1, 129.4 (2C), 125.5, 119.0, 117.6, 112.9 (2C), 110.7, 43.2, 26.5, 26.3, 21.8; **HRMS (ES+)** Calculated for $C_{17}H_{19}N_2O$ ($M+H^+$): 267.1497; found: 267.1494.

Propyl 2-(benzyloxy)acetate - 125

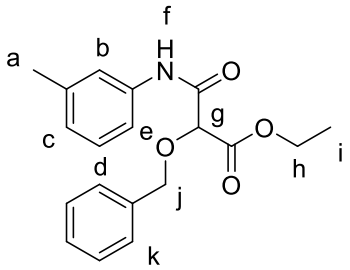


Synthesis according to Sadhukhan *et al.*[255] NaH (60% oil dispersion, 260 mg, 6.6 mmol) was suspended in dry THF (8 mL) under N_2. A solution of benzyl alcohol (620 µL, 6.0 mmol) in

dry THF (2 mL) was added dropwise at the reaction was stirred at rt for 2 h. Ethyl bromoacetate (660 µL, 6.0 mmol) was added dropwise at 0 °C and the reaction was slowly warmed to rt and stirred at this temperature for 16 h. The reaction mixture was poured into ice water (50 mL), neutralised with HCl (1 M) and the aqueous phase was extracted with EtOAc (3 x 50 mL). The combined organic phases were washed with brine (100 mL), dried over Na_2SO_4, filtered and concentrated under rotary evaporation. The crude product was purified by flash column chromatography (10 % EtOAc in pentane) to yield ester **125** as a colourless oil (691 mg, 60 %).

^{1}H NMR (400 MHz, $CDCl_3$) δ 7.41 – 7.27 (m, 5H, 5 x CH-*a*), 4.63 (s, 2H, CH_2-*b*), 4.23 (q, *J* = 7.1 Hz, 2H, CH_2-*d*), 4.09 (s, 2H, CH_2-*c*), 1.28 (t, *J* = 7.1 Hz, 3H, CH_3-*e*); **^{13}C NMR** (101 MHz, $CDCl_3$) δ 170.5, 137.2, 128.6 (2C), 128.2 (2C), 128.1, 73.4, 67.3, 61.0, 14.3; **HRMS (ES+)** Calculated for $C_{11}H_{15}O_3$ ($M+H^+$): 195.1021; found: 195.1026. These spectroscopic data correspond to previously reported data.[255,256]

(±)-Ethyl 2-(benzyloxy)-3-oxo-3-(*m*-tolylamino)propanoate – 126

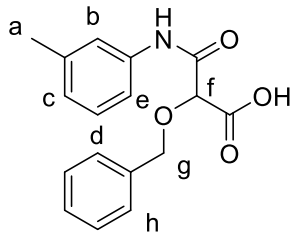


To a solution of diisopropylamine (440 µL, 3.16 mmol) in dry THF (2.5 mL) was added *n*-BuLi (2.5 M in hexanes, 1.35 mL) dropwise at -78 °C under N_2. The solution was stirred at 0 °C for 20 min before the dropwise addition of a solution of ester **125** (691 mg, 2.12 mmol) in dry THF (5 mL) at -78 °C. The reaction was stirred for 30 min at this temperature followed by the addition of a solution of *m*-tolyl *iso*cyanate (330 µL, 2.54 mmol) in dry THF (2.5 mL). The reaction was stirred at -78 °C for 2 h and then the reaction mixture was quenched with saturated aq. NH_4Cl at 0 °C. The aqueous phase was extracted with DCM (20 mL x 3). The

combined organic phases were combined, dried over Na_2SO_4 and purified by flash column chromatography (30 % EtOAc in pentane) giving amide **126** as an off-white solid (333 mg, 40 %).

^{1}H NMR (400 MHz, $CDCl_3$) δ 8.32 (s, 1H, NH-*f*), 7.44 – 7.34 (m, 6H, 5 x CH-*k* + CH-*b*), 7.31 (d, *J* = 8.0 Hz, 1H, CH-*e*), 7.20 (t, *J* = 7.8 Hz, 1H, CH-*d*), 6.94 (d, *J* = 7.5 Hz, 1H, CH-*c*), 4.79 (d, *J* = 11.5 Hz, 1H, CH-*j*), 4.63 (d, *J* = 11.5 Hz, 1H, CH-*j*), 4.56 (s, 1H, CH-*g*), 4.27 (q, *J* = 7.1 Hz, 2H, CH_2-*h*), 2.32 (s, 3H, CH_3-*a*), 1.31 (t, *J* = 7.1 Hz, 3H, CH_3-*i*); **^{13}C NMR** (101 MHz, $CDCl_3$) δ 167.5, 163.5, 139.1, 136.8, 135.7, 129.0, 128.9 (2C), 128.9, 128.7 (2C), 125.8, 120.6, 117.1, 79.3, 73.2, 62.4, 21.6, 14.2.

(±)-2-(Benzyloxy)-3-oxo-3-(*m*-tolylamino)propanoic acid – 127



To a solution of amide **126** (333 mg, 1.11 mmol) in MeOH (10 mL) was added NaOH (1 M, 2.2 mL) and the reaction was stirred at rt for 2 h. The solvent was removed under rotary evaporation then H_2O (10 mL) was added and the solution was acidified to pH 3 (1 M HCl). The aqueous phase was extracted using EtOAc (3 x 20 mL) and the combined organic phases were washed with brine (30 mL) and dried over Na_2SO_4. After filtration the solvent was removed by rotary evaporation to obtain the carboxylic acid **127** as a white solid (229 mg, 69 %).

^{1}H NMR (400 MHz, MeOD) δ 7.49 – 7.43 (m, 2H, CH-*b* + CH-*e*), 7.43 – 7.31 (m, 5H, 5 x CH-*h*), 7.21 (t, *J* = 7.8 Hz, 1H, CH-*d*), 6.98 (d, *J* = 7.5 Hz, 1H, CH-*c*), 4.75 (dd, *J* = 27.5, 11.7 Hz, 2H, CH_2-*g*), 4.62 (s, 1H, CH-*f*), 2.34 (s, 3H, CH_3-*a*); **^{13}C NMR** (101 MHz, MeOD) δ 170.6,

167.0, 139.9, 138.6, 137.9, 129.7, 129.6 (4C), 129.4, 126.6, 122.3, 118.8, 80.5, 73.7, 21.5; **HRMS (ES+)** Calculated for $C_{17}H_{18}NO_4$ ($M+H^+$): 300.1236; found: 300.1234.

7.3. Synthetic Procedures: Part 2

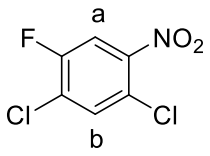
General Procedure A: S_NAr in MeCN

Based on reported procedure by Sanchez *et al.*[233] To a suspension/solution of boron difluoride chelate (1.0 equiv.) in MeCN (0.04 M) was added an amine (2.4 equiv.) and the reaction was heated at 50 °C for 18 h. The reaction was cooled to rt, concentrated under rotary evaporation and then EtOH (0.017 M) was added to the resulting residue, followed by NEt_3 (0.17 M). The suspension/solution was stirred at reflux for 18 h, cooled to rt and concentrated under rotary evaporation. The solid was suspended in H_2O (0.006 M) and basified to pH 13 (1 M NaOH) before removal of the resultant precipitate. The pH of the filtrate was adjusted to pH 4 (1 M HCl) and the resulting precipitate was filtered, washing with H_2O. The solid was dissolved in DCM, dried over Na_2SO_4 and concentrated under rotary evaporation.

General Procedure B: S_NAr in Pyridine

To a suspension/solution of boron difluoride chelate (1.0 equiv.) in pyridine (0.05 M) was added an amine (2.4 equiv.) and the reaction was stirred at rt for 18 h. The reaction was concentrated under rotary evaporation and the solid was dissolved in DCM and washed with an equal quantity of H_2O (x 3). The organic phase was dried over Na_2SO_4, concentrated under rotary evaporation and then EtOH (0.017 M) was added to the resulting residue, followed by NEt_3 (0.17 M). The suspension/solution was stirred at reflux for 18 h and then cooled and concentrated under rotary evaporation. The solid was suspended in H_2O (0.006 M) and basified to pH 13 (1 M NaOH) before filtration of insoluble impurities. The pH of the filtrate was adjusted to pH 4 (1 M HCl) and the resulting precipitate was filtered, washing with H_2O. The solid was dissolved in DCM, dried over Na_2SO_4 and concentrated under rotary evaporation.

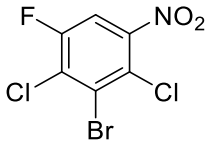
1,5-Dichloro-2-fluoro-4-nitrobenzene - 136



Synthesis according to Wang *et al.*[226] To a solution of conc. H_2SO_4 (5.6 mL, 0.11 mol) and water (1 mL) was added conc. HNO_3 (3.5 mL, 0.085 mol) drop wise at 0 °C followed by the drop wise addition of 2,4-dichlorofluorobenzene (3.5 mL, 0.030 mol). The reaction was heated to 55 °C for 6 h and was then poured into ice water (60 mL). The aqueous phase was extracted using DCM (3 x 40 mL). The combined organic phases were dried over $MgSO_4$, filtered and the solvent was evaporated under reduced pressure before purification by column chromatography (2 % EtOAc in pentane) to yield nitrobenzene **136** as a yellow liquid (4.0 g, 63 %).

^{1}H NMR (400 MHz, $CDCl_3$) δ 7.79 (d, *J* = 7.9 Hz, 1H, CH-*a*), 7.66 (d, *J* = 6.5 Hz, 1H, CH-*b*); **^{13}C NMR** (101 MHz, $CDCl_3$) δ 156.29 (d, J_{CF}= 255.1 Hz), 133.5, 127.4, 127.2, 123.6 (d, J_{CF} = 4.8 Hz), 114.5 (d, J_{CF} = 26.9 Hz); **MS (EI+)** *m/z* 210 ($M+H^+$). These spectroscopic data correspond to previously reported data.[226]

3-Bromo-2,4-dichloro-1-fluoro-5-nitrobenzene - 137

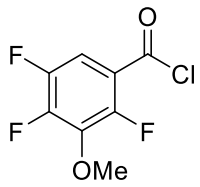


Based on reported procedure by Derbyshire *et al.*[229] To a solution of nitrobenzene **136** (1.0 g, 4.8 mmol) in conc. H_2SO_4 (9 mL) and water (1 mL) was added bromine (0.30 mL, 5.7 mmol) followed by silver sulfate (1.5 g, 4.8 mmol) and the reaction was heated at reflux for 48 h until the red colour had disappeared and silver bromide precipitate had formed. The

reaction was poured into ice water (50 mL) and any remaining bromine was quenched with $Na_2S_2O_3$ (5 mL). The aqueous phase was then extracted with Et_2O (3 x 30 mL) and the combined organic phases were washed with H_2O (2 x 50 mL) and brine (50 mL) then dried over $MgSO_4$ before filtration and evaporation of the solvent. This furnished bromobenzene **137** as a yellow solid (0.85 g, 62 %).

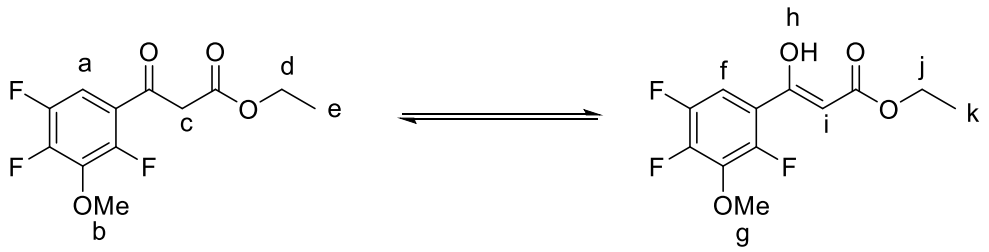
^{1}H NMR (400 MHz, $CDCl_3$) δ 7.68 (d, *J* = 7.5 Hz, 1H); **^{13}C NMR** (101 MHz, $CDCl_3$) δ 156.4 (d, J_{CF} = 256.5 Hz), 133.5, 129.3 (d, J_{CF} = 19.0 Hz), 128.5, 124.9 (d, J_{CF} = 5.0 Hz), 112.2 (d, J_{CF} = 27.6 Hz); **MS (EI+)** *m/z* 290 ($M+H^+$). These spectroscopic data correspond to previously reported data.[229]

2,4,5-Trifluoro-3-methoxybenzoyl chloride - 140



Synthesis according to Sanchez *et al*.[233] To a solution of 3-methoxy-2,4,5-trifluorobenzoic acid (1.0 g, 4.8 mmol) in dry DCM (15 mL) was added DMF (0.1 mL) and the solution was cooled to 0 °C before the drop wise addition of oxalyl chloride (0.51 mL, 6.1 mmol) and the reaction was then stirred at rt for 18 h and concentrated under rotary evaporation. Residual DMF and oxalyl chloride was removed by azeotroping with PhMe (x 3). The material was used without further purification.

Ethyl 3-oxo-3-(2,4,5-trifluoro-3-methoxyphenyl)propanoate - 141

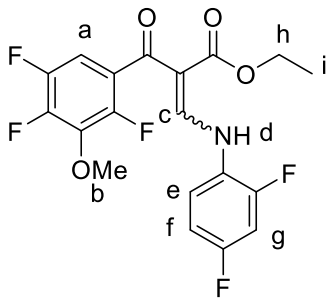


Synthesis according to Sanchez *et al*.[233] To a solution of monoethyl malonate (1.15 mL, 9.74 mmol) in dry THF (30 mL) was added 2,2'-bipyridyl (1 mg, 5 µmol) and the solution was cooled to −20 °C before the drop wise addition of *n*-BuLi (2.5 M in hexanes, 9.70 mL) over 1 h until a persistent pink colour was observed at −5 °C. The reaction was cooled to −78 °C and acyl chloride **140** (1.09 g, 4.85 mmol) in dry THF (20 mL) was added over 30 min. After completed addition the reaction was stirred at −30 °C for 2 h. The mixture was poured into HCl (12 M, 40 mL) and the aqueous phase was extracted with EtOAc (3 x 50 mL) and the combined organic phases were washed with H_2O (2 x 50 ml), dried over $MgSO_4$, filtered and the solvent was evaporated. The residue was purified by column chromatography (10 % EtOAc in pentane) to yield ketoester **141** as a light yellow solid (0.94 g, 70 %). The product existed as a 1.18:1 mixture of its keto-enol tautomers respectively.

^{1}H NMR (400 MHz, $CDCl_3$) δ 12.70 (s, 1H, OH-*h*), 7.54–7.34 (overlapping m, 2H, CH-*a* + *f*), 5.81 (s, 1H CH-*i*), 4.25 (overlapping q, 4H, CH-*d* + *j*), 4.06 (t, *J* = 1.0 Hz, 3H, CH-*b*), 4.04 (t, *J* = 1.0 Hz, 3H, CH-*g*) 3.95 (d, *J* = 3.9 Hz, 2H, CH-*c*), 1.34 (t, *J* = 7.1 Hz, 3H, CH-*k*), 1.27 (t, *J* = 7.1 Hz, 3H, CH-*e*); **^{13}C NMR** (126 MHz, $CDCl_3$) δ 188.1, 173.3, 167.1 (d, J_{CF} = 1.6 Hz), 164.2, 152.4 (d, J_{CF} = 253.3 Hz), 150.7 (d, J_{CF} = 253.9 Hz), 148.3 (ddd, J_{CF} = 259.8, 15.4, 5.3 Hz), 147.8 (ddd, J_{CF} = 248.7, 11.5, 2.3 Hz), 147.3 (ddd, J_{CF} = 246.2, 11.3, 3.2 Hz), 145.8 (ddd, J_{CF} = 255.7, 15.1, 5.0 Hz), 138.5 (dd, J_{CF} = 16.6, 11.5 Hz), 120.7 – 120.0 (m), 118.0 – 117.6 (m), 110.7 (dd, J_{CF} = 20.6, 1.9 Hz), 109.5 (dd, J_{CF} = 20.9, 1.6 Hz), 93.4 (d, J_{CF} = 15.2 Hz), 62.5, 61.7, 60.9, 49.8 (d, J_{CF} = 7.9 Hz), 14.4, 14.2; **^{19}F NMR** (377 MHz, $CDCl_3$) δ -129.8 (s, 1F), -130.8 – -131.0 (m, 1F), -138.1 – -138.5 (m, 1F), -139.8 (dt, *J* = 21.5, 12.5 Hz, 1F), -

141.1 – -141.6 (m, 1F), -146.2 – -146.5 (m, 1F); **HRMS (ES+)** Calculated for $C_{12}H_{12}F_3O_4$ ($M+H^+$): 277.0688; found: 277.0700. These spectroscopic data correspond to previously reported data.[233]

Ethyl 3-(2,4-difluorophenylamino)-2-(2,4,5-trifluoro-3-methoxybenzoyl)acrylate – *E*/*Z* mixture - 142

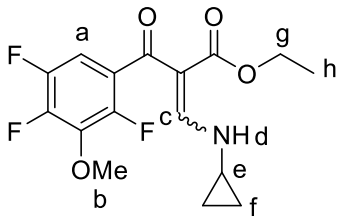


Based on reported procedure by Sanchez *et al.*[233] To a solution of ketoester **141** (0.77 g, 2.8 mmol) in Ac_2O (20 mL) was added triethyl orthoformate (0.70 mL, 4.2 mmol) and the reaction was stirred at reflux for 6 h. The reaction mixture was concentrated under rotary evaporation and dried further by the azeotropic removal of volatiles with PhMe (x 3) The resulting residue was dissolved in EtOH (30 mL). The solution was cooled to 0 ºC before the drop-wise addition of 2,4-difluoroaniline. During the addition a precipitate formed and the reaction was stirred at rt for further 2 h. The precipitate was filtered, washed with EtOH (30 mL) and concentrated under rotary evaporation to yield enamine **142** as a light yellow solid (0.78 g). The filtrate was concentrated under rotary evaporation and purified by column chromatography (10 % EtOAc in pentane) to yield enamine **142** as an orange solid (0.28 g) and this combined was an inseperable mixture of 2:1 *E* and *Z* isomers respectively (1.06 g, 90 %).

Mp ($CHCl_3$) 103–105 °C; **IR V_{max} / cm^{-1}**: 3080, 2987, 1707, 1627, 1470, 1416, 1253, 1099, 855, 802; **^{1}H NMR** (400 MHz, $CDCl_3$) δ 12.47 (d, *J* = 13.1 Hz, 1H, NH-*d* (*E*)), 11.13 (d, *J* = 13.8 Hz, 1H, NH-*d* (*Z*)), 8.50 (d, *J* = 13.1 Hz, 1H, CH-*c* (*E*)), 8.39 (d, *J* = 13.8 Hz, 1H, CH-*c* (*Z*)), 7.43–7.30 (overlapping m, 2H, CH-*g* (*E* + *Z*)), 7.10 (ddd, *J* = 9.8, 8.3, 5.9 Hz, 1H, CH-*a*

(*Z*)), 7.04–6.92 (m, 5H, CH-*a* (*E*) + CH-*e* + CH-*f* (*E* + *Z*)), 4.17–4.07 (overlapping q, 4H, CH-*h* (*E* + *Z*)), 4.02 (s, 6H, CH-*b* (*E* + *Z*)), 1.12 (t, *J* = 7.1 Hz, 3H, CH-*i* (*E*)), 1.03 (t, *J* = 7.1 Hz, 3H, CH-*i* (*Z*)); **^{13}C NMR** (126 MHz, $CDCl_3$) δ 189.2, 186.6, 168.1, 166.3, 161.0, 160.3 (dd, J_{CF} = 249.2, 11.0 Hz), 153.5 (dd, J_{CF} = 250.9, 12.2 Hz), 152.6, 151.6, 148.8 (d, J_{CF} = 246.9 Hz), 147.2 (ddd, J_{CF} = 246.5, 11.4, 2.5 Hz), 145.6 (ddd, J_{CF} = 253.6, 15.1, 5.2 Hz), 137.7 – 137.1 (m), 126.4 – 125.8 (m), 124.0 (dd, J_{CF} = 11.0, 3.8 Hz), 118.8 (d, J_{CF} = 9.3 Hz), 118.0 (d, J_{CF} = 10.1 Hz), 112.5 (dd, J_{CF} = 22.9, 3.5 Hz), 110.2 (dd, J_{CF} = 20.2, 3.4 Hz), 109.4 (dd, J_{CF} = 20.6, 3.8 Hz), 106.0 – 105.1 (m), 105.0, 62.2 (t, J_{CF} = 3.0 Hz), 60.6, 14.1; **^{19}F NMR** (377 MHz, $CDCl_3$) δ -111.9 (d, *J* = 4.7 Hz, 1F), -113.0 (d, *J* = 4.7 Hz, 0.5F), -124.0 (d, *J* = 4.7 Hz, 1F), -125.2 (d, *J* = 4.7 Hz, 0.5F), -133.5 (dd, *J* = 12.6, 7.5 Hz, 0.5F), -134.3 (dd, *J* = 12.6, 7.5 Hz, 1F), -140.5 (td, *J* = 20.6, 13.2 Hz, 1.5F), -147.7 (dd, *J* = 20.6, 7.5 Hz, 0.5F), -148.6 (dd, *J* = 20.6, 7.5 Hz, 1F); **HRMS (ES+)** Calculated for $C_{19}H_{15}F_5NO_4$ ($M+H^+$): 416.0921; found: 416.0924. These spectroscopic data correspond to previously reported data.[257]

Ethyl 2-(3-Methoxy-2,4,5-trifluorobenzoyl)-3-(cyclopropylamino)acrylate – *E*/*Z* mixture - 143

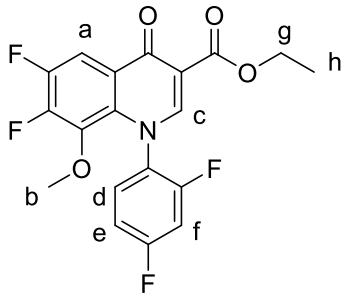


Synthesis according to Sanchez *et al*.[233] To a solution of ketoester **141** (0.20 g, 0.72 mmol) in Ac_2O (5 mL) was added triethylorthoformate (0.18 mL, 1.1 mmol) and the reaction was stirred at reflux for 18 h. The reaction mixture was concentrated under rotary evaporation and dried further by the azeotropic removal of volatiles with PhMe (x 3) and the resulting residue was dissolved in EtOH (5 mL). The solution was cooled at 0 °C before the drop-wise addition of freshly distilled cyclopropylamine (75 µL, 1.1 mmol) and the reaction was warmed to rt and stirred for 18 h. The reaction was diluted with H_2O (15 mL) and the aqueous phase

was extracted with EtOAc (10 mL x 3). The combined organic phases were then dried over $MgSO_4$, filtered and concentrated under rotary evaporation and the resulting residue was purified by column chromatography (20 % EtOAc in pentane) to yield enamine **143** as a white solid and an inseperable mixture of 2.7:1 *E* and *Z* isomers respectively (0.164 g, 66 %).

^{1}H NMR (400 MHz, $CDCl_3$) δ 10.87 (d, *J* = 11.6 Hz, 1H, NH-*d* (*E*)), 9.45 (d, *J* = 12.9 Hz, 1H, NH-*d* (*Z*)), 8.20 (overlapping d, 2H, CH-*c* (*E* +*Z*)), 6.99 (ddd, *J* = 9.9, 8.4, 5.8 Hz, 1H, CH-*a* (*Z*)), 6.85 (ddd, *J* = 9.7, 8.2, 5.7 Hz, 1H, CH-*a* (*Z*)), 4.09 – 3.96 (m, 10H, CH-*b* + CH-*g* (*E* + *Z*)), 3.07–2.85 (m, 2H, CH-*e* (*E* + *Z*)), 1.08 (t, *J* = 7.1 Hz, 3H, CH-*h* (*E*)), 0.98–0.78 (m, 7H, CH-*f* (*E* + *Z*)+ CH-*h* (*Z*)); **^{13}C NMR** (126 MHz, $CDCl_3$) δ 188.3, 186.2, 168.6, 166.7, 161.0, 160.7, 148.34 (d, J_{CF} = 246.2 Hz), 147.2 (ddd, J_{CF} = 245.9, 11.3, 3.1 Hz), 145.1 (ddd, J_{CF} = 252.3, 15.2, 5.7 Hz), 137.6 – 137.0 (m), 127.3 – 126.7 (m), 109.89 (dd, J_{CF} = 20.2, 3.7 Hz), 109.0 (dd, J_{CF} = 20.4, 4.1 Hz), 101.8, 62.2, 60.0, 59.7, 30.6, 30.3, 29.8, 14.1, 13.8, 6.7; **^{19}F NMR** (377 MHz, $CDCl_3$) δ -135.5 (dd, *J* = 12.9, 6.4 Hz, 1F), -141.1 (dd, *J* = 20.5, 12.9 Hz, 1F), -150.3 (dd, *J* = 20.5, 6.4 Hz, 1F); **HRMS (ES+)** Calculated for $C_{16}H_{17}F_3NO_4$ ($M+H^+$): 344.1110; found: 344.1121. These spectroscopic data correspond to previously reported data.[257]

Ethyl 1-(2,4-difluorophenyl)-6,7-difluoro-8-methoxy-4-oxo-1,4-dihydroquinoline-3-carboxylate - 144

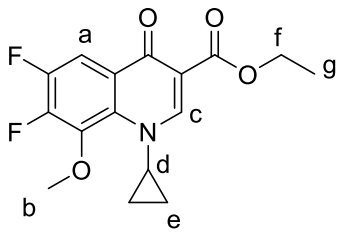


Based on reported procedure by Sanchez *et al.*[233] To a solution of enamine **142** (2.6 g, 6.3 mmol) in MeCN (60 mL) was added K_2CO_3 (0.81 g, 6.3 mmol) and the reaction was stirred at

reflux under N_2 for 16 h. The reaction was cooled to rt and concentrated under rotary evaporation. The resulting residue was dissolved in DCM (50 mL) and washed with H_2O (100 mL x 3). The organic phase was dried over $MgSO_4$, filtered and concentrated under rotary evaporation to yield quinolone **144** as an orange solid (2.14 g, 85%).

Mp ($CHCl_3$) 190-192 °C; **IR V_{max} / cm^{-1}**: 3060, 1730, 1694, 1647. **^{1}H NMR** (400 MHz, $CDCl_3$) δ 8.23 (s, 1H, CH-*c*), 8.06 (dd, *J* = 10.2, 8.6 Hz, 1H, CH-*a*), 7.58 (td, *J* = 8.6, 5.6 Hz, 1H, CH-*f*), 7.12–6.98 (m, 2H, CH-*d* + CH-*e*), 4.41 (q, *J* = 7.1 Hz, 2H, CH-*g*), 3.48 (d, *J* = 1.7 Hz, 3H, CH-*b*), 1.38 (t, *J* = 7.1 Hz, 3H, CH-*d*); **^{13}C NMR** (126 MHz, $CDCl_3$) δ 172.5, 164.9, 162.9 (dd, J_{CF} = 253.5, 10.9 Hz), 157.8 (dd, J_{CF} = 254.3, 12.5 Hz), 151.3, 149.4 (dd, J_{CF} = 252.6, 12.0 Hz), 148.1 (dd, J_{CF} = 255.1, 15.5 Hz), 139.2 (d, J_{CF} = 12.1 Hz), 131.0, 128.8 (dd, J_{CF} = 13.6, 4.3 Hz), 128.6 (d, J_{CF} = 10.0 Hz), 125.4 (d, J_{CF} = 5.3 Hz), 112.1 (dd, J_{CF} = 22.7, 3.5 Hz), 111.5, 109.0 (d, J_{CF} = 19.0 Hz), 105.0 (dd, J_{CF} = 26.4, 23.1 Hz), 62.1 (d, J_{CF} = 6.7 Hz), 61.5, 14.5; **^{19}F NMR** (377 MHz, $CDCl_3$) δ -105.9 (d, *J* = 7.9 Hz, 1F), -116.6 (d, *J* = 7.9 Hz, 1F), -135.8 (d, *J* = 21.4 Hz, 1F), -144.3 (d, *J* = 21.4 Hz, 1F); **HRMS (ES+)** Calculated for $C_{19}H_{14}F_4NO_4$ ($M+H^+$): 396.0859; found: 396.0848. These spectroscopic data correspond to previously reported data.[257]

Ethyl 1-Cyclopropyl-6,7-difluoro-1,4-dihydro-8-methoxy-4-oxo-3-quinolinecarboxylate - 145

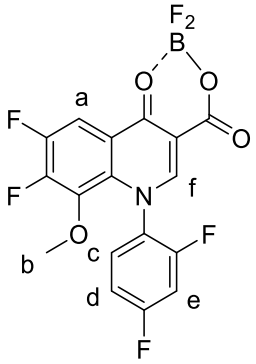


Synthesis according to Sanchez *et al*.[233] To a solution of enamine **143** (110 mg, 0.31 mmol) in MeCN (3 mL) was added K_2CO_3 (41 mg, 0.32 mmol) and the reaction was stirred at reflux under N_2 for 16 h. Reaction cooled to rt and concentrated under rotary evaporation and the

resulting residue was dissolved in DCM (15 mL) and washed with H_2O (20 mL x 3). The organic phase was dried over $MgSO_4$, filtered and concentrated under rotary evaporation to yield quinolone **145** as a white solid (90 mg, 88%).

^{1}H NMR (400 MHz, $CDCl_3$) δ 8.60 (s, 1H, CH-*c*), 8.04 (dd, *J* = 10.2, 8.6 Hz, 1H, CH-*a*), 4.38 (q, *J* = 7.1 Hz, 2H, CH-*f*), 4.08 (d, *J* = 2.1 Hz, 3H, CH-*b*), 4.04–3.94 (m, 1H, CH-*d*), 1.40 (t, *J* = 7.1 Hz, 3H, CH-*g*), 1.27 –1.15 (m, 2H, CH-*e*), 1.09–1.00 (m, 2H, CH-*e*); **^{13}C NMR** (126 MHz, $CDCl_3$) δ 172.5, 165.5, 150.9, 149.3 (dd, J_{CF} = 251.6, 12.5 Hz), 148.3 (dd, J_{CF} = 253.9, 15.6 Hz), 140.4 (d, J_{CF} = 11.1 Hz), 131.7 (d, J_{CF} = 2.8 Hz), 126.2 (d, J_{CF} = 6.0 Hz), 110.3, 108.9 (d, J_{CF} = 18.8 Hz), 63.0 (d, J_{CF} = 7.6 Hz), 61.2, 39.8, 14.6, 9.2 (2C); **^{19}F NMR** (377 MHz, $CDCl_3$) δ -136.3 (d, *J* = 21.5 Hz, 1F), -144.6 (d, *J* = 21.6 Hz, 1F); **HRMS (ES+)** Calculated for $C_{16}H_{16}F_2NO_4$ ($M+H^+$): 324.1047; found: 324.1052. These spectroscopic data correspond to previously reported data.[257]

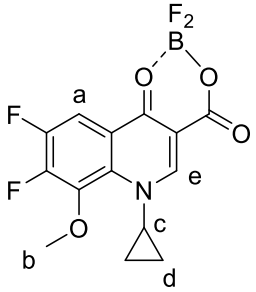
1-(2,4-Dimethylphenyl)-6,7-difluoro-4-oxo-1,4-dihydroquinoline-3-carboxylic acid-boron difluoride chelate - 146



Based on reported procedure by Sanchez *et al.*[233] To a solution of quinolone **144** (0.35 g, 0.89 mmol) in dry THF (10 mL) was added boron trifluoride etherate (3 mL) and the mixture was heated at reflux under N_2 for 16 h. The reaction was allowed to cool to rt followed by the addition of Et_2O (10 mL). The resulting precipitate was filtered, washed with Et_2O (20 mL) and dried to yield boron difluoride chelate **146** as a white solid (0.266 g, 72 %).

IR V_{max} / cm^{-1}: 3065, 1712, 1477, 1026, 931, 854; **^{1}H NMR** (400 MHz, DMSO) δ 9.43 (s, 1H, CH-*f*), 8.45 (dd, *J* = 9.7, 8.1 Hz, 1H, CH-*a*), 7.96 (td, *J* = 8.8, 5.8 Hz, 1H, CH-*c*), 7.68 (ddd, *J* = 10.5, 9.1, 2.7 Hz, CH-*d*), 7.46–7.30 (m, 1H, CH-*e*), 3.49 (d, *J* = 1.2 Hz, 3H, CH-*b*); **^{13}C NMR** (126 MHz, DMSO) δ 214.1 (d, J_{CF} = 1.9 Hz), 208.2, 202.4, 200.6 (dd, J_{CF} = 249.9, 11.5 Hz), 196.6, 194.1 (dd, J_{CF} = 252.5, 13.7 Hz), 192.3, 190.0, 188.3 (dd, J_{CF} = 255.7, 12.5 Hz), 187.2 (dd, J_{CF} = 259.0, 15.4 Hz), 177.7 (d, J_{CF} = 12.2 Hz), 170.8 (d, J_{CF} = 4.1 Hz), 166.8 (d, J_{CF} = 10.6 Hz), 165.3 (dd, J_{CF} = 13.7, 3.7 Hz), 156.5 (d, J_{CF} = 9.1 Hz), 149.7 (dd, J_{CF} = 23.2, 2.6 Hz), 145.1, 144.5 (d, J_{CF} = 19.7 Hz), 142.4 (dd, J_{CF} = 27.7, 23.1 Hz), 100.5 (d, J_{CF} = 6.0 Hz), 63.73; **^{19}F NMR** (377 MHz, DMSO) δ -106.1 (qd, *J* = 8.7, 5.7 Hz, 1F), -117.4 (q, *J* = 9.2 Hz, 1F), -129.1 (dd, *J* = 22.5, 9.6 Hz, 1F), -136.5 (dd, *J* = 22.5, 7.7 Hz, 1F), -139.7 (dd, *J* = 71.6, 23.8 Hz, 1F), -140.8 (dd, *J* = 71.6, 23.8 Hz, 1F); **HRMS (ES+)** Calculated for $C_{17}H_{12}BF_6N_2O_4$ ($M+NH_4^+$): 433.0794; found: 433.0819. These spectroscopic data correspond to previously reported data.[257]

1-Cyclopropyl-6,7-difluoro-1,4-dihydro-8-methoxy-4-oxo-3-quinolinecarboxylic acid-boron difluoride chelate - 147

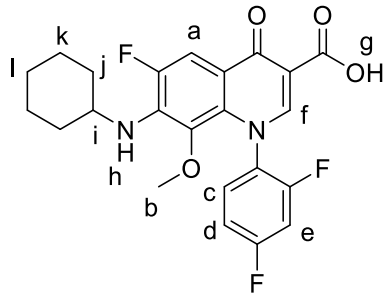


Reaction carried out in the same manner described for boron difluoride chelate **146** with quinolone **145** (110 mg, 0.34 mmol) in dry THF (3 mL) and boron trifluoride etherate (1 mL). The reaction yielded boron difluoride chelate **147** as a white solid, (76 mg, 65 %).

^{1}H NMR (400 MHz, CD_3CN) δ 9.18 (s, 1H, CH-*e*), 8.18 (dd, *J* = 9.7, 8.1 Hz, 1H, CH-*a*), 4.55–4.43 (m, 1H, CH-*c*), 4.18 (d, *J* = 2.4 Hz, 3H, CH-*b*), 1.41–1.29 (m, 2H, CH-*d*), 1.29–1.18 (m, 2H, CH-*d*); **^{13}C NMR** (101 MHz, DMSO) δ 168.9, 159.2, 152.4, 150.4 (dd, J_{CF} = 254.9, 12.9

Hz), 149.5 (dd, J_{CF} = 257.2, 15.4 Hz), 141.7 (d, J_{CF} = 11.7 Hz), 134.2 (d, J_{CF} = 4.2 Hz), 119.2 (d, J_{CF} = 9.4 Hz), 106.4, 106.0 (d, J_{CF} = 19.5 Hz), 63.6 (d, J_{CF} = 7.2 Hz), 43.6, 8.7 (2C); **^{19}F NMR** (377 MHz, CD_3CN) δ -131.2 (d, *J* = 20.0 Hz, 1F), -138.6 (d, *J* = 20.0 Hz, 1F), -143.7 (d, *J* = 23.3 Hz, 2F); **HRMS (ES+)** Calculated for $C_{14}H_{11}BF_4NO_4$ ($M+H^+$): 344.0717; found: 344.0728; *m/z* 385.1 ($M+MeCN+H^+$). These spectroscopic data correspond to previously reported data.[257]

7-(Cyclohexylamino)-1-(2,4-difluorophenyl)-6-fluoro-8-methoxy-4-oxo-1,4-dihydroquinoline-3-carboxylic acid - 150

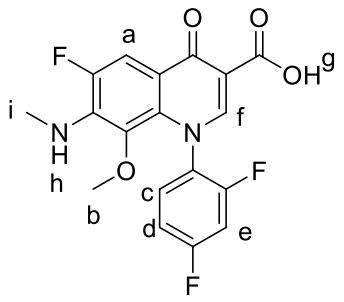


Following the general procedure **A**, the reaction of boron difluoride chelate **146** (50 mg, 0.12 mmol) with cyclohexylamine (33 µL, 0.29 mmol) in MeCN (3 mL) followed by hydrolysis of the chelate in EtOH (7 mL) and NEt_3 (0.7 mL) afforded carboxylic acid **150** as a yellow solid (28 mg, 52 %) after acid-base work up, with purity of ≥95 % by LC-MS analysis.

Mp ($CHCl_3$) 240-241 °C; **IR V_{max} / cm^{-1}**: 3319, 2937, 1709, 1623, 1436, 1321, 857, 807; **^{1}H NMR** (400 MHz, $CDCl_3$) δ 14.88 (s, 1H, OH-*g*), 8.45 (s, 1H, CH-*f*), 7.95 (d, *J* = 12.6 Hz, 1H, CH-*a*), 7.47 (td, *J* = 8.7, 5.5 Hz, 1H, CH-*c*), 7.12–6.94 (m, 2H, CH-*d* + CH-*e*), 4.31 (d, *J* = 6.7 Hz, 1H, NH-*h*), 3.83–3.61 (m, 1H, CH-*i*), 3.16 (s, 3H, CH_3-*b*), 2.01 (*app*-br s, 2H, CH_2-*j*), 1.75 (m, 2H, CH_2-*j*), 1.65 (m, 1H, CH-*l*), 1.48–1.28 (m, 2H, CH_2-*k*), 1.29–1.03 (m, 3H, CH-*l* + CH_2-*k*); **^{13}C NMR** (101 MHz, $CDCl_3$) δ 177.3 (d, J_{CF} = 2.8 Hz), 166.7, 162.9 (dd, J_{CF} = 253.5, 10.5 Hz), 157.5 (dd, J_{CF} = 254.6, 12.6 Hz), 151.1 (d, J_{CF} = 247.1 Hz), 150.2, 136.6 (d, J_{CF} = 12.1 Hz), 136.1 (d, J_{CF} = 6.9 Hz), 132.1, 128.6 (dd, J_{CF} = 13.6, 4.0 Hz), 127.8 (d, J_{CF} = 10.0 Hz), 116.5 (d, J_{CF} = 8.7 Hz), 111.8 (dd, J_{CF} = 22.6, 3.6 Hz), 108.9 (d, J_{CF} = 22.8 Hz), 108.4,

105.0 (dd, J_{CF} = 26.7, 22.8 Hz), 60.3, 53.3 (d, J = 7.7 Hz), 34.8 (2C), 25.6 (2C), 24.8 (d, J = 5.4 Hz); **^{19}F NMR** (377 MHz, $CDCl_3$) δ -105.9 (d, J = 8.1 Hz, 1F), -116.0 (s, 1F), -127.1 (s, 1F); **HRMS (ES+)** Calculated for $C_{23}H_{22}F_3N_2O_4$ ($M+H^+$): 447.1532; found: 447.1520.

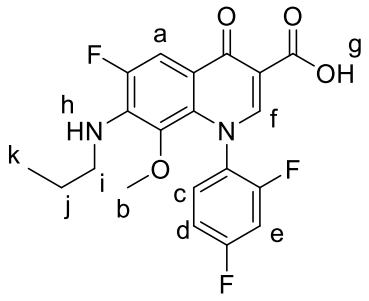
1-(2,4-Difluorophenyl)-6-fluoro-8-methoxy-7-(methylamino)-4-oxo-1,4-dihydroquinoline-3-carboxylic acid - 151



Following the general procedure **A**, the reaction of boron difluoride chelate **146** (50 mg, 0.12 mmol) with methylamine (2 M in MeOH, 140 µL) in MeCN (3 mL) followed by hydrolysis of the chelate in EtOH (7 mL) and NEt_3 (0.7 mL) afforded carboxylic acid **151** as a yellow solid (28 mg, 52 %) after acid-base work up, with purity of ≥95 % by LC-MS analysis.

Mp ($CHCl_3$) 171-174 °C; **IR V_{max} / cm^{-1}**: 3328, 2941, 1718, 1616, 1451, 1426, 1315, 1058, 931, 804; **^{1}H NMR** (400 MHz, $CDCl_3$) δ 14.87 (s, 1H, OH-*g*), 8.44 (s, 1H, CH-*f*), 7.92 (d, J = 12.6 Hz, 1H, CH-*a*), 7.50 (td, J = 8.6, 5.5 Hz, 1H, CH-*c*), 7.12–6.94 (m, 2H, CH-*d* + CH-*e*), 4.50 (br s, 1H, NH-*h*), 3.20–3.10 (m, 6H, CH_3-*b* + CH_3-*i*); **^{13}C NMR** (101 MHz, $CDCl_3$) δ 177.3 (d, J_{CF} = 3.2 Hz), 166.7, 162.9 (dd, J_{CF} = 253.6, 10.9 Hz), 157.6 (dd, J_{CF} = 255.0, 12.5 Hz), 151.2 (d, J_{CF} = 247.2 Hz), 150.3, 138.6 (d, J_{CF} = 11.5 Hz), 135.8 (d, J_{CF} = 6.7 Hz), 132.2, 128.6 (dd, J_{CF} = 13.3, 4.1 Hz), 127.9 (d, J_{CF} = 9.9 Hz), 116.5 (d, J_{CF} = 8.3 Hz), 111.8 (dd, J_{CF} = 22.8, 3.6 Hz), 108.8 (d, J_{CF} = 22.2 Hz), 108.4, 104.9 (dd, J_{CF} = 26.5, 23.0 Hz), 60.5, 32.7 (d, J = 8.0 Hz); **^{19}F NMR** (377 MHz, $CDCl_3$) δ -105.8 (d, J = 7.8 Hz, 1F), -115.9 (d, J = 7.8 Hz, 1F), -128.2 (s, 1F); **HRMS (ES+)** Calculated for $C_{18}H_{14}F_3N_2O_4$ ($M+H^+$): 379.0906; found: 379.0923.

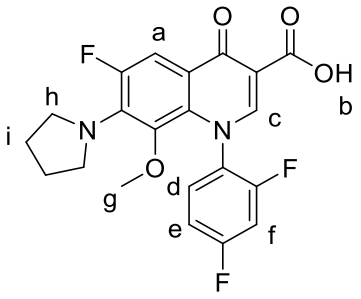
1-(2,4-Difluorophenyl)-6-fluoro-8-methoxy-4-oxo-7-(propylamino)-1,4-dihydroquinoline-3-carboxylic acid - 152



Following general procedure **A**, the reaction of boron difluoride chelate **146** (50 mg, 0.12 mmol) with propylamine (24 µL, 0.29 mmol) in MeCN (3 mL) followed by hydrolysis of the chelate in EtOH (7 mL) and NEt_3 (0.7 mL) afforded carboxylic acid **152** as a yellow solid (47 mg, 95 %) after acid-base work up, with purity of ≥95 % by LC-MS analysis.

Mp ($CHCl_3$) 248-250°C; **IR V_{max} / cm^{-1}**: 3315, 2969, 1721, 1616, 1432, 1321, 1280, 1102, 962, 854, 804; **^{1}H NMR** (400 MHz, $CDCl_3$) δ 14.87 (s, 1H, OH-*g*), 8.45 (s, 1H, CH-*f*), 7.93 (d, *J* = 12.6 Hz, 1H, CH-*a*), 7.49 (td, *J* = 8.6, 5.5 Hz, 1H, CH-*c*), 7.14–6.94 (m, 2H, CH-*d* + CH-*e*), 4.44 (s, 1H, NH-*h*), 3.43 (ddd, *J* = 8.7, 7.1, 2.5 Hz, 2H, CH_2-*i*), 3.17 (s, 3H, CH_3-*b*), 1.62 (m, 2H, CH_2-*j*), 0.96 (t, *J* = 7.3 Hz, 3H, CH_3-*k*); **^{13}C NMR** (101 MHz, $CDCl_3$) δ 177.4 (d, J_{CF} = 2.9 Hz), 166.7, 162.9 (dd, J_{CF} = 253.3, 10.9 Hz), 157.5 (dd, J_{CF} = 243.9, 11.0 Hz), 151.2 (d, J_{CF} = 247.2 Hz), 150.3, 137.7 (d, J_{CF} = 11.8 Hz), 136.0 (d, J_{CF} = 6.9 Hz), 132.2, 128.6 (dd, J_{CF} = 13.2, 4.3 Hz), 127.8 (d, J_{CF} = 10.0 Hz), 116.5 (d, J_{CF} = 8.5 Hz), 111.8 (dd, J_{CF} = 22.7, 3.6 Hz), 108.8 (d, J_{CF} = 22.7 Hz), 108.4, 105.0 (dd, J_{CF} = 26.6, 23.1 Hz), 60.4, 47.2 (d, *J* = 7.4 Hz), 24.2, 11.3; **^{19}F NMR** (377 MHz, $CDCl_3$) δ -105.9 (d, *J* = 7.9 Hz, 1F), -116.0 (d, *J* = 7.9 Hz, 1F), -127.7 (s, 1F); **HRMS (ES+)** Calculated for $C_{20}H_{18}F_3N_2O_4$ ($M+H^+$): 407.1219; found: 407.1219.

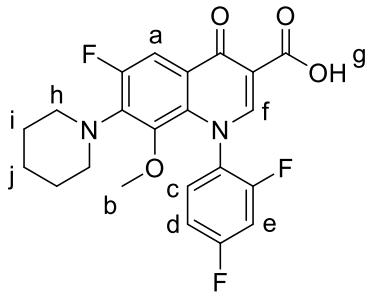
1-(2,4-Difluorophenyl)-6-fluoro-8-methoxy-4-oxo-7-(pyrrolidin-1-yl)-1,4-dihydroquinoline-3-carboxylic acid - 153



Following the general procedure **B**, the reaction of boron difluoride chelate **146** (50 mg, 0.12 mmol) with pyrrolidine (24 µL, 0.29 mmol) in pyridine (3 mL) followed by hydrolysis of the chelate in EtOH (7 mL) and NEt_3 (0.7 mL) afforded carboxylic acid **153** as a yellow solid (50 mg, 90 %) after acid-base work up, with purity of ≥95 % by LC-MS analysis.

Mp ($CHCl_3$) 182-185 °C; **IR V_{max} / cm^{-1}**: 3071, 2957, 1728, 1617, 1503, 1433, 1318, 1144, 966, 855, 810; **^{1}H NMR** (400 MHz, $CDCl_3$) δ 14.92 (s, 1H, OH-*b*), 8.45 (s, 1H, CH-*c*), 7.87 (d, *J* = 13.9 Hz, 1H, CH-*a*), 7.49 – 7.36 (m, 1H, CH-*d*), 7.09 – 6.94 (m, 2H, CH-*e* + CH-*f*), 3.69 – 3.51 (m, 2H, CH_2-*h*), 3.51 – 3.37 (m, 2H, CH_2-*h*), 3.06 (s, 3H, CH_3-*g*), 2.04 – 1.79 (m, 4H, 2 x CH_2-*i*); **^{13}C NMR** (101 MHz, $CDCl_3$) δ 177.2 (d, J_{CF} = 3.1 Hz), 166.8, 162.7 (dd, J_{CF} = 252.7, 10.9 Hz), 157.3 (dd, J_{CF} = 254.5, 12.5 Hz), 154.0 (d, J_{CF} = 251.4 Hz), 150.3, 139.6 (d, J_{CF} = 7.6 Hz), 137.7 (d, J_{CF} = 11.1 Hz), 133.4, 129.5 (dd, J_{CF} = 13.4, 4.0 Hz), 127.3 (d, J_{CF} = 10.1 Hz), 117.7 (d, J_{CF} = 8.9 Hz), 111.7 (dd, J_{CF} = 22.8, 3.7 Hz), 108.4, 108.1 (d, J_{CF} = 24.3 Hz), 104.9 (dd, J_{CF} = 26.5, 23.0 Hz), 60.1, 51.6 (d, *J* = 6.8 Hz), 26.1; **^{19}F NMR** (377 MHz, $CDCl_3$) δ -106.6 (d, *J* = 7.9 Hz, 1F), -116.7 (d, *J* = 7.9 Hz, 1F), -119.8 (s, 1F); **HRMS (ES+)** Calculated for $C_{21}H_{18}F_3N_2O_4$ ($M+H^+$): 419.1219; found: 419.1208.

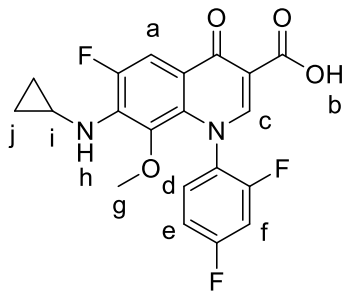
1-(2,4-Dimethylphenyl)-6-fluoro-4-oxo-7-(piperidin-1-yl)-1,4-dihydroquinoline-3-carboxylic acid - 154



Following the general procedure **A,** the reaction of boron difluoride chelate **146** (36 mg, 0.087 mmol) with piperidine (20 µL, 0.20 mmol) in MeCN (2 mL) followed by hydrolysis of the chelate in EtOH (5 mL) and NEt_3 (0.5 mL) afforded carboxylic acid **154** as a yellow solid (24 mg, 65 %) after acid-base work up, with purity of ≥95 % by LC-MS analysis.

Mp ($CHCl_3$) 160-162 °C; **IR V_{max} / cm^{-1}**: 2792, 1728, 1617, 1502, 1432, 1315, 962, 855; **^{1}H NMR** (400 MHz, $CDCl_3$) δ 14.69 (s, 1H, OH-*f*), 8.47 (s, 1H, CH-*f*), 7.92 (d, *J* = 12.3 Hz, 1H, CH-*a*), 7.44 (m, 1H, CH-*c*), 7.10–6.98 (m, 2H, CH-*e* + CH-*d*), 3.35–3.22 (m, 5H, CH_2-*h* + CH_3-*b*), 3.22–3.11 (m, 2H, CH_2-*h*), 1.76–1.54 (m, 6H, 2 x CH_2-*i* + CH_2-*j* + H_2O); **^{13}C NMR** (101 MHz, $CDCl_3$) δ 177.6 (d, J_{CF} = 2.6 Hz), 166.6, 162.8 (dd, J_{CF} = 253.3, 10.9 Hz), 157.4 (dd, J_{CF} = 254.5, 12.6 Hz), 157.1 (d, J_{CF} = 252.3 Hz), 150.6, 144.3 (d, J_{CF} = 6.0 Hz), 140.5 (d, J_{CF} = 12.2 Hz), 132.9, 129.4 (dd, J_{CF} = 13.7, 4.3 Hz), 127.5 (d, J_{CF} = 10.0 Hz), 121.0 (d, J_{CF} = 9.1 Hz), 111.9 (dd, J_{CF} = 22.8, 3.6 Hz), 108.5, 108.2 (d, J_{CF} = 23.9 Hz), 105.0 (dd, J_{CF} = 26.6, 23.1 Hz), 61.1, 52.0 (d, *J* = 4.7 Hz, 2C), 26.7 (2C), 24.2; **^{19}F NMR** (377 MHz, $CDCl_3$) δ -106.2 (d, *J* = 7.8 Hz, 1F), -116.8 (d, *J* = 7.8 Hz, 1F), -118.2 (s, 1F); **HRMS (ES+)** Calculated for $C_{22}H_{20}F_3N_2O_4$ ($M+H^+$): 433.1375; found: 433.1377.

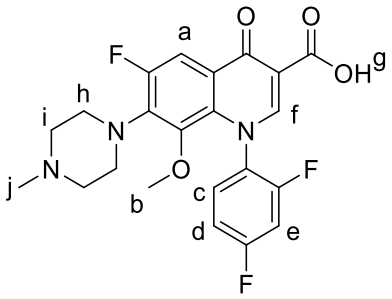
7-(Cyclopropylamino)-1-(2,4-difluorophenyl)-6-fluoro-8-methoxy-4-oxo-1,4-dihydroquinoline-3-carboxylic acid - 155



Following the general procedure **B**, the reaction of boron difluoride chelate **146** (50 mg, 0.12 mmol) with cyclopropylamine (25 µL, 0.36 mmol) in pyridine (3 mL) followed by hydrolysis of the chelate in EtOH (7 mL) and NEt_3 (0.7 mL) afforded carboxylic acid **155** as a yellow solid (25 mg, 51 %) after acid-base work up.

Mp (MeOH) 242-245 °C; **IR V_{max} / cm^{-1}**: 3284, 2928, 1712, 1620, 1452, 1433, 1347, 1312, 1268, 966, 858, 807; **^{1}H NMR** (400 MHz, DMSO) δ 15.05 (s, 1H, OH-*b*), 8.48 (s, 1H, CH-*c*), 8.02 (td, *J* = 8.9, 5.9 Hz, 1H, CH-*d*), 7.82 (d, *J* = 12.9 Hz, 1H, CH-*a*), 7.51 (ddd, *J* = 10.7, 8.9, 2.8 Hz, 1H, CH-*e*), 7.35 – 7.26 (m, 1H, CH-*f*), 6.48 (t, *J* = 2.4 Hz, 1H, NH-*h*), 3.01 (s, 3H, CH_3-*g*), 2.97 – 2.87 (m, 1H, CH-*i*), 0.71 – 0.54 (m, 4H, 2 x CH_2-*j*); **^{13}C NMR** (101 MHz, DMSO) δ 176.5 (d, J_{CF} = 2.8 Hz), 165.5, 162.1 (dd, J_{CF} = 248.4, 11.5 Hz), 157.1 (dd, J_{CF} = 251.5, 13.3 Hz), 150.9, 150.5 (d, J_{CF} = 247.9 Hz), 138.0 (d, J_{CF} = 10.8 Hz), 135.8 (d, J_{CF} = 7.5 Hz), 132.0, 128.8 (d, J_{CF} = 10.4 Hz), 128.5 (dd, J_{CF} = 13.2, 3.9 Hz), 114.7 (d, J_{CF} = 8.0 Hz), 111.7 (dd, J_{CF} = 22.8, 2.5 Hz), 107.6 (d, J_{CF} = 22.2 Hz), 106.9, 104.3 (dd, J_{CF} = 27.3, 23.7 Hz), 60.4, 27.1, 7.9 (dd, *J* = 26.9, 3.7 Hz, 2C); **^{19}F NMR** (376 MHz, DMSO) δ -108.1 (d, *J* = 8.1 Hz, 1F), -117.5 (d, *J* = 8.0 Hz, 1F), -124.7 (s, *J* = 10.7 Hz, 1F); **HRMS (ES+)** Calculated for $C_{20}H_{16}F_3N_2O_4$ (M+ H^+): 405.1062; found: 405.1059.

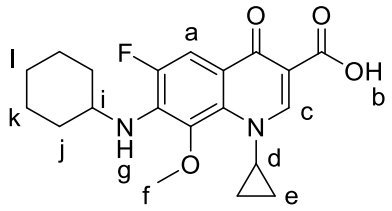
1-(2,4-Difluorophenyl)-6-fluoro-8-methoxy-7-(4-methylpiperazin-1-yl)-4-oxo-1,4-dihydroquinoline-3-carboxylic acid - 156



Following the general procedure **A,** the reaction of boron difluoride chelate **146** (50 mg, 0.12 mmol) with 1-methylpiperazine (32 µL, 0.29 mmol) in MeCN (3 mL) followed by hydrolysis of the chelate in EtOH (7 mL) and NEt_3 (0.7 mL) afforded carboxylic acid **156** as a yellow solid (42 mg, 77 %) after acid-base work up, with purity of ≥ 95% by LC-MS analysis.

Mp ($CHCl_3$) 180-184 °C; **IR V_{max} / cm^{-1}**: 2941, 1728, 1616, 1502, 1429, 1318, 1105, 854, 807; **^{1}H NMR** (400 MHz, $CDCl_3$) δ 8.46 (s, 1H, CH-*f*), 7.91 (d, *J* = 12.3 Hz, 1H, CH-*a*), 7.57–7.35 (td, *J* = 8.6, 5.5 Hz, 1H, CH-*c*), 7.18–6.90 (m, 2H, CH-*d* + CH-*e*), 3.48–3.33 (m, 2H, CH_2-*h*), 3.33–3.17 (m, 5H, CH_2-*h* + CH_3-*b*), 2.63–2.41 (m, 4H, 2 x CH_2-*i*), 2.33 (s, 3H, CH_3-*j*); **^{13}C NMR** (101 MHz, $CDCl_3$) δ 177.5 (d, J_{CF} = 2.5 Hz), 166.4, 162.8 (dd, J_{CF} = 253.3, 11.1 Hz), 157.3 (dd, J_{CF} = 254.3, 12.6 Hz), 156.7 (d, J_{CF} = 252.3 Hz), 150.7, 144.2 (d, J_{CF} = 5.5 Hz), 139.5 (d, J_{CF} = 12.0 Hz), 132.9, 129.2 (dd, J_{CF} = 13.6, 4.4 Hz), 127.5 (d, J_{CF} = 10.0 Hz), 121.3 (d, J_{CF} = 9.2 Hz), 111.9 (dd, J_{CF} = 22.8, 3.6 Hz), 108.5 (d, J_{CF} = 10.2 Hz), 108.2, 105.0 (dd, J_{CF} = 26.6, 23.1 Hz), 61.4 (2C), 55.6 (2C), 50.4 (d, *J* = 4.6 Hz), 46.5; **^{19}F NMR** (377 MHz, MeOD) δ -109.1 (d, *J* = 7.9 Hz, 1F), -119.5 (d, *J* = 7.9 Hz, 1F), -120.8 (s, 1F); **HRMS (ES+)** Calculated for $C_{24}H_{24}F_3N_4O_4$ (M+MeCN+H$^+$): 489.1750; found: 489.1750.

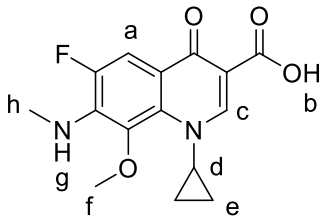
7-(Cyclohexylamino)-1-cyclopropyl-6-fluoro-8-methoxy-4-oxo-1,4-dihydroquinoline-3-carboxylic acid - 157



Following the general procedure **B**, the reaction of boron difluoride chelate **147** (50 mg, 0.15 mmol) with cyclohexylamine (41 µL, 0.36 mmol) in pyridine (3 mL) followed by hydrolysis of the chelate in EtOH (7 mL) and NEt_3 (0.7 mL) afforded carboxylic acid **157** as a brown solid (50 mg, 87 %) after acid-base work up, with purity of ≥95 % by LC-MS analysis.

Mp ($CHCl_3$) 193-195 °C; **IR V_{max} / cm^{-1}**: 3405, 2938, 1722, 1623, 1445, 1318, 1042, 804; **^{1}H NMR** (400 MHz, $CDCl_3$) δ 15.03 (s, 1H, OH-*b*), 8.76 (s, 1H, CH-*c*), 7.86 (d, *J* = 12.5 Hz, 1H, CH-*a*), 4.48 (d, *J* = 7.5 Hz, 1H, NH-*g*), 4.03 – 3.92 (m, 1H, CH-*d*), 3.87 – 3.74 (m, 1H, CH-*i*), 3.72 (s, 3H, CH_3-*f*), 2.08 (dd, *J* = 12.4, 3.2 Hz, 2H, CH_2-*j*), 1.85 – 1.74 (m, 2H, CH_2-*j*), 1.74 – 1.63 (m, 1H, CH-*l*), 1.49 – 1.34 (m, 2H, CH_2-*k*), 1.31 – 1.14 (m, 5H, CH_2-*k*, + CH-*l* + CH_2-*e*), 1.04 – 0.96 (m, 2H, CH_2-*e*); **^{13}C NMR** (101 MHz, $CDCl_3$) δ 177.1 (d, J_{CF} = 3.3 Hz), 167.2, 151.1 (d, J_{CF} = 246.5 Hz), 149.6, 137.4 (d, J_{CF} = 6.4 Hz), 136.6 (d, J_{CF} = 12.0 Hz), 117.3 (d, J_{CF} = 8.0 Hz), 116.8, 113.4, 108.6 (d, J_{CF} = 22.7 Hz), 107.6, 61.2, 53.2 (d, *J* = 7.1 Hz), 39.7, 34.8 (2C), 25.7, 24.9 (2C), 9.7 (2C); **^{19}F NMR** (377 MHz, $CDCl_3$) δ -127.7 (s, 1F); **HRMS (ES+)** Calculated for $C_{20}H_{24}FN_2O_4$ ($M+H^+$): 375.1720; found: 375.1714.

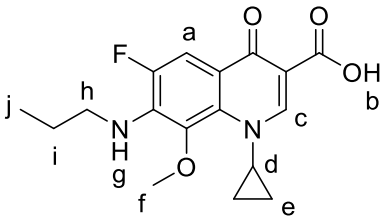
1-Cyclopropyl-6-fluoro-8-methoxy-7-(methylamino)-4-oxo-1,4-dihydroquinoline-3-carboxylic acid - 158



Following the general procedure **B**, the reaction of boron difluoride chelate **147** (50 mg, 0.15 mmol) with methylamine (2 M in MeOH, 0.18 mL) in pyridine (3 mL) followed by hydrolysis of the chelate in EtOH (7 mL) and NEt_3 (0.7 mL) afforded carboxylic acid **158** as a yellow solid (40 mg, 89 %) after acid-base work up, with purity of ≥95 % by LC-MS analysis.

Mp ($CHCl_3$) 193-196 °C; **IR V_{max} / cm^{-1}**: 3405, 2938, 1722, 1623, 1445, 1318, 1042, 941, 804; **^{1}H NMR** (400 MHz, $CDCl_3$) δ 15.03 (s, 1H, OH-*b*), 8.75 (s, 1H, CH-*c*), 7.85 (d, *J* = 12.5 Hz, 1H, CH-*a*), 4.65 (s, 1H, NH-*g*), 4.04 – 3.92 (m, 1H, CH-*d*), 3.72 (s, 3H, CH_3-*f*), 3.23 (d, *J* = 4.0 Hz, 3H, CH_3-*h*), 1.24 – 1.15 (m, 2H, CH_2-*e*), 1.06 – 0.96 (m, 2H, CH_2-*e*); **^{13}C NMR** (101 MHz, $CDCl_3$) δ 177.1 (d, J_{CF} = 3.1 Hz), 167.2, 151.2 (d, J_{CF} = 246.7 Hz), 149.6, 138.7 (d, J_{CF} = 11.5 Hz), 137.1 (d, J_{CF} = 6.3 Hz), 133.3, 117.1 (d, J_{CF} = 8.4 Hz), 108.6 (d, J_{CF} = 22.1 Hz), 107.6, 61.4, 39.7, 32.9 (d, *J* = 7.7 Hz), 9.7 (2C); **^{19}F NMR** (377 MHz, $CDCl_3$) δ -128.7 (s, 1F); **HRMS (ES+)** Calculated for $C_{15}H_{16}FN_2O_4$ ($M+H^+$): 307.1094; found: 307.1093.

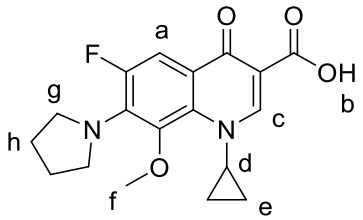
1-Cyclopropyl-6-fluoro-8-methoxy-4-oxo-7-(propylamino)-1,4-dihydroquinoline-3-carboxylic acid - 159



Following the general procedure **B**, the reaction of boron difluoride chelate **147** (50 mg, 0.15 mmol) with *n*-propylamine (31 µL, 0.36 mmol) in pyridine (3 mL) followed by hydrolysis of the chelate in EtOH (7 mL) and NEt_3 (0.7 mL) afforded carboxylic acid **159** as a yellow solid (35 mg, 71 %) after acid-base work up, with purity of ≥95 % by LC-MS analysis.

Mp ($CHCl_3$) 124-125 °C; **IR V_{max} / cm^{-1}**: 3354, 2960, 1712, 1617, 1534, 1436, 1309, 1049, 807; **^{1}H NMR** (400 MHz, $CDCl_3$) δ 15.05 (s, 1H, OH-*b*), 8.74 (s, 1H, CH-*c*), 7.83 (d, *J* = 12.5 Hz, 1H, CH-*a*), 4.63 (s, 1H, NH-*g*), 4.03 – 3.93 (m, 1H, CH-*d*), 3.72 (s, 3H, CH_3-*f*), 3.52 (ddd, *J* = 8.5, 7.2, 2.4 Hz, 2H, CH_2-*h*), 1.80 – 1.61 (m, 2H, CH_2-*i*), 1.23 – 1.15 (m, 2H, CH_2-*e*), 1.05 – 0.95 (m, 5H, CH_2-*e* + CH_3-*j*); **^{13}C NMR** (101 MHz, $CDCl_3$) δ 177.0 (d, J_{CF} = 3.2 Hz), 167.2, 151.1 (d, J_{CF} = 246.6 Hz), 149.6, 137.7 (d, J_{CF} = 11.9 Hz), 137.2 (d, J_{CF} = 6.3 Hz), 133.3, 117.1 (d, J_{CF} = 8.3 Hz), 108.5 (d, J_{CF} = 22.4 Hz), 107.6, 61.3, 47.3 (d, *J* = 7.2 Hz), 39.7, 24.2, 11.4, 9.7 (2C); **^{19}F NMR** (377 MHz, $CDCl_3$) δ -128.2 (s, 1F); **HRMS (ES+)** Calculated for $C_{17}H_{20}FN_2O_4$ ($M+H^+$): 335.1407; found: 335.1403.

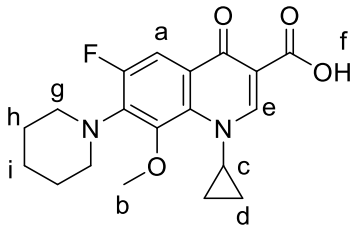
1-Cyclopropyl-6-fluoro-8-methoxy-4-oxo-7-(pyrrolidin-1-yl)-1,4-dihydroquinoline-3-carboxylic acid - 160



Following the general procedure **B**, the reaction of boron difluoride chelate **147** (50 mg, 0.15 mmol) with pyrrolidine (30 µL, 0.36 mmol) in pyridine (3 mL) followed by hydrolysis of the chelate in EtOH (7 mL) and NEt_3 (0.7 mL) afforded carboxylic acid **160** as a yellow solid (50 mg, 98 %) after acid-base work up, with purity of ≥95 % by LC-MS analysis.

^{1}H NMR (400 MHz, $CDCl_3$) δ 15.10 (s, 1H, OH-*b*), 8.75 (s, 1H, CH-*c*), 7.76 (d, *J* = 13.9 Hz, 1H, CH-*a*), 4.05 – 3.95 (m, 1H, CH-*d*), 3.63 (td, *J* = 6.6, 2.8 Hz, 4H, 2 x CH_2-*g*), 3.53 (s, 3H, CH_3-*f*), 2.02 – 1.94 (m, 4H, 2 x CH_2-*h*), 1.23 – 1.12 (m, 2H, CH_2-*e*), 1.02 – 0.92 (m, 2H, CH_2-*e*); **^{13}C NMR** (101 MHz, $CDCl_3$) δ 177.2 (d, J_{CF} = 3.0 Hz), 167.6, 154.2 (d, J_{CF} = 251.2 Hz), 150.0, 141.1 (d, J_{CF} = 7.0 Hz), 138.0 (d, J_{CF} = 11.2 Hz), 134.9, 118.5 (d, J_{CF} = 9.0 Hz), 108.2 (d, J_{CF} = 24.0 Hz), 108.0, 61.2, 52.0 (d, *J* = 6.8 Hz, 2C), 40.9, 26.5 (2C), 9.9 (2C); **^{19}F NMR** (377 MHz, $CDCl_3$) δ -120.6 (s, 1F); **HRMS (ES+)** Calculated for $C_{18}H_{20}FN_2O_4$ ($M+H^+$): 347.1407; found: 347.1414. These spectroscopic data correspond to previously reported data.[258]

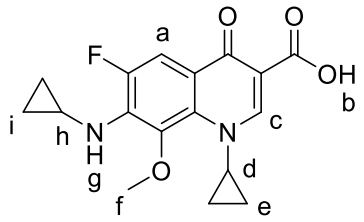
1-Cyclopropyl-6-fluoro-8-methoxy-4-oxo-7-(piperidin-1-yl)-1,4-dihydroquinoline-3-carboxylic acid - 161



Following the general procedure **A**, the reaction of boron difluoride chelate **147** (30 mg, 0.087 mmol) with piperidine (21 µL, 0.21 mmol) in MeCN (2 mL) followed by hydrolysis of the chelate in EtOH (5 mL) and NEt_3 (0.5 mL) afforded carboxylic acid **161** as a yellow solid (20 mg, 70 %) after acid-base work up.

^{1}H NMR (400 MHz, $CDCl_3$) δ 14.88 (s, 1H, OH-*f*), 8.78 (s, 1H, CH-*e*), 7.81 (d, *J* = 12.2 Hz, 1H, CH-*a*), 4.08 – 3.99 (m, 1H), 3.77 (s, 3H), 3.38 – 3.28 (m, 4H), 1.76 – 1.64 (m, 6H), 1.27 – 1.15 (m, 2H), 1.02 – 0.93 (m, 2H); **^{13}C NMR** (101 MHz, $CDCl_3$) δ 177.1 (d, J_{CF} = 2.9 Hz), 166.9, 156.5 (d, J_{CF} = 251.7 Hz), 149.7, 145.4 (d, J_{CF} = 5.9 Hz), 140.6 (d, J_{CF} = 12.0 Hz), 134.0, 121.2 (d, J_{CF} = 9.1 Hz), 108.0 (d, J_{CF} = 23.5 Hz), 107.6, 62.2, 52.1 (d, *J* = 4.6 Hz, 2C), 40.6, 26.6 (2C), 24.2, 9.5 (2C); **^{19}F NMR** (377 MHz, $CDCl_3$) δ -119.1 (s, 1F); **HRMS (ES+)** Calculated for $C_{19}H_{22}FN_2O_4$ ($M+H^+$): 361.1564; found: 361.1583.

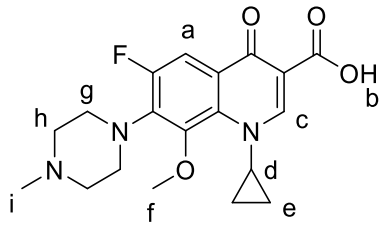
1-Cyclopropyl-7-(cyclopropylamino)-6-fluoro-8-methoxy-4-oxo-1,4-dihydroquinoline-3-carboxylic acid - 162



Following the general procedure **B**, the reaction of boron difluoride chelate **147** (50 mg, 0.15 mmol) with cyclopropylamine (25 µL, 0.36 mmol) in pyridine (3 mL) followed by hydrolysis of the chelate in EtOH (7 mL) and NEt_3 (0.7 mL) afforded carboxylic acid **162** as a yellow solid (37 mg, 87 %) after acid-base work up, with purity of ≥95 % by LC-MS analysis.

Mp ($CHCl_3$) 165-168 °C; **IR V_{max} / cm^{-1}**: 3315, 2935, 1712, 1617, 1525, 1442, 1312, 1042, 807; **^{1}H NMR** (400 MHz, $CDCl_3$) δ 15.01 (s, 1H, OH-*b*), 8.75 (s, 1H, CH-*c*), 7.86 (d, *J* = 12.2 Hz, 1H, CH-*a*), 4.86 (s, 1H, NH-*g*), 4.02 – 3.89 (m, 1H, CH-*d*), 3.69 (s, 3H, CH_3-*f*), 3.11 – 2.95 (m, 1H, CH-*h*), 1.23 – 1.14 (m, 2H, CH_2-*e*), 1.04 – 0.95 (m, 2H, CH_2-*e*), 0.89 – 0.80 (m, 2H, CH_2-*i*), 0.69 – 0.59 (m, 2H, CH_2-*i*); **^{13}C NMR** (101 MHz, $CDCl_3$) δ 177.1 (d, J_{CF} = 3.1 Hz), 167.2, 150.9 (d, J_{CF} = 249.0 Hz), 149.6, 137.9 (d, J_{CF} = 11.7 Hz), 137.0 (d, J_{CF} = 6.3 Hz), 133.0, 117.5 (d, J_{CF} = 8.0 Hz), 108.8 (d, J_{CF} = 22.1 Hz), 107.6, 61.5, 39.6, 27.8 (d, *J* = 6.6 Hz), 9.7 (2C), 9.0 (d, *J* = 3.9 Hz, 2C); **^{19}F NMR** (377 MHz, $CDCl_3$) δ -126.2 (s, 1F); **HRMS (ES+)** Calculated for $C_{17}H_{18}FN_2O_4$ ($M+H^+$): 333.1251; found: 333.1246.

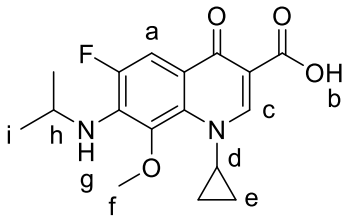
1-Cyclopropyl-6-fluoro-8-methoxy-7-(4-methylpiperazin-1-yl)-4-oxo-1,4-dihydroquinoline-3-carboxylic acid - 163



Following the general procedure **B**, the reaction of boron difluoride chelate **147** (50 mg, 0.15 mmol) with 1-methylpiperazine (40 µL, 0.36 mmol) in pyridine (3 mL) followed by hydrolysis of the chelate in EtOH (7 mL) and NEt_3 (0.7 mL). After acid-base work up, the resulting solid was purified by column chromatography (5 % MeOH in $CHCl_3$) to yield carboxylic acid **163** as a white solid (20 mg, 30 %), with purity of ≥95 % by LC-MS analysis.

^{1}H NMR (400 MHz, $CDCl_3$) δ 14.77 (s, 1H, OH-*b*), 8.79 (s, 1H, CH-*c*), 7.84 (d, *J* = 12.1 Hz, 1H, CH-*a*), 4.10 – 3.97 (m, 1H, CH-*d*), 3.77 (s, 3H, CH_3-*f*), 3.54 – 3.40 (m, 4H, 2 x CH_2-*g*), 2.64 – 2.54 (m, 4H, 2 x CH_2-*h*), 2.41 (s, 3H, CH_3-*i*), 1.24 – 1.15 (m, 2H, CH_2-*e*), 1.04 – 0.94 (m, 2H, CH_2-*e*); **^{13}C NMR** (101 MHz, $CDCl_3$) δ 177.0 (d, J_{CF} = 2.6 Hz), 166.8, 156.1 (d, J_{CF} = 251.6 Hz), 149.9, 145.4 (d, J_{CF} = 5.3 Hz), 139.5 (d, J_{CF} = 11.8 Hz), 134.0, 121.8 (d, J_{CF} = 9.3 Hz), 108.2 (d, J_{CF} = 23.6 Hz), 107.8, 62.6, 55.6 (2C), 50.4 (d, *J* = 4.2 Hz, 2C), 46.2, 40.5, 9.5 (2C); **^{19}F NMR** (377 MHz, $CDCl_3$) δ -119.3 (s, 1F); **HRMS (ES+)** Calculated for $C_{21}H_{26}FN_4O_4$ (M+MeCN+H^+): 417.1938, found: 417.1964. These spectroscopic data correspond to previously reported data.[233]

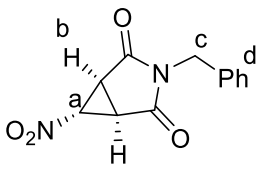
1-Cyclopropyl-6-fluoro-7-(isopropylamino)-8-methoxy-4-oxo-1,4-dihydroquinoline-3-carboxylic acid - 164



Following the general procedure **B**, the reaction of boron difluoride chelate **147** (50 mg, 0.15 mmol) with *iso*propylamine (31 µL, 0.36 mmol) in pyridine (3 mL) followed by hydrolysis of the chelate in EtOH (7 mL) and NEt_3 (0.7 mL) afforded carboxylic acid **164** as a yellow solid (40 mg, 88 %) after acid-base work up, with purity of ≥95 % by LC-MS analysis.

Mp ($CHCl_3$) 176-178 °C; **IR V_{max} / cm^{-1}**: 3367, 2973, 1725, 1626, 1426, 1312, 1055, 947, 801; **^{1}H NMR** (400 MHz, $CDCl_3$) δ 15.02 (s, 1H, OH-*b*), 8.74 (s, 1H, CH-*c*), 7.83 (d, *J* = 12.4 Hz, 1H, CH-*a*), 4.37 (dd, *J* = 8.9, 2.4 Hz, 1H, NH-*g*), 4.25 – 4.10 (m, 1H, CH-*h*), 4.03 – 3.92 (m, 1H, CH-*d*), 3.72 (s, 3H, CH_3-*f*), 1.27 (d, *J* = 6.1 Hz, 6H, 2 x CH_3-*i*), 1.23 – 1.16 (m, 2H, CH_2-*e*), 1.03 – 0.96 (m, 2H, CH_2-*e*); **^{13}C NMR** (101 MHz, $CDCl_3$) δ 176.7 (d, J_{CF} = 3.1 Hz), 166.8, 150.8 (d, J_{CF} = 246.8 Hz), 149.3, 137.1 (d, J_{CF} = 6.5 Hz), 136.5 (d, J_{CF} = 12.3 Hz), 133.1, 117.1 (d, J_{CF} = 8.4 Hz), 108.1 (d, J_{CF} = 22.8 Hz), 107.2, 60.8, 45.9 (d, *J* = 7.2 Hz), 39.5, 23.9 (2C), 9.4 (2C); **^{19}F NMR** (377 MHz, $CDCl_3$) δ -127.8 (s, 1F); **HRMS (ES+)** Calculated for $C_{17}H_{20}FN_2O_4$ ($M+H^+$): 335.1407; found: 335.1407.

1α, 5α, 6α-3-Benzyl-6-nitro-2,4-dioxo-3-azabicyclo[3.1.0]hexane - 166



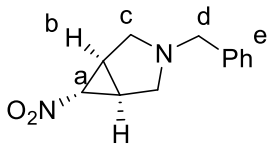
Synthesis according to Sun *et al.*[235] To a solution of *N*-benzylmaleimide (1.0 g, 5.3 mmol) in MeCN (30 mL) was added K_2CO_3 (0.74 g, 5.3 mmol) followed by slow addition of

bromonitromethane (0.37 mL, 5.3 mmol) over 4 h. The reaction was stirred at rt and more bromonitromethane (74 µL x 5 portions, 5.3 mmol) was added over 48 h. The reaction was concentrated under rotary evaporation and the resulting brown residue was purified by column chromatography (20 % EtOAc in pentane) to yield 3-azabicyclo[3.1.0]hexane **166** as a white solid (0.368 g, 28 %).

^{1}H NMR (400 MHz, $CDCl_3$) δ 7.39–7.27 (m, 5H, CH-*d*), 4.54 (s, 2H, CH-*c*), 4.48 (t, *J* = 1.6 Hz, 1H, CH-*a*), 3.36 (d, *J* = 1.6 Hz, 2H, CH-*b*); **^{13}C NMR** (101 MHz, $CDCl_3$) δ 168.5 (2C), 134.9, 129.0 (2C), 128.7 (2C), 128.5, 62.4, 42.7, 27.6. These spectroscopic data correspond to previously reported data.[235]

A mass could not be obtained for this compound through a range of techniques.

1α, 5α, 6α-3-Benzyl-6-nitro-3-azabicyclo[3.1.0]hexane - 167

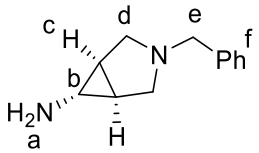


Synthesis according to Sun *et al.*[235] To a solution of 3-azabicyclo[3.1.0]hexane **166** (0.74 g, 3.0 mmol) in THF (20 mL) was added borane tetrahydrofuran complex solution (12 mL, 1.0 M in THF) and the mixture was heated at reflux under N_2 for 3 h. The reaction was then cooled at 0 °C before the careful addition of MeOH (10 mL) followed by reflux for 30 min. The reaction was concentrated under rotary evaporation and the resulting residue was dissolved in DCM (20 mL), washed with H_2O (2 x 50 mL) and then dried over $MgSO_4$ to produce 3-azabicyclo[3.1.0]hexane **167** as a pale yellow oil (0.60 g, 92 %).

^{1}H NMR (400 MHz, $CDCl_3$) δ 7.37–7.17 (m, 5H, CH-*e*), 4.63 (s, 1H, CH-*a*), 3.59 (s, 2H, CH-*d*), 3.14 (d, *J* = 9.1 Hz, 2H, CH-*b*), 2.50 (d, *J* = 8.1 Hz, 4H, CH-*c*); **^{13}C NMR** (101 MHz, $CDCl_3$) δ 138.4, 128.4 (2C), 128.3 (2C), 127.2, 61.1, 58.3, 53.4, 30.3, 29.8; **HRMS (ES+)** Calculated for $C_{12}H_{15}N_2O_2$ ($M+H^+$): 219.1134; found: 219.1140; Calculated for $C_{14}H_{18}N_3O_2$

(M+MeCN+H$^+$): 260.1399; found: 260.1416. These spectroscopic data correspond to previously reported data.[235]

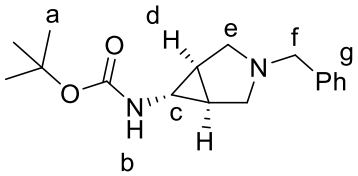
(1α,5α,6α)-3-Benzyl-6-amino-3-azabicyclo[3.1.0]hexane - 168



Synthesis according to Norris *et al.*[237] To a solution of 3-azabicyclo[3.1.0]hexane **167** (0.47 g, 2.2 mmol) in MeOH (20 mL) was added platinum on carbon (0.18 g, 0.92 mmol) and the mixture was hydrogenated at rt in a Parr shaker under 3 atm pressure of H_2 for 24 h. The catalyst was removed by filtration through celite and the filtrate was concentrated under rotary evaporation and dried under reduced pressure to yield primary amine **168** as a light yellow oil (0.345 g, 87 %) which was used without further purification.

^{1}H NMR (400 MHz, CDCl3) δ 7.36 – 7.17 (m, 5H, 5 x CH-*f*), 3.54 (s, 2H, CH_2-*e*), 2.94 (d, *J* = 8.8 Hz, 2H, CH_2-*d*), 2.64 (s, 1H, CH-*b*), 2.37 (d, *J* = 8.8 Hz, 2H, CH_2-*d*), 1.35 – 1.30 (m, 2H, 2 x CH-*c*); **^{13}C NMR** (101 MHz, $CDCl_3$) δ 139.4, 128.5 (2C), 128.4 (2C), 126.7, 59.3, 54.5 (2C), 32.5, 25.8 (2C); **HRMS (ES+)** Calculated for $C_{12}H_{17}N_2$ (M+H$^+$): 189.1392; found: 189.1398. These spectroscopic data correspond to previously reported data.[235]

(1α, 5α, 6α)-3-Benzyl-6-*tert*-butyloxycarbonylamino-3-aza-bicyclo[3.1.0]hexane - 169

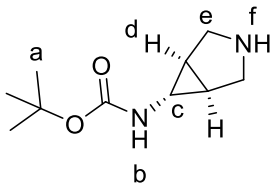


Synthesis according to Madhusudhan *et al.*[259] To a solution of primary amine **168** (0.72 g, 3.8 mmol) in THF (30 mL) was added NEt_3 (1.1 mL, 7.7 mmol) followed by decarbonate

Boc_2O (1.1 g, 5.0 mmol). The reaction was stirred at rt under N_2 for 5 h after which the solvent was evaporated and the residue was dry loaded onto silica and purified by column chromatography (20 % EtOAc in pentane) to yield Boc-protected amine **169** as a white solid (0.46 g, 42 %).

^{1}H NMR (400 MHz, $CDCl_3$) δ 7.34–6.15 (m, 5H, CH-*g*), 4.59 (s, 1H, NH-*b*), 3.55 (s, 2H, CH-*f*), 3.06 (d, *J* = 8.8 Hz, 2H, CH-*e*), 2.89 (s, 1H, CH-*c*), 2.38 (d, *J* = 8.8 Hz, 2H, CH-*e*), 1.48 (s, 2H, CH-*d*), 1.43 (s, 9H, CH_3-*a*); **^{13}C NMR** (101 MHz, $CDCl_3$) δ 156.5, 139.6, 128.5 (2C), 128.3 (2C), 126.9, 79.5, 59.0, 54.2 (2C), 30.6, 28.5 (3C), 24.7 (2C); **HRMS (ES+)** Calculated for $C_{17}H_{25}N_2O_2$ ($M+H^+$): 289.1916; found: 289.1916. These spectroscopic data correspond to previously reported data.[259]

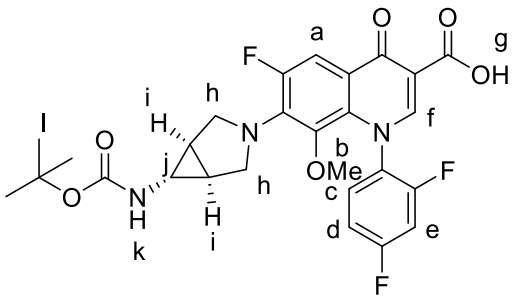
(1α,5α,6α)-6-*Tert*-butyloxycarbonylamino-3-azabicyclo[3.1.0]hexane - 170



Synthesis according to Sun *et al.*[235] To a solution of Boc-protected amine **169** (180 mg, 0.62 mmol) in MeOH (7 mL) was added $Pd(OH)_2$/C (90 mg, 0.64 mmol) catalyst under N_2 and the mixture was hydrogenated at 3.5 atm for 6 h. The catalyst was removed by filtration through Celite® and the filtrate was concentrated under rotary evaporation and dried under vacuum to yield 3-azabicyclo[3.1.0]hexane **170** as a light yellow solid, (125 mg, >99 %).

^{1}H NMR (400 MHz, CDCl3) δ 4.64 (br s, 1H, NH-*b*), 3.12 (d, *J* = 11.5 Hz, 2H, CH_2-*e*), 2.91 (d, *J* = 11.5 Hz, 1H, CH_2-*e*), 2.29 (s, 1H, CH-*c*), 1.95 (s, 3H, NH-*f* + 2 x CH-*d*), 1.43 (s, 9H, CH_3-*a*); **^{13}C NMR** (101 MHz, $CDCl_3$) δ 156.4, 79.8, 48.7 (2C), 30.5 28.5 (3C), 26.4 (2C); **HRMS (ES+)** Calculated for $C_{12}H_{22}N_3O_2$ ($M+MeCN+H^+$): 240.1712; found: 240.1653. These spectroscopic data correspond to previously reported data.[235]

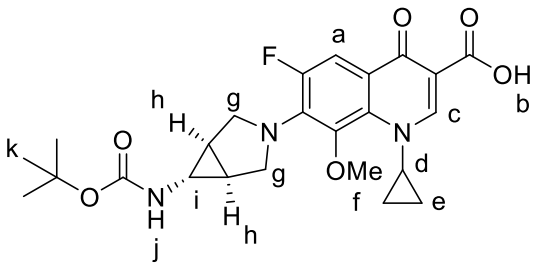
7-{(1*R*,5*S*,6*s*)-6-[(*Tert*-butoxycarbonyl)amino]-3-azabicyclo[3.1.0]hex-3-yl}-1-(2,4-difluorophenyl)-6-fluoro-8-methoxy-4-oxo-1,4-dihydroquinoline-3-carboxylic acid - 171



Following the general procedure **B**, the reaction of boron difluoride chelate **146** (88 mg, 0.21 mmol) with 3-azabicyclo[3.1.0]hexane **170** (100 mg, 0.50 mmol) in pyridine (5 mL) followed by hydrolysis of the chelate in EtOH (10 mL) and NEt_3 (1 mL) afforded carboxylic acid **171** as a yellow solid (56 mg, 46 %) after acid-base work up.

^{1}H NMR (400 MHz, $CDCl_3$) δ 14.70 (s, 1H, OH-*g*), 8.47 (s, 1H, CH-*f*), 7.88 (d, *J* = 13.4 Hz, 1H, CH-*a*), 7.53–7.35 (m, 1H, CH-*c*), 7.15–6.92 (m, 2H, CH-*d* + CH-*e*), 4.70 (br s, 1H, NH-*k*), 3.93 (d, *J* = 10.4 Hz, 1H, CH-*i*), 3.65 (*app*-s, 2H, CH_2-*h*), 3.40 (d, *J* = 9.7 Hz, 1H, CH-*i*), 3.08 (s, 3H, CH_3-*b*), 2.46 (*app*-s, 1H, CH-*j*), 1.72 (*app*-s, 2H, 2 x CH-*i*), 1.43 (s, 9H, 3 x CH_3-*l*); **^{13}C NMR** (101 MHz, $CDCl_3$) δ 177.4 (d, J_{CF} = 2.7 Hz), 166.5, 162.8 (dd, J_{CF} = 253.2, 11.0 Hz), 157.3 (dd, J_{CF} = 254.3, 12.5 Hz), 156.3, 155.5 (d, J_{CF} = 252.4 Hz), 150.6, 142.6 (d, J_{CF} = 6.3 Hz), 136.5 (d, J_{CF} = 11.4 Hz), 133.0, 129.2 (dd, J_{CF} = 13.3, 4.2 Hz), 127.3 (d, J_{CF} = 10.1 Hz), 119.9 (d, J_{CF} = 9.3 Hz), 111.9 (dd, J_{CF} = 22.7, 3.3 Hz), 108.5 (d, J_{CF} = 29.2 Hz), 108.0, 105.0 (dd, J_{CF} = 26.6, 23.0 Hz), 80.0, 60.8, 51.6 (dd, *J* = 66.5, 7.1 Hz, 2C), 29.7, 28.5 (3C), 24.5 (2C); **^{19}F NMR** (377 MHz, $CDCl_3$) δ -106.2 (d, *J* = 7.9 Hz, 1F), -116.8 (d, *J* = 7.9 Hz, 1F), -117.3 (s, 1F); **HRMS (ES+)** Calculated for $C_{27}H_{27}F_3N_3O_6$ ($M+H^+$): 546.1852; found: 546.1852. These spectroscopic data correspond to previously reported data.[257]

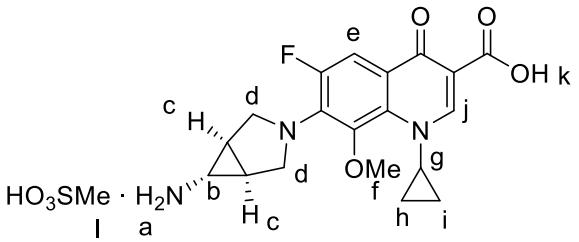
7-((1*R*,5*S*,6*s*)-6-(*Tert*-butoxycarbonylamino)-3-azabicyclo[3.1.0]hexan-3-yl)-1-cyclopropyl-6-fluoro-8-methoxy-4-oxo-1,4-dihydroquinoline-3-carboxylic acid - 172



Following the general procedure **B**, the reaction of boron difluoride chelate **147** (40 mg, 0.12 mmol) with 3-azabicyclo[3.1.0]hexane **170** (55 mg, 0.28 mmol) in pyridine (3 mL) followed by hydrolysis of the chelate in EtOH (7 mL) and NEt_3 (0.7 mL) afforded carboxylic acid **172** as a yellow solid (53 mg, 90 %) after acid-base work up.

^{1}H NMR (400 MHz, $CDCl_3$) δ 14.88 (s, 1H, OH-*b*), 8.76 (s, 1H, CH-*c*), 7.76 (d, *J* = 13.3 Hz, 1H, CH-*a*), 4.81 (s, 1H), 4.78 (s, 1H, NH-*j*), 3.99 (ddd, *J* = 11.2, 7.3, 4.1 Hz, 1H, CH-*d*), 3.91 (d, *J* = 10.2 Hz, 2H, CH_2-*g*), 3.64 (d, *J* = 9.4, 2H, CH_2-*g*) 3.57 (s, 3H, CH_3-*f*), 2.54 (s, 1H, CH-*i*), 1.79 (s, 2H, 2 x CH-*h*), 1.44 (s, 9H, 3 x CH_3-*k*), 1.21 – 1.13 (m, 2H, CH_2-*e*), 0.99 – 0.92 (m, 2H, CH_2-*e*); **^{13}C NMR** (101 MHz, $CDCl_3$) δ 176.9 (d, J_{CF} = 2.7 Hz), 166.9, 155.0 (d, J_{CF} = 252.9 Hz), 149.8, 143.7 (d, J_{CF} = 6.4 Hz), 136.4 (d, J_{CF} = 11.3 Hz), 134.1, 120.3 (d, J_{CF} = 9.1 Hz), 107.9 (d, J_{CF} = 24.2 Hz), 107.7, 79.8, 61.6, 51.8 (d, *J* = 7.2 Hz, 2C), 40.5, 31.8, 28.4 (3C), 24.6 (2C), 9.5 (2C); **^{19}F NMR** (377 MHz, $CDCl_3$) δ -117.9 (s, 1F); **HRMS (ES+)** Calculated for $C_{24}H_{29}FN_3O_6$ ($M+H^+$): 474.2040; found: 474.2052. These spectroscopic data correspond to previously reported data.[257]

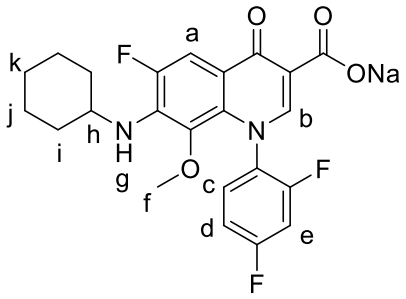
(1*R*,5*S*,6*s*)-3-(3-Carboxy-1-cyclopropyl-6-fluoro-8-methoxy-4-oxo-1,4-dihydroquinolin-7-yl)-3-azabicyclo[3.1.0]hexan-6-aminium methanesulfonate - 174



To a solution of carboxylic acid **172** (150 mg, 0.32 mmol) in THF (5 mL) was added methanesulfonic acid (41 µL, 0.63 mmol) and the solution was heated to reflux for 16 h resulting in precipitate formation. The solvent was decanted, washing with THF (10 mL) to yield mesylate salt **174** as a light brown solid (49 mg, 28 %), with purity of ≥95 % by LC-MS analysis.

Mp (MeOH) 206-207 °C; **^{1}H NMR** (400 MHz, DMSO) δ 14.96 (s, 1H, OH-*k*), 8.68 (s, 1H), 8.18 (s, 3H, NH_3-*a*), 7.70 (d, *J* = 13.2 Hz, 1H, CH-*e*), 4.20 – 4.11 (m, 1H, CH-*g*), 3.75 (d, *J* = 10.3 Hz, 2H), 3.68 – 3.55 (m, 5H, CH_3-*f*), 3.36 (m, 1H, CH-*b*), 2.34 (s, 3H, CH_3-*l*), 2.07 (d, *J* = 12.9 Hz, 2H, 2 x CH-*c*), 1.17 – 1.06 (m, 2H, CH_2-*h*), 1.05 – 0.97 (m, 2H, CH_2-*i*); **^{13}C NMR** (101 MHz, DMSO) δ 176.2 (d, J_{CF} = 2.6 Hz), 165.7, 154.6 (d, J_{CF} = 250.0 Hz), 150.6, 144.6 (d, J_{CF} = 6.3 Hz), 135.7 (d, J_{CF} = 11.2 Hz), 134.2, 119.8 (d, J_{CF} = 9.2 Hz), 106.6, 106.3, 62.2 (2C), 50.9 (d, *J* = 6.4 Hz), 40.8, 29.6, 20.6 (2C), 9.0 (2C); **^{19}F NMR** (376 MHz, DMSO) δ -118.7 (s, 1F); **HRMS (ES+)** Calculated for $C_{21}H_{24}FN_4O_4$ (M+MeCN+H^+): 415.1782; found: 415.1791.

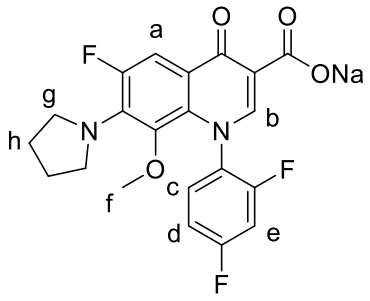
Sodium 7-(cyclohexylamino)-1-(2,4-difluorophenyl)-6-fluoro-8-methoxy-4-oxo-1,4-dihydroquinoline-3-carboxylate - 175



To a suspension of carboxylic acid **150** (90 mg, 0.20 mmol) in EtOH (3 mL) was added NaOH (1 M, 0.20 mL) resulting in a solution which was stirred at rt for 3 h resulting in precipitation. The EtOH was decanted, washing the solid with fresh EtOH (10 mL) to yield sodium salt **175** as a light yellow solid (60 mg, 64 %).

Mp (MeOH) 244-247 °C; **IR V_{max} / cm^{-1}**: 2935, 1636, 1509, 1461, 1401, 1303, 1268, 1093, 1045, 845, 823; **^{1}H NMR** (400 MHz, DMSO + D_2O) δ 7.91 (s, 1H, CH-*b*), 7.71 (td, *J* = 8.8, 5.8 Hz, 1H, CH-*c*), 7.65 (d, *J* = 13.3 Hz, 1H, CH-*a*), 7.26 – 7.10 (m, 2H, CH-*d* + CH-*e*), 3.56 – 3.38 (m, 1H, CH-*h*), 3.01 (s, 3H, CH_3-*f*), 1.88 – 1.70 (m, 2H, CH_2-*i*), 1.69 – 1.54 (m, 2H, CH_2-*i*), 1.48 (m, 1H, CH-*k*), 1.22 – 0.99 (m, 5H, 2 x CH_2-*j* + CH-*k*); **^{13}C NMR** (101 MHz, DMSO + D_2O) δ 175.5 (d, J_{CF} = 2.3 Hz), 170.5, 162.9 (dd, J_{CF} = 248.8, 11.7 Hz), 158.4 (dd, J_{CF} = 252.1, 12.4 Hz), 151.4 (d, J_{CF} = 243.3 Hz), 148.9, 137.6 (d, J_{CF} = 6.6 Hz), 135.6 (d, J_{CF} = 12.0 Hz), 132.8, 129.9 (d, J_{CF} = 16.6 Hz), 129.4 (d, J_{CF} = 9.7 Hz), 120.1, 119.5 (d, J_{CF} = 6.9 Hz), 113.0 (d, J_{CF} = 25.4 Hz), 108.8 (d, J_{CF} = 22.2 Hz), 105.3 (t, J_{CF} = 25.7 Hz), 61.4, 54.2 (d, *J* = 7.3 Hz), 34.7 (d, *J* = 3.9 Hz, 2C), 26.2 (2C), 25.7 (d, *J* = 12.4 Hz); **^{19}F NMR** (376 MHz, DMSO + D_2O) δ -108.3 (d, *J* = 7.3 Hz, 1F), -118.0 (d, *J* = 7.3 Hz, 1F), -128.67 (s, 1F); **HRMS (ES+)** Calculated for $C_{23}H_{22}F_3N_2O_4$ ($M+H^+$): 447.1532; found: 447.1545.

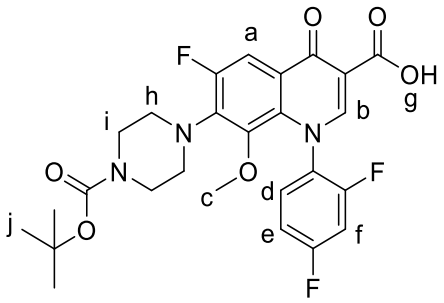
Sodium 1-(2,4-difluorophenyl)-6-fluoro-8-methoxy-4-oxo-7-(pyrrolidin-1-yl)-1,4-dihydroquinoline-3-carboxylate - 176



Following the procedure described for the preparation of sodium salt **175**, the title compound was prepared from carboxylic acid **153** (89 mg, 0.21 mmol) in EtOH (3 mL) with NaOH (1 M, 0.21 mL) to yield sodium salt **176** as an off-white solid (72 mg, 68 %).

Mp (MeOH) >250 °C; **^{1}H NMR** (400 MHz, MeOD + D_2O) δ 8.11 (s, 1H, CH-*b*), 7.73 (d, *J* = 14.5 Hz, 1H, CH-*a*), 7.70 – 7.61 (m, 1H, CH-*c*), 7.19 – 7.10 (m, 2H, CH-*d* + CH-*e*), 3.55 (m, *J* = 6.2 Hz, 2H), 3.03 (s, 3H), 2.00 – 1.88 (m, 2H), 1.88 – 1.75 (m, 2H); **^{13}C NMR** (101 MHz, MeOD + D_2O) δ 176.4 (d, J_{CF} = 2.3 Hz), 172.5, 163.48 (dd, J_{CF} = 249.1, 11.0 Hz), 158.6 (dd, J_{CF} = 251.5, 12.9 Hz), 154.9 (d, J_{CF} = 247.5 Hz), 149.6, 141.1 (d, J_{CF} = 7.0 Hz), 137.2 (d, J_{CF} = 11.8 Hz), 134.1, 130.8 (dd, J_{CF} = 13.3, 4.0 Hz), 128.8 (d, J_{CF} = 10.1 Hz), 120.7 (d, J_{CF} = 8.0 Hz), 119.0, 112.7 (dd, J_{CF} = 22.9, 3.3 Hz), 108.2 (d, J_{CF} = 24.0 Hz), 105.1 (dd, J_{CF} = 26.9, 24.0 Hz), 60.7 (2C), 52.0 (d, *J* = 6.3 Hz), 26.7 (2C); **^{19}F NMR** (377 MHz, MeOD + D_2O) δ -108.5 (d, *J* = 7.7 Hz, 1F), -118.0 (d, *J* = 7.7 Hz, 1F), -121.9 (s, 1F); **HRMS (ES+)** Calculated for $C_{21}H_{18}F_3N_2O_4$ ($M+H^+$): 419.1219; found: 419.1228.

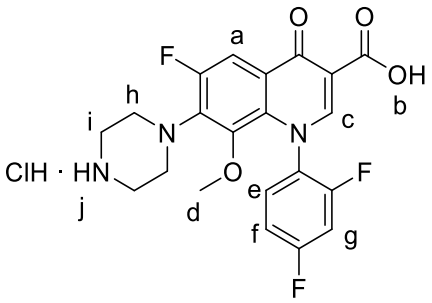
7-(4-(*Tert*-butoxycarbonyl)piperazin-1-yl)-1-(2,4-difluorophenyl)-6-fluoro-8-methoxy-4-oxo-1,4-dihydroquinoline-3-carboxylic acid - 177a



Following the general procedure **B**, the reaction of boron difluoride chelate **146** (50 mg, 0.12 mmol) with 1-boc-piperazine (54 mg, 0.29 mmol) in pyridine (2 mL) followed by hydrolysis of the chelate in EtOH (7 mL) and NEt_3 (0.7 mL) afforded Boc-protected carboxylic acid **177a** as a yellow solid (50 mg, 75 %) after acid-base work up.

IR V_{max} / cm^{-1}: 2928, 1731, 1696, 1620, 1420, 1137, 855, 807; **^{1}H NMR** (400 MHz, $CDCl_3$) δ 14.51 (s, 1H, OH-*g*), 8.47 (s, 1H, CH-*b*), 7.93 (d, *J* = 12.2 Hz, 1H, CH-*a*), 7.48 (td, *J* = 8.6, 5.5 Hz, 1H, CH-*d*), 7.12 – 6.97 (m, 2H, CH-*e* + CH-*f*), 3.61 – 3.42 (m, 4H, 2 x CH_2-*i*), 3.36 – 3.24 (m, 5H, CH_2-*h* + CH_3-*c*), 3.24 – 3.12 (m, 2H, CH_2-*h*), 1.46 (s, 9H, 3 x CH_3-*j*); **^{13}C NMR** (101 MHz, $CDCl_3$) δ 177.5 (d, J_{CF} = 2.5 Hz), 166.3, 162.9 (dd, J_{CF} = 253.5, 10.8 Hz), 157.3 (dd, J_{CF} = 254.6, 12.6 Hz), 156.7 (d, J_{CF} = 252.1 Hz), 154.8, 150.9, 144.4 (d, J_{CF} = 5.6 Hz), 139.3 (d, J_{CF} = 12.1 Hz), 132.8, 129.1 (dd, J_{CF} = 13.3, 4.4 Hz), 127.5 (d, J_{CF} = 9.8 Hz), 121.8 (d, J_{CF} = 9.1 Hz), 112.0 (dd, J_{CF} = 22.8, 3.4 Hz), 108.7, 108.4, 105.1 (dd, J_{CF} = 26.5, 23.0 Hz), 80.3, 61.3, 50.5 (d, *J* = 4.3 Hz, 4C), 28.5 (3C); **^{19}F NMR** (377 MHz, $CDCl_3$) δ -105.8 (d, J = 8.1 Hz, 1F), -116.7 (d, J = 8.1 Hz, 1F), -118.5 (s, 1F); **HRMS (ES+)** Calculated for $C_{26}H_{27}F_3N_3O_6$ ($M+H^+$): 534.1852; found: 534.1851.

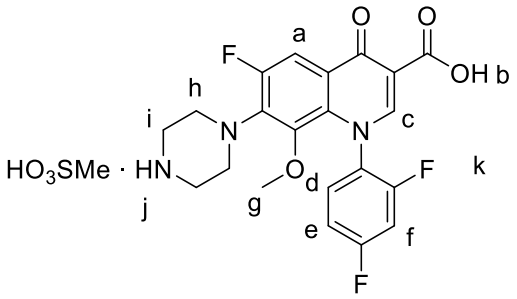
1-(2,4-Difluorophenyl)-6-fluoro-8-methoxy-4-oxo-7-(piperazin-1-yl)-1,4-dihydroquinoline-3-carboxylic acid hydrochloride - 177



HCl (2 M in Et_2O, 1.5 mL) was added to Boc-protected carboxylic acid **177a** (50 mg, 0.094 mmol) and the suspension was stirred at rt for 18 h. The reaction was diluted with Et_2O (3 mL) and the solvent was decanted before the addition of more Et_2O (3 mL). This process was repeated until the additional Et_2O appeared colourless. The precipitate was dried under high vacuum to yield HCl salt **177** as a yellow solid, (45 mg, 100 %) with purity of ≥95 % by LC-MS analysis.

Mp (MeOH) >250 °C; **^{1}H NMR** (500 MHz, DMSO) δ 14.58 (s, 1H, OH-*b*), 9.13 (s, *J* = 51.0 Hz, 2H, NH_2-*j*), 8.60 (s, 1H, CH-*c*), 7.98 (td, *J* = 9.0, 5.9 Hz, 1H, CH-*e*), 7.92 (d, *J* = 12.1 Hz, 1H, CH-*c*), 7.55 (ddd, *J* = 10.6, 9.0, 2.8 Hz, 1H, CH-*f*), 7.33 (m, 1H, CH-*g*), 3.53 – 3.43 (m, 2H, CH_2-*h*), 3.42 – 3.29 (m, 2H, CH_2-*h*), 3.24 (s, 3H, CH_3-*d*), 3.18 (s, 4H, 2 x CH_2-*i*); **^{13}C NMR** (126 MHz, DMSO) δ 176.7 (d, J_{CF} = 1.8 Hz), 165.1, 162.1 (dd, J_{CF} = 248.6, 11.7 Hz), 156.8 (dd, J_{CF} = 251.2, 13.5 Hz), 156.0 (d, J_{CF} = 250.5 Hz), 151.9, 144.9 (d, J_{CF} = 5.1 Hz), 137.9 (d, J_{CF} = 12.3 Hz), 132.7, 128.7 (d, J_{CF} = 9.9 Hz), 121.5 (d, J_{CF} = 9.1 Hz), 111.9 (dd, J_{CF} = 22.3, 2.4 Hz), 107.8, 107.1 (d, J_{CF} = 23.1 Hz), 104.5 (dd, J_{CF} = 27.3, 23.9 Hz), 61.8, 47.0 (2C), 43.3 (2C); **^{19}F NMR** (471 MHz, DMSO) δ -107.9 (d, *J* = 7.9 Hz, 1F), -118.2 (d, *J* = 7.9 Hz, 1F), -119.2 (s, 1F); **HRMS (ES+)** Calculated for $C_{23}H_{22}F_3N_4O_4$ (M+MeCN+H$^+$): 475.1593, found: 475.1585.

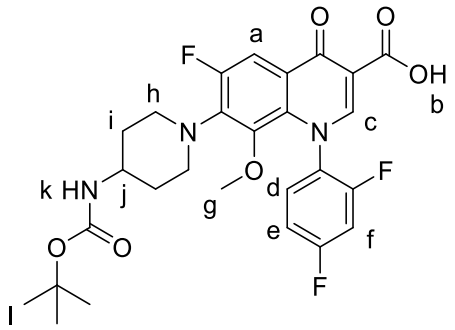
4-(3-Carboxy-1-(2,4-difluorophenyl)-6-fluoro-8-methoxy-4-oxo-1,4-dihydroquinolin-7-yl)piperazin-1-ium mesylate - 178



To a solution of Boc-protected carboxylic acid **177a** (80 mg, 0.14 mmol) in THF (5 mL) was added methanesulfonic acid (45 µL, 0.69 mmol) and the solution was heated to reflux for 16 h resulting in precipitate formation. The solvent was decanted, washing with THF (10 mL) to yield mesylate salt **178** as a white solid (71 mg, 98 %) with purity of ≥95 % by LC-MS analysis.

Mp (MeOH), >250 °C; **IR V_{max} / cm^{-1}**: 3024 (NH_2), 2757, 1731, 1617, 1503, 1436, 1211, 1144, 1042, 944, 807, 775; **^{1}H NMR** (400 MHz, DMSO) δ 8.75 (br s, 2H, NH_2-*j*), 8.61 (s, 1H, CH-*c*), 8.05 – 7.87 (m, 2H, CH-*a* + CH-*d*), 7.62 – 7.49 (m, 1H, CH-*e*), 7.40 – 7.25 (m, 1H, CH-*f*), 3.26 – 3.14 (m, 7H, CH_3-*g* + 2 x CH_2-*h*), 2.32 (s, 4H, 2 x CH_2-*i*); **^{13}C NMR** (101 MHz, DMSO) δ 176.7 (d, J_{CF} = 2.3 Hz), 165.1, 162.2 (dd, J_{CF} = 248.8, 11.2 Hz), 157.3, 156.9 (dd, J_{CF} = 251.2, 13.4 Hz), 156.0 (d, J_{CF} = 250.1 Hz), 154.8, 151.9, 144.9 (d, J_{CF} = 5.3 Hz), 137.9 (d, J_{CF} = 12.2 Hz), 132.7, 128.8 (d, J_{CF} = 12.7 Hz), 128.7 (d, J_{CF} = 10.2 Hz), 121.5 (d, J_{CF} = 9.1 Hz), 111.9 (dd, J_{CF} = 22.8, 2.8 Hz), 107.8, 107.2 (d, J_{CF} = 23.4 Hz), 104.5 (dd, J_{CF} = 27.1, 23.4 Hz), 61.8, 47.0 (2C), 43.5 (2C); **^{19}F NMR** (377 MHz, DMSO) δ -107.9 (d, *J* = 7.9 Hz, 1F), -118.2 (d, *J* = 7.9 Hz, 1F), -119.23 (s, 1F); **HRMS (ES+)** Calculated for $C_{23}H_{22}F_3N_4O_4$ (M+MeCN+H^+): 475.1593, found: 475.1588.

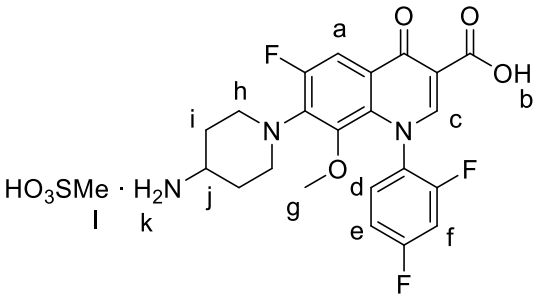
7-(4-((*Tert*-butoxycarbonyl)amino)piperidin-1-yl)-1-(2,4-difluorophenyl)-6-fluoro-8-methoxy-4-oxo-1,4-dihydroquinoline-3-carboxylic acid - 179a



Following the general procedure **B**, the reaction of boron difluoride chelate **146** (100 mg, 0.24 mmol) with *tert*-butyl piperidin-4-yl carbamate (116 mg, 0.58 mmol) in pyridine (5 mL) followed by hydrolysis of the chelate in EtOH (14 mL) and NEt_3 (1.4 mL) afforded Boc-protected carboxylic acid **179a** as a brown oil (102 mg, 78 %) after acid-base work up.

IR V_{max} / cm^{-1}: 3354, 2938, 1703, 1620, 1506, 1436, 1363, 1322, 1147, 807, 737; **^{1}H NMR** (400 MHz, $CDCl_3$) δ 14.61 (s, 1H, OH-*b*), 8.49 (s, 1H, CH-*c*), 7.95 (d, *J* = 12.2 Hz, 1H, CH-*a*), 7.48 – 7.37 (m, 1H, CH-*d*), 7.12 – 6.96 (m, 2H, CH-*e* + CH-*f*), 4.49 (br s, 1H, NH-*k*), 3.73 – 3.52 (m, 1H, CH-*j*), 3.41 (dd, *J* = 31.9, 12.9 Hz, 2H, CH_2-*h*), 3.28 – 3.17 (m, 4H, CH_3-*g* + CH-*h*), 3.11 (t, *J* = 11.9 Hz, 1H, CH-*h*), 2.01 (dd, *J* = 8.8, 3.7 Hz, 2H, CH_2-*i*), 1.57 – 1.46 (m, 2H, CH_2-*i* under H_2O), 1.45 (s, 9H, 3 x CH_3-*l*); **^{13}C NMR** (101 MHz, $CDCl_3$) δ 177.5 (d, J_{CF} = 2.5 Hz), 166.4, 162.9 (dd, J_{CF} = 253.7, 10.9 Hz), 157.4 (dd, J_{CF} = 254.4, 12.6 Hz), 156.9 (d, J_{CF} = 251.9 Hz), 155.2, 150.8, 144.3 (d, J_{CF} = 5.6 Hz), 139.8 (d, J_{CF} = 12.3 Hz), 132.9, 129.2 (dd, J_{CF} = 13.5, 4.3 Hz), 127.5 (d, J_{CF} = 9.9 Hz), 121.4 (d, J_{CF} = 9.3 Hz), 111.9 (dd, J_{CF} = 22.7, 3.6 Hz), 108.6, 108.4 (d, J_{CF} = 23.9 Hz), 105.1 (dd, J_{CF} = 26.6, 23.0 Hz), 79.7, 61.3 (2C), 49.8 (dd, *J* = 34.2, 4.1 Hz), 47.7, 33.4 (d, *J* = 14.4 Hz, 2C)), 28.5 (3C); **^{19}F NMR** (377 MHz, $CDCl_3$) δ -105.9 (d, *J* = 8.1 Hz 1F), -116.7 (d, *J* = 8.1 Hz, 1F), -118.36 (s, 1F); **HRMS (ES+)** Calculated for $C_{27}H_{29}F_3N_3O_6$ ($M+H^+$): 548.2008; found: 548.2009.

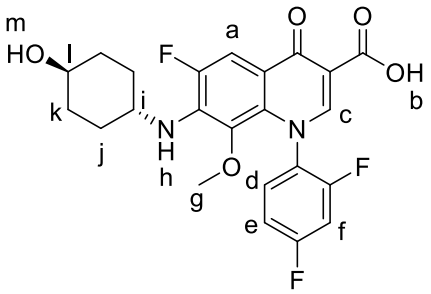
1-(3-Carboxy-1-(2,4-difluorophenyl)-6-fluoro-8-methoxy-4-oxo-1,4-dihydroquinolin-7-yl)piperidin-4-aminium mesylate - 179



Following the procedure described for the preparation of mesylate salt **178**, the title compound was prepared from Boc-protected carboxylic acid **179a** (102 mg, 0.19 mmol) in THF (5 mL) with methanesulfonic acid (60 µL, 0.92 mmol) to yield mesylate salt **179** as a light yellow solid (76 mg, 92 %) with purity of ≥95 % by LC-MS analysis.

Mp (MeOH) >250 °C; **IR V_{max} / cm^{-1}**: 3062, 2947, 2843, 1725, 1623, 1499, 1449, 1325, 1191, 1042, 779; **^{1}H NMR** (400 MHz, DMSO) δ 8.58 (s, 1H, CH-*c*), 7.93 – 7.80 (m, 5H, CH-*a* + CH-*d* + $^{+}NH_3$-*k*), 7.55 (ddd, *J* = 10.7, 9.0, 2.8 1H, CH-*e*), 7.36 – 7.28 (m, 1H, CH-*f*), 3.19 (s, 6H, CH_3-*g* + CH-*j* + CH_2-*h*), 3.13 – 3.01 (m, 2H, CH_2-*h*), 2.34 (s, 3H, CH_3-*l*), 1.93 (s, 2H, CH_2-*i*), 1.73 – 1.52 (m, 2H, CH_2-*i*); **^{13}C NMR** (101 MHz, DMSO) δ 176.7 (d, J_{CF} = 1.7 Hz), 165.1, 162.1 (dd, J_{CF} = 248.7, 11.6 Hz), 156.8 (dd, J_{CF} = 251.2, 13.3 Hz), 156.0 (d, J_{CF} = 249.9 Hz), 151.7, 144.4 (d, J_{CF} = 5.6 Hz), 138.9 (d, J_{CF} = 12.3 Hz), 132.8, 128.8 (dd, J_{CF} = 13.3, 3.8 Hz), 128.6 (d, J_{CF} = 10.2 Hz), 120.4 (d, J_{CF} = 9.0 Hz), 112.1 – 111.5 (m), 107.6, 107.0 (d, J_{CF} = 23.4 Hz), 104.4 (dd, J_{CF} = 27.2, 23.9 Hz), 61.6 (2C), 49.1 – 47.8 (m), 47.4, 30.2 (d, *J* = 26.7 Hz, 2C); **^{19}F NMR** (377 MHz, DMSO) δ -107.98 (d, *J* = 7.5 Hz, 1F), -118.3 (d, *J* = 7.5 Hz, 1F), -119.3 (s, 1F); **HRMS (ES+)** Calculated for $C_{22}H_{21}F_3N_3O_4$ ($M+H^+$): 448.1484; found: 448.1489.

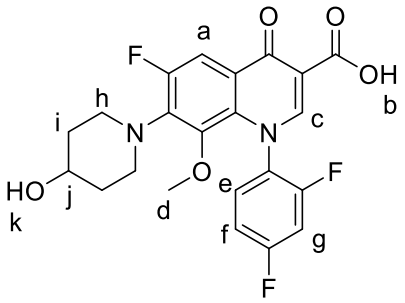
1-(2,4-Difluorophenyl)-6-fluoro-7-((1*r*,4*r*)-4-hydroxycyclohexylamino)-8-methoxy-4-oxo-1,4-dihydroquinoline-3-carboxylic acid - 180



Following the general procedure **B**, the reaction of boron difluoride chelate **146** (50 mg, 0.12 mmol) with *trans*-4-amino-cyclohexanol (33 mg, 0.29 mmol) in pyridine (3 mL) followed by hydrolysis of the chelate in EtOH (7 mL) and NEt_3 (0.7 mL) afforded carboxylic acid **180** as a yellow solid (50 mg, 90 %) after acid-base work up, with purity of ≥95 % by LC-MS analysis.

Mp (MeOH) >250 °C; **IR V_{max} / cm^{-1}**: 3513, 3316, 2938, 1719, 1620, 1499, 1436, 1322, 1083, 966, 804; **^{1}H NMR** (400 MHz, DMSO) δ 15.04 (s, 1H, OH-*b*), 8.49 (s, 1H, CH-*c*), 8.03 (td, *J* = 9.0, 5.9 Hz, 1H, CH-*d*), 7.81 (d, *J* = 13.4 Hz, 1H, CH-*a*), 7.52 (ddd, *J* = 10.8, 9.0, 2.8 Hz, 1H, CH-*e*), 7.35 – 7.28 (m, 1H, CH-*f*), 5.68 (dd, *J* = 8.8, 1.6 Hz, 1H, OH-*m*), 4.55 (d, *J* = 3.8 Hz, 1H, NH-*h*), 3.61 (m, 1H, CH-*i*), 3.46 – 3.30 (m, 1H, CH-*l* under H_2O), 3.06 (s, 3H, CH_3-*g*), 1.93 – 1.70 (m, 4H, 2 x CH_2-*j*), 1.47 – 1.30 (m, 2H, CH_2-*k*), 1.29 – 1.06 (m, 2H, CH_2-*k*); **^{13}C NMR** (126 MHz, DMSO) δ 176.5 (d, J_{CF} = 2.2 Hz), 165.5, 162.1 (dd, J_{CF} = 248.3, 11.4 Hz), 157.1 (dd, J_{CF} = 251.3, 13.5 Hz), 151.0, 150.3 (d, J_{CF} = 246.2 Hz), 136.6 (d, J_{CF} = 11.0 Hz), 136.1 (d, J_{CF} = 7.5 Hz), 132.2, 128.8 (d, J_{CF} = 10.5 Hz), 128.5 (dd, J_{CF} = 13.0, 3.4 Hz), 114.6 (d, J_{CF} = 8.4 Hz), 111.7 (dd, J_{CF} = 22.8, 2.4 Hz), 107.7 (d, J_{CF} = 22.7 Hz), 107.0, 104.3 (dd, J_{CF} = 27.3, 23.7 Hz), 68.2, 60.2, 52.9 (d, *J* = 9.2 Hz), 34.0 (d, *J* = 11.2 Hz, 2C), 31.6 (2C); **^{19}F NMR** (377 MHz, DMSO) δ -108.1 (d, *J* = 8.0 Hz, 1F), -117.6 (d, *J* = 8.0 Hz, 1F), -126.37 (s, 1F); **HRMS (ES+)** Calculated for $C_{23}H_{22}F_3N_2O_5$ ($M+H^+$): 463.1481; found: 463.1489.

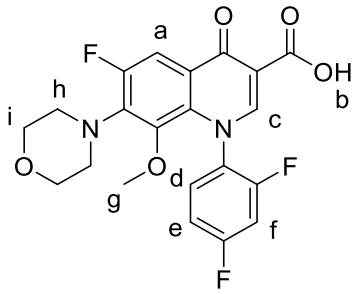
1-(2,4-Difluorophenyl)-6-fluoro-7-(4-hydroxypiperidin-1-yl)-8-methoxy-4-oxo-1,4-dihydroquinoline-3-carboxylic acid - 181



Following the general procedure **B**, the reaction of boron difluoride chelate **146** (50 mg, 0.12 mmol) with 4-hydroxypiperidine (29 mg, 0.29 mmol) in pyridine (3 mL) followed by hydrolysis of the chelate in EtOH (7 mL) and NEt_3 (0.7 mL) afforded carboxylic acid **181** as a yellow solid (39 mg, 75 %) after acid-base work up, with purity of ≥95 % by LC-MS analysis.

Mp (MeOH) 237-240 °C; **IR V_{max} / cm^{-1}**: 3408, 2938, 1719, 1623, 1499, 1436, 1322, 1074, 972, 804; **^{1}H NMR** (400 MHz, DMSO) δ 14.72 (s, 1H, OH-*b*), 8.55 (s, 1H, CH-*c*), 7.95 (td, *J* = 8.9, 5.9 Hz, 1H, CH-*e*), 7.83 (d, *J* = 12.3 Hz, 1H, CH-*a*), 7.59 – 7.48 (m, 1H, CH-*f*), 7.36 – 7.24 (m, 1H, CH-*g*), 4.76 (d, *J* = 4.0 Hz, 1H, OH-*k*), 3.71 – 3.57 (m, 1H, CH-*j*), 3.39 – 3.23 (m, 2H, CH_2-*h* under H_2O), 3.22 – 3.06 (m, 4H, CH_3-*d* + CH-*h*), 2.99 (t, *J* = 10.5 Hz, 1H, CH-*h*), 1.90 – 1.71 (m, 2H, CH_2-*i*), 1.59 – 1.37 (m, 2H, CH_2-*i*); **^{13}C NMR** (101 MHz, MeOD) δ 176.7 (d, J_{CF} = 2.3 Hz), 165.2, 162.1 (dd, J_{CF} = 248.9, 11.9 Hz), 156.8 (dd, J_{CF} = 250.1, 12.9 Hz), 156.1 (d, J_{CF} = 249.9 Hz), 151.5, 144.1 (d, J_{CF} = 5.7 Hz), 139.5 (d, J_{CF} = 12.0 Hz), 132.9, 128.9 (dd, J_{CF} = 13.0, 3.9 Hz), 128.5 (d, J_{CF} = 10.2 Hz), 120.0 (d, J_{CF} = 9.2 Hz), 111.8 (dd, J_{CF} = 22.9, 3.1 Hz), 107.5, 106.9 (d, J_{CF} = 23.3 Hz), 104.5 (dd, J_{CF} = 26.9, 24.3 Hz), 65.6, 61.4, 48.2 (dd, *J* = 25.8, 3.2 Hz), 34.9 (d, *J* = 18.2 Hz); **^{19}F NMR** (377 MHz, DMSO) δ -108.0 (d, *J* = 7.7 Hz, 1F), -118.4 (d, *J* = 7.7 Hz, 1F), -119.0 (s, 1F); **HRMS (ES+)** Calculated for $C_{22}H_{20}F_3N_2O_5$ ($M+H^+$): 449.1324; found: 449.1330.

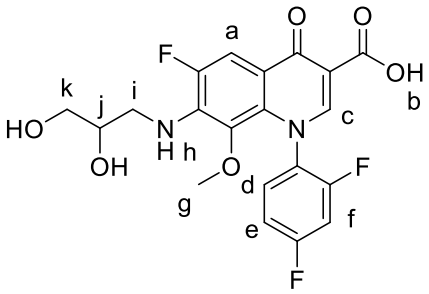
1-(2,4-Difluorophenyl)-6-fluoro-8-methoxy-7-morpholino-4-oxo-1,4-dihydroquinoline-3-carboxylic acid - 182



Following the general procedure **B**, the reaction of boron difluoride chelate **146** (100 mg, 0.24 mmol) with morpholine (51 µL, 0.58 mmol) in pyridine (5 mL) followed by hydrolysis of the chelate in EtOH (14 mL) and NEt_3 (1.4 mL) afforded carboxylic acid **182** as a yellow solid (90 mg, 85 %) after acid-base work up, with purity of ≥95 % by LC-MS analysis.

Mp (MeOH) 231-233 °C; **^{1}H NMR** (400 MHz, DMSO) δ 14.75 (br s, 1H, OH-*b*), 8.57 (s, 1H, CH-*c*), 7.95 (td, *J* = 8.9, 5.9 Hz, 1H, CH-*d*), 7.87 (d, *J* = 12.4 Hz, 1H, CH-*a*), 7.56 – 7.47 (m, 1H, CH-*e*), 7.35 – 7.27 (m, 1H, CH-*f*), 3.71 – 3.64 (m, 4H, 2 x CH_2-*h*), 3.33 – 3.25 (m, 2H, CH_2-*i*), 3.22 (s, 3H, CH_3-*g*), 3.18 – 3.09 (m, 2H, CH_2-*i*); **^{13}C NMR** (101 MHz, DMSO) δ 176.8 (d, J_{CF} = 2.3 Hz), 165.4, 162.2 (dd, J_{CF} = 248.6, 11.5 Hz), 156.9 (dd, J_{CF} = 251.1, 13.4 Hz), 156.1 (d, J_{CF} = 250.3 Hz), 151.8, 144.5 (d, J_{CF} = 5.8 Hz), 138.7 (d, J_{CF} = 11.6 Hz), 133.0, 128.9 (dd, J_{CF} = 13.4, 3.7 Hz), 128.7 (d, J_{CF} = 10.3 Hz), 120.7 (d, J_{CF} = 9.2 Hz), 112.0 (dd, J_{CF} = 22.6, 2.5 Hz), 107.8, 107.2 (d, J_{CF} = 23.4 Hz), 104.6 (dd, J_{CF} = 27.3, 23.7 Hz), 66.7 (2C), 61.6, 50.5 (d, *J* = 3.8 Hz, 2C). **^{19}F NMR** (377 MHz, DMSO) δ -107.9 (d, *J* = 7.9 Hz, 1F), -118.3 (d, *J* = 7.9 Hz, 1F), -119.3 (s, 1F); **HRMS (ES+)** Calculated for $C_{21}H_{18}F_3N_2O_5$ ($M+H^+$): 435.1168; found: 435.1171.

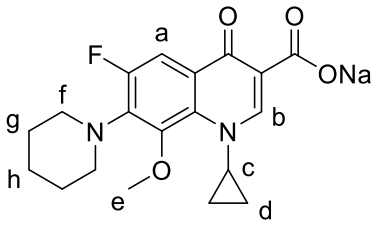
(±)-1-(2,4-Difluorophenyl)-7-((2,3-dihydroxypropyl)amino)-6-fluoro-8-methoxy-4-oxo-1,4-dihydroquinoline-3-carboxylic acid - 183



Following the general procedure **B**, the reaction of boron difluoride chelate **146** (100 mg, 0.24 mmol) with 3-aminopropane-1,2-diol (45 µL, 0.58 mmol) in pyridine (5 mL) followed by hydrolysis of the chelate in EtOH (14 mL) and NEt_3 (1.4 mL) afforded carboxylic acid **183** as a yellow solid (90 mg, 84 %) after acid-base work up.

^{1}H NMR (400 MHz, MeOD) δ 8.53 (s, 1H, OH-*b*), 7.90 – 7.80 (m, 2H, CH-*c* + CH-*d*), 7.29 – 7.17 (m, 2H, CH-*e* + CH-*f*), 3.86 – 3.75 (m, 1H, CH-*k*), 3.74 – 3.63 (m, 1H, CH-*j*), 3.59 – 3.54 (m, 2H, CH_2-*i*), 3.49 – 3.39 (m, 1H, CH-*k*), 3.22 (s, 3H, CH_3-*g*); **^{13}C NMR** (101 MHz, MeOD) δ 178.6 (d, J_{CF} = 3.2 Hz), 169.0, 164.5 (dd, J_{CF} = 250.6, 11.1 Hz), 159.2 (dd, J_{CF} = 258.1, 4.7 Hz), 152.6 (dd, J_{CF} = 246.3, 5.2 Hz), 139.3 (d, J_{CF} = 11.6), 137.8 (d, J_{CF} = 6.0 Hz), 133.8, 130.0 (dd, J_{CF} = 12.9, 3.9 Hz), 129.6 (t, J_{CF} = 10.2 Hz), 117.0 (d, J_{CF} = 7.9 Hz), 112.8 (dd, J_{CF} = 22.7, 3.3 Hz), 108.9 (dd, J_{CF} = 22.6, 5.0 Hz), 108.5, 105.6 (ddd, J_{CF} = 27.3, 23.8, 3.0 Hz), 105.2, 72.3 (d, J = 13.0 Hz), 65.3, 61.2, 30.7; **^{19}F NMR** (377 MHz, MeOD) δ -109.0 (t, J = 7.8 Hz, 1F), -118.7 (dd, J = 41.1, 7.4 Hz, 1F), -128.6 (d, J = 21.3 Hz, 1F).

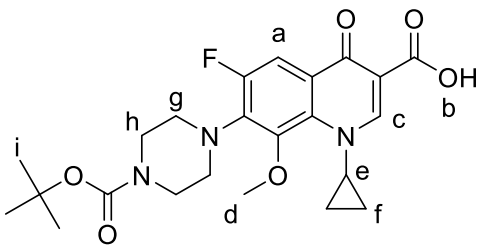
Sodium 1-cyclopropyl-6-fluoro-8-methoxy-4-oxo-7-(piperidin-1-yl)-1,4-dihydroquinoline-3-carboxylate - 184



Following the procedure described for the preparation of sodium salt **175**, the title compound was prepared from carboxylic acid **161** (40 mg, 0.11 mmol) in EtOH (3 mL) with NaOH (1 M, 0.11 mL) to yield sodium salt **184** as a light yellow solid solid (20 mg, 47 %).

IR V_{max} / cm^{-1}: 3386, 2935, 1617, 1588, 1445, 1277, 1055, 950, 823; **^{1}H NMR** (400 MHz, DMSO + D_2O) δ 8.35 (s, 1H, CH-*b*), 7.56 (d, *J* = 12.8 Hz, 1H, CH-*a*), 3.97 – 3.86 (m, 1H, CH-*c*), 3.66 (s, 3H, CH_3-*e*), 3.15 (br s, 4H, 2 x CH_2-*f*), 1.57 (br s, 6H, 2 x CH_2-*g* + CH_2-*h*), 1.08 – 0.94 (m, 2H, CH_2-*d*), 0.85 – 0.72 (m, 2H, CH_2-*d*); **^{13}C NMR** (101 MHz, DMSO + D_2O) δ 175.0, 170.4, 156.2 (d, J_{CF} = 246.5 Hz), 149.5, 146.6 (d, J_{CF} = 5.3 Hz), 139.5 (d, J_{CF} = 12.1 Hz), 134.4, 124.5 (d, J_{CF} = 7.6 Hz), 118.6, 107.8 (d, J_{CF} = 22.7 Hz), 63.5, 52.7 (2C), 40.4, 27.3 (2C), 24.7, 9.8 (2C); **^{19}F NMR** (377 MHz, DMSO + D_2O) δ -123.1 (s, 1F).

7-(4-(*Tert*-butoxycarbonyl)piperazin-1-yl)-1-cyclopropyl-6-fluoro-8-methoxy-4-oxo-1,4-dihydroquinoline-3-carboxylic acid - 185a

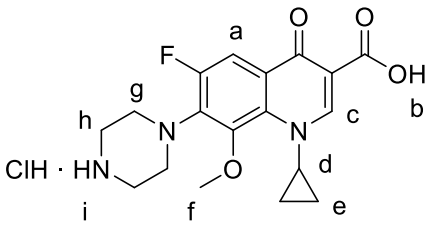


Following the general procedure **B**, the reaction of boron difluoride chelate **147** (80 mg, 0.23 mmol) with 1-boc-piperazine (104 mg, 0.56 mmol) in pyridine (3 mL) followed by hydrolysis

of the chelate in EtOH (7 mL) and NEt_3 (0.7 mL) afforded Boc-protected carboxylic acid **185a** as a yellow solid (73 mg, 65 %) after acid-base work up.

IR V_{max} / cm^{-1}: 2979, 1731, 1693, 1620, 1449, 1169, 807; **^{1}H NMR** (400 MHz, $CDCl_3$) δ 14.68 (s, 1H, OH-*b*), 8.77 (s, 1H, CH-*c*), 7.81 (d, *J* = 12.1 Hz, 1H, CH-*a*), 4.02 (ddd, *J* = 11.1, 7.4, 4.0 Hz, 1H, CH-*e*), 3.79 (s, 3H, CH_3-*d*), 3.65 – 3.54 (m, 4H, 2 x CH_2-*h*), 3.41 – 3.28 (m, 4H, 2 x CH_2-*g*), 1.48 (s, 9H, 3 x CH_3-*i*), 1.28 – 1.14 (m, 2H, CH_2-*f*), 1.06 – 0.89 (m, 2H, CH_2-*f*); **^{13}C NMR** (126 MHz, $CDCl_3$) δ 177.0 (d, J_{CF} = 2.0 Hz), 166.6, 156.0 (d, J_{CF} = 251.5 Hz), 154.7, 150.0, 145.5 (d, J_{CF} = 5.2 Hz), 139.3 (d, J_{CF} = 11.9 Hz), 133.8, 122.1 (d, J_{CF} = 9.2 Hz), 108.3 (d, J_{CF} = 23.4 Hz), 107.7, 80.1, 62.4, 50.6 (d, *J* = 4.1 Hz, 4C), 40.5, 28.4 (3C), 9.5 (2C); **^{19}F NMR** (377 MHz, $CDCl_3$) δ -119.4 (s, 1F); **HRMS (ES+)** Calculated for $C_{23}H_{29}FN_3O_6$ ($M+H^+$): 462.2040; found: 462.2049.

1-Cyclopropyl-6-fluoro-8-methoxy-4-oxo-7-(piperazin-1-yl)-1,4-dihydroquinoline-3-carboxylic acid hydrochloride - 185

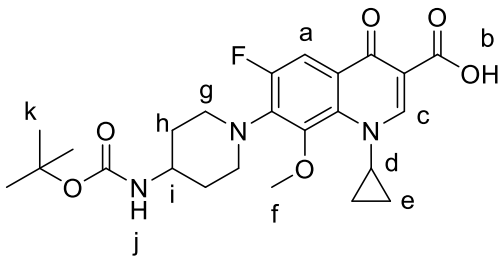


Following the procedure described for the preparation of HCl salt **177**, the title compound was prepared from Boc-protected carboxylic acid **185a** (46 mg, 0.10 mmol) in HCl (2 M in Et_2O, 1.5 mL) to afford HCl salt **185** as a light yellow solid (38 mg, 96 %) with purity of ≥95 % by LC-MS analysis.

Mp (MeOH) 224-227 °C; **^{1}H NMR** (400 MHz, DMSO) δ 9.53 (s, 2H, NH_2-*i*), 8.72 (s, 1H, CH-*c*), 7.79 (d, *J* = 12.0 Hz, 1H, CH-*a*), 4.23 – 4.12 (m, 1H, CH-*d*), 3.81 (s, 3H, CH_3-*f*), 3.64 – 3.48 (m, 4H, 2 x CH_2-*g* overlapping with H_2O), 3.24 (s, 4H, 2 x CH_2-*h*), 1.18 – 1.00 (m, 4H, 2 x CH_2-*e*), OH-*b* very broad – could not be integrated; **^{13}C NMR** (101 MHz, MeOD) δ 178.4 (d,

J_{CF} = 0.6 Hz), 169.1, 157.58 (d, J_{CF} = 249.5 Hz), 152.3, 148.1 (d, J_{CF} = 4.4 Hz), 139.6 (d, J_{CF} = 12.2 Hz), 135.5, 124.4 (d, J_{CF} = 9.1 Hz), 108.7 (d, J_{CF} = 23.5 Hz), 108.2, 63.7, 45.4 (2C), 42.0 (2C), 30.7, 10.0 (2C); **^{19}F NMR** (377 MHz, MeOD) δ -121.7 (s, 1F); **HRMS (ES+)** Calculated for $C_{18}H_{21}FN_3O_4$ ($M+H^+$): 362.1516; found: 362.1522 and calculated for $C_{20}H_{24}FN_4O_4$ ($M+MeCN+H^+$): 403.1782; found: 403.1803.

7-(4-((*Tert*-butoxycarbonyl)amino)piperidin-1-yl)-1-cyclopropyl-6-fluoro-8-methoxy-4-oxo-1,4-dihydroquinoline-3-carboxylic acid - 186a

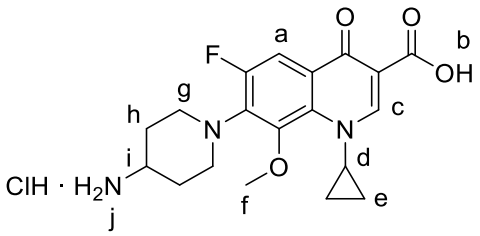


Following the general procedure **B**, the reaction of boron difluoride chelate **147** (50 mg, 0.15 mmol) with *tert*-butyl piperidin-4-ylcarbamate (72 mg, 0.36 mmol) in pyridine (3 mL) followed by hydrolysis of the chelate in EtOH (7 mL) and NEt_3 (0.7 mL) afforded Boc-protected carboxylic acid **186a** as a yellow solid (70 mg, 99 %) after acid-base work up.

IR V_{max} / cm^{-1}: 3309, 2973, 2941, 2855, 1731, 1674, 1620, 1509, 1452, 1388, 1315, 1236, 1166, 1030, 944, 807; **^{1}H NMR** (400 MHz, $CDCl_3$) δ 14.79 (s, 1H, OH-*b*), 8.79 (s, 1H, CH-*c*), 7.84 (d, *J* = 12.1 Hz, 1H, CH-*a*), 4.56 (br s, 1H, NH-*j*), 4.07 – 3.97 (m, 1H, CH-*d*), 3.80 – 3.60 (m, 4H, CH_3-*f* + CH-*i*), 3.53 (d, *J* = 12.7 Hz, 2H, CH_2-*g*), 3.27 (dd, *J* = 12.7, 11.5 Hz, 2H, CH_2-*g*), 2.07 (dd, *J* = 12.4, 2.8 Hz, 2H, CH_2-*h*), 1.59 (ddd, *J* = 23.5, 11.5, 4.0 Hz, 2H, CH_2-*h*), 1.46 (s, 9H, 3 x CH_3-*k*), 1.27 – 1.17 (m, 2H, CH_2-*e*), 1.03 – 0.94 (m, 2H, CH_2-*e*); **^{13}C NMR** (101 MHz, $CDCl_3$) δ 177.2 (d, J_{CF} = 2.7 Hz), 166.9, 156.4 (d, J_{CF} = 251.3 Hz), 155.3, 150.0, 145.6 (d, J_{CF} = 5.5 Hz), 140.0 (d, J_{CF} = 12.2 Hz), 134.1, 121.9 (d, J_{CF} = 9.2 Hz), 108.3 (d, J_{CF} = 23.5 Hz), 107.9, 79.7, 62.6, 50.2 (d, *J* = 4.1 Hz, 2C), 47.9, 40.7, 33.5 (2C), 28.6 (3C), 9.7

(2C); **^{19}F NMR** (377 MHz, $CDCl_3$) δ -119.3 (s, 1F); **HRMS (ES+)** Calculated for $C_{24}H_{31}FN_3O_6$ (M+ H^+): 476.2197; found: 476.2198.

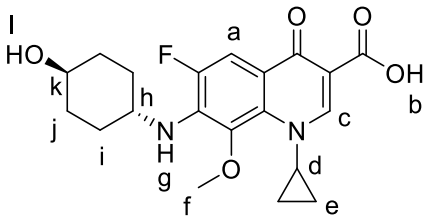
7-(4-Aminopiperidin-1-yl)-1-cyclopropyl-6-fluoro-8-methoxy-4-oxo-1,4-dihydroquinoline-3-carboxylic acid hydrochloride - 186



Following the procedure described for the preparation of **177**, the title compound was prepared from Boc-protected carboxylic acid **186a** (60 mg, 1.2 mmol) in HCl (4 M in dioxane, 1.5 mL) to yield HCl salt **186** as a yellow solid (50 mg, 98 %), with purity of ≥95 % by LC-MS analysis.

Mp (MeOH) >250 °C; **IR V_{max} / cm^{-1}**: 2941, 2852, 2589, 2512, 1696, 1623, 1496, 1430, 1318, 1220, 1115, 1033; **^{1}H NMR** (400 MHz, DMSO) δ 8.69 (s, 1H, CH-*c*), 8.36 (br s, 3H, $^+NH_3$-*j*), 7.74 (d, *J* = 12.1 Hz, 1H, CH-*a*), 4.22 – 4.11 (m, 1H, CH-*d*), 3.56 (s, 3H, CH_3-*f*), 3.51 (d, *J* = 12.7 Hz, 2H, CH_2-*g*), 3.34 – 3.15 (m, 3H, CH-*i* + CH_2-*g*), 2.04 (dd, *J* = 12.2, 2.5 Hz, 2H, CH_2-*h*), 1.78 (qd, *J* = 12.2, 3.9 Hz, 2H, CH_2-*h*), 1.18 – 0.95 (m, 4H, 2 x CH_2-*e*); **^{13}C NMR** (101 MHz, DMSO) δ 176.3 (d, *J* = 2.3 Hz), 165.6, 155.6 (d, *J* = 249.3 Hz), 150.5, 146.1 (d, *J* = 5.5 Hz), 139.2 (d, *J* = 11.9 Hz), 134.1, 120.9 (d, *J* = 9.3 Hz), 106.6 (d, *J* = 9.0 Hz), 106.4, 66.3 (2C), 62.9, 48.7 (d, *J* = 3.7 Hz), 47.4, 30.3 (2C), 9.00 (2C); **^{19}F NMR** (377 MHz, DMSO) δ -120.2 (s, 1F); **HRMS (ES+)** Calculated for $C_{19}H_{23}FN_3O_4$ (M+ H^+): 376.1673; found: 376.1671.

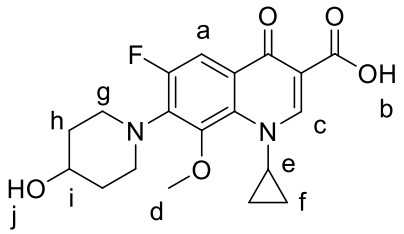
1-Cyclopropyl-6-fluoro-7-((1*r*,4*r*)-4-hydroxycyclohexylamino)-8-methoxy-4-oxo-1,4-dihydroquinoline-3-carboxylic acid - 187



Following the general procedure **B**, the reaction of boron difluoride chelate **147** (50 mg, 0.15 mmol) with *trans*-4-amino-cyclohexanol (41 mg, 0.36 mmol) in pyridine (3 mL) followed by hydrolysis of the chelate in EtOH (7 mL) and NEt_3 (0.7 mL) afforded carboxylic acid **187** as a yellow solid (50 mg, 91 %) after acid-base work up, with purity of ≥95 % by LC-MS analysis.

Mp (MeOH) 208-210 °C; **IR V_{max} / cm^{-1}**: 3446, 3417, 2935, 1693, 1623, 1525, 1445, 1331, 1045, 902, 807; **^{1}H NMR** (400 MHz, DMSO) δ 15.21 (s, 1H, OH-*b*), 8.62 (s, 1H, CH-*c*), 7.70 (d, *J* = 13.0 Hz, 1H, CH-*a*), 5.61 (dd, *J* = 8.9, 1.9 Hz, 1H, OH-*l*), 4.57 (d, *J* = 3.9 Hz, 1H, NH-*g*), 4.20 – 4.07 (m, 1H, CH-*d*), 3.76 – 3.59 (m, 4H, CH_3-*f* + CH-*h*), 3.47 – 3.35 (m, 1H, CH-*k*), 1.98 – 1.77 (m, 4H, 2 x CH_2-*i*), 1.43 (dd, *J* = 24.0, 11.3 Hz, 2H, CH_2-*j*), 1.24 (m, 2H, CH_2-*j*), 1.15 – 1.05 (m, 2H, CH_2-*e*), 1.05 – 0.94 (m, 2H, CH_2-*e*); **^{13}C NMR** (101 MHz, DMSO) δ 176.1 (d, J_{CF} = 2.8 Hz), 165.9, 150.3 (d, J_{CF} = 245.4 Hz), 150.1, 137.6 (d, J_{CF} = 7.2 Hz), 136.7 (d, J_{CF} = 11.2 Hz), 133.4, 115.6 (d, J_{CF} = 8.4 Hz), 107.1 (d, J_{CF} = 22.8 Hz), 106.0, 68.2, 61.3, 52.8 (d, *J* = 8.1 Hz), 34.0 (2C), 31.6 (2C), 9.1 (2C); **^{19}F NMR** (377 MHz, DMSO) δ -127.0 (s, 1F); **HRMS (ES+)** Calculated for $C_{20}H_{24}FN_2O_5$ ($M+H^+$): 391.1669; found: 391.1672.

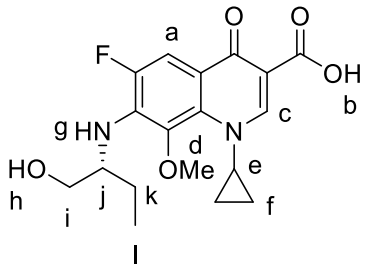
1-Cyclopropyl-6-fluoro-7-(4-hydroxypiperidin-1-yl)-8-methoxy-4-oxo-1,4-dihydroquinoline-3-carboxylic acid - 188



Following the general procedure **B**, the reaction of boron difluoride chelate **147** (50 mg, 0.15 mmol) with 4-hydroxypiperidine (36 mg, 0.36 mmol) in pyridine (3 mL) followed by hydrolysis of the chelate in EtOH (7 mL) and NEt_3 (0.7 mL) afforded carboxylic acid **188** as a yellow solid (40 mg, 70 %) after acid-base work up, with purity of ≥95 % by LC-MS analysis.

Mp (MeOH) 206-208 °C; **^{1}H NMR** (400 MHz, DMSO) δ 14.95 (s, 1H, OH-*b*), 8.67 (s, 1H, CH-*c*), 7.67 (d, *J* = 12.2 Hz, 1H, CH-*a*), 4.80 (d, *J* = 2.4 Hz, 1H, OH-*j*), 4.22 – 4.10 (m, 1H, CH-*e*), 3.81 – 3.62 (m, 4H, CH_3-*d* + CH-*i*), 3.53 – 3.42 (m, 2H, CH_2-*g*), 3.17 (t, *J* = 10.9 Hz, 2H, CH_2-*g*), 1.96 – 1.80 (m, 2H, CH_2-*h*), 1.62 – 1.49 (m, 2H, CH_2-*h*), 1.17 – 1.08 (m, 2H, CH_2-*f*), 1.06 – 0.96 (m, 2H, CH_2-*f*); **^{13}C NMR** (101 MHz, DMSO) δ 176.8 (d, J_{CF} = 2.4 Hz), 166.2, 156.1 (d, J_{CF} = 249.5 Hz), 150.8, 146.3 (d, J_{CF} = 5.6 Hz), 140.2 (d, J_{CF} = 11.8 Hz), 134.6, 120.9 (d, J_{CF} = 9.0 Hz), 107.0 (d, J_{CF} = 11.8 Hz), 106.8, 66.2, 63.1, 48.9 (d, *J* = 3.8 Hz, 2C), 41.3, 35.5 (2C), 9.4 (2C); **^{19}F NMR** (377 MHz, DMSO) δ -120.0 (s, 1F); **HRMS (ES+)** Calculated for $C_{19}H_{22}FN_2O_5$ ($M+H^+$): 377.1513; found: 377.1523.

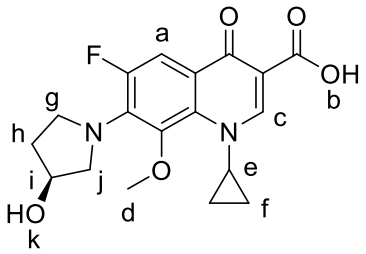
(*R*)-1-Cyclopropyl-6-fluoro-7-(1-hydroxybutan-2-ylamino)-8-methoxy-4-oxo-1,4-dihydroquinoline-3-carboxylic acid - 189



Following the general procedure **B**, the reaction of boron difluoride chelate **147** (50 mg, 0.15 mmol) with (*R*)-2-aminobutan-1-ol (34 µL, 0.36 mmol) in pyridine (3 mL) followed by hydrolysis of the chelate in EtOH (7 mL) and NEt_3 (0.7 mL) afforded carboxylic acid **189** as a yellow solid (31 mg, 40 %) after acid-base work up, with purity of ≥95 % by LC-MS analysis.

Mp ($CHCl_3$) 107-108 °C; **IR V_{max} / cm^{-1}**: 3411, 2925, 1703, 1623, 1442, 1312, 1032, 950, 804; **^{1}H NMR** (400 MHz, $CDCl_3$) δ 15.04 (s, 1H, OH-*b*), 8.73 (s, 1H, CH-*c*), 7.81 (d, *J* = 12.6 Hz, 1H, CH-*a*), 4.78 (d, *J* = 8.6 Hz, 1H, NH-*g*), 4.05 – 3.90 (m, 2H, CH-*e* + CH-*j*), 3.84 (dd, *J* = 11.1, 3.6 Hz, 1H, CH-*i*), 3.79 – 3.68 (m, 4H, CH_3-*d* + CH-*i*), 2.15 (br s, 1H, OH-*h*), 1.81 – 1.59 (m, 2H with H_2O peak, CH_2-*k*), 1.28 – 1.17 (m, 2H, CH_2-*f*), 1.09 – 0.94 (m, 5H, CH_2-*f* + CH_3-*l*); **^{13}C NMR** (101 MHz, $CDCl_3$) δ 176.8 (d, J_{CF} = 3.1 Hz), 167.1, 151.2 (d, J_{CF} = 246.6 Hz), 149.8, 149.5, 137.5 (d, J_{CF} = 6.4 Hz), 137.3 (d, J_{CF} = 11.6 Hz), 133.3, 117.1 (d, J_{CF} = 8.5 Hz), 108.3 (d, J_{CF} = 22.8 Hz), 107.3, 64.16, 61.30, 57.2 (d, *J* = 6.9 Hz), 39.7, 25.6, 10.7, 9.6 (d, *J* = 9.0 Hz, 2C); **^{19}F NMR** (377 MHz, $CDCl_3$) δ -126.7 (s, 1F); **HRMS (ES+)** Calculated for $C_{18}H_{22}FN_2O_5$ ($M+H^+$): 365.1513; found: 365.1518; **$[\alpha]^{35}_D$**: 26.1 ° (c = 0.30, $CHCl_3$).

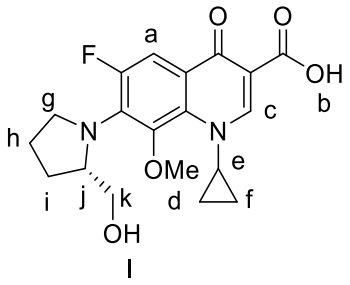
(*S*)-1-Cyclopropyl-6-fluoro-7-(3-hydroxypyrrolidin-1-yl)-8-methoxy-4-oxo-1,4-dihydroquinoline-3-carboxylic acid - 190



Following the general procedure **B**, the reaction of boron difluoride chelate **147** (50 mg, 0.15 mmol) with (*S*)-3-hydroxypyrrolidine (29 µL, 0.36 mmol) in pyridine (3 mL) followed by hydrolysis of the chelate in EtOH (7 mL) and NEt_3 (0.7 mL) afforded carboxylic acid **190** as a yellow solid (24 mg, 30 %) after acid-base work up, with purity of ≥95 % by LC-MS analysis.

Mp (MeOH) 229-233 °C; **IR V_{max} / cm^{-1}**: 3424, 3268, 2928, 1728, 1617, 1433, 1325, 1052, 804; **^{1}H NMR** (400 MHz, DMSO) δ 15.20 (s, 1H, OH-*b*), 8.64 (s, 1H, CH-*c*), 7.64 (d, *J* = 14.0 Hz, 1H, CH-*a*), 5.02 (d, *J* = 3.1 Hz, 1H, OH-*k*), 4.40 (br s, 1H, CH-*i*), 4.19 – 4.08 (m, 1H, CH-*e*), 3.96 – 3.77 (m, 2H, CH_2-*j*), 3.53 (s, 4H, CH_3-*d* + CH-*g*), 3.42 – 3.26 (m, 1H, CH-*g*), 2.08 – 1.80 (m, 2H, CH_2-*h*), 1.20 – 0.87 (m, 4H, 2 x CH_2-*f*); **^{13}C NMR** (101 MHz, DMSO) δ 176.5 (d, J_{CF} = 2.8 Hz), 166.4, 153.5 (d, J_{CF} = 248.9 Hz), 150.6, 141.3 (d, J_{CF} = 7.6 Hz), 137.5 (d, J_{CF} = 10.7 Hz), 135.0, 117.4 (d, J_{CF} = 8.5 Hz), 106.9, 106.7 (d, J_{CF} = 5.5 Hz), 69.5, 61.6, 60.0 (d, *J* = 5.1 Hz), 49.5 (d, *J* = 6.9 Hz), 34.2, 9.9, 8.9 (2C); **^{19}F NMR** (377 MHz, DMSO) δ -121.4 (s, 1F); **HRMS (ES+)** Calculated for $C_{18}H_{20}FN_2O_5$ ($M+H^+$): 363.1356; found: 363.1356; **$[\alpha]^{32}_D$**: -152.5 ° (c = 0.65, DMSO).

(*S*)-1-Cyclopropyl-6-fluoro-7-(2-(hydroxymethyl)pyrrolidin-1-yl)-8-methoxy-4-oxo-1,4-dihydroquinoline-3-carboxylic acid - 191



I

Following the general procedure **B**, the reaction of boron difluoride chelate **147** (50 mg, 0.15 mmol) with (*S*)-prolinol (35 µL, 0.36 mmol) in pyridine (3 mL) followed by hydrolysis of the chelate in EtOH (7 mL) and NEt_3 (0.7 mL) afforded carboxylic acid **191** as a yellow solid (42 mg, 70 %) after acid-base work up, with purity of ≥95 % by LC-MS analysis.

Mp ($CHCl_3$) 168-170 °C; **IR V_{max} / cm^{-1}**: 3427, 2928, 1709, 1623, 1439, 1325, 1039, 801; **^{1}H NMR** (400 MHz, $CDCl_3$) δ 14.98 (s, 1H, OH-*b*), 8.77 (s, 1H, CH-*c*), 7.79 (d, *J* = 13.2 Hz, 1H, CH-*a*), 4.29 (m, 1H, CH-*e*), 4.05 (ddd, *J* = 11.2, 7.5, 4.0 Hz, 1H, CH-*j*), 3.98 – 3.88 (m, 1H, 1H-*g*), 3.76 – 3.66 (m, 4H, CH-*k* + CH_3-*d*), 3.62 (dd, *J* = 11.5, 2.1 Hz, 1H, CH-*k*), 3.38 (t, *J* = 8.2 Hz, 1H, CH-*g*), 2.30 – 2.17 (m, 1H, CH-*i*), 2.17 – 2.07 (m, 1H, CH-*i*), 2.07 – 1.82 (m, 2H, CH_2-*h*) 1.68 (s, 1H, OH-*l*), 1.40 – 1.29 (m, 1H, CH-*f*), 1.18 (dtd, *J* = 10.5, 6.6, 3.9 Hz, 1H, CH-*f*), 1.09 (m, 1H, CH-*f*), 0.94 – 0.81 (m, 1H, CH-*f*); **^{13}C NMR** (126 MHz, $CDCl_3$) δ 176.72 (d, J_{CF} = 2.7 Hz), 166.9, 155.4 (d, J_{CF} = 252.3 Hz), 149.6, 143.3 (d, J_{CF} = 7.2 Hz), 136.2 (d, J_{CF} = 12.0 Hz), 134.2, 119.8 (d, J_{CF} = 9.0 Hz), 107.9 (d, J_{CF} = 23.4 Hz), 107.5, 63.1, 61.2 (d, *J* = 4.9 Hz), 61.0, 53.5 (d, *J* = 5.9 Hz), 40.6, 29.7, 28.3, 25.5, 10.4, 8.5 (2C); **^{19}F NMR** (377 MHz, $CDCl_3$) δ -118.2 (s, 1F); **HRMS (ES+)** Calculated for $C_{19}H_{22}FN_2O_5$ ($M+H^+$): 377.1540; found: 377.1527; **$[\alpha]^{35}_D$**: 290.8 ° (c = 0.18, $CHCl_3$).

7.4. Biological Testing – Part 1

7.4.1. Ex vivo Parasite Experiments

Performed by Tom Blake of the Baum Group at Imperial College London

Parasite Culture

P. falciparum strain D10-PHG[260] were cultured at pH 7.4 in plastic petri dishes using human type O^+ erythrocytes. Cultures were maintained at 4 % haematocrit with 5 % parasitaemia in a RPMI-1640-HEPES medium containing 50 µg/mL hypoxanthine, 20 µg/mL gentamicin, 250 µg/ml L-glutamine and 0.45 % (w/v) Albumax II at 37 °C in an atmosphere of 3% oxygen, 5% carbon dioxide and 92% nitrogen.

Late Stage Schizont and Merozoite Purification

Parasite synchronisation was carried out using 5% sorbitol. Early to mid-stage schizonts (40-44 h post-invasion) were isolated (>95 % purity) for use in the GIA from uninfected erythrocytes with a MAC magnetic separation column (Miltenyi Biotec). For isolation of merozoites, this was followed by incubation of the purified schizonts with E64 (Sigma) in culture media for 6-8 h and subsequently the schizonts were pelleted by centrifugation and resuspended in fresh culture media. The parasites were then filtered using an Acrodisc 32-mm syringe filter (1.2 µm, Pall) and purified merozoites were used in the IIA.

Invasion Inhibition Assays

Purified merozoites were resuspended in a minimal volume of culture media and added directly (without dilution) to a 96 well plate in triplicate, with and without Blebbistatin derivatives at the appropriate concentration in DMSO with a CytoD control (500 nM). After 40 minutes of incubation (37°C, 400 rpm) the parasites were stained with ethidium bromide (EtBr) (5 µg/mL, in 100 µL) in the dark (10 min, RT). The parasites were then washed once in phosphate-buffered saline (PBS) and resuspended in 150 µL PBS for analysis. Gates

were set for RBCs and single cells, then parasitaemia was quantified by selecting the GFP+/EtBr- population.

Growth Inhibition Assays

Late stage parasites were suspended in culture medium (100 µL) and added at 100- or 500-fold dilution to 180 µL RPMI 1640 media with a final haematocrit of 0.2 %, with and without Blebbistatin derivatives at the appropriate concentration in DMSO. The experiment was set up in triplicate in a 96 well plate with a CytoD control (500 nM). After 16 h of incubation, the parasites were washed with PBS and stained using SYBR Green I (Sigma) which was diluted 1:5000 (100 µL/well) in PBS, for 15 min in the dark. The parasites were washed 3 more times with PBS and then resuspended into PBS (150 µL) before quantification of parasitaemia by flow cytometry with gates set for RBC's, single cells and SYBR Green-positive cells.

7.4.2. *In vitro* ATPase Assay

Buffer and Solution Compositions

KMg50 buffer = KCl (50 mM), $MgCl_2$ (2 mM), EGTA (1 mM), imidazole pH 7.4 (10 mM), DTT (1 mM).

Mg buffer = $MgCl_2$ (2 mM), EGTA (1 mM), imidazole pH 7.4 (10 mM), DTT (1 mM).

NADH cocktail = NADH (1.75 mM), lactic dehydrogenase (100 U/mL), pyruvate kinase (150 U/mL), phospho-enol pyruvate (2.5 mM), made up to volume with Mg buffer.

Assay Procedure

Prior to the ATPase assay, F-actin (100 µL, purified from chicken pectoral muscle) was polymerised by dialysis in KMg50 buffer (1 L) for 24 h at 4 °C, with 2 buffer changes to remove free ATP. The assay was assembled in a Greiner UV-star 96 well transparent flat-bottom plate with a final volume of 200 µL. The recombinant *Pf*MyoA complex (final conc.

0.3 μM, purified from *Spodoptera frugiperda* cells) was added to each well containing NADH cocktail (40 μL/well). The Bleb derivatives (final conc. 100 μM, or DMSO or buffer) were added along with Mg buffer (18 μL) and the mixture was incubated at rt for 15 min. F-actin (final conc. 50 μM) was then added to each well followed by ATP (final conc. 2 mM) and the ATPase activity was promptly read by measuring the decrease in absorbance over time at 340 nm (Tecan Infinite M200 Pro). Readings were taken every 10-30 seconds at 25 °C for 300 seconds.

7.5. Biological Testing: Part 2

7.5.1. RSK4 Cell-based Assay

Assay Procedure

10^6 HEK-293T cells transduced with RSK4 lentivirus were seeded into 35-mm dishes and incubated at 37 ºC overnight. The fluoroquinolone inhibitors (50 μM), DMSO only or UO126 (10 μM) were then added followed by incubation for 2 h. 20 min prior to the end of the incubation period, EGF (final conc. 20 nM) was added to the cells and on completion of the incubation time, the medium was removed, and the plates were washed with PBS twice. Subsequent treatment of the plates with hot lysis buffer (40 μL) was followed by cell scrapping and samples were placed in Eppendorf tubes and boiled (95 ºC) for 10 min. Lysate concentrations were measured using Nanodrop or using a DC™ Protein Assay (BioRad). Phosphorylation of RSK4 was then analysed by western blotting by standard techniques using monoclonal rabbit phospho-p90RSK (Ser380) antibody (Cell Signalling Technology, #12032) and monoclonal rabbit GFP antibody (Cell Signalling Technology, #2956). ImageJ was used to quantify the intensities of the bands in the western blot and the final relative quantification values were the ratio of the net loading control band of each lane to the net protein band.

8. References

(1) Talevi, A. Drug Repositioning: Current Approaches and Their Implications in the Precision Medicine Era. *Expert Rev. Precis. Med. Drug Dev.* **2018**, *3* (1), 49–61.

(2) Klug, D. M.; Gelb, M. H.; Pollastri, M. P. Repurposing Strategies for Tropical Disease Drug Discovery. *Bioorganic Med. Chem. Lett.* **2016**, *26* (11), 2569–2576.

(3) Ashburn, T. T.; Thor, K. B. Drug Repositioning: Identifying and Developing New Uses for Existing Drugs. *Nat. Rev. Drug Discov.* **2004**, *3* (8), 673–683.

(4) Nzila, A.; Ma, Z.; Chibale, K. Drug Repositioning in the Treatment of Malaria and TB. *Future Med. Chem.* **2011**, *3* (11), 1413–1426.

(5) Galvin, B. D.; Li, Z.; Villemaine, E.; Poole, C. B.; Chapman, M. S.; Pollastri, M. P.; Wyatt, P. G.; Carlow, C. K. S. A Target Repurposing Approach Identifies N-Myristoyltransferase as a New Candidate Drug Target in Filarial Nematodes. *PLoS Negl. Trop. Dis.* **2014**, *8* (9).

(6) Gould, M. K.; De Koning, H. P. Cyclic-Nucleotide Signalling in Protozoa. *FEMS Microbiol. Rev.* **2011**, *35* (3), 515–541.

(7) Yu, Z.; Brannigan, J. A.; Moss, D. K.; Brzozowski, A. M.; Wilkinson, A. J.; Holder, A. A.; Tate, E. W.; Leatherbarrow, R. J. Design and Synthesis of Inhibitors of Plasmodium FalciparumN -Myristoyltransferase, A Promising Target for Antimalarial Drug Discovery. *J. Med. Chem.* **2012**, *55* (20), 8879–8890.

(8) Nicola Nosengo. Can You Teach Old Drugs New Tricks? *Nature* **2016**, *534* (7607), 314–316.

(9) Bryan, J. How Minoxidil Was Transformed from an Antihypertensive to Hair-Loss Drug. *Pharm. J.* **2011**, *287*, 137.

(10) World Malaria Report 2015. *Geneva: World Health Organization*. Geneva 2015, pp 1–280.

(11) World Malaria Report 2017. *Geneva: World Health Organization*. 2017, pp 1–196.

(12) Cowman, A. F.; Tonkin, C. J.; Tham, W. H.; Duraisingh, M. T. The Molecular Basis of Erythrocyte Invasion by Malaria Parasites. *Cell Host Microbe* **2017**, *22* (2), 232–245.

(13) Cowman, A. F.; Berry, D.; Baum, J. The Cellular and Molecular Basis for Malaria Parasite Invasion of the Human Red Blood Cell. *J. Cell Biol.* **2012**, *198* (6), 961–971.

(14) Wright, G. J.; Rayner, J. C. Plasmodium Falciparum Erythrocyte Invasion: Combining Function with Immune Evasion. *PLoS Pathog.* **2014**, *10* (3), 1–7.

(15) Gilson, P. R.; Crabb, B. S. Morphology and Kinetics of the Three Distinct Phases of Red Blood Cell Invasion by Plasmodium Falciparum Merozoites. *Int. J. Parasitol.* **2009**, *39* (1), 91–96.

(16) Dvorak, J. A.; Miller, L. H.; Whitehouse, W. C.; Shiroishi, T. Invasion of Erythrocytes by Malaria Merozoites. *Science* **1975**, *187* (4178), 748–750.

(17) Williams, M. J.; Alonso, H.; Enciso, M.; Egarter, S.; Sheiner, L.; Meissner, M.; Striepen, B.; Smith, B. J.; Tonkin, C. J. Two Essential Light Chains Regulate the MyoA Lever Arm to Promote Toxoplasma Gliding Motility. *MBio* **2015**, *6* (5).

(18) Wells, T. N. C.; Alonso, P. L.; Gutteridge, W. E. New Medicines to Improve Control and Contribute to the Eradication of Malaria. *Nat. Rev. Drug Discov.* **2009**, *8* (11), 879–891.

(19) Achan, J.; Talisuna, A. O.; Erhart, A.; Yeka, A.; Tibenderana, J. K.; Baliraine, F. N.; Rosenthal, P. J.; D'Alessandro, U. Quinine, an Old Anti-Malarial Drug in a Modern World: Role in the Treatment of Malaria. *Malar. J.* **2011**, *10* (1), 144.

(20) Olliaro, P. L.; Yuthavong, Y. An Overview of Chemotherapeutic Targets for Antimalarial Drug Discovery. *Pharmacol. Ther.* **1999**, *81* (2), 91–110.

(21) Petersen, I.; Eastman, R.; Lanzer, M. Drug-Resistant Malaria: Molecular Mechanisms and Implications for Public Health. *FEBS Lett.* **2011**, *585* (11), 1551–1562.

(22) Al-Bari, M. A. A. Chloroquine Analogues in Drug Discovery: New Directions of Uses, Mechanisms of Actions and Toxic Manifestations from Malaria to Multifarious Diseases. *J. Antimicrob. Chemother.* **2015**, *70* (6), 1608–1621.

(23) Uhlemann, a C.; Krishna, S. Antimalarial Multi-Drug Resistance in Asia: Mechanisms and Assessment. *Curr. Top. Microbiol. Immunol.* **2005**, *295*, 39–53.

(24) Eastman, R. T.; Fidock, D. A. Artemisinin-Based Combination Therapies: A Vital Tool in Efforts to Eliminate Malaria. *Nat. Rev. Microbiol.* **2009**, *7* (12), 864–874.

(25) Meshnick, S. R.; Taylor, T. E.; Kamchonwongpaisan, S. Artemisinin and the Antimalarial Endoperoxides: From Herbal Remedy to Targeted Chemotherapy. *Microbiol. Rev.* **1996**, *60* (2), 301–315.

(26) White, N. Antimalarial Drug Resistance and Combination Chemotherapy. *Philos. Trans. R. Soc. B Biol. Sci.* **1999**, *354* (1384), 739–749.

(27) Price, R. N. Artemisinin Drugs: Novel Antimalarial Agents. *Expert Opin. Investig. Drugs* **2000**, *9* (8), 1815–1827.

(28) Noedl, H.; Se, Y.; Sriwichai, S.; Schaecher, K.; Teja-Isavadharm, P.; Smith, B.; Rutvisuttinunt, W.; Bethell, D.; Surasri, S.; Fukuda, M. M.; et al. Artemisinin Resistance in Cambodia: A Clinical Trial Designed to Address an Emerging Problem in Southeast Asia. *Clin. Infect. Dis.* **2010**, *51* (11), e82–e89.

(29) Ashley, E. A.; Dhorda, M.; Fairhurst, R. M.; Amaratunga, C.; Lim, P.; Suon, S.; Sreng, S.; Anderson, J. M.; Mao, S.; Sam, B.; et al. Spread of Artemisinin Resistance in Plasmodium Falciparum Malaria. *N. Engl. J. Med.* **2014**, *371* (5), 411–423.

(30) Lu, F.; Culleton, R.; Zhang, M.; Ramaprasad, A.; von Seidlein, L.; Zhou, H.; Zhu, G.; Tang, J.; Liu, Y.; Wang, W.; et al. Emergence of Indigenous Artemisinin-Resistant Plasmodium Falciparum in Africa. *N. Engl. J. Med.* **2017**, *376* (10), 991–993.

(31) Wells, T. N. C.; van Huijsduijnen, R. H.; Van Voorhis, W. C. Malaria Medicines: A Glass Half Full? *Nat. Rev. Drug Discov.* **2015**, *14* (6), 424–442.

(32) Allingham, J. S.; Smith, R.; Rayment, I. The Structural Basis of Blebbistatin Inhibition

and Specificity for Myosin II. *Nat. Struct. Mol. Biol.* **2005**, *12* (4), 378–379.

(33) Geeves, M. A. Review: The ATPase Mechanism of Myosin and Actomyosin. *Biopolymers* **2016**, *105* (8), 483–491.

(34) Bond, L. M.; Tumbarello, D. A.; Kendrick-Jones, J.; Buss, F. Small-Molecule Inhibitors of Myosin Proteins. *Future Med. Chem.* **2013**, *5* (1), 41–52.

(35) Kendrick-Jones, J.; Buss, F. Editorial Overview: Myosins in Review. *Traffic* **2016**, *17* (8), 819–821.

(36) Syamaladevi, D. P.; Spudich, J. A.; Sowdhamini, R. Structural and Functional Insights on the Myosin Superfamily. *Bioinform. Biol. Insights* **2012**, *6*, 11–21.

(37) Lodish, H.; Berk, A.; Zipursky, S. Section 18.3 Myosin: The Actin Motor Protein. In *Molecular Cell Biology*; W. H. Freeman and Company: New York, 2000.

(38) Bähler, M.; Rhoads, A. Calmodulin Signaling via the IQ Motif. *FEBS Lett.* **2002**, *513* (1), 107–113.

(39) Tuxworth, R. I.; Titus, M. A. Unconventional Myosins: Anchors in the Membrane Traffic Relay. *Traffic* **2000**, *1* (1), 11–18.

(40) Hartman, M. A.; Finan, D.; Sivaramakrishnan, S.; Spudich, J. A. Principles of Unconventional Myosin Function and Targeting. *Annu. Rev. Cell Dev. Biol.* **2011**, *27* (1), 133–155.

(41) Cooper, G. M. Actin, Myosin, and Cell Movement. In *The Cell: A Molecular Approach*; Sinauer Associates Inc.: Sunderland (MA), 2000.

(42) Kalhammer, G.; Bähler, M. Unconventional Myosins. *Essays Biochem.* **2000**, *35* (1), 33–42.

(43) Woolner, S.; Bement, W. M. Unconventional Myosins Acting Unconventionally. *Trends Cell Biol.* **2009**, *19* (6), 245–252.

(44) Sweeney, H. L.; Houdusse, A. Structural and Functional Insights into the Myosin Motor Mechanism. *Annu. Rev. Biophys.* **2010**, *39* (1), 539–557.

(45) Preller, M.; Manstein, D. J. Myosin Structure, Allostery, and Mechano-Chemistry. *Structure* **2013**, *21* (11), 1911–1922.

(46) Roman, B. I.; Verhasselt, S.; Stevens, C. V. Medicinal Chemistry and Use of Myosin II Inhibitor (S)-Blebbistatin and Its Derivatives. *J. Med. Chem.* **2018**, A-S.

(47) Zuccala, E. S.; Satchwell, T. J.; Angrisano, F.; Tan, Y. H.; Wilson, M. C.; Heesom, K. J.; Baum, J. Quantitative Phospho-Proteomics Reveals the Plasmodium Merozoite Triggers Pre-Invasion Host Kinase Modification of the Red Cell Cytoskeleton. *Sci. Rep.* **2016**, *6* (February), 19766.

(48) Shaw, M. A.; Ostap, E. M.; Goldman, Y. E.; Pennsyl, V.; Uni, V. Mechanism of Inhibition of Skeletal Muscle Actomyosin by N-Benzyl-p-Toluenesulfonamide. *Biochemistry* **2003**, *42* (0006–2960 (Print)), 6128–6135.

(49) Ostap, E. M. 2,3-Butanedione Monoxime (BDM) as a Myosin Inhibitor. *J. Muscle Res. Cell Motil.* **2002**, *23* (4), 305–308.

(50) Chinthalapudi, K.; Taft, M. H.; Martin, R.; Heissler, S. M.; Preller, M.; Hartmann, F. K.; Brandstaetter, H.; Kendrick-Jones, J.; Tsiavaliaris, G.; Gutzeit, H. O.; et al. Mechanism and Specificity of Pentachloropseudilin-Mediated Inhibition of Myosin Motor Activity. *J. Biol. Chem.* **2011**, *286* (34), 29700–29708.

(51) Islam, K.; Chin, H. F.; Olivares, A. O.; Saunders, L. P.; De-la-cruz, E. M.; Kapoor, T. M. A Myosin-V Inhibitor Based on Privileged Chemical Scaffolds. *Angew. Chemie - Int. Ed.* **2010**, *49* (45), 8484–8488.

(52) Heissler, S. M.; Selvadurai, J.; Bond, L. M.; Fedorov, R.; Kendrick-Jones, J.; Buss, F.; Manstein, D. J. Kinetic Properties and Small-Molecule Inhibition of Human Myosin-6. *FEBS Lett.* **2012**, *586* (19), 3208–3214.

(53) Kovacs, M.; Toth, J.; Hetenyi, C.; Malnasi-Csizmadia, A.; Sellers, J. R. Mechanism of Blebbistatin Inhibition of Myosin II. *J. Biol. Chem.* **2004**, *279* (34), 35557–35563.

(54) Limouze, J.; Straight, A. F.; Mitchison, T.; Sellers, J. R. Specificity of Blebbistatin, an Inhibitor of Myosin II. *J. Muscle Res. Cell Motil.* **2004**, *25* (4–5), 337–341.

(55) Straight, A. F.; Cheung, A.; Limouze, J.; Chen, I.; Westwood, N. J.; Sellers, J. R.; Mitchison, T. J. Dissecting Temporal and Spatial Control of Cytokinesis with a Myosin II Inhibitor. *Science* **2003**, *299* (5613), 1743–1747.

(56) Smith, C. A.; Rayment, I. X-Ray Structure of the Magnesium (II)⊙ ADP⊙ Vanadate Complex of the Dictyostelium Discoideum Myosin Motor Domain to 1.9 Å Resolution. *Biochemistry* **1996**, *35* (17), 5404–5417.

(57) Lucas-Lopez, C.; Allingham, J. S.; Lebl, T.; Lawson, C. P. a T.; Brenk, R.; Sellers, J. R.; Rayment, I.; Westwood, N. J. The Small Molecule Tool (S)-(-)-Blebbistatin: Novel Insights of Relevance to Myosin Inhibitor Design. *Org. Biomol. Chem.* **2008**, *6* (12), 2076–2084.

(58) Verhasselt, S.; Roman, B. I.; Bracke, M. E.; Stevens, C. V. Improved Synthesis and Comparative Analysis of the Tool Properties of New and Existing D-Ring Modified (S)-Blebbistatin Analogs. *Eur. J. Med. Chem.* **2017**, *136*, 85–103.

(59) Kolega, J. Phototoxicity and Photoinactivation of Blebbistatin in UV and Visible Light. *Biochem. Biophys. Res. Commun.* **2004**, *320* (3), 1020–1025.

(60) Várkuti, B. H.; Képiró, M.; Horváth, I. Á.; Végner, L.; Ráti, S.; Zsigmond, Á.; Hegyi, G.; Lenkei, Z.; Varga, M.; Málnási-Csizmadia, A. A Highly Soluble, Non-Phototoxic, Non-Fluorescent Blebbistatin Derivative. *Sci. Rep.* **2016**, *6* (1), 26141.

(61) Verhasselt, S.; Stevens, C. V.; Van den broecke, T.; Bracke, M. E.; Roman, B. I. Insights into the Myosin II Inhibitory Potency of A-Ring-Modified (S)-Blebbistatin Analogs. *Bioorganic Med. Chem. Lett.* **2017**, *27* (13), 2986–2989.

(62) Verhasselt, S.; Roman, B. I.; De Wever, O.; Van Hecke, K.; Van Deun, R.; Bracke, M. E.; Stevens, C. V. Discovery of (S)-3′-Hydroxyblebbistatin and (S)-3′-Aminoblebbistatin: Polar Myosin II Inhibitors with Superior Research Tool Properties. *Org. Biomol. Chem.* **2017**, *15* (9), 2104–2118.

(63) Lawson, C. P. A. T.; Slawin, A. M. Z.; Westwood, N. J. Application of the Copper Catalysed N-Arylation of Amidines in the Synthesis of Analogues of the Chemical Tool, Blebbistatin. *Chem. Commun.* **2011**, *47* (3), 1057–1059.

(64) Roman, B. I.; Verhasselt, S.; Mangodt, C. W.; De Wever, O.; Stevens, C. V. Synthesis of C-Ring-Modified Blebbistatin Derivatives and Evaluation of Their Myosin II ATPase Inhibitory Potency. *Bioorganic Med. Chem. Lett.* **2018**, *28* (13), 2261–2264.

(65) Képiró, M.; Várkuti, B. H.; Bodor, A.; Hegyi, G.; Drahos, L.; Kovács, M.; Málnási-Csizmadia, A. Azidoblebbistatin, a Photoreactive Myosin Inhibitor. *Proc. Natl. Acad. Sci. U. S. A.* **2012**, *109* (24), 9402–9407.

(66) Wetzel, D. M.; Håkansson, S.; Hu, K.; Roos, D.; Sibley, L. D. Actin Filament Polymerization Regulates Gliding Motility by Apicomplexan Parasites. *Mol. Biol. Cell* **2003**, *14* (2), 396–406.

(67) Baum, J.; Richard, D.; Healer, J.; Rug, M.; Krnajski, Z.; Gilberger, T. W.; Green, J. L.; Holder, A. A.; Cowman, A. F. A Conserved Molecular Motor Drives Cell Invasion and Gliding Motility across Malaria Life Cycle Stages and Other Apicomplexan Parasites. *J. Biol. Chem.* **2006**, *281* (8), 5197–5208.

(68) Yusuf, N. A.; Green, J. L.; Wall, R. J.; Knuepfer, E.; Moon, R. W.; Schulte-Huxel, C.; Stanway, R. R.; Martin, S. R.; Howell, S. A.; Douse, C. H.; et al. The Plasmodium Class XIV Myosin, MyoB, Has a Distinct Subcellular Location in Invasive and Motile Stages of the Malaria Parasite and an Unusual Light Chain. *J. Biol. Chem.* **2015**, *290* (19), 12147–12164.

(69) Bookwalter, C. S.; Tay, C. L.; McCrorie, R.; Previs, M. J.; Lu, H.; Krementsova, E. B.; Fagnant, P. M.; Baum, J.; Trybus, K. M. Reconstitution of the Core of the Malaria Parasite Glideosome with Recombinant Plasmodium Class XIV Myosin A and Plasmodium Actin. *J. Biol. Chem.* **2017**, *292* (47), 19290–19303.

(70) Ménard, R. Gliding Motility and Cell Invasion by Apicomplexa: Insights from the Plasmodium Sporozoite. *Cell. Microbiol.* **2001**, *3* (2), 63–73.

(71) Pinder, J. C.; Fowler, R. E.; Dluzewski, a R.; Bannister, L. H.; Lavin, F. M.; Mitchell, G. H.; Wilson, R. J.; Gratzer, W. B. Actomyosin Motor in the Merozoite of the Malaria Parasite, Plasmodium Falciparum: Implications for Red Cell Invasion. *J. Cell Sci.* **1998**, *111*, 1831–1839.

(72) McLellan, M. A.; Rosenthal, N. A.; Pinto, A. R. Cre- Lox P-Mediated Recombination: General Principles and Experimental Considerations. In *Current Protocols in Mouse Biology*; John Wiley & Sons, Inc.: Hoboken, NJ, USA, 2017; pp 1–12.

(73) Jones, M. L.; Das, S.; Belda, H.; Collins, C. R.; Blackman, M. J.; Treeck, M. A Versatile Strategy for Rapid Conditional Genome Engineering Using LoxP Sites in a Small Synthetic Intron in Plasmodium Falciparum. *Sci. Rep.* **2016**, *6* (February), 1–9.

(74) Opitz, C.; Soldati, D. “The Glideosome”: A Dynamic Complex Powering Gliding Motion and Host Cell Invasion by Toxoplasma Gondii. *Mol. Microbiol.* **2002**, *45* (3), 597–604.

(75) Farrow, R. E.; Green, J.; Katsimitsoulia, Z.; Taylor, W. R.; Holder, A. A.; Molloy, J. E. The Mechanism of Erythrocyte Invasion by the Malarial Parasite, Plasmodium Falciparum. *Semin. Cell Dev. Biol.* **2011**, *22* (9), 953–960.

(76) Kumpula, E. P.; Kursula, I. Towards a Molecular Understanding of the Apicomplexan Actin Motor: On a Road to Novel Targets for Malaria Remedies? *Acta Crystallogr. Sect. FStructural Biol. Commun.* **2015**, *71*, 500–513.

(77) Thomas, J. C.; Green, J. L.; Howson, R. I.; Simpson, P.; Moss, D. K.; Martin, S. R.; Holder, A. A.; Cota, E.; Tate, E. W. Interaction and Dynamics of the Plasmodium Falciparum MTIP-MyoA Complex, a Key Component of the Invasion Motor in the Malaria Parasite. *Mol. Biosyst.* **2010**, *6* (3), 494–498.

(78) Sibley, L. D. How Apicomplexan Parasites Move in and out of Cells. *Curr. Opin. Biotechnol.* **2010**, *21* (5), 592–598.

(79) Anderson, A. C. The Process of Structure-Based Drug Design. *Chem. Biol.* **2003**, *10*, 787–797.

(80) Šali, A.; Blundell, T. L. Definition of General Topological Equivalence in Protein Structures. A Procedure Involving Comparison of Properties and Relationships through Simulated Annealing and Dynamic Programming. *J. Mol. Biol.* **1990**, *212* (2), 403–428.

(81) Wiltgen, M.; Tilz, G. P. Homology Modelling: A Review about the Method on Hand of the Diabetic Antigen GAD 65 Structure Prediction. *Wiener Medizinische Wochenschrift* **2009**, *159* (5–6), 112–125.

(82) Schrödinger Release 2016-1. Maestro. Schrödinger, LLC, New York, NY 2016.

(83) Larkin, M. A.; Blackshields, G.; Brown, N. P.; Chenna, R.; McGettigan, P. A.; McWilliam, H.; Valentin, F.; Wallace, I. M.; Wilm, A.; Lopez, R.; et al. Clustal W and Clustal X Version 2.0. *Bioinformatics* **2007**, *23* (21), 2947–2948.

(84) Kelley, L. A.; Mezulis, S.; Yates, C. M.; Wass, M. N.; Sternberg, M. J. E. The Phyre2 Web Portal for Protein Modelling, Prediction and Analysis. *Nat. Protoc.* **2015**, *10* (6), 845–858.

(85) Arnold, K.; Bordoli, L.; Kopp, J.; Schwede, T. The SWISS-MODEL Workspace: A Web-Based Environment for Protein Structure Homology Modelling. *Bioinformatics* **2006**, *22* (2), 195–201.

(86) Friesner, R. A.; Banks, J. L.; Murphy, R. B.; Halgren, T. A.; Klicic, J. J.; Mainz, D. T.; Repasky, M. P.; Knoll, E. H.; Shelley, M.; Perry, J. K.; et al. Glide: A New Approach for Rapid, Accurate Docking and Scoring. 1. Method and Assessment of Docking Accuracy. *J. Med. Chem.* **2004**, *47* (7), 1739–1749.

(87) Rössle, M.; Christoffers, J. The Source of Oxygen in Cerium-Catalyzed α-Hydroxylation of β-Dicarbonyl Compounds. *Tetrahedron* **2009**, *65* (52), 10941–10944.

(88) Liang, Y. F.; Jiao, N. Highly Efficient C-H Hydroxylation of Carbonyl Compounds with Oxygen under Mild Conditions. *Angew. Chemie - Int. Ed.* **2014**, *53* (2), 548–552.

(89) Kornet, M. J.; Thio, P. A.; Tan, S. I. Borane Reduction of Amido Esters. *J. Org. Chem.* **1968**, *33* (9), 3637–3639.

(90) Cossy, J.; Mirguet, O.; Pardo, D. G.; Desmurs, J. R. A Formal Synthesis of (-)-Paroxetine by Enantioselective Ring Enlargement of a Trisubstituted Prolinol. *European J. Org. Chem.* **2002**, No. 21, 3543–3551.

(91) Volkov, A.; Tinnis, F.; Slagbrand, T.; Trillo, P.; Adolfsson, H. Chemoselective Reduction of Carboxamides. *Chem. Soc. Rev.* **2016**, *45* (24), 6685–6697.

(92) Igarashi, M.; Fuchikami, T. Transition-Metal Complex-Catalyzed Reduction of Amides with Hydrosilanes: A Facile Transformation of Amides to Amines. *Tetrahedron Lett.* **2001**, *42* (10), 1945–1947.

(93) Kuwano, R.; Takahashi, M.; Ito, Y. Reduction of Amides to Amines via Catalytic Hydrosilylation by a Rhodium Complex. *Tetrahedron Lett.* **1998**, *39* (9), 1017–1020.

(94) Motoyama, Y.; Mitsui, K.; Ishida, T.; Nagashima, H. Self-Encapsulation of Homogeneous Catalyst Species into Polymer Gel Leading to a Facile and Efficient Separation System of Amine Products in the Ru-Catalyzed Reduction of Carboxamides with Polymethylhydrosiloxane (PMHS). *J. Am. Chem. Soc.* **2005**, *127* (38), 13150–13151.

(95) Das, S.; Addis, D.; Zhou, S.; Junge, K.; Beller, M. Zinc-Catalyzed Reduction of Amides: Unprecedented Selectivity and Functional Group Tolerance. *J. Am. Chem. Soc.* **2010**, *132* (6), 1770–1771.

(96) Ozturk, T.; Ertas, E.; Mert, O. Use of Lawesson's Reagent in Organic Syntheses. *Chem. Rev.* **2007**, *107* (11), 5210–5278.

(97) Hussaini, S. R.; Moloney, M. G. Cis-Selective Synthesis of 2,5-Disubstituted Pyrrolidines. *Tetrahedron Lett.* **2004**, *45* (6), 1125–1127.

(98) Lajoie, G.; Lepine, F.; Maziak, L.; Belleau, B. Facile Regioelective Formation of Thiopeptide Linkages from Oligopeptides With New Thionation Reagents. *Tetrahedron Lett.* **1983**, *24* (36), 3815–3818.

(99) Lecher, H. Z.; Greenwood, R. A.; Whitehouse, K. C.; Chao, T. H. The Phosphonation of Aromatic Compounds with Phosphorus Pentasulfide. *J. Am. Chem. Soc.* **1956**, *78* (19), 5018–5022.

(100) Sherer, B. A.; Brugger, N. Heterocyclic Compounds as NAV Channel Inhibitors and Uses Thereof. US 2015/0266862 A1, 2015.

(101) Geoghegan, K.; Bode, J. W. Bespoke SnAP Reagents for the Synthesis of C-Substituted Spirocyclic and Bicyclic Saturated N-Heterocycles. *Org. Lett.* **2015**, *17* (8), 1934–1937.

(102) Herold, P.; Mah, R.; Stutz, S.; Stojanovic, A.; Tschinke, V.; Jotterand, N. Organic Compounds. WO 2005/061457 A1, 2005.

(103) Wolfe, J. P.; Buchwald, S. L. Scope and Limitations of the Pd/BINAP-Catalyzed Amination of Aryl Bromides. *J. Org. Chem.* **2000**, *65* (4), 1144–1157.

(104) Zhou, C.; Pasternak, A.; Morriello, G.; Guo, L.; Pan, Y.; Yang, L.; Patchett, A. Somatostatin Agonists. US 6387932 B1, 2002.

(105) Ullmann, F.; Bielecki, J. Ueber Synthesen in Der Biphenylreihe. *Berichte der Dtsch. Chem. Gesellschaft* **1901**, *34* (2), 2174–2185.

(106) Ma, D.; Cai, Q.; Zhang, H. Mild Method for Ullmann Coupling Reaction of Amines and Aryl Halides. *Org. Lett.* **2003**, *5* (14), 2453–2455.

(107) Sambiagio, C.; Marsden, S. P.; Blacker, A. J.; McGowan, P. C. Copper Catalysed Ullmann Type Chemistry: From Mechanistic Aspects to Modern Development. *Chem.*

Soc. Rev. **2014**, *43* (10), 3525–3550.

(108) Bing, W. N-(1-Hydroxy-3-(Pyrrolidinyl)Propan-2-Yl)Pyrrolidine-3-Carboxamide Derivatives as Glucosylceramide Synthase Inhibitors. WO 2015/065937 A1, 2015.

(109) McCarthy, T. D.; Naylor, A. Heterocyclic Compounds and Methods for Their Use. WO 2013/110134 A1, 2013.

(110) Lihammar, R.; Millet, R.; Bäckvall, J. E. An Efficient Dynamic Kinetic Resolution of N-Heterocyclic 1,2-Amino Alcohols. *Adv. Synth. Catal.* **2011**, *353* (13), 2321–2327.

(111) Ju, Y.; Varma, R. S. Aqueous N-Heterocyclization of Primary Amines and Hydrazines with Dihalides: Microwave-Assisted Syntheses of N-Azacycloalkanes, Isoindole, Pyrazole, Pyrazolidine, and Phthalazine Derivatives. *J. Org. Chem.* **2006**, *71* (1), 135–141.

(112) Mancuso, A. J.; Swern, D. Activated Dimethyl Sulfoxide. *Synthesis (Stuttg).* **1981**, *1* (9), 165–185.

(113) Kharasch, M. S.; Reinmuth, O. *Grignard Reactions of Nonmetallic Substances*; New York, Prentice-Hall, 1954.

(114) Weiberth, F. J.; Hall, S. S. Copper(I)-Activated Addition of Grignard Reagents to Nitriles. Synthesis of Ketimines, Ketones, and Amines. *J. Org. Chem.* **1987**, *52* (17), 3901–3904.

(115) Mentzel, M.; Hoffmann, H. M. R. N-Methoxy-N-Methylamides (Weinreb Amides) in Modern Organic Synthesis. *J. für Prakt. Chemie/Chemiker-Zeitung* **1997**, *339* (1), 517–524.

(116) Iriarte, I.; Vera, S.; Badiola, E.; Mielgo, A.; Oiarbide, M.; García, J. M.; Odriozola, J. M.; Palomo, C. Asymmetric Assembly of All-Carbon Tertiary/Quaternary Nonadjacent Stereocenters through Organocatalytic Conjugate Addition of α-Cyanoacetates to a Methacrylate Equivalent. *Chem. - A Eur. J.* **2016**, *22* (38), 13690–13696.

(117) Prosser, A. R.; Liotta, D. C. One-Pot Transformation of Esters to Analytically Pure Ketones: Methodology and Application in Process Development. *Tetrahedron Lett.* **2015**, *56* (23), 3005–3007.

(118) Gilman, H.; St. John, E. L.; St. John, N. B.; Lichtenwalter, M. Relative Reactivities of Organometallic Compounds. XI Grignard Reagents. *Recl. des Trav. Chim. des Pays-Bas* **2010**, *55* (7), 577–585.

(119) Gröbel, B.-T.; Seebach, D. Umpolung of the Reactivity of Carbonyl Compounds Through Sulfur-Containing Reagents. *Synthesis (Stuttg).* **1977**, *1977* (06), 357–402.

(120) Eymur, S.; Göllü, M.; Tanyeli, C. Umpolung Strategy: Advances in Catalytic C-C Bond Formations. *Turkish J. Chem.* **2013**, *37* (4), 586–609.

(121) Seebach, D.; Corey, E. J. Generation and Synthetic Applications of 2-Lithio-1,3-Dithianes. *J. Org. Chem.* **1975**, *40* (2), 231–237.

(122) Burghardt, T. E. Developments in the Deprotection of Thioacetals. *J. Sulfur Chem.* **2005**, *26* (4–5), 411–427.

(123) Kamata, M.; Otogawa, H.; Hasegawa, E. Deprotection of 1,3-Dithianes by Antimony Pentachloride via Single Electron Transfer Processes. *Tetrahedron Lett.* **1991**, *32* (50), 7421–7424.

(124) Porter, Q. N.; Utley, J. H. P. Electrochemical Removal of 1,3-Dithian Protecting Groups. *J. Chem. Soc. Chem. Commun.* **1978**, No. 6, 255.

(125) Ghorbani-vaghei, R.; Veisi, H. Solvent-Free Oxidative Deprotection of 1,3-Dithianes and 1,3-Dithiolanes Using Poly(N,N'-Dibromo-N-Ethyl-Benzene-1,3-Disulfonamide), N,N,N',N'-Tetrabromobenzene-1,3-Disulfonamide and NBS. *Arkivoc* **2009**, *2009*, 44–51.

(126) Bates, S. B.; O'Doherty, J. Phase Transfer Catalyzed Hydrolysis of Thioacetals Using Pyridinium Hydrobromide Perbromide. *Am. Chem. Soc.* **1981**, *46* (8), 1745–1747.

(127) Stork, G.; Zhao, K. A Simple Method of Dethioacetalization. *Tetrahedron Lett.* **1989**, *30* (3), 287–290.

(128) Smith, A. B.; Dorsey, B. D.; Maeda, T.; Malamas, M. S.; Visnick, M. Synthesis of (-)-Bertyadionol. *J. Am. Chem. Soc.* **1986**, *108* (11), 3110–3112.

(129) Krüger, S.; Gaich, T. Total Syntheses of Vellosimine, N-Methylvellosimine, and 10-Methoxyvellosimine and Formal Synthesis of 16-Epinormacusine B through a [5+2] Cycloaddition. *European J. Org. Chem.* **2016**, *2016* (28), 4893–4899.

(130) Narasaka, K.; Sakashita, T.; Mukaiyama, T. A Convenient Method for Hydrolysis of 1,3-Dithiane Derivatives Using Cupric Chloride. *Bulletin of the Chemical Society of Japan*. 1972, p 3724.

(131) Zweifel, G. S.; Nantz, M. H.; Somfai, P. *Modern Organic Synthesis: An Introduction*, 2nd Ed.; John Wiley & Sons, Inc., 2017.

(132) Paytash, P. L.; Sparrow, E.; Gathe, J. C. The Reaction of Itaconic Acid with Primary Amines. *J. Am. Chem. Soc.* **1950**, *72* (3), 1415–1416.

(133) Jones, A.; Kemps, M. I.; Stockley, M. L.; Woodrow, M. D. 1-Cyano-Pyrrolidine Derivatives as DBU Inhibitors. WO 2017/163078 A1, 2017.

(134) Blanc, F.; Isabet, T.; Benisty, H.; Sweeney, H. L.; Cecchini, M.; Houdusse, A. An Intermediate along the Recovery Stroke of Myosin VI Revealed by X-Ray Crystallography and Molecular Dynamics. *Proc. Natl. Acad. Sci.* **2018**, *115* (24), 6213–6218.

(135) Planelles-Herrero, V. J.; Hartman, J. J.; Robert-Paganin, J.; Malik, F. I.; Houdusse, A. Mechanistic and Structural Basis for Activation of Cardiac Myosin Force Production by Omecamtiv Mecarbil. *Nat. Commun.* **2017**, *8* (1), 190.

(136) Wulf, S. F.; Ropars, V.; Fujita-Becker, S.; Oster, M.; Hofhaus, G.; Trabuco, L. G.; Pylypenko, O.; Sweeney, H. L.; Houdusse, A. M.; Schröder, R. R. Force-Producing ADP State of Myosin Bound to Actin. *Proc. Natl. Acad. Sci.* **2016**, *113* (13), E1844–E1852.

(137) Sirigu, S.; Hartman, J. J.; Planelles-Herrero, V. J.; Ropars, V.; Clancy, S.; Wang, X.; Chuang, G.; Qian, X.; Lu, P.-P.; Barrett, E.; et al. Highly Selective Inhibition of Myosin Motors Provides the Basis of Potential Therapeutic Application. *Proc. Natl. Acad. Sci.*

2016, *113* (47), E7448–E7455.

(138) Lucas-Lopez, C.; Patterson, S.; Blum, T.; Straight, A. F.; Toth, J.; Slawin, A. M. Z.; Mitchison, T. J.; Sellers, J. R.; Westwood, N. J. Absolute Stereochemical Assignment and Fluorescence Tuning of the Small Molecule Tool, (-)-Blebbistatin. *European J. Org. Chem.* **2005**, No. 9, 1736–1740.

(139) Orrling, K. M.; Wu, X.; Russo, F.; Larhed, M. Fast, Acid-Free, and Selective Lactamization of Lactones in Ionic Liquids. *J. Org. Chem.* **2008**, *73* (21), 8627–8630.

(140) Racine, E.; Monnier, F.; Vors, J.-P.; Taillefer, M. Direct N-Cyclopropylation of Secondary Acyclic Amides Promoted by Copper. *Chem. Commun.* **2013**, *49* (67), 7412.

(141) Thomas, A. M.; Sujatha, A.; Anilkumar, G. Goldberg Reaction: Development, Mechanistic Insights and Applications. *Mini. Rev. Org. Chem.* **2015**, *12* (1), 3–23.

(142) Guazzelli, G.; Duffy, L. A.; Procter, D. J. A Samarium(II)-Mediated, Stereoselective Cyclization for the Synthesis of Azaspirocycles. *Org. Lett.* **2008**, *10* (19), 4291–4294.

(143) Verkade, J. M. M.; van Hemert, L. J. C.; Quaedflieg, P. J. L. M.; Alsters, P. L.; van Delft, F. L.; Rutjes, F. P. J. T. Mild and Efficient Deprotection of the Amine Protecting P-Methoxyphenyl (PMP) Group. *Tetrahedron Lett.* **2006**, *47* (46), 8109–8113.

(144) Taylor, J. E.; Bull, S. D.; Williams, J. M. J. Amidines, Isothioureas, and Guanidines as Nucleophilic Catalysts. *Chem. Soc. Rev.* **2012**, *41* (6), 2109.

(145) Aly, A. A.; Nour-El-Din, A. M. Functionality of Amidines and Amidrazones. *Arkivoc* **2008**, *2008* (1), 153–194.

(146) Wolff, H.; Hartke, K. Zur Rotationshinderung N,N,N′-Trisubstituierter Amidine. *Arch. Pharm. (Weinheim).* **1980**, *313* (3), 215–220.

(147) Li, J.; Jiao, J.; Zhang, C.; Shi, M.; Zhang, J. Facile Syntheses of N-Heterocyclic Carbene Precursors through I2- or NIS-Promoted Amidiniumation of N-Alkenyl Formamidines. *Chem. - An Asian J.* **2016**, *11* (9), 1361–1365.

(148) Méndez, M. V.; Heredia, D. A.; Larghi, E. L.; Bracca, A. B. J.; Kaufman, T. S. Efficient Total Synthesis of Neocryptolepine and Synthetic Access to 6-Methylquinindoline from a Common Intermediate. *RSC Adv.* **2017**, *7* (45), 28298–28307.

(149) Abarghaz, M.; Kerbal, A.; Bourguignon, J.-J. Regioselective Alkylation of the Exocyclic Nitrogen of Heterocyclic Amidines via the Mitsunobu Reaction. *Tetrahedron Lett.* **1995**, *36* (36), 6463–6466.

(150) Contini, A.; Erba, E.; Trimarco, P. Efficient Alkylation of N-N′disubstituted Formamidines Using Mitsunobu's Reagents. *Arkivoc* **2009**, *2009* (2), 126.

(151) Egger, N.; Hoesch, L.; Dreiding, A. S. 3,3-Dialkyltriazencarbonsäure-Derivate Durch Oxydative Hydro-Acyl-Elimination von 3,3-Dialkyltriazan-1,2-Dicarbonsäure-Derivaten. *Helv. Chim. Acta* **1983**, *66* (5), 1416–1426.

(152) Kanzian, T.; Mayr, H. Electrophilic Reactivities of Azodicarboxylates. *Chem. - A Eur. J.* **2010**, *16* (38), 11670–11677.

(153) Tsunoda, T.; Yamamiya, Y.; Itô, S. 1,1′-(Azodicarbonyl)Dipiperidine-Tributylphosphine, a New Reagent System for Mitsunobu Reaction. *Tetrahedron Lett.* **1993**, *34* (10), 1639–1642.

(154) Buckle, D. R.; Pinto, I. L. Functions Bearing Two Nitrogens. In *Comprehensive Organic Functional Group Transformations*; Katritzky, A. R., Rees, C. W., Meth-Cohn, O., Eds.; Elsevier, 1995; pp 403–449.

(155) Bénard, S.; Neuville, L.; Zhu, J. Copper-Promoted N-Cyclopropylation of Anilines and Amines by Cyclopropylboronic Acid. *Chem. Commun.* **2010**, *46* (19), 3393.

(156) Wu, W.; Ma, B.; Wu, J. I. C.; Von Ragué Schleyer, P.; Mo, Y. Is Cyclopropane Really the σ-Aromatic Paradigm? *Chem. - A Eur. J.* **2009**, *15* (38), 9730–9736.

(157) Mao, Y.; Lin, N.; Tian, W.; Han, X.; Han, X.; Huang, Z.; An, J. Design, Synthesis, and Biological Evaluation of New Diaminoquinazolines as β-Catenin/Tcf4 Pathway Inhibitors. *J. Med. Chem.* **2012**, *55* (3), 1346–1359.

(158) Moon, B. S.; Lee, B. S.; Chi, D. Y. Syntheses and Binding Affinities of 6-Nitroquipazine Analogues for Serotonin Transporter. Part 4: 3-Alkyl-4-Halo-6-Nitroquipazines. *Bioorg. Med. Chem.* **2005**, *13* (16), 4952–4959.

(159) Blackburn, C.; LaMarche, M. J.; Brown, J.; Che, J. L.; Cullis, C. A.; Lai, S.; Maguire, M.; Marsilje, T.; Geddes, B.; Govek, E.; et al. Identification and Characterization of Amino-Piperidinequinolones and Quinazolinones as MCHr1 Antagonists. *Bioorg. Med. Chem. Lett.* **2006**, *16* (10), 2621–2627.

(160) Bei, A. K.; Desimone, T. M.; Badiane, A. S.; Ahouidi, A. D.; Ndiaye, D.; Sarr, O.; Ndir, O.; Mboup, S.; Manoj, T. A Flow Cytometry-Based Assay for Measuring Invasion of Red Blood Cells by Plasmodium Falciparum. *Am. J. Hematol.* **2011**, *85* (4), 234–237.

(161) Otto, T. D.; Wilinski, D.; Assefa, S.; Keane, T. M.; Sarry, L. R.; Böhme, U.; Lemieux, J.; Barrell, B.; Pain, A.; Berriman, M.; et al. New Insights into the Blood-Stage Transcriptome of Plasmodium Falciparum Using RNA-Seq. *Mol. Microbiol.* **2010**, *76* (1), 12–24.

(162) Tonkin-Hill, G. Q.; Trianty, L.; Noviyanti, R.; Nguyen, H. H. T.; Sebayang, B. F.; Lampah, D. A.; Marfurt, J.; Cobbold, S. A.; Rambhatla, J. S.; McConville, M. J.; et al. The Plasmodium Falciparum Transcriptome in Severe Malaria Reveals Altered Expression of Genes Involved in Important Processes Including Surface Antigen–encoding Var Genes. *PLOS Biol.* **2018**, *16* (3), e2004328.

(163) National Cancer Institute. What Is Cancer? https://www.cancer.gov/about-cancer/understanding/what-is-cancer (accessed Aug 15, 2018).

(164) Lung cancer https://www.cancerresearchuk.org/health-professional/cancer-statistics-for-the-uk (accessed May 15, 2015).

(165) Belani, C. P.; Marts, S.; Schiller, J.; Socinski, M. a. Women and Lung Cancer: Epidemiology, Tumor Biology, and Emerging Trends in Clinical Research. *Lung Cancer* **2007**, *55* (1), 15–23.

(166) Langevin, S. M.; Kratzke, R. a; Kelsey, K. T. Epigenetics of Lung Cancer. *Transl. Res.* **2015**, *165* (1), 74–90.

(167) Liu, H.; Gu, Y.; Yin, J.; Zheng, G.; Wang, C.; Zhang, Z.; Deng, M.; Liu, J.; Jia, X.; He, Z. SET-Mediated NDRG1 Inhibition Is Involved in Acquisition of Epithelial-to-Mesenchymal Transition Phenotype and Cisplatin Resistance in Human Lung Cancer Cell. *Cell. Signal.* **2014**, *26* (12), 2710–2720.

(168) Ashkenazi, R.; Gentry, S. N.; Jackson, T. L. Pathways to Tumorigenesis--Modeling Mutation Acquisition in Stem Cells and Their Progeny. *Neoplasia* **2008**, *10* (11), 1170–1182.

(169) de Groot, P.; Munden, R. F. Lung Cancer Epidemiology, Risk Factors, and Prevention. *Radiol. Clin. North Am.* **2012**, *50* (5), 863–876.

(170) Brambilla, E.; Gazdar, A. Pathogenesis of Lung Cancer Signalling Pathways: Roadmap for Therapies. *Eur. Respir. J.* **2009**, *33* (6), 1485–1497.

(171) Sharma, S. V.; Bell, D. W.; Settleman, J.; Haber, D. A. Epidermal Growth Factor Receptor Mutations in Lung Cancer. *Nat. Rev. Cancer* **2007**, *7* (3), 169–181.

(172) Nicholson, R. I.; Gee, J. M.; Harper, M. E. EGFR and Cancer Prognosis. *Eur. J. Cancer* **2001**, *37 Suppl 4*, S9-15.

(173) Brambilla, E.; Gazzeri, S.; Lantuejoul, S.; Coll, J. L.; Moro, D.; Negoescu, A.; Brambillo, C. P53 Mutant Immunophenotype and Deregulation of P53 Transcription Pathway (Bcl2, Bax and Waf1) in Precursor Bronchial Lesions of Lung Cancer. *Clin. Cancer Res.* **1998**, *4*, 1609–1618.

(174) Giacinti, C.; Giordano, A. RB and Cell Cycle Progression. *Oncogene* **2006**, *25* (38), 5220–5227.

(175) Viard-Leveugle, I.; Veyrenc, S.; French, L. E.; Brambilla, C.; Brambilla, E. Frequent Loss of Fas Expression and Function in Human Lung Tumours with Overexpression of FasL in Small Cell Lung Carcinoma. *J. Pathol.* **2003**, *201* (2), 268–277.

(176) Zhang, J.; Yang, P. L.; Gray, N. S. Targeting Cancer with Small Molecule Kinase Inhibitors. *Nat. Rev. Cancer* **2009**, *9* (1), 28–39.

(177) Endicott, J. a.; Noble, M. E. M.; Johnson, L. N. The Structural Basis for Control of Eukaryotic Protein Kinases. *Annu. Rev. Biochem.* **2012**, *81* (1), 587–613.

(178) Miller, R. M.; Taunton, J. *Targeting Protein Kinases with Selective and Semipromiscuous Covalent Inhibitors*, 1st ed.; Elsevier Inc., 2014; Vol. 548.

(179) Zappa, C.; Mousa, S. A. Non-Small Cell Lung Cancer: Current Treatment and Future Advances. *Transl. Lung Cancer Res.* **2016**, *5* (3), 288–300.

(180) Hanna, N.; Johnson, D.; Temin, S.; Baker, S.; Brahmer, J.; Ellis, P. M.; Giaccone, G.; Hesketh, P. J.; Jaiyesimi, I.; Leighl, N. B.; et al. Systemic Therapy for Stage IV Non–small-Cell Lung Cancer: American Society of Clinical Oncology Clinical Practice Guideline Update. *J. Clin. Oncol.* **2017**, *35* (30), 3484–3515.

(181) Hirsch, F. R.; Scagliotti, G. V.; Mulshine, J. L.; Kwon, R.; Curran, W. J.; Wu, Y. L.; Paz-Ares, L. Lung Cancer: Current Therapies and New Targeted Treatments. *Lancet* **2017**, *389* (10066), 299–311.

(182) Pao, W.; Miller, V. A. Epidermal Growth Factor Receptor Mutations, Small-Molecule

Kinase Inhibitors, and Non-Small-Cell Lung Cancer: Current Knowledge and Future Directions. *J. Clin. Oncol.* **2005**, *23* (11), 2556–2568.

(183) Chan, B. A.; Hughes, B. G. M. Targeted Therapy for Non-Small Cell Lung Cancer: Current Standards and the Promise of the Future. *Transl. Lung Cancer Res.* **2015**, *4* (1), 36–54.

(184) Zhao, Y.; Bjorbaek, C.; Moller, D. E. Regulation and Interaction of Pp90rsk Isoforms with Mitogen-Activated Protein Kinases. *J. Biol. Chem.* **1996**, *271* (47), 29773–29779.

(185) Romeo, Y.; Zhang, X.; Roux, P. P. Regulation and Function of the RSK Family of Protein Kinases. *Biochem. J.* **2012**, *441* (2), 553–569.

(186) Ikuta, M.; Kornienko, M.; Byrne, N.; Reid, J. C.; Mizuarai, S.; Kotani, H.; Munshi, S. K. Crystal Structures of the N-Terminal Kinase Domain of Human RSK1 Bound to Three Different Ligands: Implications for the Design of RSK1 Specific Inhibitors. *Protein Sci.* **2007**, *16* (12), 2626–2635.

(187) Fisher, T. L.; Blenis, J. Evidence for Two Catalytically Active Kinase Domains in Pp90rsk. *Mol. Cell. Biol.* **1996**, *16* (3), 1212–1219.

(188) Frödin, M.; Gammerltoft, S. Role and Regulation of 90 KDa Ribosomal S6 Kinase (RSK) in Signal Transduction. *Mol. Cell. Endocrinol.* **1999**, *151*, 65–77.

(189) Kang, S.; Dong, S.; Gu, T.-L.; Guo, A.; Cohen, M. S.; Lonial, S.; Khoury, H. J.; Fabbro, D.; Gilliland, D. G.; Bergsagel, P. L.; et al. FGFR3 Activates RSK2 to Mediate Hematopoietic Transformation through Tyrosine Phosphorylation of RSK2 and Activation of the MEK/ERK Pathway. *Cancer Cell* **2007**, *12* (3), 201–214.

(190) Torres, M. A.; Eldar-Finkelman, H.; Krebs, E. G.; Moon, R. T. Regulation of Ribosomal S6 Protein Kinase-P90(Rsk), Glycogen Synthase Kinase 3, and Beta-Catenin in Early Xenopus Development. *Mol. Cell. Biol.* **1999**, *19* (2), 1427–1437.

(191) De Cesare, D.; Jacquot, S.; Hanauer, A.; Sassone-Corsi, P. Rsk-2 Activity Is Necessary for Epidermal Growth Factor-Induced Phosphorylation of CREB Protein and Transcription of c-Fos Gene. *Proc. Natl. Acad. Sci. U. S. A.* **1998**, *95* (21), 12202–12207.

(192) Wang, Z.; Zhang, B.; Wang, M.; Carr, B. I. Persistent ERK Phosphorylation Negatively Regulates CAMP Response Element-Binding Protein (CREB) Activity via Recruitment of CREB-Binding Protein to Pp90 RSK. *J. Biol. Chem.* **2003**, *278* (13), 11138–11144.

(193) Joel, P. B.; Smith, J.; Sturgill, T. W.; Fisher, T. L.; Blenis, J.; Lannigan, D. A. Pp90rsk1 Regulates Estrogen Receptor-Mediated Transcription through Phosphorylation of Ser-167. *Mol. Cell. Biol.* **1998**, *18* (4), 1978–1984.

(194) López-Vicente, L.; Pons, B.; Coch, L.; Teixidó, C.; Hernández-Losa, J.; Armengol, G.; Ramon Y Cajal, S. RSK4 Inhibition Results in Bypass of Stress-Induced and Oncogene-Induced Senescence. *Carcinogenesis* **2011**, *32* (4), 470–476.

(195) Ruiz, E. J.; Vilar, M.; Nebreda, A. R. A Two-Step Inactivation Mechanism of Myt1 Ensures CDK1/Cyclin B Activation and Meiosis I Entry. *Curr. Biol.* **2010**, *20* (8), 717–723.

(196) Shimamura, A.; Ballif, B. A.; Richards, S. A.; Blenis, J. Rsk1 Mediates a MEK-MAP

Kinase Cell Survival Signal. *Curr. Biol.* **2000**, *10* (3), 127–135.

(197) Anjum, R.; Roux, P. P.; Ballif, B. A.; Gygi, S. P.; Blenis, J. The Tumor Suppressor DAP Kinase Is a Target of RSK-Mediated Survival Signaling. *Curr. Biol.* **2005**, *15* (19), 1762–1767.

(198) Casalvieri, K. A.; Matheson, C. J.; Backos, D. S.; Reigan, P. Selective Targeting of RSK Isoforms in Cancer. *Trends in Cancer* **2017**, *3* (4), 302–312.

(199) Smith, J. A.; Poteet-Smith, C. E.; Xu, Y.; Errington, T. M.; Hecht, S. M.; Lannigan, D. A. Identification of the First Specific Inhibitor of P90 Ribosomal S6 Kinase (RSK) Reveals an Unexpected Role for RSK in Cancer Cell Proliferation. *Cancer Res.* **2005**, *65* (3), 1027–1034.

(200) Clark, D. E.; Errington, T. M.; Smith, J. A.; Frierson, H. F. J.; Weber, M. J.; Lannigan, D. A. The Serine/Threonine Protein Kinase, P90 Ribosomal S6 Kinase, Is an Important Regulator of Prostate Cancer Cell Proliferation. *Cancer Res.* **2005**, *65* (8), 3108–3116.

(201) Kang, S.; Elf, S.; Lythgoe, K.; Hitosugi, T.; Taunton, J.; Zhou, W.; Xiong, L.; Wang, D.; Muller, S.; Fan, S.; et al. P90 Ribosomal S6 Kinase 2 Promotes Invasion and Metastasis of Human Head and Neck Squamous Cell Carcinoma Cells. *J. Clin. Invest.* **2010**, *120* (4), 1165–1177.

(202) Elf, S.; Blevins, D.; Jin, L.; Chung, T.-W.; Williams, I. R.; Lee, B. H.; Lin, J.-X.; Leonard, W. J.; Taunton, J.; Khoury, H. J.; et al. P90RSK2 Is Essential for FLT3-ITD- but Dispensable for BCR-ABL-Induced Myeloid Leukemia. *Blood* **2011**, *117* (25), 6885–6894.

(203) Cho, Y.-Y.; Yao, K.; Kim, H.-G.; Kang, B. S.; Zheng, D.; Bode, A. M.; Dong, Z. Ribosomal S6 Kinase 2 Is a Key Regulator in Tumor Promoter Induced Cell Transformation. *Cancer Res.* **2007**, *67* (17), 8104–8112.

(204) Sulzmaier, F. J.; Young-Robbins, S.; Jiang, P.; Geerts, D.; Prechtl, A. M.; Matter, M. L.; Kesari, S.; Ramos, J. W. RSK2 Activity Mediates Glioblastoma Invasiveness and Is a Potential Target for New Therapeutics. *Oncotarget* **2016**, *7* (48), 79869–79884.

(205) Bignone, P. A.; Lee, K. Y.; Liu, Y.; Emilion, G.; Finch, J.; Soosay, A. E. R.; Charnock, F. M. L.; Beck, S.; Dunham, I.; Mungall, A. J.; et al. RPS6KA2, a Putative Tumour Suppressor Gene at 6q27 in Sporadic Epithelial Ovarian Cancer. *Oncogene* **2007**, *26* (5), 683–700.

(206) Thakur, A.; Sun, Y.; Bollig, A.; Wu, J.; Biliran, H.; Banerjee, S.; Sarkar, F. H.; Liao, D. J. Anti-Invasive and Antimetastatic Activities of Ribosomal Protein S6 Kinase 4 in Breast Cancer Cells. *Clin. Cancer Res.* **2008**, *14* (14), 4427–4436.

(207) Lara, R.; Mauri, F. a; Taylor, H.; Derua, R.; Shia, a; Gray, C.; Nicols, a; Shiner, R. J.; Schofield, E.; Bates, P. a; et al. An SiRNA Screen Identifies RSK1 as a Key Modulator of Lung Cancer Metastasis. *Oncogene* **2011**, *30* (32), 3513–3521.

(208) Larrea, M. D.; Hong, F.; Wander, S. A.; da Silva, T. G.; Helfman, D.; Lannigan, D.; Smith, J. A.; Slingerland, J. M. RSK1 Drives P27Kip1 Phosphorylation at T198 to Promote RhoA Inhibition and Increase Cell Motility. *Proc. Natl. Acad. Sci.* **2009**, *106* (23), 9268–9273.

(209) Nguyen, T. Targeting RSK: An Overview of Small Molecule Inhibitors. *Anticancer. Agents Med. Chem.* **2008**, *8* (7), 710–716.

(210) Cohen, M. S.; Zhang, C.; Shokat, K. M.; Taunton, J. Structural Bioinformatics-Based Design of Selective, Irreversible Kinase Inhibitors. *Science* **2005**, *308* (5726), 1318–1321.

(211) Bain, J.; Plater, L.; Elliott, M.; Shpiro, N.; Hastie, C. J.; Mclauchlan, H.; Klevernic, I.; Arthur, J. S. C.; Alessi, D. R.; Cohen, P. The Selectivity of Protein Kinase Inhibitors: A Further Update. *Biochem. J.* **2007**, *408* (3), 297–315.

(212) Cohen, M. S.; Hadjivassiliou, H.; Taunton, J. A Clickable Inhibitor Reveals Context-Dependent Autoactivation of P90 RSK. *Nat. Chem. Biol.* **2007**, *3* (3), 156–160.

(213) Hammoud, L.; Adams, J. R.; Loch, A. J.; Marcellus, R. C.; Uehling, D. E.; Aman, A.; Fladd, C.; McKee, T. D.; Jo, C. E. B.; Al-Awar, R.; et al. Identification of RSK and TTK as Modulators of Blood Vessel Morphogenesis Using an Embryonic Stem Cell-Based Vascular Differentiation Assay. *Stem Cell Reports* **2016**, *7* (4), 787–801.

(214) Beauchamp, E. M.; Kosciuczuk, E. M.; Serrano, R.; Nanavati, D.; Swindell, E. P.; Viollet, B.; O'Halloran, T. V.; Altman, J. K.; Platanias, L. C. Direct Binding of Arsenic Trioxide to AMPK and Generation of Inhibitory Effects on Acute Myeloid Leukemia Precursors. *Mol. Cancer Ther.* **2015**, *14* (1), 202–212.

(215) Lara, R.; Seckl, M. J.; Pardo, O. E. The P90 RSK Family Members: Common Functions and Isoform Specificity. *Cancer Res.* **2013**, *73* (17), 5301–5308.

(216) Dümmler, B. a; Hauge, C.; Silber, J.; Yntema, H. G.; Kruse, L. S.; Kofoed, B.; Hemmings, B. a; Alessi, D. R.; Frödin, M. Functional Characterization of Human RSK4, a New 90-KDa Ribosomal S6 Kinase, Reveals Constitutive Activation in Most Cell Types. *J. Biol. Chem.* **2005**, *280* (14), 13304–13314.

(217) Berns, K.; Hijmans, E. M.; Mullenders, J.; Brummelkamp, T. R.; Velds, A.; Heimerikx, M.; Kerkhoven, R. M.; Madiredjo, M.; Nijkamp, W.; Weigelt, B.; et al. A Large-Scale RNAi Screen in Human Cells Identifies New Components of the P53 Pathway. *Nature* **2004**, *428* (6981), 431–437.

(218) LLeonart, M. E.; Vidal, F.; Gallardo, D.; Diaz-Fuertes, M.; Rojo, F.; Cuatrecasas, M.; López-Vicente, L.; Kondoh, H.; Blanco, C.; Carnero, A.; et al. New P53 Related Genes in Human Tumors: Significant Downregulation in Colon and Lung Carcinomas. *Oncol. Rep.* **2006**, *16* (3), 603–608.

(219) Bender, C.; Ullrich, A. PRKX, TTBK2 and RSK4 Expression Causes Sunitinib Resistance in Kidney Carcinoma- and Melanoma-Cell Lines. *Int. J. Cancer* **2012**, *131* (2), E45–E55.

(220) Fan, L.; Li, P.; Yin, Z.; Fu, G.; Liao, D. J.; Liu, Y.; Zhu, J.; Zhang, Y.; Wang, L.; Yan, Q.; et al. Ribosomal S6 Protein Kinase 4: A Prognostic Factor for Renal Cell Carcinoma. *Br. J. Cancer* **2013**, *109* (5), 1137–1146.

(221) Sun, Y.; Cao, S.; Yang, M.; Wu, S.; Wang, Z.; Lin, X.; Song, X.; Liao, D. J. Basic Anatomy and Tumor Biology of the RPS6KA6 Gene That Encodes the P90 Ribosomal S6 Kinase-4. *Oncogene* **2013**, *32* (14), 1794–1810.

(222) Sharma, P. C.; Jain, A.; Jain, S. Fluoroquinolone Antibacterials: A Review on

Chemistry, Microbiology and Therapeutic Prospects. *Acta Pol. Pharm. - Drug Res.* **2009**, *66* (6), 587–604.

(223) Zhanel, G. G.; Walkty, A.; Vercaigne, L.; Karlowsky, J. A.; Embil, J.; Gin, A. S.; Hoban, D. J. The New Fluoroquinolones: A Critical Review. *Can. J. Infect. Dis.* **1999**, *10* (3), 207–238.

(224) Reece, R. J.; Maxwell, A. DNA Gyrase: Structure and Function. *Crit. Rev. Biochem. Mol. Biol.* **1991**, *26* (3–4), 335–375.

(225) Drlica, K.; Zhao, X. DNA Gyrase, Topoisomerase IV, and the 4-Quinolones. *Microbiol. Mol. Biol. Rev.* **1997**, *61* (3), 377–392.

(226) Wang, Y.; Chen, R.; Nan, H. Process for Preparing a Quinolone-Carboxylic Acid. US 2003/0166936 A1, 2003.

(227) Groweiss, A. Use of Sodium Bromate for Aromatic Bromination: Research and Development. *Org. Process Res. Dev.* **2000**, *4* (1), 30–33.

(228) Rajesh, K.; Somasundaram, M.; Saiganesh, R.; Balasubramanian, K. K. Bromination of Deactivated Aromatics: A Simple and Efficient Method. *J. Org. Chem.* **2007**, *72* (15), 5867–5869.

(229) Derbyshire, D. H.; Waters, W. A. 108. The Significance of the Bromine Cation in Aromatic Substitution. Part II. Preparative Applicability. *J. Chem. Soc.* **1950**, 573.

(230) Clayden, J.; Greeves, N.; Warren, S.; Wothers, P. *Organic Chemistry*; Oxford University Press Inc., New York: Oxford, 2001.

(231) Aalten, H. L.; van Koten, G.; Grove, D. M.; Kuilman, T.; Piekstra, O. G.; Hulshof, L. A.; Sheldon, R. A. The Copper Catalysed Reaction of Sodium Methoxide with Aryl Bromides. A Mechanistic Study Leading to a Facile Synthesis of Anisole Derivatives. *Tetrahedron* **1989**, *45* (17), 5565–5578.

(232) Davies, K.; Kiyoi, T.; Mistry, A. D.; Ray, P. C.; Reid, M.; Wishart, G. Tricyclic Heterocyclic Derivatives. WO 2010/103001 A1, 2010.

(233) Sanchez, J. P.; Gogliotti, R. D.; Domagala, J. M.; Gracheck, S. J.; Huband, M. D.; Sesnie, J. A.; Cohen, M. A.; Shapiro, M. A. The Synthesis, Structure-Activity, and Structure-Side Effect Relationships of a Series of 8-Alkoxy- and 5-Amino-8-Alkoxyquinolone Antibacterial Agents. *J. Med. Chem.* **1995**, *38* (22), 4478–4487.

(234) Mich, T. F.; Sanchez, J. P.; Domagala, J. M.; Trehan, A. K. 1-Cyclopropyl-6,7-Dihalo-1,4-Dihydro-4-Oxo-1,8-Naphthyridine-3-Carboxylic Acid and Their Esters, Useful as Intermediates for Preparing the 7-Amine Substituted Naphthyridines. 4663457, 1987.

(235) Sun, Q.; Zhu, R.; Foss, F. W.; Macdonald, T. L. Mechanisms of Trovafloxacin Hepatotoxicity: Studies of a Model Cyclopropylamine-Containing System. *Bioorganic Med. Chem. Lett.* **2007**, *17* (24), 6682–6686.

(236) Hutton, H. M.; Schaefer, T. Proton Coupling Constants in Substituted Cyclopropanes. *Can. J. Chem.* **1963**, *41* (3), 684–689.

(237) Norris, T.; Braish, T. F.; Butters, M.; DeVries, K. M.; Hawkins, J. M.; Massett, S. S.; Rose, P. R.; Santafianos, D.; Sklavounos, C. Synthesis of Trovafloxacin Using

Various (1α,5α,6α)-3-Azabicyclo[3.1.0]Hexane Derivatives. *J. Chem. Soc. Perkin Trans. 1* **2000**, *4* (10), 1615–1622.

(238) Blokhina, S. V.; Sharapova, A. V.; Ol'khovich, M. V.; Volkova, T. V.; Perlovich, G. L. Solubility, Lipophilicity and Membrane Permeability of Some Fluoroquinolone Antimicrobials. *Eur. J. Pharm. Sci.* **2016**, *93*, 29–37.

(239) Firestone, B. a.; Dickason, M. a.; Tran, T. Solubility Characteristics of Three Fluoroquinolone Ophthalmic Solutions in an in Vitro Tear Model. *Int. J. Pharm.* **1998**, *164* (1–2), 119–128.

(240) Ortega, L. M.; Khan, M.; Bagwan, N.; Nayer, A. Journal of Nephropathology Crystal-Induced Acute Kidney Injury Due to Ciprofloxacin. *J Nephropathol* **2015**, *4* (1), 29–31.

(241) Walker, M. A. Novel Tactics for Designing Water-Soluble Molecules in Drug Discovery. *Expert Opin. Drug Discov.* **2014**, *9* (12), 1421–1433.

(242) Elder, D. P.; Holm, R.; De Diego, H. L. Use of Pharmaceutical Salts and Cocrystals to Address the Issue of Poor Solubility. *Int. J. Pharm.* **2013**, *453* (1), 88–100.

(243) Florindo, C.; Costa, A.; Matos, C.; Nunes, S. L.; Matias, A. N.; Duarte, C. M. M.; Rebelo, L. P. N.; Branco, L. C.; Marrucho, I. M. Novel Organic Salts Based on Fluoroquinolone Drugs: Synthesis, Bioavailability and Toxicological Profiles. *Int. J. Pharm.* **2014**, *469* (1), 179–189.

(244) Joel, P. B.; Smith, J.; Sturgill, T. W.; Fisher, T. L.; Blenis, J.; Lannigan, D. A. Pp90rsk1 Regulates Estrogen Receptor-Mediated Transcription through Phosphorylation of Ser-167. *Mol. Cell. Biol.* **1998**, *18* (4), 1978–1984.

(245) Hoye, T. R.; Eklov, B. M.; Ryba, T. D.; Voloshin, M.; Yao, L. J. No-D NMR (No-Deuterium Proton NMR) Spectroscopy: A Simple yet Powerful Method for Analyzing Reaction and Reagent Solutions. *Org. Lett.* **2004**, *6* (6), 953–956.

(246) Lui, Y. Enantioselective Synthesis of α-Fluoro-β-Hydroxy Esters and Amides and Ni-Catalyzed Asymmetric 1,4-Addition to Vinylnitriles, Ph.D. Thesis, Swiss Federal Institute of Technology Zurich, 2006.

(247) Heinrich, T.; Zenke, F.; Calderini, M.; Djordje, M. Pyrrolidinones as Metap-2 Inhibitors. US 2013/0296274 A1, 2013.

(248) Banerjee, S.; Vogel, E. R.; Hinton, D.; Sterling, M.; Masterson, D. S. An Enantiodivergent Synthesis of Cα-Methyl Nipecotic Acid Analogues from δ-Lactam Derivatives Obtained through a Highly Stereoselective Cyclization Strategy. *Tetrahedron: Asymmetry* **2015**, *26* (21–22), 1292–1299.

(249) Bull, R. J.; Ray, N. C. 2-(9H-Xanthen-9-Yl)-Oxazol Derivatives as M3 Muscarinic Receptor Antagonists for the Treatment of Asthma and Chronic Obstructive Lung Disease. WO 2009/098455 A1, 2009.

(250) Yu, C. J.; Li, R.; Gu, P. Intermolecular Schmidt Reaction of Alkyl Azides with Acyl Silanes. *Tetrahedron Lett.* **2016**, *57* (31), 3568–3570.

(251) Toukoniitty, E.; Mäki-Arvela, P.; Kuzma, M.; Villela, A.; Neyestanaki, A. K.; Salmi, T.; Murzin, D. Y.; Sjöholm, R.; Leino, R.; Laine, E. Enantioselective Hydrogenation of 1-Phenyl-1, 2-Propanedione. *J. Catal.* **2001**, *204* (2), 281–291.

(252) North, M.; Omedes-Pujol, M.; Young, C. Kinetics and Mechanism of the Racemic Addition of Trimethylsilyl Cyanide to Aldehydes Catalysed by Lewis Bases. *Org. Biomol. Chem.* **2012**, *10* (21), 4289–4298.

(253) Griffioen, G.; Van Dooren, T.; Rojas De La Parra, V.; Marchand, A.; Allasia, S.; Kilonda, A.; Chaltin, P. Indole Amide Derivatives and Related Compounds for the Use in the Treatment of Neurodegenerative Diseases. WO 2010/142801 A1, 2010.

(254) Takao, K.; Noda, K.; Morita, Y.; Nishimura, K.; Ikeda, Y. Molecular and Crystal Structures of Uranyl Nitrate Complexes with N -Alkylated 2-Pyrrolidone Derivatives: Design and Optimization of Promising Precipitant for Uranyl Ion. *Cryst. Growth Des.* **2008**, *8* (7), 2364–2376.

(255) Sadhukhan, S.; Zhang, G. F.; Tochtrop, G. P. Modular Isotopomer Synthesis of γ-Hydroxybutyric Acid for a Quantitative Analysis of Metabolic Fates. *ACS Chem. Biol.* **2014**, *9* (8), 1706–1711.

(256) Tian, C.; Wang, M.; Han, Z.; Fang, F.; Zhang, Z.; Wang, X.; Liu, J. Design, Synthesis and Biological Evaluation of Novel 6-Substituted Pyrrolo [3,2- d] Pyrimidine Analogues as Antifolate Antitumor Agents. *Eur. J. Med. Chem.* **2017**, *138*, 630–643.

(257) Anquetin, G.; Greiner, J.; Mahmoudi, N.; Santillana-Hayat, M.; Gozalbes, R.; Farhati, K.; Derouin, F.; Aubry, A.; Cambau, E.; Vierling, P. Design, Synthesis and Activity against Toxoplasma Gondii, Plasmodium Spp., and Mycobacterium Tuberculosis of New 6-Fluoroquinolones. *Eur. J. Med. Chem.* **2006**, *41* (12), 1478–1493.

(258) Garza, I.; Wallace, M. J.; Fernando, D.; Singh, A.; Lee, R. E.; Gerding, J. S.; Franklin, C.; Yendapally, R. Synthesis and Evaluation of Thiazolidine Amide and N-Thiazolyl Amide Fluoroquinolone Derivatives. *Arch. Pharm. (Weinheim).* **2017**, *350* (6), 1–7.

(259) Madhusudhan, G.; Balraju, V.; Rajesh, T.; Narayana, B. V.; Reddy, R. N. Synthesis of an Amino Moiety in Trovafloxacin by Using an Inexpensive Amidine Base, N,N-Diethylacetamidine. *Indian J. Chem.* **2009**, *48B*, 569–573.

(260) Wilson, D. W.; Crabb, B. S.; Beeson, J. G. Development of Fluorescent Plasmodium Falciparum for in Vitro Growth Inhibition Assays. *Malar. J.* **2010**, *9* (1), 152.